The catalytic oxidative dehydrogenation of n-octane over iron and other metal molybdates

Thesis submitted in accordance with requirements of the University of Cardiff for the qualification of Doctor of Philosophy

Keith Bugler
May 2017

ACKNOWLEDGEMENTS

SUMMARY

Metal molybdates of iron, cobalt and nickel, were found to be catalysts for the gas phase oxidative dehydrogenation of *n*-octane to octenes. Other products formed included; carbon oxides, aromatic species, cracked oxygenate species and cracked hydrocarbon products of the octane.

Iron molybdate in the ferrous form was shown to exhibit much greater selectivity to octenes than when in the ferric form. Cobalt and nickel molybdates were also tested and found to be active catalysts, but exhibited greater selectivity to carbon oxide and aromatic products than iron, which produced the greatest selectivity to octenes.

A variety of conditions were tested for the catalytic oxidative dehydrogenation of *n*-octane, including; reactor bed temperature, contact time, carbon to oxygen ratio in the gas feed and concentration of *n*-octane. This was done to discover the optimal conditions for the catalytic production of octenes. A maximum selectivity of 85.4% to octenes with an *n*-octane conversion of 7.8% was found.

Investigations were carried out to elucidate the mechanism and route of formation of the products found, including comparison with previous literature on the molybdenum based catalysts for the oxidative dehydrogenation of hydrocarbons. It was found that the ferrous iron molybdate phase, $FeMoO_4$, was responsible for the production of octenes. Molybdenum oxides of the dioxide and trioxide form were associated with the production of aromatic species. While lattice oxygen was used in producing octenes via oxidative dehydrogenation, suggesting a Mars and van Krevelen style mechanism, carbon oxide production was found to be produced via oxygen from the gas feed.

Analysis of the catalysts before and after the reaction was carried out with a variety of techniques including X-ray powder diffraction, Raman Spectroscopy and X-ray photoelectron spectroscopy.

ABSTRACT

This work studies the gas phase oxidative dehydrogenation (ODH) of *n*-octane to produce octenes, catalysed by metal molybdates of the formula $AMoO_4$, where A equals iron, cobalt or nickel in the +2 oxidation state. An *in-situ* reduction study from previous work had shown that iron molybdate where iron is in the +2 oxidation state is a superior catalyst to an iron molybdate catalyst with iron in the +3 state. This was tested and found to be the case. Subsequently all iron molybdate catalyst testing was performed with iron molybdate where iron is in the +2 oxidation state. This was achieved through a pre-reduction step in catalyst preparation.

The pre-reduced iron molybdate catalyst with a 2.7:1 molar excess of molybdenum to iron was found to be composed of the species $FeMoO_4 + Mo_4O_{11}$. This catalyst exhibited high selectivity to octenes from an *n*-octane feedstock at 400 °C in a plug flow reactor. Changes in gas hourly velocity (GHSV) and temperature (ranging from 350-550 °C) affected catalyst activity and selectivity, as did varying the ratio of carbon to oxygen in the gas feed.

Optimum conditions for the production of octene were found to be; 400 °C reactor bed temperature, 4000 h^{-1} GHSV and an 8:1 carbon to oxygen ratio, no carbon oxides were observed at these conditions. Increasing temperature results in higher conversion of *n*-octane but lower selectivity to octenes. Aromatic species become the major products at higher temperatures. Carbon oxide selectivity also rises with temperature.

Increasing partial pressure of oxygen in the gas feed leads to higher conversion but the major products formed are carbon oxides. Lowering the level of oxygen from an 8:1 carbon to oxygen ratio saw lower conversions with similar selectivity. This suggested oxidative dehydrogenation was occurring.

Lowering the GHSV from 4000 h^{-1} to 1000 h^{-1} resulted in product selectivity to aromatic species, ethyl benzene, xylene and styrene. Higher conversion as a result of greater contact time between catalyst and product was observed. Styrene and xylene selectivity increased in line with temperature, while selectivity to ethyl benzene fell,

suggesting a competing pathway between aromatic formation, or that ethyl benzene underwent further dehydrogenation to styrene.

Increasing GHSV to 6000 h^{-1} resulted in an even greater selectivity to octenes than 4000 h^{-1}. However conversion was lower, likely due to contact time effects. These findings suggested that the product selectivity from n-octane over an iron molybdate catalyst has a strongly kinetic element.

Increasing the concentration of n-octane in the gas feed showed a shift in the optimal conditions for the production of octene. A higher GHSV was required to yield octenes as the dominant product, this had the unfortunate effect of lowering conversion percentage. While this was off-set in some way by the increased concertation of n-octane it does suggest future difficulties on scaling up the process.

Time on line studies showed the catalyst was stable at temperatures of 550 °C for 20 hours or more.

In addition anaerobic studies were carried out on the catalyst were tested to elucidate the mechanism of the catalyst. The change in selectivity and activity showed the catalyst most likely operates by a Mars and van-Krevelen type system. After oxygen deprivation for 25 hours catalyst deactivation occurred. Analysis showed both carbon laydown and reduction of the molybdenum lattice from Mo_4O_{11} had occurred.

Product selectivity analysis indicated that lattice oxygen from the iron molybdate or the bulk Mo_4O_{11} phase was responsible for the ODH of n-octane to octene. Carbon oxides were formed via oxygen in the gas feed.

Stoichiometric nickel molybdates and cobalt molybdates were prepared and compared against nickel and cobalt molybdates with a molybdenum molar excess of 1.5:1 for the catalytic conversion of n-octane to octene. These catalysts were then compared against stoichiometric iron molybdate ($FeMoO_4$) to compare catalytic effectiveness. Iron molybdate outperformed nickel molybdate and cobalt molybdate which have been more heralded ODH catalysts in the literature. Cobalt molybdate was found to exhibit high selectivity to aromatic species while nickel molybdate produced carbon oxides and cracked hydrocarbon products. Nickel molybdate and cobalt molybdate

with an excess of molybdenum performed better as catalysts than stoichiometric nickel and cobalt molybdates.

GLOSSARY OF TERMS

BE – Binding Energy

C:O ratio – Carbon to Oxygen ratio

EDX – Energy Dispersive X-rays

GC – Gas Chromatograph

GHSV – Gas Hourly Space Velocity

MP-AES – Multi Plasma Atomic Emission Spectroscopy

MvK – Mars-Van Krevelen

ODH – Oxidative dehydrogenation

TGA – Thermogravimetric analysis

XPS – X-ray photoelectron spectroscopy

XRD – X-ray Diffraction

XRPD – X-ray Powder Diffraction

CONTENTS

CHAPTER 1 – LITERATURE REVIEW AND INTRODUCTION

1.1 OVERVIEW OF CATALYSIS

Catalysis is a term coined by Berzelius from the Greek "*kata*" which means down and "*lysis*" which translates as loosening.[1,2] It can be defined as a substance or material which increases the rate at which a chemical reaction reaches equilibrium without being consumed or chemically altered.

Berzelius defined a catalyst as "a material that enhances the rate and selectivity of a chemical reaction without itself being consumed in the reaction".

For molecules to react, a minimum activation energy (E_{act}) must be reached. A catalyst allows the activation energy to be lowered by providing an alternative reaction pathway.[3] As a result a greater number of molecules have a Gibbs free energy which is greater than that of the activation energy and thus more reactant molecules can come together and react. The Gibbs free energy (ΔG) is equal to the sum of enthalpy and the product of temperature and entropy within a system. This is shown as

$$\Delta G = \Delta H - T\Delta S$$

Where

ΔH is the change in enthalpy

T is temperature

ΔS is the change in entropy.

Catalysts affect the rate of the reaction and not the thermodynamics, this was shown by Ostwald.[3] This means they can be used to improve the rate of reactions that may otherwise take a long time or require high levels of pressure and heat.
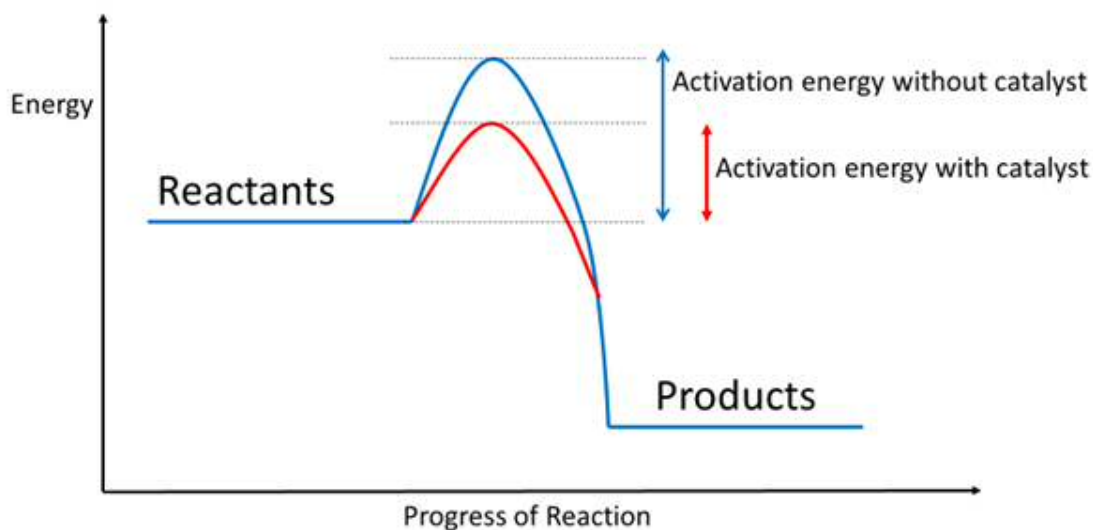
Figure 1.1 – Basic illustration of the concept of catalysis and its effect on E$_{act}$.

When considering Figure 1.1 it can be seen there are reaction barriers. These are represented by the raised curves. The top of the curve can be referred to as $\Delta G^{\ddagger}$ which is the Gibbs free energy of the transition state, between the reactant and product. This is linked to the ideas of Arrhenius who observed the rate of a reaction is dependent upon temperature.

$$\Delta G^{\ddagger} = -RTlnK$$

Where

R is the ideal gas constant

T is the absolute temperature

K is the equilibrium constant

The relationship between the activation energy and the rate constant (k) can be shown by Arrhenius equation.

$$k = Ae^{-\Delta G^{\ddagger}/RT}$$

Where A is the Arrhenius constant and k is the rate constant.

This leads to:

$$lnk = (-\Delta G^{\ddagger} / RT) + constant$$

When ΔG‡ is at zero the rate constant is given as k_0. This is a diffusion limited constant and can be given as.

$$k = k_0 \, e \, [-\Delta G‡ / RT]$$

In summary a catalyst lowers the activation energy barrier of a reaction, this allows more molecules to reach a transition state, this then results in an increase of the rate at which chemical equilibrium is reached.

Catalysis is divided into two main groups. Homogeneous and heterogeneous catalysis. Homogeneous catalysis is when the catalyst is in the same phase as the reactants and heterogenous catalysis is when the catalyst is in a different phase. Homogeneous catalysis is generally liquid-liquid processes.[4] A common example would be acid/base catalysed hydrolysis of esters.[5] Advantages of homogeneous catalysis is that product selectivity is high and low reaction temperatures (≤200 °C) are required. The challenges associated with homogeneous are separation of products and recycling of the catalyst.[6]

Heterogeneous catalysis generally occurs with a solid catalyst with gaseous and/or liquid reactants.[7] This approach tends to give high activity but challenges arise with selectivity to the desired product. Higher reaction temperatures are used in heterogeneous catalysis (rising to 600 °C).[8] Separation of the catalyst is relatively easy but the high temperatures mean the reactions can be very energy intensive. An example of heterogeneous catalysis all chemists will be familiar with is the Haber-Bosch process for ammonia production.[9]

As this work focuses on the heterogeneous catalytic process of oxidative dehydrogenation of alkanes with molybdates, the next part of this chapter looks at heterogeneous catalysis in more detail.

1.2 HETEROGENEOUS CATALYSIS

It has been reported that a clear majority (80%) of all catalytic processes performed in industry are heterogeneous.[10]

In addition to the aforementioned Haber-Bosch process, many other processes rely on heterogeneous catalysts. Methanol synthesis form syngas on a copper catalyst supported on zirconia,[11] nitric acid synthesis using a platinum gauze, ethylene epoxidation[12] are just three examples.

As it relates to a similar field to the study of this work, it is worth mentioning the Fischer Tropsch (FT) process which converts syngas (CO and H_2) to alkanes. Often cobalt based catalysts are used.[13] The syngas is produced from coal and natural gas and is then converted into liquid alkane products.

Although not exclusively true[14], an overview of the literature shows that most heterogeneous catalysts are transition metal based. Precious metals such as Pt, Au and Ag on ceramic supports are widely used.[15–17] Ceramic oxides include MgO, SiO_2 and Al_2O_3 among others. The advantages of these ceramic supports are their high degree of thermal stability and lack of reactivity. It should be noted that here is an entire field of catalytic science that looks at catalyst support interactions. However recent research has shown that metal oxide supports can interact with the catalyst in ways previously unthought of[18] so these ceramic and metal oxide supports should not be blithely dismissed as mere spectators in heterogeneous catalysis.

Mixed metal oxides such as $MMoO_4$ where M is a transition metal, or metal vanadate species[19,20] are also widely used in alkane activation and partial oxidation. These catalysts exhibit versatility due to their redox properties, and the differing phases present.

1.3 THE PETROCHEMICAL INDUSTRY AND THE ACTIVATION OF ALKANES

Alkanes come in a variety of masses, from so called "light" hydrocarbons such as ethane, to medium length liquid hydrocarbons such as octane, through to "heavier" species such as dodecane. Increasing the carbon number in this manner ends up yielding waxes. While alkanes are the most commonly occurring hydrocarbon species, alkenes and alkynes possess greater functionality and are thus more desirable from an industrial standpoint.

Light alkenes such ethane are often produced via steam cracking.[21] Steam cracking is an non-catalytic process. The process works by a hydrocarbon feedstock such as naptha being vaporised with superheated steam. The naptha is then cracked to to small hydrocarbon moelcules via a free radical mechanism. Temperatures used can range from 750-1100 °C.[22] The light alkene products are then manufactured into plastics, fibres and pharmaceuticals.[23, 24] As would be expected this process is incredibly energy intensive. Naptha pyrolysis consumes an estimated 75% of the energy input.[22] Following pyrolysis the hydrocarbons are passed along transfer line exchangers, which leads to heat dissipating. Aromatic and gasoline products are condensed and fractioned.
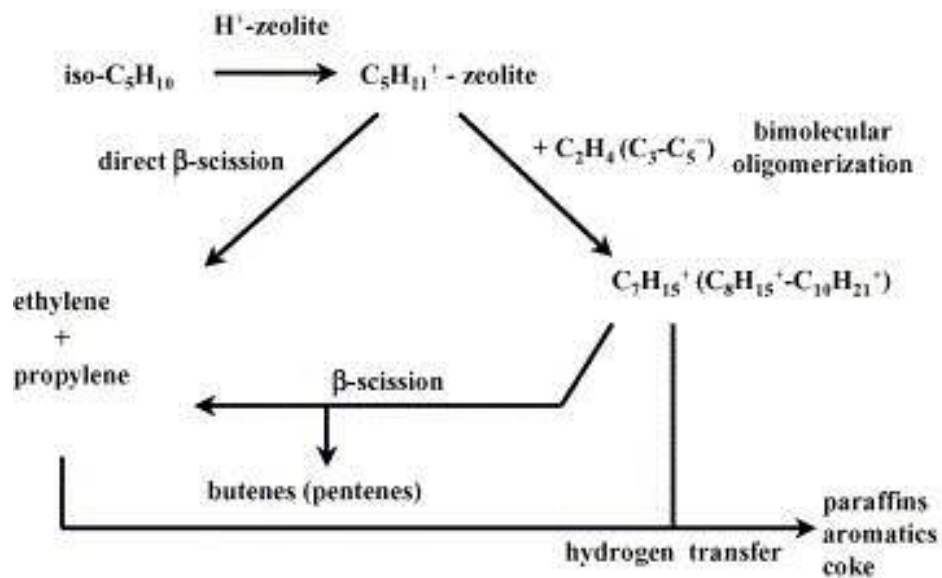
Figure 1.2 Scheme of isopentene cracking on H-zeolites as outlined and from Bortnovsky *et al.*[24]

As steam cracking is so energy intensive catalytic cracking offers a lower energy route to obtaining light alkenes. Zeolites are a common catalyst used to crack larger hydrocarbons into lighter fractions.[25,26] A zeolite is a hydrated aluminosilicate which has a complex 3-D structure which can be used as a molecular sieve. They often have acidic properties. Fluidised catalytic cracking (FCC) is an acid cracking process catalysed by ZSM zeolites, which possess Bronsted acid sites.[27,28] FCC is estimated to produce 30% of the world's propene via naptha cracking. The operating conditions for FCC are at 600 °C or lower, which makes it a less energy consuming procedure than steam reforming processes.[22]

The reason zeolites are used in FCC is that one of the challenges in maximising yield and conversion of short chain alkenes is prevention of branched alkanes (isomers of the original feedstock) forming. The structure of the zeolite can act as a shape selective molecular sieve which prevents branched isomers from forming.

Catalytic dehydrogenation is a catalytic process that has huge industrial impact, as "it represents a route to obtain alkenes from low cost saturated hydrocarbons".[29,30] Early work in the area (*ca.*1970) looked at converting *n*-butane to butene and butadiene which are precursors to synthetic rubber.[29] over time propene and isobutene became increasingly important products from this process, with propene being a prerequisite for polypropylene and isobutene having applications as a fuel additive. As a result of this, there is far more literature on the catalytic dehydrogenation of short chain alkanes than intermediate ($C_6 – C_{10}$) saturated hydrocarbons.

The CATOFIN process is used industrially by Lummus to produced propene and isobutene. Selectivity to isobutene from isobutene exceeds 90 mol%, while selectivity to propene from propane exceeds 86 mol%. The catalyst is used CrO_x/Al_2O_3 system[31] first reported by Freye and Huppke in 1933.[32] Operating temperatures are around 600-650 °C.

Another industrial process that involves dehydrogenation of alkanes is the Honeywell UOP Oleflex process.[33] This is used for C_3 and C_4 hydrocarbons and boasts an alkene selectivity of *ca.*91%. A $Pt/Sn/Al_2O_3$ catalyst is used.

Honeywell UOP also conducts the PACOL process[34] "which can be applied to the dehydrogenation of heavy paraffins in the C_6 - C_{20} range".[34] A platinum dehydrogenation deposited on alumina (which can be modified with rhenium) catalyst is used.[35] Platinum has been shown to exhibit high catalytic activity for the conversion of alkanes to alkenes. This was originally found by Bloch, who found that Pt catalysts can be used to dehydrogenate medium-long chain alkanes to mono-alkenes. This was of importance as there are multiple sites on a longer alkane for dehydrogenation to occur.[36]

The main drawback of dehydrogenation are the thermodynamic constraints. The reaction is strongly endothermic,[37] this requires high temperatures to be maintained in the reactor to drive the reaction. Temperatures of over 550 °C are typically required. The high temperatures can lead to undesirable side reactions such as coke depositing which can lead to catalyst deactivation over time. As the catalysts for the Honeywell processes are made from expensive materials this is doubly unwanted. Le Chatelier's principle limits alkane dehydrogenation and so higher conversion requires lower pressures or higher temperatures.[38] As a result of these issues, oxidative dehydrogenation has emerged as a potential rival process.

1.4 OXIDATIVE DEHYDROGENATION

The oxidative dehydrogenation (ODH) of alkanes is another pathway for the formation of alkenes. It poses less thermodynamic constraints, as it is an exothermic reaction it can be operated under milder conditions, as a result it does not need the elevated reactor temperatures required for dehydrogenation. While catalytic dehydrogenation requires continuous catalyst regeneration,[39] this is not required for alkane ODH.

The idea behind ODH is that oxygen in the gas feed reacts with the hydrogen that is abstracted in the dehydrogenation step and forms water.[40] It is this, the oxygen accepting the hydrogen and forming water that makes it an endothermic reaction. The overall equation is shown here.

$$C_nH_{2n+2} + 1/2O_2 \rightarrow C_nH_{2n} + H_2O$$
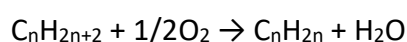
The formation of water also removes hydrogen from the system, which shifts the equilibrium towards the formation of more dehydrogenated products due to le Chatelier's principle. Coke deposits that occur on the catalyst surface in dehydrogenation are burnt off with the oxygen present in the system, this can extend catalyst lifetime.

However, catalytic ODH has several drawbacks. Firstly the levels of oxygen and alkane in the gas feed must be monitored to prevent the reaction mixture being within explosive limits. Secondly, the presence of oxygen can lead to side reactions or competing reactions (such as combustion) which lower selectivity and ultimately alkene yield. Stern and Grasselli[41] proposed a reaction mechanism for the ODH of propane to propene, and attempted to answer why aldehyde and carboxylic acids were resulting products. In Figure 1.3 shows the mechanism proposed by Stern and Grasselli. They state that oxidative dehydrogenation occurs in step 1 yielding "propylene as the exclusive primary product". They propose that propylene then undergoes a secondary oxidation step to acrylaldehyde (also known as acrolein).

They state that "the relative rate of acrolein formation from propylene is 3.5 times that of propylene formation from propane, the rate of CO_x formation from acrolein is 13 times that of acrolein formation from propylene, and the rate of CO_x formation from acrolein is 46 times that of propylene formation from propane." So from a kinetic perspective reaction pathway 1 in Figure 1.3 is the slowest and reaction pathway 3 is the fastest.
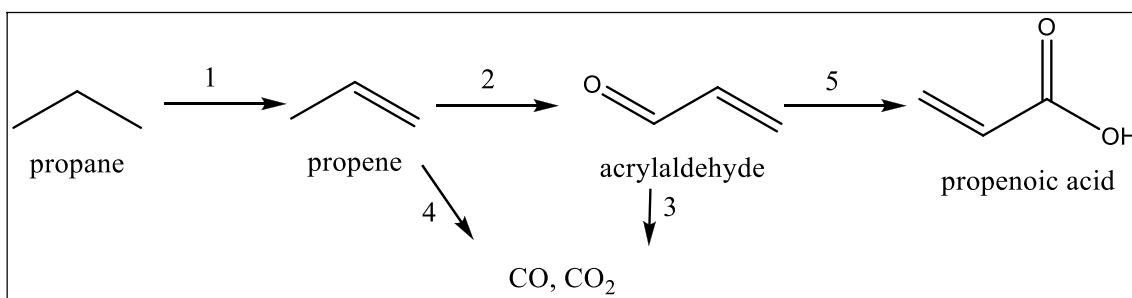
Figure 1.3 Proposed mechanism for the ODH of propane by Stern and Grasselli.[41]

The selective oxidation of propane to propylene (pathway 1) and propylene to acrolein (pathway 2) are both reported by Stern and Grasselli to be zero order with regards to oxygen and first order regarding hydrocarbon (propane and propylene, respectively).[41] The oxidation reaction leading to the formation of CO and CO_2 was found to be half order in oxygen, and with a Langmuir style dependence regarding propylene. Stern and Grasselli also found that propylene competed for the same metal oxide sites as

propane molecules, with the reported effectiveness being on the same order of magnitude.[41]

The concentration of oxygen in the gas feed relative to the alkane can affect the selectivity to products.[42] An excess of oxygen results in higher conversion, but can lead to combustion and the formation of carbon oxides. ODH will be mostly selective to alkenes.[43] Limiting the steps 2 and 5 in Figure 1.3 is the strength of relative allylic bonds. The allylic bond of the alkane is notably weaker than that of its corresponding alkene.[44,45]

Recently the oxidative dehydrogenation of longer chain alkanes (C_6 and larger) has been investigated.[42] Friedrich *et al* have looked at the ODH of hexane[46] over a nickel molybdate catalyst. Other work has examined the effect of a cobalt molybdate on *n*-octane ODH.[47] Hydrotalcite catalysts have also been investigated for *n*-oxctane ODH.[48] Other work has examined the catalytic activity of vanadium based catalysts for *n*-octane ODH.[49]

Both molybdenum[50] and vanadium[51,52] based ODH catalysts tend to proceed via a catalytic mechanism known as the Mars van-Krevelen reaction.[53,54] It is this which will be next examined.

1.5 THE MARS-VAN KREVELEN MECHANISM

Within heterogeneous catalysis, a molecule adsorbs onto the catalyst surface, reacts with another molecule and a molecular product desorbs.

Thus it is of interest to elucidate the mechanism by which this happens. If the reactants adsorb from the gas phase and react together at the surface the reaction mechanism is labelled as a Langmuir-Hinshelwood mechanism.[55] If only one of the reactant (species A) adsorbs to the catalyst surface and then reacts with the other reactant molecule (reactant B) this is labelled an Eley-Rideal style mechanism.[56]
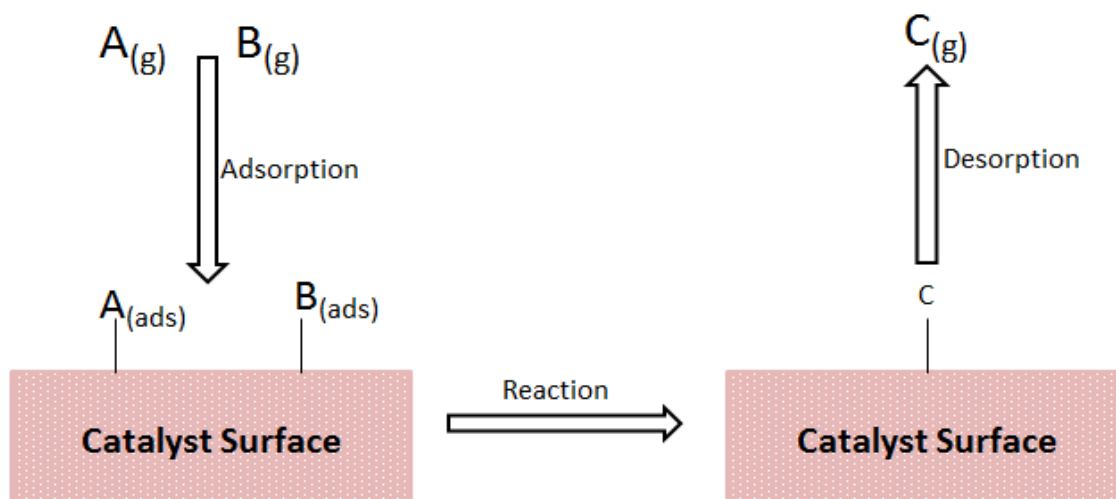
Figure 1.4 Schematic of a simplified Langmuir-Hinshelwood reaction mechanism.
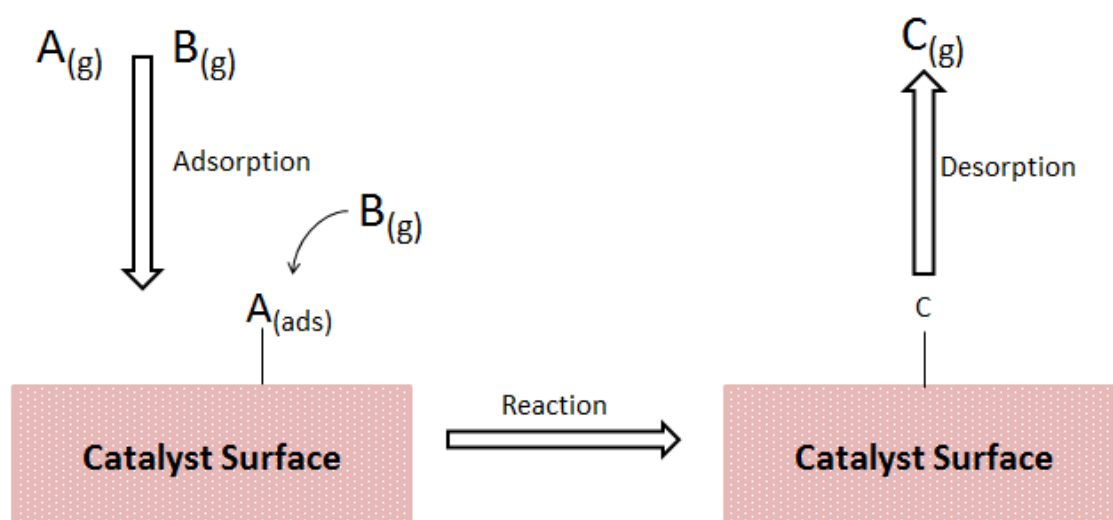
Figure 1.5 Schematic of a simplified Eley-Rideal reaction mechanism.

This work however focuses on molybdenum based mixed metal oxide catalysts, which activate the C-H bond of an alkane molecule, and through oxygen insertion at the adsorbed alkyl species catalyse oxidative dehydrogenation. The mechanism by which this occurs is called the Mars-Van Krevelen mechanism.

Lattice oxygen from the catalyst abstracts 2 hydrogen atoms from the alkane, forming water. The hydrocarbon molecule then desorbs from the catalyst surface as an alkene.
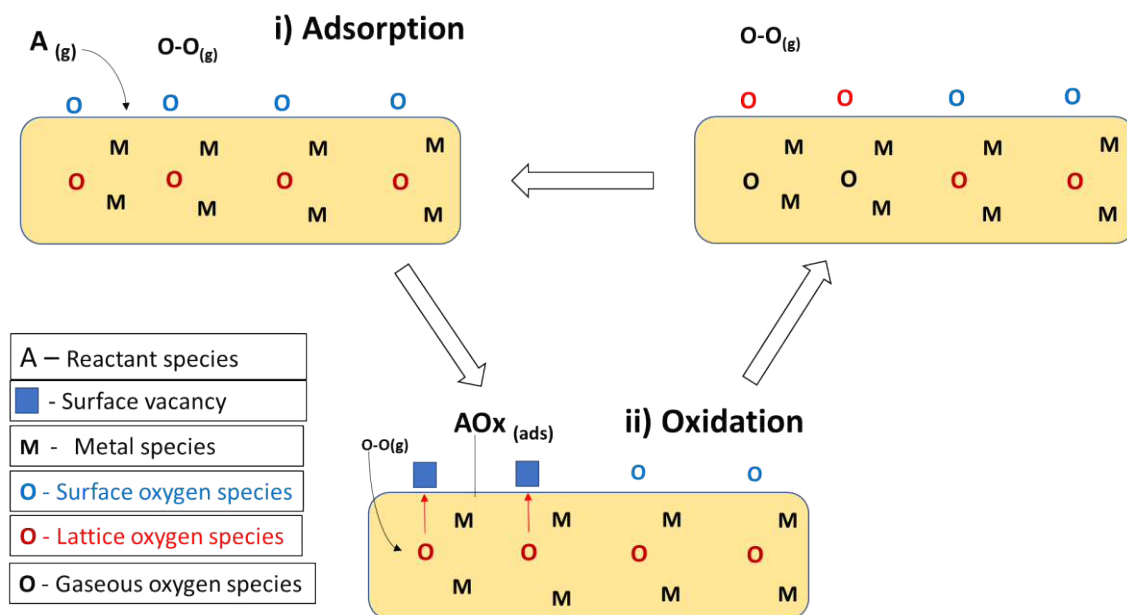
Figure 1.6 Representation of the Mars-Van Krevelen mechanism.

As a catalyst should be definition not be consumed by the reaction, the gaseous oxygen in the reaction gas feed replenishes the catalyst.

1.6 OBJECTIVES OF THIS RESEARCH.

This work examines the activity and selectivity of metal molybdate catalysts for the oxidative dehydrogenation of *n*-octane. The overall aim is to develop a catalyst capable of highly active and selective ODH of medium to long chain alkanes to mono-alkenes. This process may eventually improve on the existing Honeywell UOP PACOL process which as mentioned earlier, is very energy intensive and requires its Pt catalyst to undergo a regeneration step due to coke deposition. This thesis builds upon previous work done by research students in Cardiff Catalysis Institute.[57,58]

1.7 LITERATURE REVIEW

1.7.1 VANADIUM CATALYSTS

Vanadium oxide based catalysts have been used for the selective oxidation of methane to formaldehyde[59], the conversion of butene to 1,3-butadiene via oxidative dehydrogenation[60], and the oxidative dehydrogenation of ethane.[61]

The production of maleic anhydride from *n*-butane using vanadium phosphate catalysts has been widely studied.[62–64] This is shown in Figure 1.7. Maleic anhydride is used for the synthesis of unsaturated polymer resins (UPR), which can then be used to produce fibreglass reinforced plastics. An estimated 700,000 tonnes of maleic anhydride is produced per annum.[64]
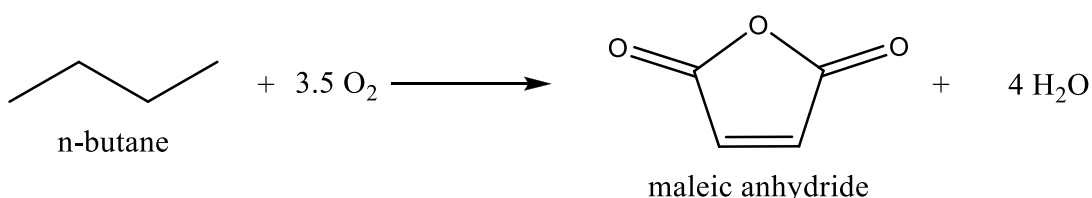
Figure 1.7 Reaction scheme of the conversion of *n*-butane to maleic anhydride.[62]

The structure of vanadium phosphates influences its catalytic activity.[65] The ratio of vanadium to phosphate, the precursor morphology and gas flow during calcination are all believed to have a factor in influencing catalytic activity and selectivity. It is believed[66] that the terminal oxygen bonded to phosphorus acts as the active centre for initiating hydrogen abstraction. Note the terminal oxygen position, a similar mechanism is suggested for molybdenum oxide catalysts (shown below). Vanadium in the +5 oxidation state is believed to be key as it offers large reduction potential. Work done by Sananes-Schulz[67] explored the ratio between V^{5+} and V^{4+} sites on VPO catalysts. Using ^{31}P NMR characterisation they could differentiate V^{4+} sites. Catalytic testing suggested the best performance came from materials which exhibited both V^{4+} cationic species and V^{4+} - V^{5+} dimers. Sananes-Schulz[67] proposed the pyrophosphate phase $(VO)_2P_2O_7$ phase where vanadium is in the +4 phase is considered catalytically inactive and thus requires the presence of V^{5+} species. Abon and Volta propose however that the $(VO)_2P_2O_7$ phase is necessary but with the presence of $VOPO_4$ which

exhibits the V^{5+} oxidation state.[68] The optimum ratio of V^{5+} to V^{4+} for the best catalytic activity, regarding the conversion of *n*-butane to maleic anhydride, has been a topic of some debate. However with related iron phosphate species it has been proposed that a ratio of Fe^{3+}/Fe^{2+} equal to two is the ratio exhibited in industrial iron phosphate catalysts.[69] When butene is used as a substrate instead of butane however it has been shown that V^{4+} is the desired oxidation state in a vanadium phosphate catalyst.[70] A recent review by Trifirò and Grasselli, when referencing the Monsanto patent on VPO catalysts, suggest that a ratio of 90% V^{4+} to 10% V^{5+} to be the optimal ratio to maximise maleic anhydride yield.[71]

Vanadium phosphate and vanadium oxide catalysts, although not used in this work, exhibit similar catalytic activity to molybdenum oxide catalysts. They have been shown to selectively oxidise and oxidatively dehydrogenate alkane species. A terminal oxygen species on the catalyst inserts into the hydrocarbon and catalyses ODH.
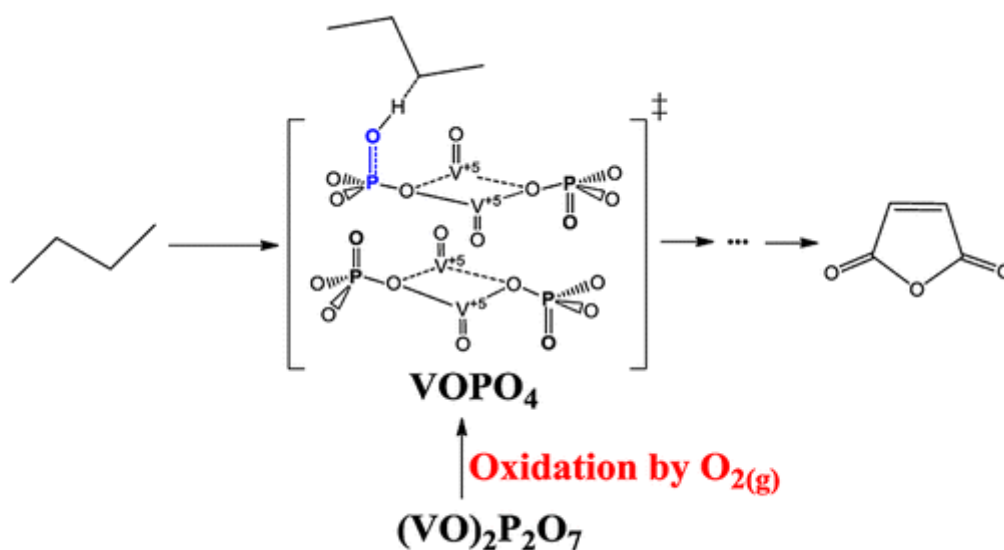
Figure 1.8 Suggested mechanism for adsorption of *n*-butane on vanadium phosphate catalyst surface. Taken from Cheng and Goddard.[66]

1.7.2 MOLYDENUM OXIDE CATALYSTS

Molydenum oxides or molybdates, have been well studied for the selective oxidation of hydrocarbons.[72] Molybdenum oxides exist in several phases, the two most common are MoO_3 where Mo is +6 oxidation state and MoO_2 where Mo is in the +4 oxidation

state. Various other lattice forms of molybdenum oxides exist, such as Mo_4O_{11} and its homologue Mo_9O_{25}.[73] In a molybdenum trioxide lattice, molybdenum atoms coordinate 6 oxygen atoms, forming MoO_6 octahedra. These are then joined by sharing edges. Molybdenum is one of the most widely studied transition metals for the activity of oxygen transfer. Over 100 oxygen transfer reactions have been characterized for molybdenum compounds.[74] These include but are not restricted to; epoxidation reactions of short-chain hydrocarbons[75], ammoxidation of alkenes to nitrile compounds[76] and as a partial oxidation catalyst.[77,78] The oxidative dehydrogenation of propane has been widely studied. Figure 1.9 shows a proposed mechanism for this.

Vedrine and Fechete have suggested that the metal site (displayed as M in Figure 1.9) for molybdenum oxide catalysis is the most likely to be an unsaturated O=Mo=O group from the MoO_3 species.[77]
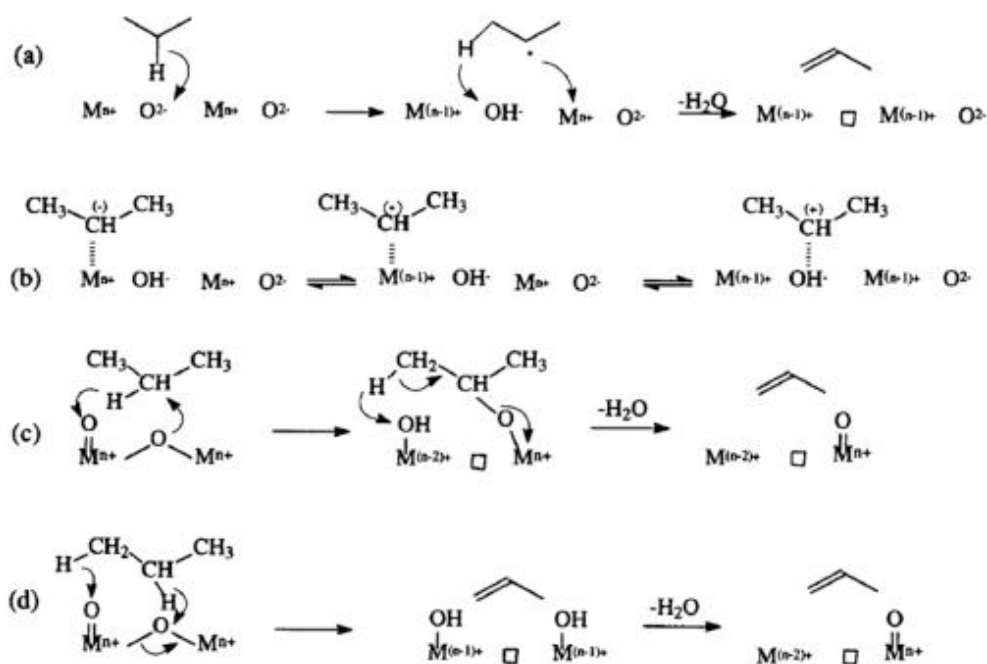
Figure 1.9 A mechanistic representation of the oxidative dehydrogenation from Centi et al.[62]

In short, molybdenum oxides when the Mo is in the +6 oxidation state take the form of MoO_3, which can be thought of as an oxidising species. When Mo is in the +4 oxidation state then molybdenum oxides take the form of MoO_2, this can be thought of as a reductive species. Which crystal face of the MoO_3 is most active is hotly debated, and

it may be that it varies from reaction to reaction. Figure 1.10 below shows the bond ordering of a MoO_3 molecule within a crystal lattice and an example of an orthorhombic crystal structure.
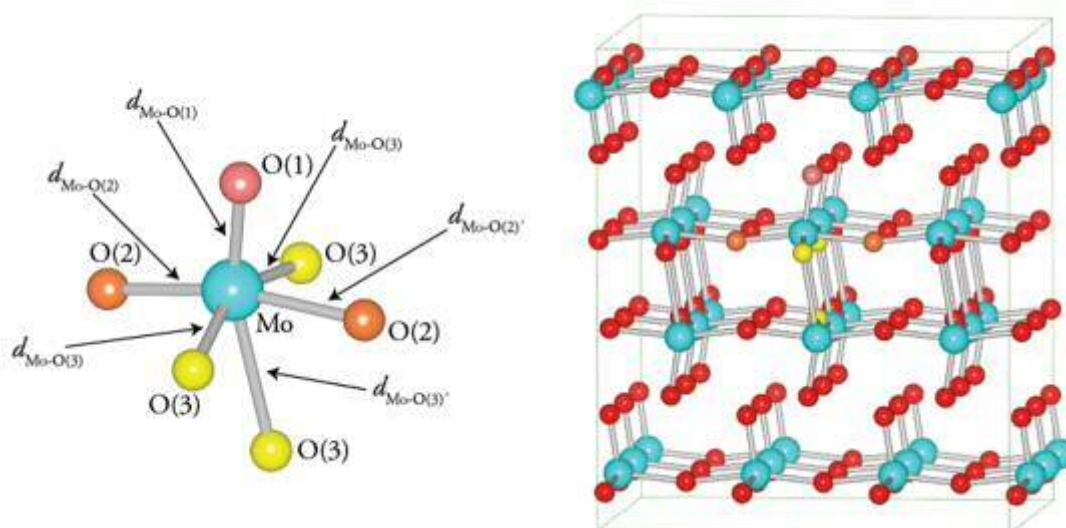
Figure 1.10 – MoO_3 distorted octahedral highlighting bond ordering (I) and the crystal structure of orthorhombic MoO_3. From Scanlon _et al_[79]

MoO_2 can be thought of as a reduced MoO_3 with the terminal oxygen removed. MoO_2 has not been as widely studied as its trioxide cousin as a catalyst, however it has been shown to be active for the partial oxidation of isooctane.[80]

"The structure of a Mo_9O_{25} structure is built up of corner-sharing distorted MO_6 octahedra in slabs of an ReO_3-type."[73] while Mo_4O_{11} can be considered a MoO_3 lattice with every 4th Mo atom losing its terminal oxygen. Mo_4O_{11} and Mo_9O_{25} are not widely reported on as catalysts in the available literature, although Delmon[81] suggested that Mo_4O_{11} was a species worthy of further investigation.

The nature of the oxygen species involved in reactions at the catalyst surface is also important. There is general agreement in the literature for alkene oxidative dehydrogenation, that electrophilic oxygen species are associated with non-selective total oxidation, thus forming carbon oxides. While nucleophilic oxygen species are believed to undergo either selective insertion in partial oxidation reactions, or hydrogen

abstraction in oxidative dehydrogenation.[82] Centi, Trifirò and Cavani have suggested that the different oxygen species can be thought of as; gaseous oxygen fed into a reactor exhibiting electrophilic character and structural oxygen from a metal oxide (such as MoO_3) possessing nucleophilic character. The authors stress that this is a simplified framework which does not take into account issues such as kinetics, the oxygen replenishment of metal oxides and the uniqueness of certain catalytic systems. In particular they state that a model which suggests that only lattice oxygen undergoes selective oxidation/oxidative dehydrogenation is a generalisation which ignores the complex catalytic chemistry occurring at a metal oxide surface.[82]

Numerous mixed metal molybdates; magnesium,[83,84] mnaganese,[85,86] vanadium[87] and bismuth[88–90] have been tested, usually as selective oxidation or ODH catalysts. However this work will focus mainly on iron, nickel and cobalt molybdates

Bismuth molybdate in particular has been an extensively studied catalytic system. Early reporting goes back to the middle of the twentieth century, with reports in 1964 of bismuth molybdate being a catalyst for the selective oxidation of butene and propene.[91]

Bismuth molybdate has also shown to be an active catalyst in the partial oxidation of propane to acrolein.[92] The reaction is thought to proceed via a hydrogen abstraction over via an allyl oxidation mechanism involving molybdenum trioxide, before acrolein desorbs from a weakened MoO_2 site.

Bismuth molybdate can manifest in several different phases.[93] α-$Bi_2Mo_3O_{12}$ β-$Bi_2Mo_2O_9$ and γ-Bi_2MoO_6 are all phases that can be present. It has been suggested[93] that a synergistic relationship exists between the phases. There is some debate in the literature over which phase is most integral, however due to its superior lattice oxygen mobility (key in a Mars-Van Krevelen reaction) γ-Bi_2MoO_6 may be the most important.[94]
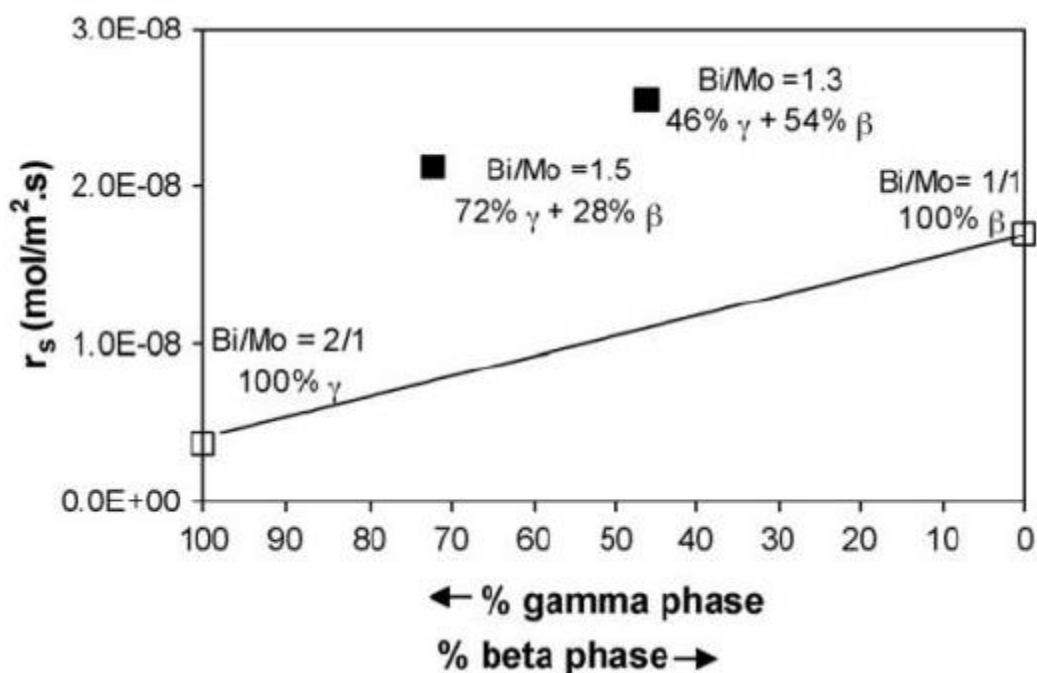
Figure 1.11 Chart showing the catalytic activity (reaction rate) for the conversion of propane to acrolein at 425 °C using gamma and beta phase bismuth molybdates. From Thang *et al*[93]

1.7.3 NICKEL MOLYBDATE CATALYSTS

Nickel molybdate has been a widely studied catalyst for oxidative dehydrogenation of alkanes, chiefly propane.[41,95] It exists in the form of $NiMoO_4$ with Ni in a +2 oxidation state. There are two forms, a low temperature α phase and a high temperature, metastable β phase.[96,97] The β phase only forms at temperatures above 600 °C.[96] Kaddouri *et al* used a sol-gel type synthesis to stabilise the β-phase at room temperature. This is because the β-phase exhibits considerably greater selectivity to propene than the α $NiMoO_4$ when used as a catalyst for propane ODH.[98]

Nickel molybdate is believed to convert propane to propene via a Mars-Van Krevelen type mechanism.[97] This is because the reaction of propane with a supply of oxygen over a $NiMoO_4$ catalyst is first order with respect to propane and zero order to oxygen.[41,99] This is consistent with the Mars-Van Krevelen mechanism.[53]

Work done by Madeira *et al*[100] on the ODH of *n*-butane over stoichiometric nickel molybdate (so $NiMoO_4$) showed stark differences in selectivity to butenes. α-$NiMoO_4$ exhibited over a 50% selectivity to carbon oxides with a total selectivity to butene and butadiene of 41%. β-$NiMoO_4$ however showed high selectivity (81%) to butene and butadienes from *n*-butane.

The main difference between α and β phase nickel molybdate is the conformation of the coordination of the MoO_6^+ ions in the bulk lattice. In the α-phase they are octahedral. This then shifts to a tetrahedral coordination when a phase transition occurs and the β is adopted.[101] In both isomorphs the Ni 2+ occupies an octahedral coordination.

Ozkan in his PhD thesis, showed that nickel molybdate catalysts with an excess of MoO_3 showed much higher selectivity to maleic anhydride from *n*-butane than when stoichiometric $NiMoO_4$ or pure MoO_3 was used. This indicates that for certain ODH reactions a molybdenum excess in a nickel molybdate catalyst is desirable.

$NiMoO_4$ has also been recently shown to catalytically perform ODH on *n*-hexane.[46] It was shown that the β was more active than the α phase. Interestingly a major product of this reaction was benzene. It was hypothesised that *n*-hexane underwent 1,6 ring closure to cyclohexane before aromatisation.
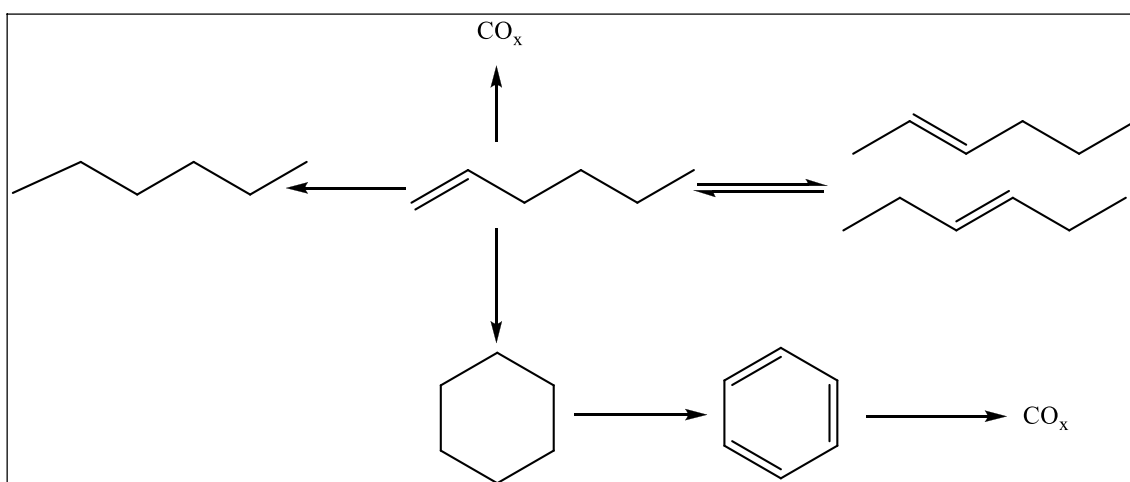
Figure 1.12 – Reaction scheme of the formation of benzene from n-hexane over a NiMoO₄ catalyst[46]

1.7.4 COBALT MOLYBDATE CATALYSTS

Cobalt molybdate catalysts possess the formula $CoMoO_4$. It shares many similar properties with $NiMoO_4$.[102] It too possesses an α and a β phase.[103] The α phase is present at room temperature and phase transitions to the meta-stable β phase at 550°C and above.

α-$CoMoO_4$ possesses Co^{2+} ions and Mo^{6+} in the octahedral conformation, while the β phase sees the molybdena shift to the tetrahedral conformation.[103] β-$CoMoO_4$ has been reported as the more active phase for catalytic ODH.
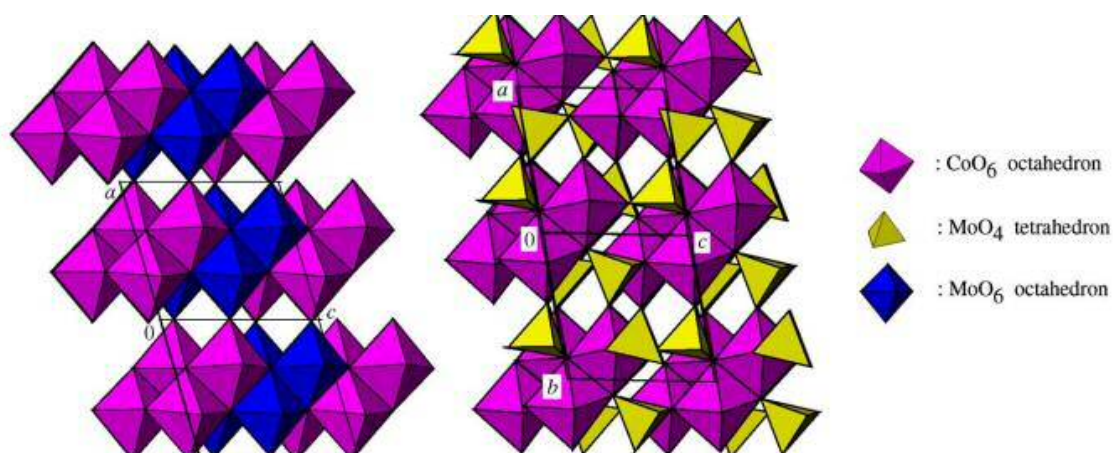
Figure 1.13 Illustration showing the conformation of α-CoMoO₄ (l) and β-CoMoO₄ (r). From Eda *et al*[103]

Cobalt nano-rods have been shown to be synthesised.[104] However as of yet no reports in the literature have suggested that nano-rod $CoMoO_4$ possesses significantly higher surface area or different catalytic activity.

Cobalt molybdate has been shown to be an active catalyst for the ODH of short chain alkanes, mainly *n*-butane and propane.[7,105,106] Cobalt molybdate has also been used as a catalyst for the selective oxidation of isobutene to methacrolein.[107] $CoMoO_4$ is also believed to perform catalytic ODH via a Mars-Van Krevelen mechanism.[99]

Cobalt molybdate with a slight molybdenum excess has been shown to be a more active and selective catalyst to maleic anhydride from 1-butene than pure phase $CoMoO_4$.[102]

Stoichiometric cobalt molybdate has also been tested for the ODH of *n*-octane.[47] The dominant products produced were C_8 aromatics (ethylbenzene, xylene and styrene). Increasing oxygen partial pressure in the gas feed led to higher selectivity to carbon oxides. Higher temperatures also produced higher levels of carbon oxide and aromatic species.

1.7.5 IRON MOLYBDATE CATALYSTS

Iron molybdate has been widely used as a catalyst.[108–110] It has two forms, ferrous molybdate, $Fe_2(MoO_4)_3$ which has been widely reported on as a catalyst for the selective oxidation of methanol to formaldehyde,[111,112] ferric molybdate possesses iron in the +3 oxidation state. The second form, ferrous molybdate, $FeMoO_4$ shows iron in the +2 oxidation state.[113] Ferric molybdate by its formula has a 3:2 molybdenum to iron ratio, while ferrous molybdate is a 1:1 ratio. Molybdenum is in the +6 oxidation state for both forms.

Iron molybdate was first reported by Adkins and Peterson in 1931.[114] It has since become the industrial standard catalyst for the production of formaldehyde from methanol. Industrial catalysts have an excess of molybdenum to iron, greater than 1.5:1 molybdenum to iron.[112]

There is some debate about whether ferric molybdate catalysts require an excess of molybdenum in the form of MoO_3.[115,116] Literature suggests there is a synergistic effect between MoO_3 and $Fe_2(MoO_4)_3$.[115]
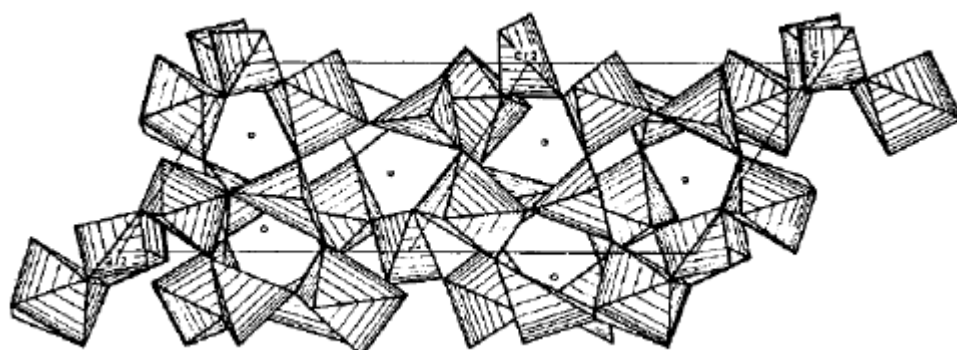
O - *possible positions of the interstitial oxygen ions.*

Figure 1.14 – Possible lattice structure and interstitial oxygen positions in an

Fe$_2$(Mo$_4$)$_3$ catalyst. From Soares *et al.*[112]

Ferric molybdate consists of Fe octahedra and Mo tetrahedral sites.[117] This is very different to ferrous molybdate which possesses Fe in tetrahedral positions and Mo as octahedra.

The industrial process of selective oxidation of methanol to formaldehyde has been widely reported on. Air or an oxygen rich gas flow is flowed over a ferric molybdate catalyst. Temperatures do not exceed 400 °C this is to stop side reactions, industrial catalysts can achieve *ca*.100% and *ca.* 96% selectivity to formaldehyde.[112] The reactions that iron molybdate catalyses are shown below:

$$H_3C\text{-}OH + \tfrac{1}{2} O_2 \rightarrow H_2CO + H_2O \quad \Delta H = -159 \text{ kJmol}^{-1} \text{ (1)}$$

$$H_3C\text{-}OH + \tfrac{1}{2} O_2 \rightarrow CO_2 + 2H_2O \quad \Delta H = -674 \text{ kJmol}^{-1} \text{ (2)}$$
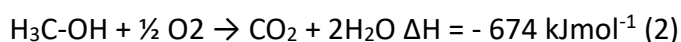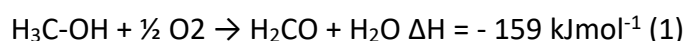
Bowker *et al* [118–120] have conducted novel work using mixed iron and molybdenum oxides instead of iron molybdates. This was of interest to observe synergistic effects between iron and molybdenum. Molybdenum trioxide in synergy with hematite produced a very active and selective catalyst for the conversion of methanol to formaldehyde. Iron molybdates and the above system were found to exhibit greater catalytic activity than molybdenum oxides. However hematite or another iron oxide on its own is considered a poor catalyst as it combusts methanol to formaldehyde. Bowker's work found that it is stoichiometric iron molybdate that is the active phase.

MoO_3 however is believed to be needed to be in excess to prevent the formation of isolated iron clusters at the surface preventing combustion.[112,115,121]

Methanol oxidation over the iron molybdate catalyst is believed to occur via a Mars-Van Krevelen type mechanism using oxygen insertion. There is a redox reaction that has been reported to occur with the ferric molybdate phase to ferrous molybdate.[112]

$$CH_3OH + Fe_2(MoO_4)_3 \rightarrow H_2CO + H_2O + (\beta\text{-}FeMoO_4) + MoO_3 \textbf{ Reduction}$$

$$2(\beta\text{-}FeMoO_4) + MoO_3 + \tfrac{1}{2} O_2 \rightarrow Fe_2(MoO_4)_3 \textbf{ Oxidation}$$
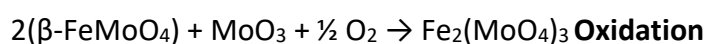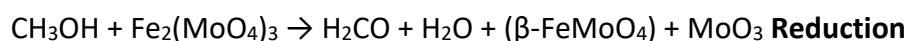
Ferrous molybdate has been shown to possess profoundly different catalytic selectivity to the ferric form for the ODH of n-decane in work done by Hutchings et al.[57]
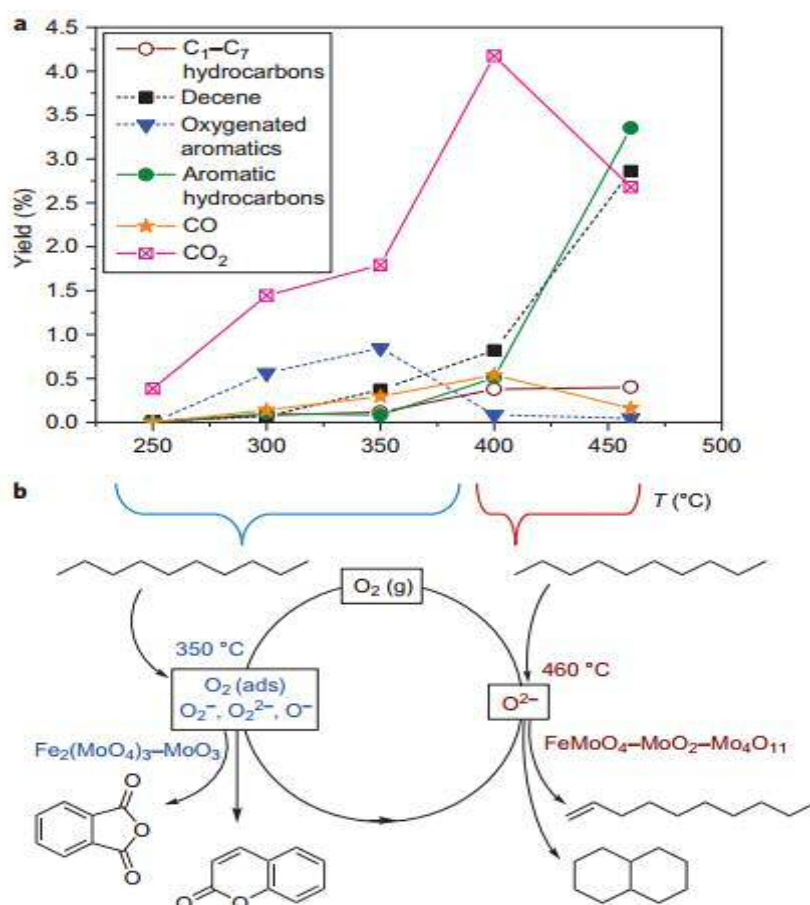
Figure 1.15 Reaction scheme of n-decane over an iron molybdate catalyst and its relation to temperature from Pradhan et al[57]

The group found that ferric molybdate inserts oxygen into *n*-decane at lower temperatures, creating aromatic oxygenate species as products. However at higher temperatures the catalyst system shifts to a ferrous molybdate species which produces linear alkenes. This is of interest and helped build the foundation this thesis is built on.

1.8 CONCLUSIONS

The literature shows that molybdates have been used extensively for the oxidative dehydrogenation of alkanes. Dehydrogenation of alkane to alkenes possesses several drawbacks and the favourable thermodynamics of ODH catalysts suggests they may one day supplant platinum catalysts used for industrial processes such as the PACOL process.

Iron molybdate was one of the first molybdates investigated for selective oxidation reactions, specifically methanol to formaldehyde. Various other molybdate species such as cobalt, nickel and bismuth have been shown to selectively oxidise hydrocarbons. They also perform ODH on short chain alkanes via a Mars-Van Krevelen mechanism. It is perhaps fitting perhaps, that recent work by this group[57] has demonstrated iron molybdate, could now be used for ODH of medium chain alkanes, once again being at the forefront of the molybdate family.

1.9 THESIS OVERVIEW

This work examines the oxidative dehydrogenation of *n*-octane to octenes and steps to maximise octene production. In addition the effect on catalytic activity and product selectivity of altering the reaction conditions, temperature, carbon to oxygen ratio, gas hourly space velocity are all examined.

Chapter one is an introduction of the area and also has a literature review of the class of catalysts used in this work. In particular oxidative dehydrogenation (ODH) and molybdates are examined.

Chapter two contains experimental details, including catalyst synthesis and preparation, analytical techniques used and reactor details. Each analytical technique is discussed in some detail and reactor schematics are included for ease of replication of work.

Chapter three examines the difference in catalytic activity and selectivity between ferrous and ferric molybdate for the oxidative dehydrogenation of *n*-octane to octenes. Variables such as gas hourly velocity, temperature and carbon to oxygen are examined here. In addition scaling up the process from 1% *n*-octane in the gas feed to 10% is tested. Also investigated is the effect of pure phase molybdenum oxides and stoichiometric iron molybdate have as catalysts. This was done to indicate the role of each species. Finally the effect of undergoing reaction is investigated in relation to the catalyst structure.

Chapter four looks at the effect of time on line studies to demonstrate catalyst stability over a range of varying temperatures over time. Oct-1-ene is then placed as a feedstock in place of *n*-octane to elucidate the mechanism by which aromatic species are formed as products, The chapter then moves onto the effect of oxygen deprivation on the catalyst, followed by reoxidation studies to observe the effect on the catalyst of *in-situ* reduction. This also gives a valuable insight into the mechanism by which the catalyst proceeds.

Chapter 5 is concerned with the comparison of nickel molybdate and cobalt molybdate with iron molybdate. Cobalt and nickel molybdates have been extensively reported in the literature as ODH catalysts for short chain alkanes. Thus it was of interest to observe their activity and selectivity as catalysts for *n*-octane ODH.

Chapter 6 is a conclusions chapter which briefly looks at findings and gives some ideas and thoughts on future work.

Bibliography

1   Wiley, http://eu.wiley.com/WileyCDA/WileyTitle/productCd-3527321209.html, (accessed 17 September 2016).
2   G. K. Boreskov, *Heterogeneous Catalysis*, Nova Publishers, 2003.
3   J. R. H. Ross, *Heterogeneous Catalysis: Fundamentals and Applications*, Elsevier, 2012.
4   Wiley, http://eu.wiley.com/WileyCDA/WileyTitle/productCd-3527335838,subjectCd-CH86.html, (accessed 17 September 2016).
5   W. W. Christie, *J. Lipid Res.*, 1982, **23**, 1072–1075.
6   A. Behr and P. Neubert, *Applied Homogeneous Catalysis*, Wiley-VCH, Weinheim, 1 edition., 2012.
7   J.-F. L. Page, *Applied Heterogeneous Catalysis: Design, Manufacture, Use of Solid Catalysts*, Editions Technip, Paris, 1987.

8   L. M. (Lars) van der Zande, E. A. (Bart) de Graaf and G. Rothenberg, *Adv. Synth. Catal.*, 2002, **344**, 884–889.

9   V. Smil, *Enriching the Earth: Fritz Haber, Carl Bosch, and the Transformation of World Food Production*, MIT Press, Cambridge, Mass., New Ed edition., 2004.

10   P. Serp and K. Philippot, *Nanomaterials in Catalysis*, John Wiley & Sons, 2012.

11   Y. Nitta, O. Suwata, Y. Ikeda, Y. Okamoto and T. Imanaka, *Catal. Lett.*, **26**, 345–354.

12   G. Boskovic, N. Dropka, D. Wolf, A. Brückner and M. Baerns, *J. Catal.*, 2004, **226**, 334–342.

13   E. Iglesia, *Appl. Catal. Gen.*, 1997, **161**, 59–78.

14   M. Carta, M. Croad, K. Bugler, K. J. Msayib and N. B. McKeown, *Polym. Chem.*, 2014, **5**, 5262–5266.

15   G. C. Bond and P. B. Wells, *Appl. Catal.*, 1985, **18**, 225–230.

16   K. Shimizu, H. Kawachi and A. Satsuma, *Appl. Catal. B Environ.*, 2010, **96**, 169–175.

17   M. Alhumaimess, Z. Lin, W. Weng, N. Dimitratos, N. F. Dummer, S. H. Taylor, J. K. Bartley, C. J. Kiely and G. J. Hutchings, *ChemSusChem*, 2012, **5**, 125–131.

18   C. T. Campbell, *Nat. Chem.*, 2012, **4**, 597–598.

19   I. E. Wachs, *Catal. Today*, 2005, **100**, 79–94.

20   M. Conte, G. Budroni, J. K. Bartley, S. H. Taylor, A. F. Carley, A. Schmidt, D. M. Murphy, F. Girgsdies, T. Ressler, R. Schlögl and G. J. Hutchings, *Science*, 2006, **313**, 1270–1273.

21   ETHYLENE TECHNOLOGIES-1: Novel ethylene technologies developing, but steam cracking remains king - Oil & Gas Journal, http://www.ogj.com/articles/print/volume-95/issue-25/in-this-issue/petrochemicals/ethylene-technologies-1-novel-ethylene-technologies-developing-but-steam-cracking-remains-king.html, (accessed 17 September 2016).

22   J. H. Gary, G. E. Handwerk, M. J. Kaiser and A. de Klerk, *Petroleum Refining: Technology and Economics, Fifth Edition*, CRC Press, 2007.

23   Y. Wei, D. Zhang, Z. Liu and B.-L. Su, *J. Catal.*, 2006, **238**, 46–57.

24   O. Bortnovsky, P. Sazama and B. Wichterlova, *Appl. Catal. Gen.*, 2005, **287**, 203–213.

25   C. N. (Massachusetts I. of T. Satterfield, .

26   P. B. Venuto and E. T. J. Habib, .

27   L. Zhang, H. Liu, X. Li, S. Xie, Y. Wang, W. Xin, S. Liu and L. Xu, *Fuel Process. Technol.*, 2010, **91**, 449–455.

28   R. B. Kasat and S. K. Gupta, *Comput. Chem. Eng.*, 2003, **27**, 1785–1800.

29   B. M. Weckhuysen and R. A. Schoonheydt, *Catal. Today*, 1999, **51**, 223–232.

30   B. M. Weckhuysen, I. E. Wachs and R. A. Schoonheydt, *Chem. Rev.*, 1996, **96**, 3327–3350.

31   C. P. Poole Jr. and D. S. MacIver, in *Advances in Catalysis*, ed. H. P. and P. B. W. D.D. Eley, Academic Press, 1967, vol. 17, p. 223–314.

32   J. J. Spivey and R. S. of Chemistry, *Catalysis*, Royal Society of Chemistry, 1994.

33   Oleflex™ Process Helping Meet Growing Demand for Key Petrochemicals in China | Honeywell UOP, https://www.uop.com/oleflex-process-helping-meet-growing-demand-for-key-petrochemicals-in-china/, (accessed 18 September 2016).

34   WO2013089859 A1, 2013. "Hydrocarbon dehydrogenation with inert diluent"L. Leonard, A.G. Bozzano, G.P.Towler

35   R. A. Meyers, *Handbook of Petroleum Refining Processes*, McGraw-Hill Education, New York, 3 edition., 2003.

36   US3254966 A, 1966."Means for effecting catalytic conversion of exhaust streams" Patent. H. Bloch, H. Vladimir

37   R. K. Grasselli, D. L. Stern and J. G. Tsikoyiannis, *Appl. Catal. Gen.*, 1999, **189**, 1–8.

38   B. V. Vora, *Top. Catal.*, 2012, **55**, 1297–1308.

39   S. K. Masoudian, S. Sadighi, A. Abbasi, F. Salehirad and A. Fazlollahi, *Chem. Eng. Technol.*, 2013, **36**, 1593–1598.

40   Oxidative Dehydrogenation of Alkanes - Handbook of Heterogeneous Catalysis - Håkonsen - Wiley Online Library,

http://onlinelibrary.wiley.com/doi/10.1002/9783527610044.hetcat0171/abstract, (accessed 18 September 2016).

41 D. L. Stern and R. K. Grasselli, *J. Catal.*, 1997, **167**, 560–569.

42 M. I. Fadlalla and H. B. Friedrich, *Catal. Sci. Technol.*, 2014, **4**, 4378–4385.

43 D. Y. Jang, H. G. Jang, G. R. Kim and G.-J. Kim, *Res. Chem. Intermed.*, 2011, **37**, 1145.

44 F. Cavani, N. Ballarini and A. Cericola, *Catal. Today*, 2007, **127**, 113–131.

45 M. Zboray, A. T. Bell and E. Iglesia, *J. Phys. Chem. C*, 2009, **113**, 12380–12386.

46 B. Pillay, M. R. Mathebula and H. B. Friedrich, *Appl. Catal. Gen.*, 2009, **361**, 57–64.

47 M. I. Fadlalla and H. B. Friedrich, *Catal. Sci. Technol.*, 2014, **4**, 4378–4385.

48 H. B. Friedrich and A. S. Mahomed, *Appl. Catal. Gen.*, 2008, **347**, 11–22.

49 V. D. B. C. Dasireddy, H. B. Friedrich and S. Singh, *South Afr. J. Chem.*, 2015, **68**, 195–200.

50 M. M. Barsan and F. C. Thyrion, *Catal. Today*, 2003, **81**, 159–170.

51 L. Lisi, G. Ruoppolo, M. P. Casaletto, P. Galli, M. A. Massucci, P. Patrono and F. Pinzari, *J. Mol. Catal. Chem.*, 2005, **232**, 127–134.

52 S. Arias-Pérez, R. García-Alamilla, M. G. Cárdenas-Galindo, B. E. Handy, S. Robles-Andrade and G. Sandoval-Robles, *Ind. Eng. Chem. Res.*, 2009, **48**, 1215–1219.

53 C. Doornkamp and V. Ponec, *J. Mol. Catal. Chem.*, 2000, **162**, 19–32.

54 T. Fransen, P. C. Berge and P. Mars, *React. Kinet. Catal. Lett.*, 1976, **5**, 445–452.

55 G. W. Roberts and C. N. Satterfield, *Ind. Eng. Chem. Fundam.*, 1965, **4**, 288–293.

56 C. T. Rettner, *J. Chem. Phys.*, 1994, **101**, 1529–1546.

57 S. Pradhan, J. K. Bartley, D. Bethell, A. F. Carley, M. Conte, S. Golunski, M. P. House, R. L. Jenkins, R. Lloyd and G. J. Hutchings, *Nat. Chem.*, 2012, **4**, 134–139.

58 B.R Yeo, 2014. PhD thesis, Cardiff University.

59 L. D. Nguyen, S. Loridant, H. Launay, A. Pigamo, J. L. Dubois and J. M. M. Millet, *J. Catal.*, 2006, **237**, 38–48.

60 C. Wan, D. Cheng, F. Chen and X. Zhan, *RSC Adv.*, 2015, **5**, 42609–42615.

61 M. D. Argyle, K. Chen, A. T. Bell and E. Iglesia, *J. Phys. Chem. B*, 2002, **106**, 5421–5427.

62 G. Centi, F. Trifiro, J. R. Ebner and V. M. Franchetti, *Chem. Rev.*, 1988, **88**, 55–80.

63 R. M. Contractor, H. E. Bergna, H. S. Horowitz, C. M. Blackstone, B. Malone, C. C. Torardi, B. Griffiths, U. Chowdhry and A. W. Sleight, *Catal. Today*, 1987, **1**, 49–58.

64 B. K. Hodnett, *Catal. Rev.*, 1985, **27**, 373–424.

65 S. Sajip, J. K. Bartley, A. Burrows, M.-T. Sananés-Schulz, A. Tuel, J. C. Volta, C. J. Kiely and G. J. Hutchings, *New J. Chem.*, 2001, **25**, 125–130.

66 M.-J. Cheng and W. A. Goddard, *J. Am. Chem. Soc.*, 2013, **135**, 4600–4603.

67 M. T. Sananes-Schulz, A. Tuel, G. J. Hutchings and J. C. Volta, *J. Catal.*, 1997, **166**, 388–392.

68 M. Abon and J.-C. Volta, *Appl. Catal. Gen.*, 1997, **157**, 173–193.

69 J. C. Vedrine, J. M. M. Millet and J. C. Volta, *Faraday Discuss. Chem. Soc.*, 1989, **87**, 207–213.

70 S. Morrison, *The Chemical Physics of Surfaces*, Springer Science & Business Media, 2012.

71 F. Trifirò and R. K. Grasselli, *Top. Catal.*, 2014, **57**, 1188–1195.

72 K. V. R. Chary, K. R. Reddy, G. Kishan, J. W. Niemantsverdriet and G. Mestl, *J. Catal.*, 2004, **226**, 283–291.

73 O. G. D'Yachenko, V. V. Tabachenko and M. Sundberg, *J. Solid State Chem.*, 1995, **119**, 8–12.

74 R. H. Holm, *Chem. Rev.*, 1987, **87**, 1401–1449.

75 J. M. Mitchell and N. S. Finney, *J. Am. Chem. Soc.*, 2001, **123**, 862–869.

76 R. K. Grasselli, *Catal. Today*, 2005, **99**, 23–31.

77 J. C. Védrine and I. Fechete, *Comptes Rendus Chim.*, 2016, **19**, 1203–1225.

78 C. J. Cassady and S. W. McElvany, *Organometallics*, 1992, **11**, 2367–2377.

79 D. O. Scanlon, G. W. Watson, D. J. Payne, G. R. Atkinson, R. G. Egdell and D. S. L. Law, *J. Phys. Chem. C*, 2010, **114**, 4636–4645.

80 O. G. Marin Flores and S. Ha, *Appl. Catal. Gen.*, 2009, **352**, 124–132.

81 P. Ruiz and B. Delmon, *New Developments in Selective Oxidation by Heterogeneous Catalysis*, Elsevier, 1992.

82 G. Centi, F. Cavani and F. Trifirò, *Selective Oxidation by Heterogeneous Catalysis*, Springer Science & Business Media, 2012. 400-406

83 Y. S. Yoon, W. Ueda and Y. Moro-oka, *Catal. Lett.*, 1995, **35**, 57–64.

84 Y. S. Yoon, K. Suzuki, T. Hayakawa, S. Hamakawa, T. Shishido and K. Takehira, *Catal. Lett.*, **59**, 165–172.

85 Y. A. Agafonov, N. V. Nekrasov, N. A. Gaidai, M. A. Botavina, P. E. Davydov and A. L. Lapidus, *Kinet. Catal.*, 2009, **50**, 577–582.

86 U. Ozkan, R. C. Gill and M. R. Smith, *J. Catal.*, 1989, **116**, 171–183.

87 T. V. Andrushkevich, L. M. Plyasova, G. G. Kuznetsova, V. M. Bondareva, T. P. Gorshkova, I. P. Olenkova and N. I. Lebedeva, *React. Kinet. Catal. Lett.*, **12**, 463–467.

88 J.-H. Park, H. Noh, J. W. Park, K. Row, K. D. Jung and C.-H. Shin, *Appl. Catal. Gen.*, 2012, **431**–**432**, 137–143.

89 J. C. Jung, H. Lee, J. G. Seo, S. Park, Y.-M. Chung, T. J. Kim, S. J. Lee, S.-H. Oh, Y. S. Kim and I. K. Song, *Catal. Today*, 2009, **141**, 325–329.

90 J. L. Callahan, R. K. Grasselli, E. C. Milberger and H. A. Strecker, *Prod. RD*, 1970, **9**, 134–142.

91 C. R. Adams, H. H. Voge, C. Z. Morgan and W. E. Armstrong, *J. Catal.*, 1964, **3**, 379–386.

92 S. Pudar, J. Oxgaard, K. Chenoweth, A. C. T. van Duin and W. A. Goddard, *J. Phys. Chem. C*, 2007, **111**, 16405–16415.

93 L. Thang, L. Bac, I. Van Driessche, S. Hoste and W. Van Well, *Catal. Today,* 2008, **131**, 566–571.

94 R. K. Grasselli, *Appl. Catal.*, 1985, **15**, 127–139.

95 N. Fujikawa, K. Wakui, K. Tomita, N. Ooue and W. Ueda, *Catal. Today*, 2001, **71**, 83–88.

96 A. Kaddouri, E. Tempesti and C. Mazzocchia, *Mater. Res. Bull.*, 2004, **39**, 695–706.

97 L. M. Madeira, M. F. Portela and C. Mazzocchia, *Catal. Rev.*, 2004, **46**, 53–110.

98 C. Mazzocchia, C. Aboumrad, C. Diagne, E. Tempesti, J. M. Herrmann and G. Thomas, *Catal. Lett.*, **10**, 181–191.

99 D. L. Stern and R. K. Grasselli, *J. Catal.*, 1997, **167**, 550–559.

100 L. M. Madeira, R. M. Martín-Aranda, F. J. Maldonado-Hódar, J. L. G. Fierro and M. F. Portela, *J. Catal.*, 1997, **169**, 469–479.

101 J. A. Rodriguez, S. Chaturvedi, J. C. Hanson, A. Albornoz and J. L. Brito, *J. Phys. Chem. B*, 1998, **102**, 1347–1355.

102 U. Ozkan and G. L. Schrader, *Appl. Catal.*, 1986, **23**, 327–338.

103 K. Eda, Y. Uno, N. Nagai, N. Sotani and M. Stanley Whittingham, *J. Solid State Chem.*, 2005, **178**, 2791–2797.

104 T. Kong, Z. Liu, Y. Song, L. Wang and H. C. Shum, *Soft Matter*, 2013, **9**, 9780–9784.

105 Y. S. Yoon, W. Ueda and Y. Moro-oka, *Top. Catal.*, 1996, **3**, 265–275.

106 T. C. Bissot and K. A. Benson, *IEC Prod. Res. Dev.*, 1963, **2**, 57–60.

107 S. R. G. Carrazán, C. Martín, V. Rives and R. Vidal, *Appl. Catal. Gen.*, 1996, **135**, 95–123.

108 V. S. Ana Paula, *Chem. Eng. Sci.*, 2003, **58**, 1315–1322.

109 W.-H. Cheng, *J. Catal.*, 1996, **158**, 477–485.

110 Abaulina, L.I., Kustova, G.N., Klevtsova, R.F., Popov, B.I., Bibin, V.N., Melekhina, V.A., Kolomiichuk, V.N., Boreskov, G.K., *Kinet Catal Engl Transl*, 1976, **17**, 1126.

111 G. Jin, W. Weng, Z. Lin, N. F. Dummer, S. H. Taylor, C. J. Kiely, J. K. Bartley and G. J. Hutchings, *J. Catal.*, 2012, **296**, 55–64.

112 A. P. V. Soares, M. F. Portela and A. Kiennemann, *Catal. Rev.*, 2005, **47**, 125–174.

113 L. Wu, L. Wu, W. Yang and A. I. Frenkel, *Catal. Sci. Technol.*, 2014, **4**, 2512–2519.

114 P. Adkins, H.; W. R., *J Am Chem Soc*, 1931, **53**, 1512.

115 K. Routray, W. Zhou, C. J. Kiely, W. Grünert and I. E. Wachs, *J. Catal.*, 2010, **275**, 84–98.

116 I. E. Wachs and K. Routray, *ACS Catal.*, 2012, **2**, 1235–1246.

117 L. M. Plyasova, *J. Struct. Chem.*, **17**, 637–640.

118 S. Chapman, C. Brookes, M. Bowker, E. K. Gibson and P. P. Wells, *Faraday Discuss.*, 2016, **188**, 115–129.

119 M. Bowker, R. Holroyd, M. House, R. Bracey, C. Bamroongwongdee, M. Shannon and A. Carley, *Top. Catal.*, 2008, **48**, 158–165.

120 C. Brookes, P. P. Wells, N. Dimitratos, W. Jones, E. K. Gibson, D. J. Morgan, G. Cibin, C. Nicklin, D. Mora-Fonz, D. O. Scanlon, C. R. A. Catlow and M. Bowker, *J. Phys. Chem. C*, 2014, **118**, 26155–26161.

121 A. P. Soares, M. Farinha Portela, A. Kiennemann, L. Hilaire and J. M. . Millet, *Appl. Catal. Gen.*, 2001, **206**, 221–229.

2

CHAPTER 2 – CATALYST PREPARATION, EXPERIMENTAL METHODS AND THEORY

2.1 INTRODUCTION

Catalyst preparation and synthesis, catalytic testing and characterisation techniques used will be discussed in this chapter. The analytical techniques of X-ray diffraction (XRD), Raman spectroscopy, thermogravimetric analysis (TGA), multi plasma atomic emission spectroscopy (MP-AES), X-ray photoelectron spectroscopy (XPS), surface area analysis and energy dispersive x-ray spectroscopy (EDX) are examined.

2.2 CATALYST PREPARATION

Pre-reduced iron molybdate catalyst

Iron chloride hexahydrate (2.70 g, $FeCl_3 \cdot 6H_2O$, 98% purity sigma-aldrich) was dissolved in 100 cm^3 of water under stirring. In a separate vessel ammonium heptamolybdate (3.53 g, $H_{24}Mo_7N_6O_{24}$, >99%purity sigma-aldrich) was dissolved in 100 cm^3 of water under stirring. The pH of the ammonium heptamolybdate solution was lowered to 2.25 through the drop-wise addition of conc. hydrochloric acid. The solution was then added dropwise to the iron hexahydrate solution. This resulted in a solution with a 2.7:1 molybdenum to iron ratio. After allowing the resulting precipitate to settle, the mixture was filtered washed and dried overnight at 110 °C. The solid precipitate (1.7g) was then calcined in flowing air (5mL/min) at 260 °C for 4 hours using a heating ramp rate of 5 °C a minute. A final reduction step was then performed by placing the catalyst in a calcination furnace under a 10% hydrogen in argon atmosphere (5mL/min) at 460 °C using a heating ramp rate of 5 °C for 2 hours.

Pure phase FeMoO₄ catalyst

FeMoO₄ (99% purity) was purchased from Sigma Aldrich and used as catalyst. XRPD confirmed its structure.

Pure phase MoO₃ catalyst

MoO₃ (>99.5% purity) was purchased from Sigma Aldrich and used as catalyst. XRPD confirmed its structure.

Pure phase MoO₂ catalyst

MoO₂ (99% purity) was purchased from Sigma Aldrich and used as catalyst. XRPD confirmed its structure.

Cobalt molybdate catalyst

Ammonium heptamolybdate (3.53 g, $H_{24}Mo_7N_6O_{24}$, >99%purity sigma-aldrich) was dissolved in 50 cm^3 of water under stirring. Ammonia was added drop wise until the solution reached pH 6. Cobalt chloride (4.74 g, $CoCl_2$, 97% purity) was dissolved in 50 cm^3 of water before being added drop wise to the solution of ammonium heptamolybdate with stirring so that an equimolar solution of cobalt and molybdenum were formed. The solution was heated to 90 °C and aged for 2 hours to allow the precipitation of cobalt molybdate. The solution was filtered and the solid collected and dried overnight at 110 °C. The solid precipitate (1.5g) was then calcined in flowing air (5mL/min) at 500 °C for 5 hours at a heating ramp rate of 5 °C a minute.

Cobalt molybdate with a molybdenum excess catalyst

Ammonium heptamolybdate (4.74 g, $H_{24}Mo_7N_6O_{24}$, >99% purity sigma-aldrich) was dissolved in 50 cm^3 of water under stirring. Ammonia was added drop wise until the solution reached pH 6. Cobalt chloride (4.74 g, $CoCl_2$, 97% purity) was dissolved in 50 cm^3 of water before being added drop wise to the solution of ammonium heptamolybdate with stirring so that a solution with a molar excess of 1.5:1 molybdenum to cobalt was formed. The solution was heated to 90 °C and aged for 2 hours to allow the precipitation of cobalt molybdate. The solution was filtered and the

solid collected and dried overnight at 110 °C. The solid precipitate (1.5g) was then calcined in flowing air (5mL/min) at 500 °C for 5 hours at a heating ramp rate of 5 °C per minute.

Nickel molybdate catalyst

Ammonium heptamolybdate (3.53 g, $H_{24}Mo_7N_6O_{24}$, >99% purity sigma-aldrich) was dissolved in 100 cm^3 of water under stirring. Ammonia was added drop wise until the solution reached pH 5.6. Nickel chloride hexahydrate (4.75 g, $NiCl_2 \cdot 6H_2O$, >97% purity sigma-aldrich) was dissolved in 100 cm^3 of water before being added drop wise to the solution of ammonium heptamolybdate with stirring giving an equimolar solution of nickel and molybdenum. The solution was heated to 85 °C and aged for 4 hours. The pH of the solution was maintained by further addition of ammonia if necessary. The solution was filtered and the solid collected and dried overnight at 110 °C. The solid precipitate (1.5g) was calcined in flowing air (5mL/min) at 500 °C for 5 hours at a heating ramp rate of 5 °C per minute .

Nickel molybdate with a molybdenum excess catalyst

Ammonium heptamolybdate (4.74 g, $H_{24}Mo_7N_6O_{24}$, >99% purity sigma-aldrich) was dissolved in 100 cm^3 of water under stirring. Ammonia was added drop wise until the solution reached pH 5.6. Nickel chloride hexahydrate(4.75 g, $NiCl_2 \cdot 6H_2O$, >97% purity sigma-aldrich) was dissolved in 100 cm^3 of water before being added drop wise to the solution of ammonium heptamolybdate with stirring, so that a solution with a molar excess of 1.5:1 molybdenum to cobalt was formed. The solution was heated to 85 °C and aged for 4 hours. The pH of the solution was maintained by further addition of ammonia if necessary. The solution was filtered and the solid collected and dried overnight at 110 °C. The solid precipitate (1.5g) was calcined in flowing air (5ml/min) at 500 °C for 5 hours at a heating ramp rate of 5 °C per minute.

Final catalyst preparation

All catalysts were pelleted at 10 tonnes of pressure for 1 minute and then sieved to 0.4-0.8mm. 0.2 cm^3 of the pelleted catalysts were then packed between quartz wool plugs in the central isothermal zone of the stainless steel reactor tube. The mass which

related to a volume of 0.2cm^3 varied for catalysts. It corresponded to 0.23g of iron molybdate catalyst and 0.27g of cobalt and nickel molybdate catalyst. These masses were kept constant throughout this work. A K-type thermocouple was inserted marginally below the catalyst bed to monitor catalyst bed temperature. The stainless steel reactor tube was then placed and secured in a Carbolite furnace (220-240 V, 382 W). Blanks of *n*-octane and oxygen concentrations were recorded prior to reaction conditions so as to calculate the carbon balance and carbon to oxygen ratios.

2.3 *N*-OCTANE REACTOR SET-UP
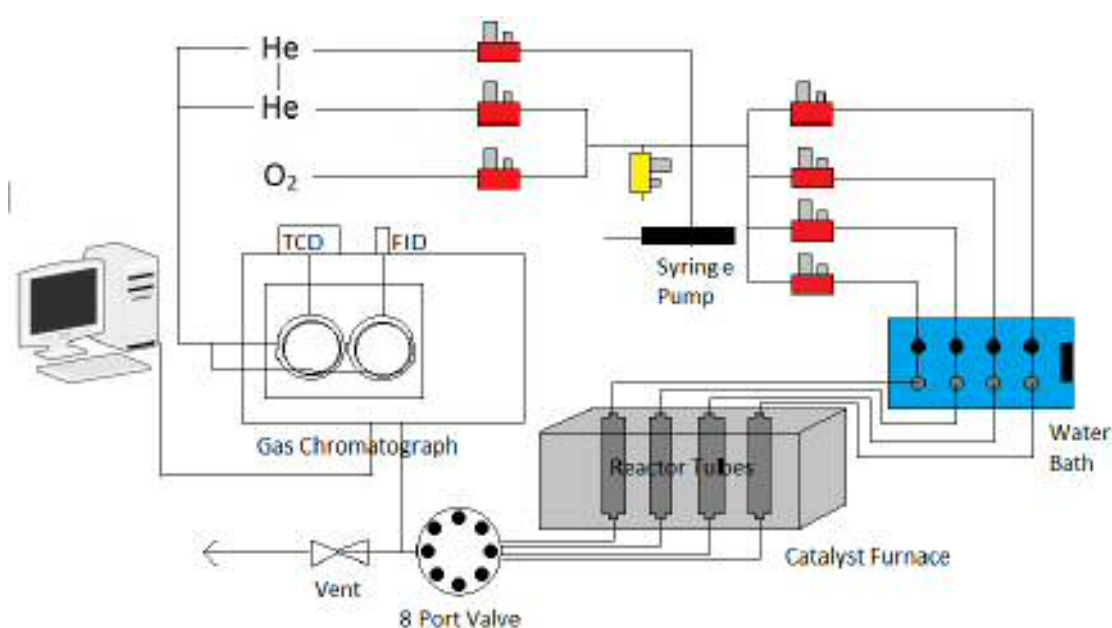
Figure 2.1 Schematic of the reactor used for catalytic testing for the oxidative dehydrogenation of *n*-octane.[1]

Catalytic testing for the oxidative dehydrogenation of *n*-octane was carried out using a multi-bed plug flow reactor shown in Figure 2.1. Reactors used were stainless steel tubes (10mm diameter). The gases of helium and oxygen (source BOC Ltd, purity ≥99.5%) were connected to the reactor via Bronckhorst mass flow controllers. Helium and oxygen lines were joined and connected to a pressure controller. The gases were passed through a saturator containing *n*-octane held in a water bath at *ca.*10 °C to give a concentration of 1% *n*-octane in helium and oxygen. When catalytic testing required a concentration of 10% *n*-octane in helium and oxygen then a high performance liquid chromatography pump was used in place of a saturator to give the required

concentration of *n*-octane. After the addition of *n*-octane to the gas feed all inlet and outlet lines were maintained at 130 °C to prevent condensation in the lines (boiling point of *n*-octane is 125.6 °C). Reaction studies were done at concentrations of 1% *n*-octane and 10% *n*-octane which were outside the lower and higher explosive limits respectively. The lower explosion of *n*-octane is 1.1% and the upper explosion limit is 7.0%. The stainless steel tubes were connected to an 8-port valco valve, allowing multiple reactions to be analysed using a Varian CP-3800 gas chromatograph.

2.4 ONLINE PRODUCT ANALYSIS FOR THE *N*-OCTANE REACTOR

A Varian CP-3800 gas chromatograph was fitted with an Agilent non-polar HP-5 column (30 m, 0.53 mm, 0.5 μm film of phenyl-methylpolysiloxane), a Hayesep Q column and a Molsieve 13X column. The HP-5 column was used to separate hydrocarbon products and led to a flame ionisation detector (FID). The Molsieve column was used to separate O_2 and CO and the Hayesep Q column to detect CO_2, these columns led to a thermal conductivity detector (TCD) or gas analysis. However CO_2 would adsorb irreversibly onto the Molsieve 13X column resulting in column deactivation. To prevent this the Molsieve 13X column was by-passed during the elution of CO_2. Between 4.75 and 8.00 minutes, the valve labelled as V2 switched from "series" to "bypass" positions. To explain this further; the Molsieve column was sealed from the rest of the system while the gas flow went via a by-pass route. This was because between 4.75 and 8.00 minutes CO_2 was eluted, which if it had come into contact with the Molsieve column would bind irreversibly and deactivate it. Figure 2.4 shows the valve configuration for this in greater detail.

The retention times and calibration of products was determined by using a syringe (5 cm^3) and a syringe pump (0.254 cm^3/h). The sample injection was controlled through a 6-port valve, the gas sampling valve (V3) allowed the gas flow through the HP-5 column and to the FID. A second valve, 10 port (V1) controlled gas flow through the Hayesep Q and 13X Molsieve columns and to the TCD. This valve is shown in Figure 2.3. A final valve (V2) controlled the position of the Molsieve 13X from series to by-pass.

Catalyst performance was quantified in molar conversion and selectivity and carbon balance. The valve labelled as V2 is shown in Figure 2.5.
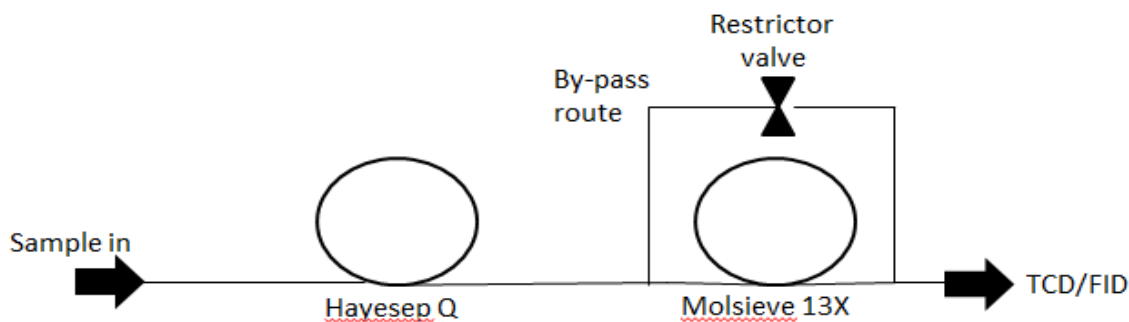
Figure 2.2 Schematic of column set-up in Varian CP-3800 gas chromatograph

Figures 2.3 to 2.5 illustrate the valve configuration and internal injection sequence of the Varian CP-3800 gas chromatograph.
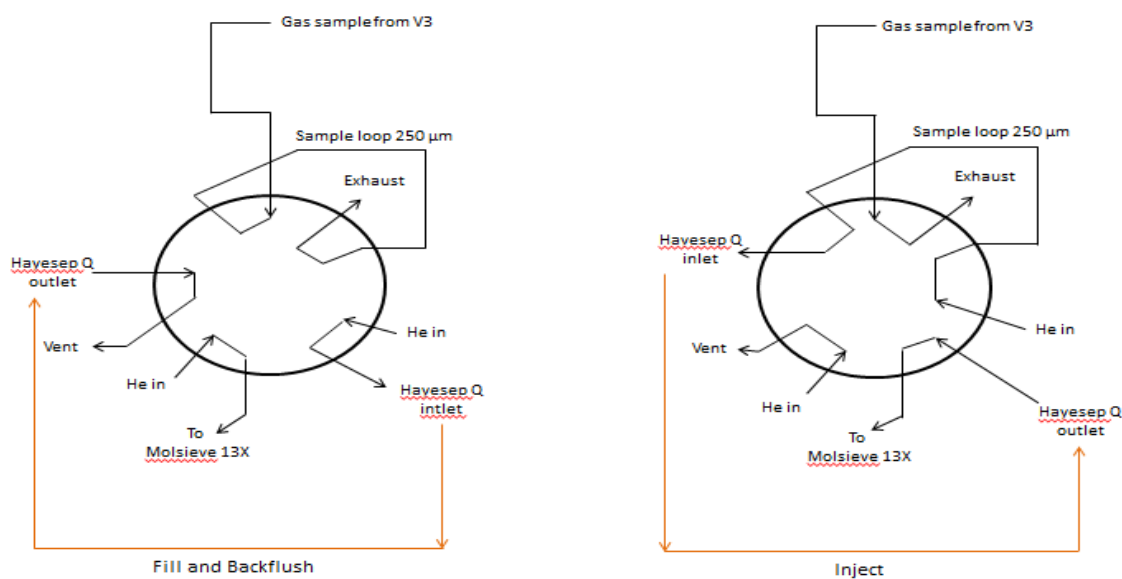
Figure 2.3 Schematic of the 10-port gas sampling valve (V1) to the Hayesep Q and Molsieve 13X columns on both the fill and backflush and inject positions.
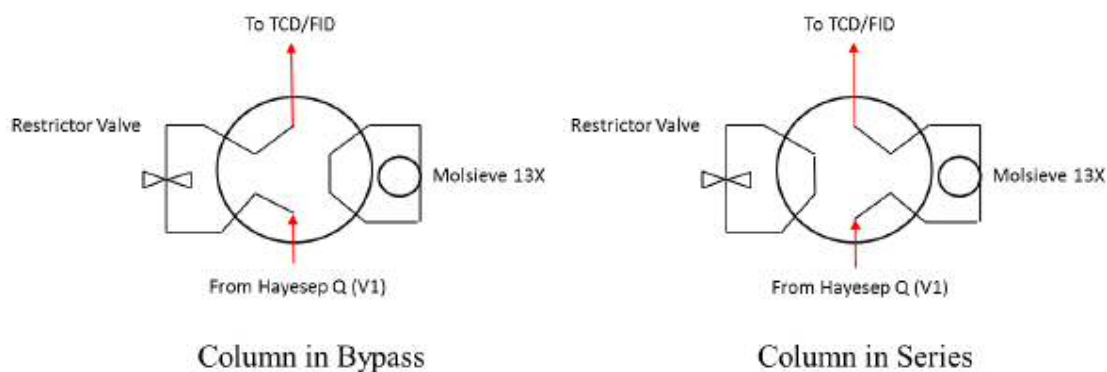
Figure 2.4 Schematic of the 6-port gas sampling valve (V2) for the Molsieve 13X column for bypass and series positions.
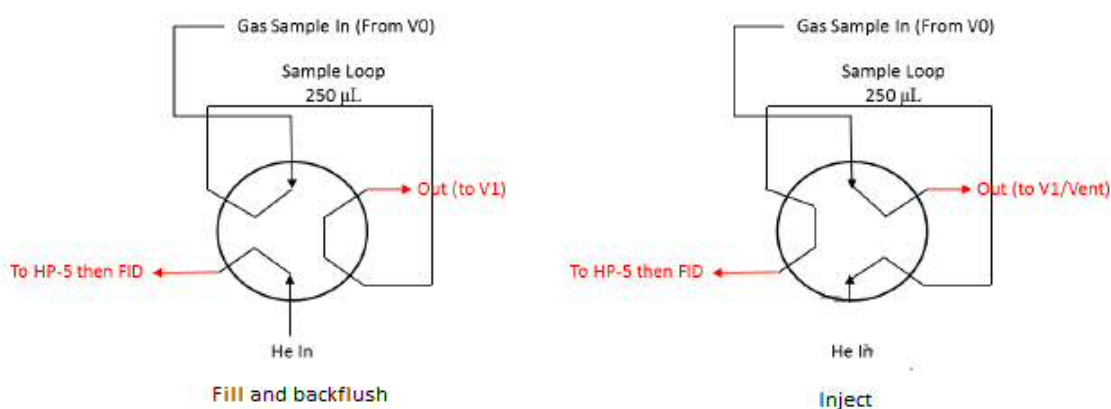
Figure 2.5 Schematic of the 6-port gas sampling valve (V3) in the fill and backflush positions.[1]

Table 2.1 shows the valve switching process for the injection for gas chromatograph runs and the time programme used.

Time (min)	Valve position		
Initial	V1 Fill and backflush	V2 Series	V3 Fill and backflush
0.01	V1 Inject	V2 Series	V3 Inject
4.75	V1 Inject	V2 Bypass	V3 Inject
8.00	V1 Inject	V2 Series	V3 Inject
60.00	V1 Fill and backflush	V2 Series	V3 Fill and backflush

Table 2.1 Valve switching program for gas chromatograph runs

Once V1 goes to the inject position at 0.01 min the gas sample goes through the Hayesep Q column and then to the Molsieve 13X column via V2 which is connected in

series. At 4.75 min V2 switches from the series position to bypass until 8.00 min. This is because the time taken for CO_2 to elute from the Hayesep Q column is between 6.00 - 7.50 min. During this time the Molsieve 13X is in bypass and is thus protected from deactivation. At 0.01 min V3 switches to the inject position. At 60.00 min both V1 and V3 revert to the fill and backflush position in readiness for another injection.

The temperature program used for a gas chromatograph oven is also important as the rate of heating will affect the separation of products. In Table 2.2 the temperature program used for a gas chromatograph run for the determination of products from the reaction of *n*-octane is shown.

Temperature (°C)	Ramp rate (°C/min)	Hold time (min)	Total time (min)
50	n/a	3.00	3.00
100	8	20.00	29.25
270	8	10.00	60.50

Table 2.2 Temperature program used for gas chromatograph runs

These conditions were chosen to give the best peak separation. The initial temperature was 50 °C which is the temperature the oven holding the columns was kept at when no run was occurring.

2.5 PROPANE REACTOR SET-UP

0.3mL of the catalyst was packed into a stainless steel tube (diameter 5 mm) which was fitted to the reactor. A mixture of propane/helium gas (BOC Ltd) containing 5002 ppm propane was flowed through the reactor at a flow rate of 19 cm^3 min^{-1}. Oxygen was flowed through the reactor at a rate of 1 cm^3 min^{-1}. The gas flows were controlled using mass flow controllers. The Gas Hourly Space Velocity (GHSV) was calculated to be 4000 h^{-1}.

The temperature of the reaction was monitored using a K-type thermocouple which was placed just below the catalyst bed and was controlled manually using a Carbolite

furnace (220-240 V, 382 W) fitted around the reactor which was set to the required temperature.

The reactions were monitored using an on-line P23 Varian GC which had a molecular sieve and an Agilent HayeSep Q column. Organic products – such as propane and propene – were detected using a FID. Gases were detected using a TCD.

Blank readings were taken at 100 °C determining the levels of propane and oxygen present in the product feed before the reaction had taken place. The reaction was monitored from 350 – 600 °C in 50 °C increments.

2.6 CALCULATIONS FOR CONVERSION, SELECTIVITY AND YIELD.

Conversion, selectivity and yield are discussed in the ensuing chapters. The data used for these came from the measurements taken from the gas chromatograph.

Conversion:

Blank measurements of oxygen and *n*-octane were taken prior to heating the reactor. These gave average area counts measured in µV. To calculate conversion as a percentage.

((average counts of blank reactant- counts from experiment)/average blank counts)) x100

This gave a percentage value for *n*-octane and oxygen conversion which could then be plotted.

Selectivity:

The area count of a product was calculated from the gas chromatograph. This value was then divided by the relative response factor (RRF) a ratio between the signal produced by an analyte and the corresponding quantity of analyte which produced the signal. The RRF of an analyte will vary. For hydrocarbons this value was then multiplied by the carbon number of the analyte. Finally that value is divided by the sum of all products and multiplied by 100 to give a percentage value. The calculation is shown below.

Area count of analyte/RRF =X

X * carbon number = Y

(Y/Sum of all products from reaction)*100 = percentage selectivity.

Yield:

This was calculated by isolating the selectivity percentage of a species (usually octene as the desired end product) and multiplying this by the overall conversion of *n*-octane to product.

Percentage selectivity x conversion percentage of *n*-octane = yield

2.7 CATALYST CHARACTERISATION TECHNIQUES

2.7.1 X-RAY POWDER DIFFRACTION

X-ray powder diffraction (XRPD) is an analytical technique that can be used to classify, identify and analyse materials. X-rays are electromagnetic radiation that occur in the region between ultraviolet and gamma rays. X-rays wavelength is in the around 10^{-10} m or 1Å, comparable to the size of an atom.

 X-ray diffraction (XRD) is a bulk technique, it is not a surface sensitive analytical tool. For XRD to work the sample being analysed must be crystalline, without crystallinity no diffraction is possible. Unit cell dimensions, crystal structure and crystallite size are all information that can be yielded from XRD. This thesis used XRPD to simply identify catalyst structure and the phases present.

The technique was invented by W.H. Bragg.[2] Diffraction patterns are produced to identify the crystalline phases present in a material. A crystalline material can is a solid with a highly regular arrangement of atoms or molecules. This arrangement should be repeating, which is referred to as being periodic. By definition a crystalline solid should be a material in which periodicity is exhibited in all three dimensions.[3] A stationary X-ray source, in this case a Cu Kα source, produces monochromatic X-rays which interact with the lattice spacing in a crystalline material to produce an X-ray diffraction pattern. X-rays scattered by atoms in an ordered lattice interfere constructively in directions given by Bragg's law.[4]
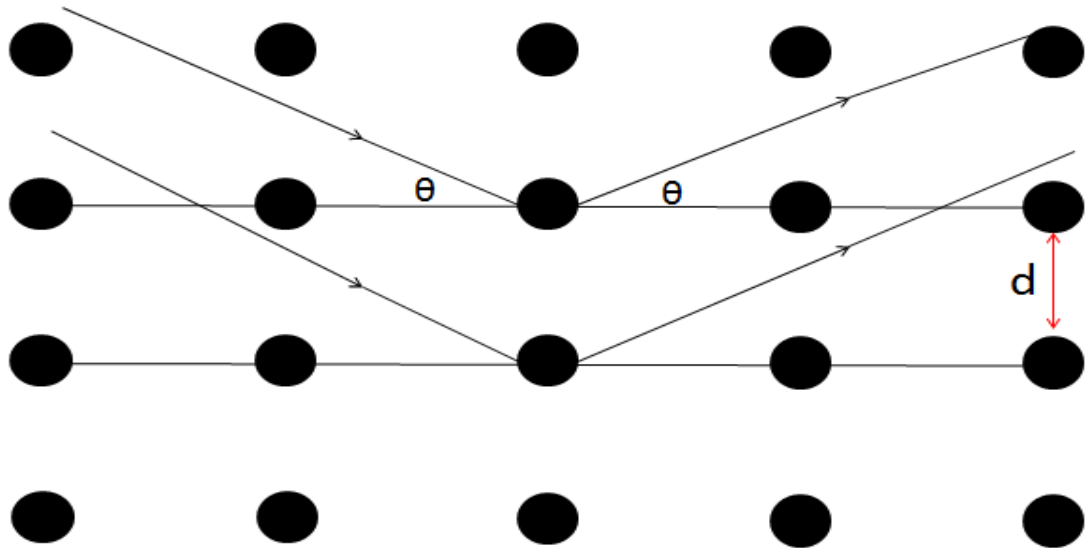
Figure 2.6 Reflection of X-rays in a crystalline solid as defined by Bragg's law.

For constructive interference to occur the additional distance travelled after diffraction from d must be an integer of the wavelength. The path-length travelled by the X-rays is affected by, the lattice spacing which is represented by d and the angle of incidence of the X-ray beam which is given by θ. This leads to the aforementioned Bragg equation which is given as.

$$n\,\lambda = 2d\sin(\theta)$$

Where

n - is an integer, the order of the reflection

λ - is the X-ray wavelength

d - is the distance between two lattice planes

θ - is the angle of incidence

X-ray powder diffraction analysis for the work detailed in this thesis was performed by a PANanalytical X'pert Pro diffractometer equipped with a Cu Kα X-ray source. All experiments were done with an applied accelerator voltage of 40kV and a current of 40mA. Each experiment was performed between 10°-80°. Patterns produced were

referenced and identified against reference patterns compiled in the international centre for diffraction data (ICDD).

2.7.2 RAMAN SPECTROSCOPY

Raman spectroscopy concerns the frequencies of light. This technique determines the vibrational, rotational modes in a system. When a molecule is exposed to monochromatic light (also referred to as incident light) at a frequency not corresponding to adsorption a small amount is scattered (referred to as). This can cause a Raman shift (Δv).[5,6]

Where

Δv = change in frequency

v_0 = frequency of incident light

v_r = frequency of scattered light

The scattering of the light can either be elastic or inelastic. Rayleigh scattering is the term used for elastic scattering, which occurs when the frequency of the scattered light is the same as the frequency of the incident light. If the molecule which has been hit by incident light gains energy this leads to Stokes radiation. If the molecule loses energy this leads to anti-Stokes radiation. Both of these are inelastic scattering.
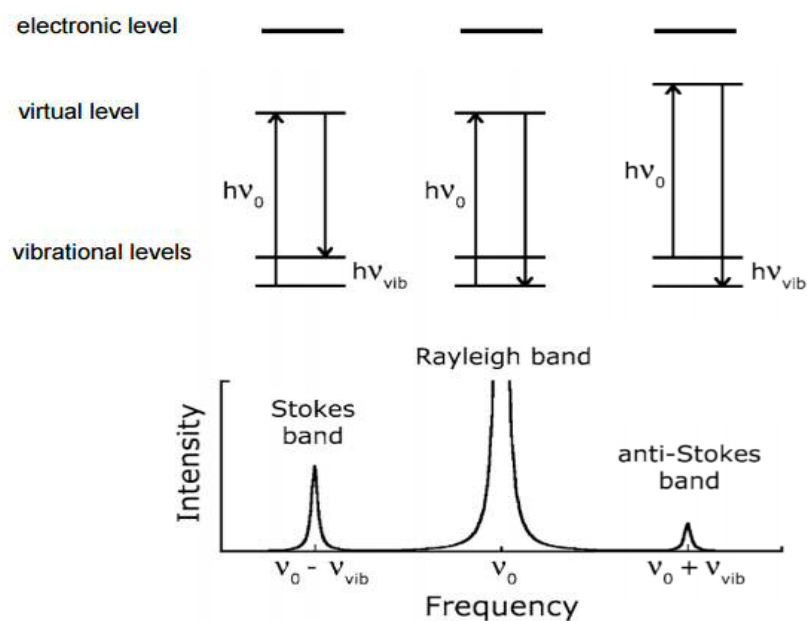
Figure 2.7 Transitions leading to Stokes radiation and Rayleigh scattering. From Hammond.[7]

The incident monochromatic light source is provided by a laser, usually in the visible, infra-red or near ultra-violet spectrum. The light interacts with the bonding electrons of the molecule causing vibrations and rotations.[8]

For a molecular vibration to be Raman active it must occur alongside a change in the polarizability of the molecule.[9] This result in a shape change, see Figure 2.8 for a visual depiction of this effect. The molecule must not possess a symmetry element to be Raman active.
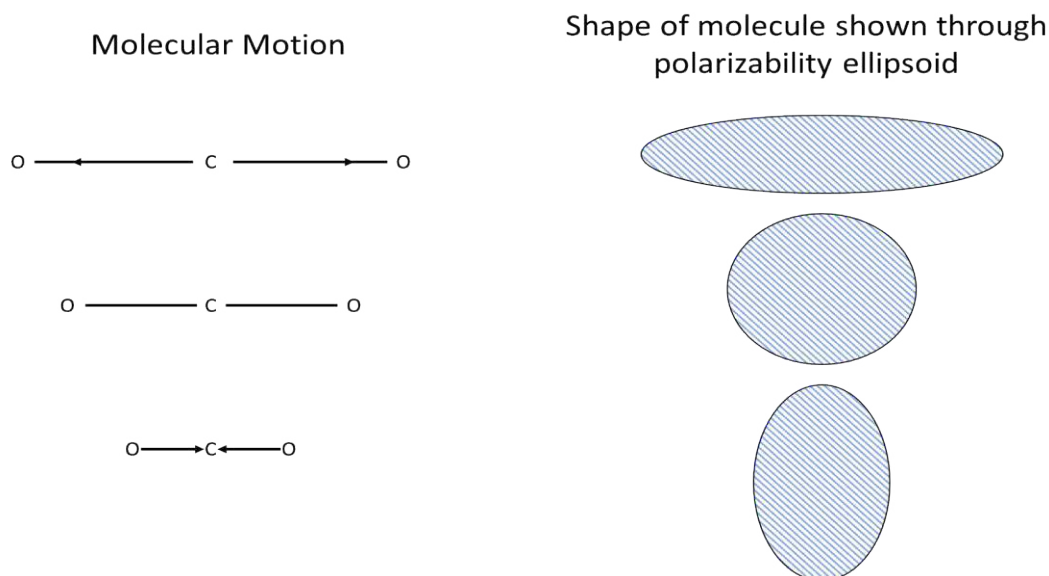
Figure 2.8 – Representation of change in polarizability of a CO_2 molecule.

Raman spectroscopy analysis for the work detailed in this thesis was performed using a Renishaw Ramascope using a Spectra physics green argon laser (λ = 514 nm) at a power of 20mW.

Ultra violet Raman spectroscopy shown in Chapter 5 was done using a Class 4 CW inVia Raman system. A Spectra physics UV laser (λ = 266 nm) was used.

2.7.3 THERMOGRAVIMETRIC ANALYSIS

Thermogravimetric analysis measures the change mass of a sample as a function of increasing temperature. The weight of the sample is measure in relation to time and temperature. Volatile products may break down and lose mass, if sample oxidation or an adsorption process occurs then mass gain may be observed.[10]

A thermogravimetric analysis profile can yield information on whether decomposition of the sample or a chemical transformation occurs at the temperatures tested.

2.7.4 MICROWAVE-PLASMA ATOMIC EMISSION SPECTROSCOPY (MP-AES)

Microwave-plasma atomic emission spectroscopy (MP-AES) can be used to quantify the ratios of elements present in a catalyst. A microwave magnetic field (2.45 GHz)

excitation generates nitrogen plasma from nitrogen gas. This is stable at atmospheric pressure and held within the torch of the MP-AES. The sample being tested is aerosolized and passed through the torch. The sample is vaporised as it passes through the torch. This leads to excitation of atoms in the sample which emit photons as they relax back to ground state.[11] The sources for atomic emission can be a microwave plasma, used here, or an inductively coupled argon plasma. The plasma can be generated via an electrical or magnetic field, in this instance an electrical field was used. The photons are funnelled towards a monochromator prior to detection via a charge coupled device measuring the conversion of photons into electrical charge. The wavelengths of light emitted are characteristic of the element that generated it and the intensity levels can be quantified which can then be used to elucidate the ratio of elements in a sample.

In this work, MP-AES was used to calculate the ratio of metal elements present in catalyst samples.

2.7.5 X-RAY PHOTOELECTRON SPECTROSCOPY (XPS)

X-ray photoelectron spectroscopy (XPS) is a widely used surface technique which gives information about the oxidation state of species present at a catalyst surface. Kai Siegbahn won the Nobel prize in physics for his work in using photoemission as an analytical tool.

The theory behind XPS lies with the Einstein relationship, which states that:

$$E_K = h\nu - E_B$$

Where

E_K is the binding energy of the ejected photoelectron.

$h\nu$ is the characteristic energy of the X-ray photon.

E_B is the binding energy of the atomic orbital from which the electron originates.[12] See Figure 2.9 for an illustration of this.
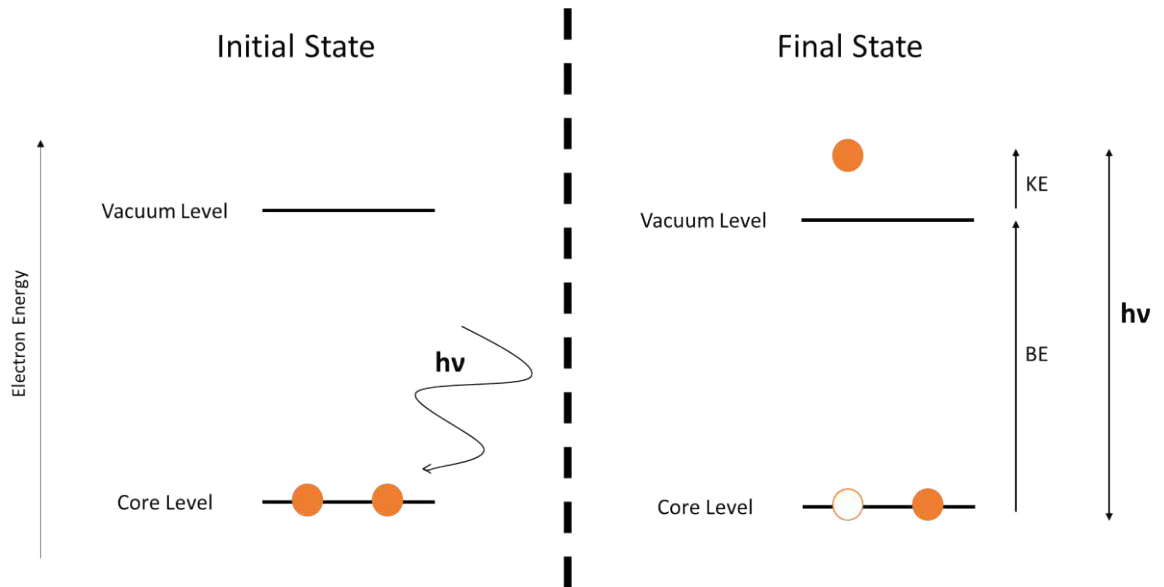
Figure 2.9 – Illustrating the Einstein relationship.

Consider Figure 2.9, the binding energy (BE) is the amount of energy required to promote an electron from the core level to its vacuum level. However the kinetic energy of the photoelectron is shown by KE which is the difference between the energy put in and the binding energy.[13]

Atoms absorb photons of a certain energy and wavelength from an X-ray source. This then leads to the emission of photelectrons from the sample surface. For this to occur the excitation energy required must be higher than the difference between a vacuum and the fermi energy level. The fermi energy level is the energy of an electron in the highest occupied molecular orbital at absolute zero. Electron orbitals deeper than the valence band can be considered "core-like" and give up photoelectrons with binding energies that are generally within 3 eV of their elemental values.
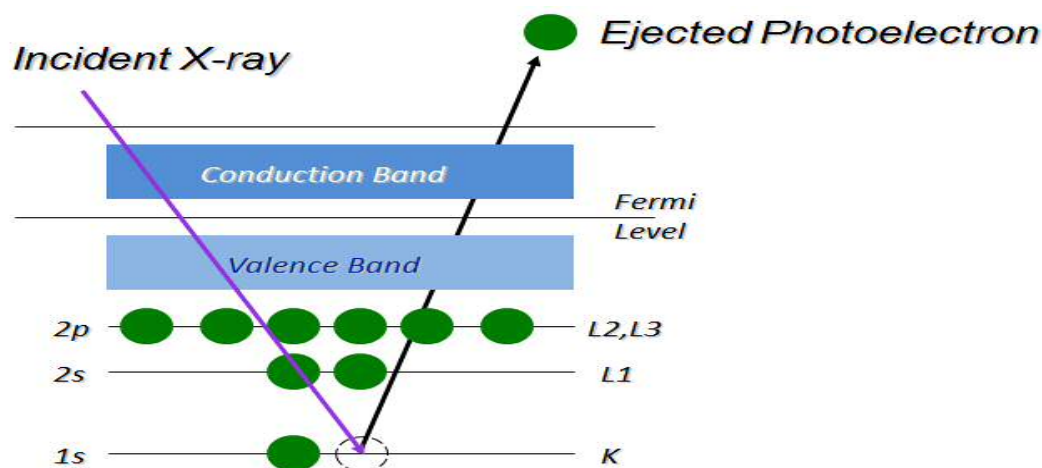
Figure 2.10 – Illustration of photoelectron emission for XPS. From Morgan.[14]

XPS analysis for this work was obtained using a ESCALAB 220 spectrometer equipped with a aluminium Kα source. Analyser pass energy of 100eV. Pressure of the chamber was maintained at 3.9×10^{-8} N/m^2. Energy resolution of spectrometer was determined from the full width half maximum of metallic gold at an energy of 20eV.

2.7.6 THE BRUNAUER-EMMET-TELLER SURFACE AREA MEASUREMENT

Surface area measurement processes involve adsorption.[15] Typically physisorption of nitrogen or argon is used, close to the condensation temperature of the adsorbed gas chosen. At 77K nitrogen can be adsorbed onto a surface and the Brunauer-Emmet-Teller (BET) model can be used to interpret the data and yield a surface area measurement.[16]

This is done by the BET equation (named after the scientists who developed it), which is an extension of the Langmuir equation. As the Langmuir equation only accounts for monolayer coverage, modification was required to represent multilayer adsorption.

The BET equation is given as:

Where

V is the volume of gas adsorbed.

P_0 is the saturation pressure

V_m is the volume of gas adsorbed at (STP) per unit mass of adsorbent, when the surface is covered by a unimolecular layer of adsorbate.

C is a constant.

There is an assumption that the first layer is adsorbed with the heat of adsorption (H_1) while subsequent layers are adsorbed with a heat of adsorption equal to the heat of evaporation (H_L). This gives the final part of the BET equation, the constant C.[17]

$$C = \exp(H_1 - H_L)\ /RT$$

This results in a plot of data, giving the monolayer coverage.[18] A nitrogen molecule occupies 16Å.

BET analysis for the work detailed in this thesis were performed on a Micromeretics Gemini 2360 surface analyser. All samples were degassed for 2 hours.

2.7.7 ENERGY DISPERSIVE X-RAY (EDX) SPECTROSCOPY

Energy dispersive X-ray (EDX) analysis is used often in conjunction with scanning electron microscopy (SEM). This work only used EDX analysis.

EDX occurs from secondary electron emission of core shell electrons.[1,19] Elements present in the catalyst sample are analysed by determination of X-ray wavelengths emitted when an atom is bombarded by high energy electrons. This gives a localised chemical analysis. In theory elements from beryllium to uranium can be detected. However not all instruments are equipped for detection of lighter elements (lower proton number than sodium). Qualitative analysis simply requires identification of lines in the X-ray spectrum. Quantitative analysis requires a comparison of the intensities of identified elements within a sample and cross-referencing these values with calibration standard of known composition. Accuracy of modern EDX analysis is

considered to be within 2%. The lower end of detection limits with regular techniques is 1000ppm.

When an atom is irradiated by an electron beam, a core electron is emitted from the atom. An electron in a higher energy orbital than the ejected electron relaxes into the now vacant lower energy orbital. The resulting loss of kinetic energy from this transition results in X-ray generation. Each element possesses a unique wavelength x-ray, as each element has a unique difference between the energies of core and higher energy electrons. X-ray lines are identified by a capital Roman letter indicating the shell containing the inner vacancy (K, L or M). When electrons are emitted from the L energy level then the spectra is more complex than when electrons are emitted from the K energy level. This is due to the L level into three sub-levels. Energy levels are measure in electron volts (eV). 1 eV is equal to 1.602^{-19} J. When discussing EDX X-rays are thought of as a photons possessing a specific energy (see Figure 2.11).[20,21]
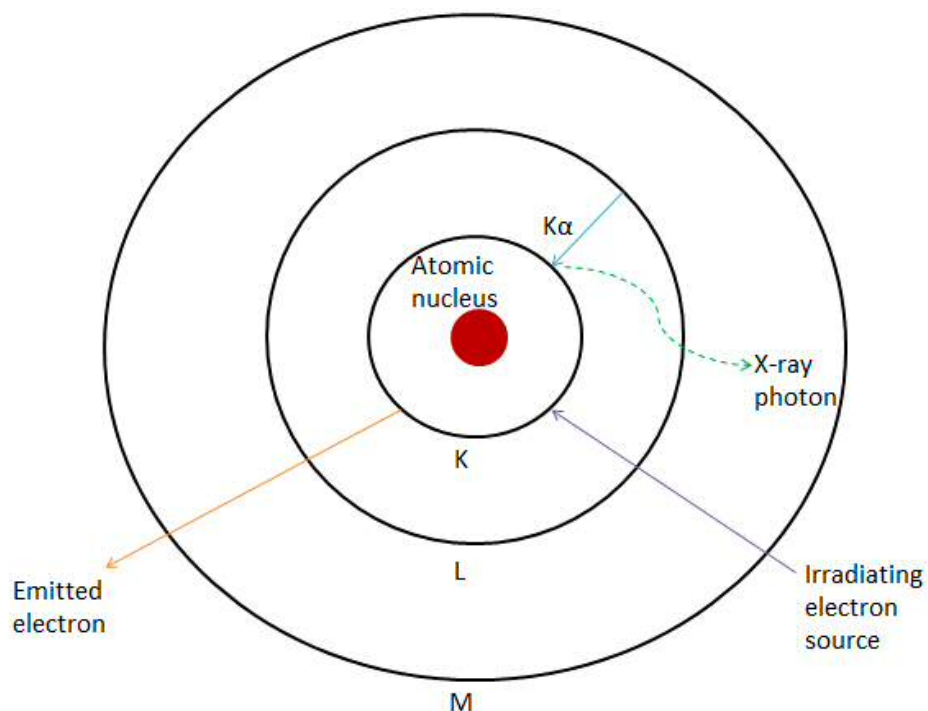
Figure 2.11 Figure illustrating the generation of X-rays for EDX spectroscopy.

X-rays once emitted are detected by a solid state detector in which a semi-conductor material usually silicon is used as a medium to detect x-rays.[22] This is shown in Figure 2.12.
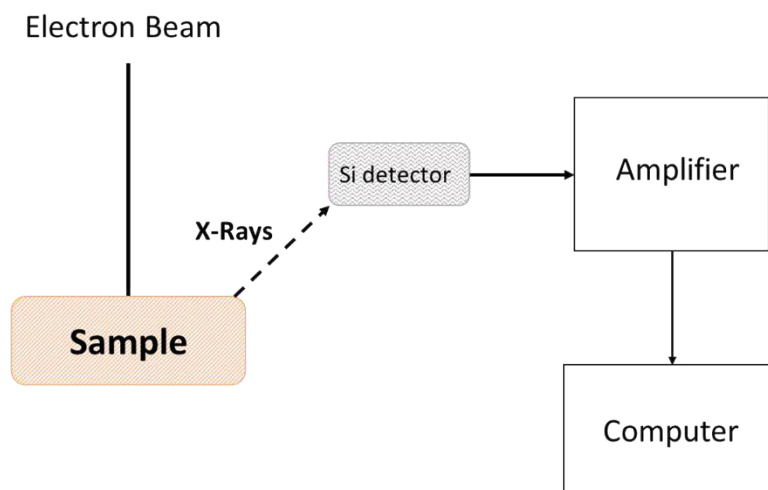
Figure 2.12 Simplified schematic of the internal working of an EDX spectrometer.

EDX analysis for this work was performed using an Oxford EDX analyser in tandem with Carl Zeiss EVO 40 SEM. Working distance used was 9mm, extra high tension was set to 25 keV, I-probe to 25 nA.

Bibliography

1   B.R. Yeo, PhD, Cardiff University, 2014.
2   M. F. Perutz, *Acta Crystallogr. A*, 1990, **46**, 633–643.
3   T. L. Malkin, B. J. Murray, A. V. Brukhno, J. Anwar and C. G. Salzmann, *Proc. Natl. Acad. Sci.*, 2012, **109**, 1041–1045.
4   W. L. Bragg, *Proc. R. Soc. Lond. Ser. Contain. Pap. Math. Phys. Character*, 1914, **89**, 468–489.
5   E. Smith and G. Dent, *Modern Raman Spectroscopy: A Practical Approach*, John Wiley & Sons, 2013.
6   P. Vandenabeele, *Practical Raman Spectroscopy: An Introduction*, John Wiley & Sons, 2013.
7   C. R. Hammond, Phd, Cardiff University, 2004.
8   P. Larkin, *Infrared and Raman Spectroscopy: Principles and Spectral Interpretation*, Elsevier, 2011.
9   I. R. Lewis and H. Edwards, *Handbook of Raman Spectroscopy: From the Research Laboratory to the Process Line*, CRC Press, 2001.
10 T. R. Crompton, *Polymer Reference Book*, iSmithers Rapra Publishing, 2006.
11 D. Briggs and M. P. Seah, *Practical Surface Analysis, Auger and X-ray Photoelectron Spectroscopy*, Wiley, 1990.
12 C.-O. A. Olsson, *Corros. Sci.*, 1995, **37**, 467–479.
13 P. van der Heide, in *X-Ray Photoelectron Spectroscopy*, John Wiley & Sons, Inc., 2011, pp. i–xvii.
14 Dr David Morgan, Cardiff University 2012, .

15   T. Allen, *Particle Size Measurement: Volume 2: Surface Area and Pore Size Determination.*, Springer Science & Business Media, 1996.

16   J. Rouquerol, F. Rouquerol, P. Llewellyn, G. Maurin and K. S. W. Sing, *Adsorption by Powders and Porous Solids: Principles, Methodology and Applications*, Academic Press, 2013.

17   T. E. Davies, Phd, Cardiff University, 2006.

18   G. Attard and C. Barnes, *SURFACES. Edition en anglais*, Oxford University Press, 1998.

19   R. A. Carlton, *Pharmaceutical Microscopy*, Springer Science & Business Media, 2011.

20   J. C. Russ, *Fundamentals of Energy Dispersive X-Ray Analysis: Butterworths Monographs in Materials*, Butterworth-Heinemann, 2013.

21   A. J. Garratt-Reed, D. C. Bell and P. Nicholson, *Scanning*, 2003, **25**, 162–162.

22   R. Schneider, in *Surface and Thin Film Analysis*, eds. G. Friedbacher and H. Bubert, Wiley-VCH Verlag GmbH & Co. KGaA, 2011, pp. 293–310.

CHAPTER 3- THE OXIDATIVE DEHYDROGENATION OF N-OCTANE

3.1 INTRODUCTION

The reaction of n-octane over a variety of iron molybdate catalysts is investigated in this chapter. Previous work carried out by this university and research group,[1,2] has looked at the reaction of medium to long chain alkanes over iron molybdate based catalysts. Recently the production of octenes from a *ca.*1% octane feed, over a variety of carbon to oxygen ratios, has been shown.[2] The conclusion was that catalytic oxidative dehydrogenation (ODH) was occurring. The ODH of short-chain alkanes has been well-reported.[3,4] The previous work was done with a catalyst provided by Johnston Matthey.

The first aim of this chapter was to produce a catalyst which could reproduce those results. The second aim was to optimise the catalyst. To this effect the reaction parameters were manipulated to give an optimal performance and maximise production of high value chemicals. Finally the catalyst was characterised pre and post reaction to indicate the active species and elucidate some information about a possible mechanism.

3.2 REACTION PARAMETERS INVESTIGATED

3.2.1 TEMPERATURE

Catalytic reactions were performed between 350-550°C unless stated otherwise. The standard temperature increase was in 50°C increments at a ramp rate of 15°C a minute. The reactor was purged and allowed to stabilise under reaction conditions for 1h before each temperature ramp occurred and following the subsequent injection from the gas chromatograph's sample loop. The temperature was monitored via a K-

type thermocouple placed below the catalyst bed, using the PicoLog Tc-08 software by Pico Technology.

3.2.2 GAS HOURLY SPACE VELOCITY (GHSV)

The effect of gas hourly space velocity (GHSV) on the reaction of n-octane over an iron molybdate catalyst was investigated. Throughout all investigations 0.2 mL of pelletized catalyst (10 tons, 800-1000 µm) was used for all the reactions studied as outlined in Chapter 2. The GHSV was altered by adjusting the flow rates controlled by the Bronckhorst mass flow controllers (MFCs). GHSV flows in this thesis were between $1000h^{-1}$ and $18,000h^{-1}$.

3.2.3 PARTIAL PRESSURES AND CARBON TO OXYGEN RATIO

The carbon to oxygen (C:O) ratio used in this investigation are mainly 8:1 carbon to oxygen. Some tests were performed at 2:1 and 12:1, so in the gas feed there are 2 carbon atoms to every oxygen atom, or 12 carbon atoms to every oxygen atom. The large majority of investigations are performed at 8:1 as this was found to be the optimal C:O ratio.[2] The following chapter investigates anaerobic conditions, where no oxygen is used. The ratios were calculated using the percentage volume (v/v%) of octane in the feed which was either *ca.*1% , *ca.*10% with the oxygen concentration altered to give the desired ratio.

3.3 CATALYST

The catalysts used in this chapter are a pre-reduced iron molybdate catalyst or an unreduced iron molybdate catalyst prepared by coprecipitation detailed in Chapter 2. The iron molybdates tested, either pre-reduced or unreduced, have a molybdenum to iron molar ratio of 2.7:1. This means free molybdenum oxides are also present. In addition pure phases such as $FeMoO_4$, MoO_3 and MoO_2 sourced from Sigma Aldrich are tested for their catalytic ability.

3.4 CALIBRATION OF N-OCTANE

Calibration of n-octane was completed with a syringe pump and the desired concentration created by adjusting the carrier gas (helium) flow. Oxygen was also calibrated by adjusting the flow rates of oxygen and helium MFCs to produce the desired concentrations.
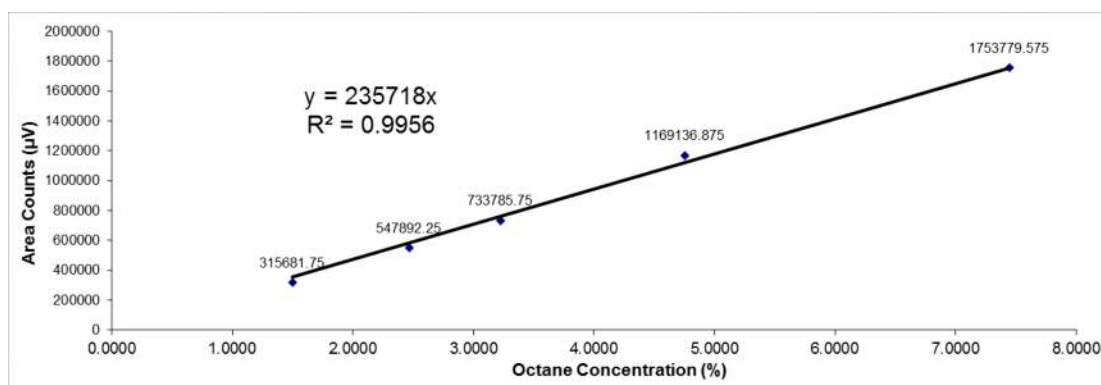
Figure 3.1 – A calibration plot showing the relationship between increasing *n*-octane concentration and area counts.
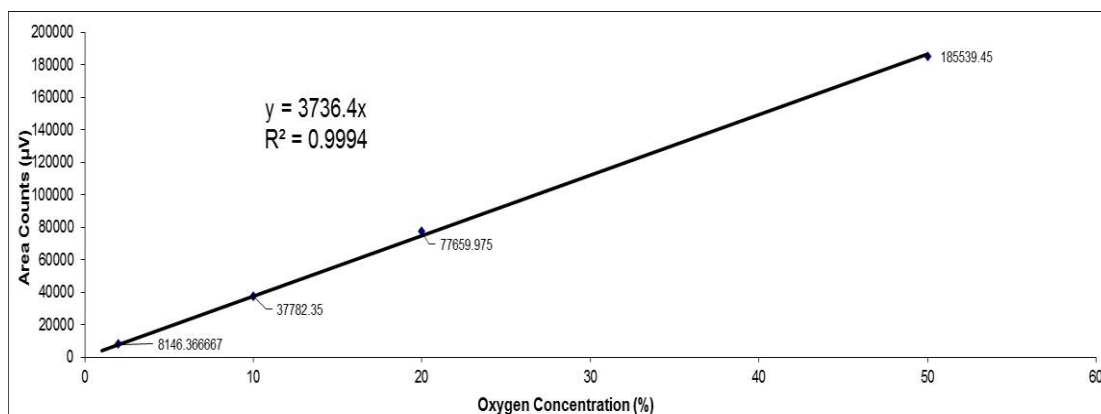
Figure 3.2 – A calibration plot showing the relationship between increasing oxygen concentration and area counts.

3.5 RESULTS AND DISCUSSION

3.5.1 CATALYTIC ACTIVITY OF A FERRIC MOLYBDATE CATALYST

An iron molybdate catalyst $Fe_2(MoO_4)_3$ with a Fe:Mo molar ratio of 1:2.7 was tested with *n*-octane (1% octane, 0.2mL catalyst C:O 8:1) and the temperature increased from 350°C to 550°C in 50°C increments as can be seen on the x-axis of Figure 3.3.
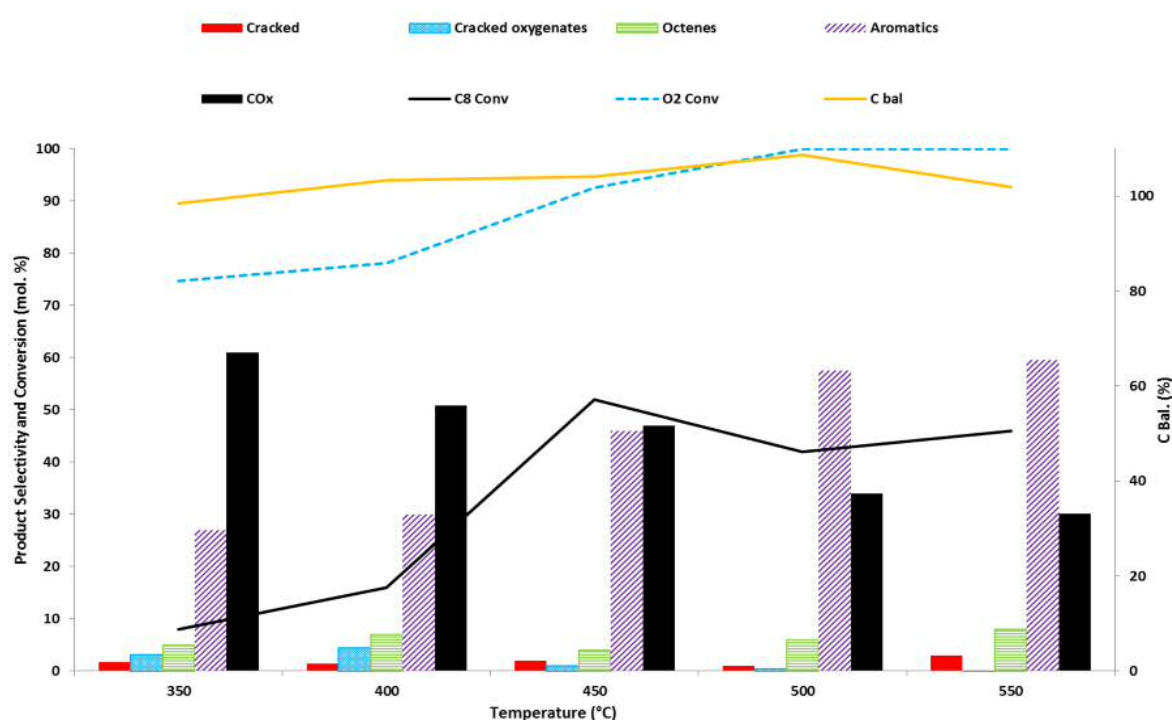
Figure 3.3 – Reaction of 1% *n*-octane (GHSV 1000h^{-1}, C:O 8:1) over a iron molybdate catalyst. Temperature range from 350-550°C

As can be seen the octane is converted to a variety of products. The main product is carbon oxides, with aromatics as the secondary product. The octane conversion increases with rising temperature despite dipping slightly after 450°C. The rise in octane conversion could be attributed to total oxygen consumption from the gas phase at 500°C and above. The literature[5–7] suggests the mechanism used by this molybdenum based catalyst is an oxidative dehydrogenation, Mars-Van Krevelen (ODH-MvK) pathway. This mechanism sees the catalytic surface oxygen atoms interact with the substrate before being abstracted to form water The lattice oxygen atoms in

63

the bulk of the catalyst are then reordered to replace vacancies at the surface. Gaseous oxygen (supplied by the gas feed) then replenishes the bulk lattice oxygen. Once the oxygen is removed from the gas feed the catalyst loses its oxygen atoms and becomes deactivated.[5] As such the drop in conversion at 500°C and above could be attributed to not enough oxygen present in the gas feed to replenish lattice oxygen.

It is thought that the alkane, in this case *n*-octane oxidatively dehydrogenates, to form the corresponding alkene, in the above experiment this is octene, predominantly *trans*-2-octene and *trans*-3-octene are observed. It may be that alkenes that are less stable, depending on the position of the double bond, cyclise and dehydrogenate further to form the aromatic species, chiefly, ethylbenzene, xylene and styrene.[1,8,9]
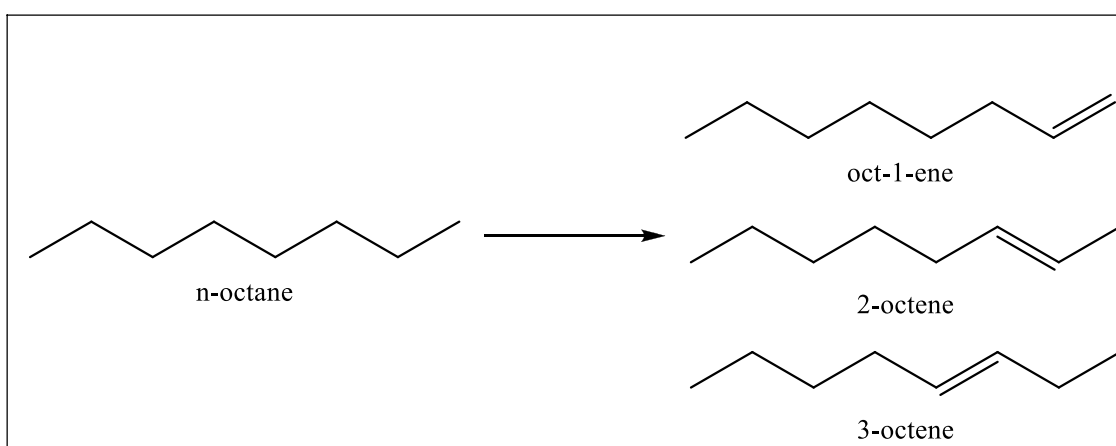
Figure 3.4 – Diagram of *n-octane* converted to octenes
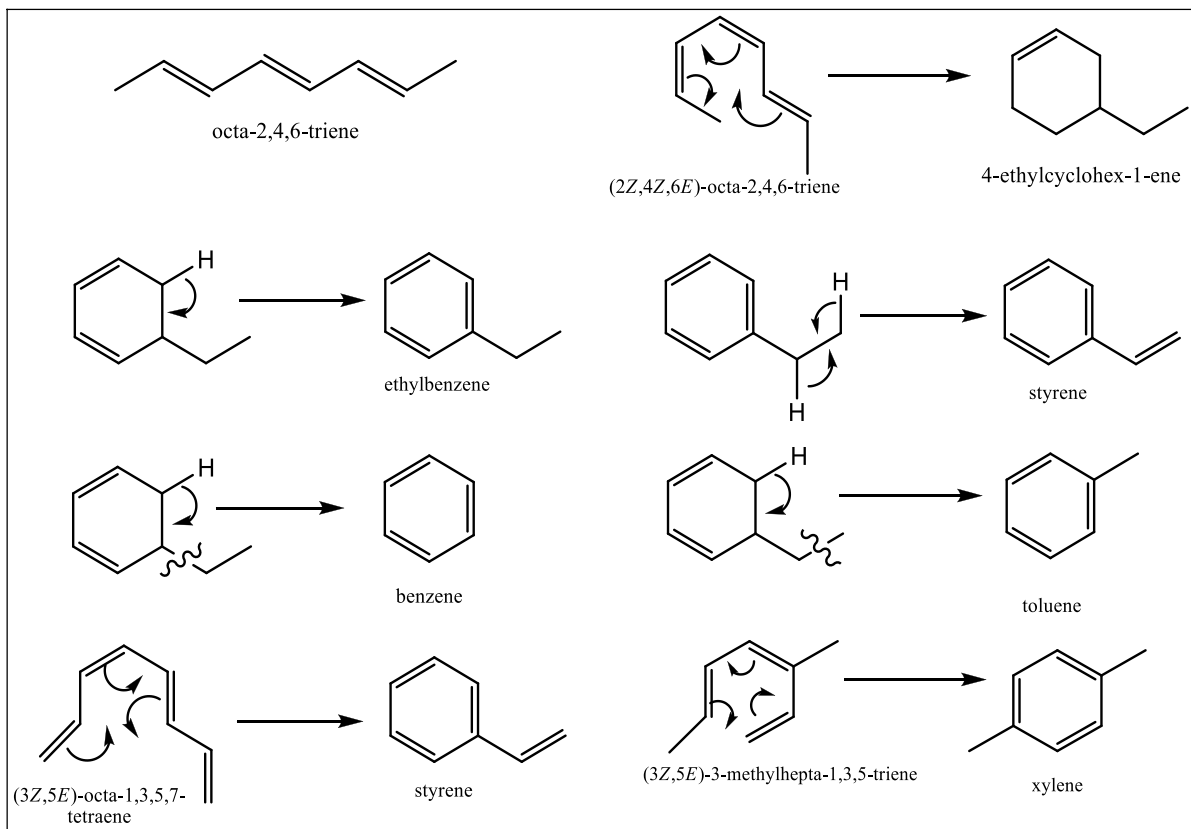
Figure 3.5 – Proposed further dehydrogenation and cyclisation mechanisms to form the aromatics observed

These findings are comparable to what previous work in this group has found[1,2]. It has been suggested the increase in conversion and selectivity to aromatics was caused by the $(Fe_2MoO_4)_3 + MoO_3$ catalyst undergoing a phase change and reduction (forming $FeMoO_4$).[2] The rapid increase in conversion at 450°C could be attributed to the phase change (see section 3.5.2) from $Fe_2(MoO_4)_3$-MoO_3 to $FeMoO_4$-Mo_4O_{11}-MoO_2 causing oxygen to be released

An *in-situ x-ray powder diffraction* (XRPD) study was carried out to investigate the phase transitions at different temperatures on an iron molybdate catalyst comprising of the species $Fe_2(MoO_4)_3 + MoO_3$. This is shown in Figure 3.6. The experiment started with the sample held at 50 °C. The temperature was then raised to 350 °C. Three scans were taken and then the temperature was raised another 50 °C to 400 °C. Three scans were taken and the sample was then raised to 450 °C. At this temperature and at 500 °C and 550 °C the temperature was held constant for 45 minutes before the heating

increase to the next increment occurred. After being held for 45 minutes at 550 °C the temperature was allowed to cool back to 50 °C.

Scans taken lasted 8 minutes 42 seconds. The heating ramp rate between increments was 5 °C a minute.

3.5.2 *IN-SITU* XRPD STUDY OF THE REDUCTION OF FERROUS MOLYBDATE TO FERRIC MOLYBDATE.
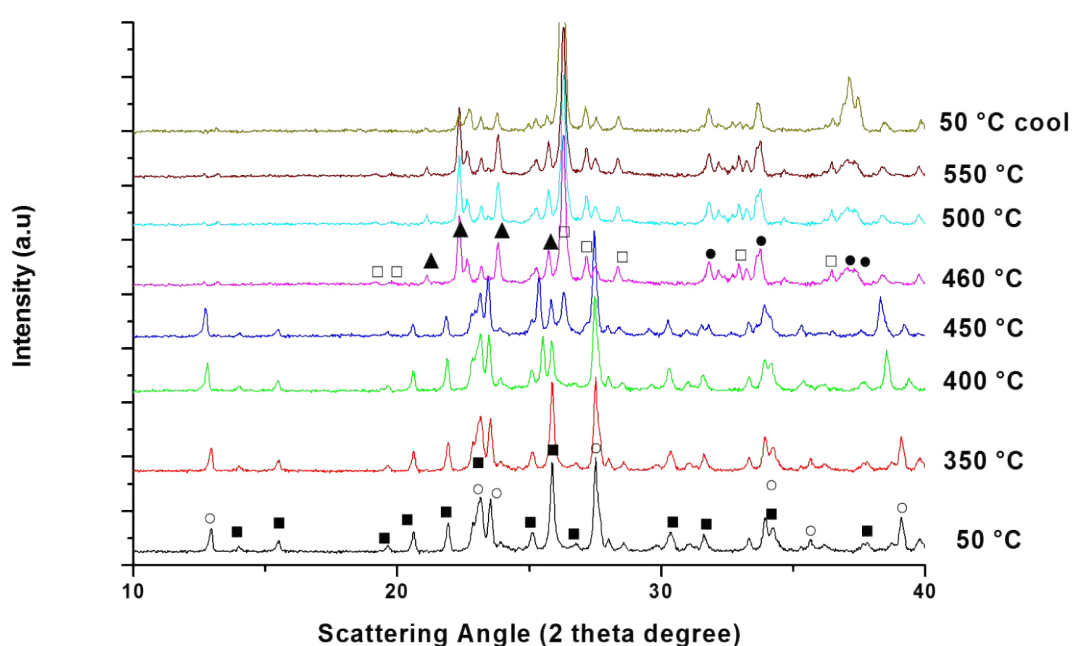
Figure 3.6: *In situ* XRPD of an iron molybdate catalyst (Mo to Fe excess of 2.7:1) with *n*-octane under aerobic conditions (C:O 8:1) to 550°C. Phases present: MoO_3 (o), $Fe_2(MoO_3)_4$ (■), β-$FeMoO_4$ (□), Mo_4O_{11}(▲), and MoO_2 (●).

A fast phase reduction at 460 °C (within 40 min) is observed with conversion of α-$Fe_2(MoO_4)_3$ to β-$FeMoO_4$, MoO_2 and Mo_4O_{11}.[2] In Figure 3.6, fresh iron molybdate is shown by the black line, held at 50°C. MoO_3 (o) and $Fe_2(MoO_3)_4$ (■) species are both present.

Species	Peak (2 theta degrees)	Lattice Plane	d-spacing (Å)
MoO$_3$	12.8	200	4.52
	33.8	111	1.38
Fe$_2$(MoO$_3$)$_4$	20.5	120	4.10
	21.8	214	3.95
	23.0	220	2.02
	31.4	032	1.43
Mo$_4$O$_{11}$	20.9	011	4.24
	22.2	211	4.00
	23.7	311	3.75
	25.5	601	3.48
MoO$_2$	31.6	101	3.12
	37.1	-211	2.42
B-FeMoO$_4$	19.0	-201	4.66
	26.2	220	3.40
	27.0	-112	3.30
	27.3	-202	3.26
	33.5	-312	2.67
	36.3	400	2.47

Table 3.1 – XRPD Peak list for Figure 3.6 with associated d-spacing and lattice planes.[10,11]

Acknowledgments for the XRPD study go to previous work done in the research group.[1,2]

What this study shows is that the iron molybdate undergoes a reductive phase change a *ca.*450°. This has also been shown in work by other groups.[12] Catalytic testing with an iron molybdate catalyst (Fe$_2$(MoO$_4$)$_3$ + MoO$_3$) with a molybdenum excess of 2.7:1 produced octenes but the highest selectivity was to carbon oxides and aromatics. However there was an increase in conversion seen at 450°C and after this point selectivity towards aromatics rose and carbon oxide production fell. This finding indicated that the reduced form of iron molybdate would be a more promising catalyst for the selective oxidation on *n*-octane to octenes. The reduced iron molybdate is in the form of β-FeMoO$_4$ where the Mo is in the +6 oxidation state and Fe is in the +2 oxidation state.

Upon cooling to 50 °C there is slight but perceptible shift with the peak at 25.5°

corresponding to the (601) lattice plane of Mo_4O_{11} decreasing when the temperature is

lowered from 550 °C to 50 °C. This corresponds with a sharp rise with the reflections at

37.1° and 37.6° which correspond to the lattice planes of (-211) and (-202) of MoO_2.

Potentially while cooling the molybdenum oxide lattice undergoes a rearrangement.

Molybdenum oxide lattice mobility at temperatures above 450 °C is well

documented,[13] suggesting a lattice reordering would be feasible. In addition the peak

at 26.2° corresponding to the (220) lattice planes of β-$FeMoO_4$ undergoes peak

broadening upon cooling to 50 °C. This may be down to a second order phase

transition with a fraction of the (220) lattice plane undergoing a rearrangement to

(202), with the majority remaining as (220). This would result in two discrete peaks but

due to the subtle nature of the transformation the data may have led to peak merging

resulting in the asymmetric broader peak around 26.2° which is observed at 50 °C.

As such the preparation method of forming iron molybdate was modified and a pre-

reduction step using a furnace at 460°C in a reductive atmosphere was added, to see if

there was an improvement on catalytic performance. This is shown in the

experimental chapter. To avoid confusion it is referred to as the "pre-reduced iron

molybdate catalyst". The majority of catalytic data shown in this chapter comes from

this catalyst and if other species (such as the pure phase components of the catalyst)

are used this is made clear.

3.5.3 STRUCTURE OF A PRE-REDUCED IRON MOLYBDATE CATALYST
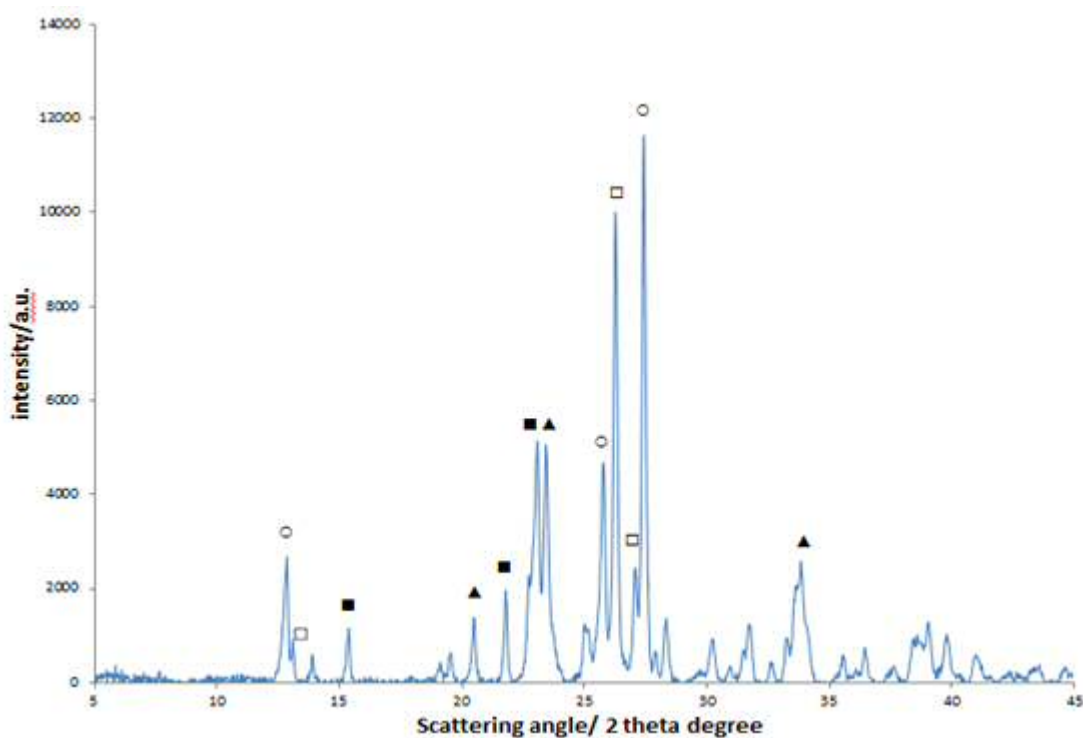
Figure 3.7- XRPD of a pre-reduced iron molybdate catalyst. Phases present: MoO₃ (o),

Fe₂(MoO₃)₄ (■), β-FeMoO₄ (□) and Mo₄O₁₁(▲)

Species	Peak (2 theta degrees)	Lattice Plane	d-spacing (Å)
MoO₃	23.0	011	3.86
	27.4	111	3.37
Fe₂(MoO₃)₄	15.8	110	4.50
	20.5	120	4.10
	23.0	220	2.02
Mo₄O₁₁	20.9	011	4.24
	23.7	311	3.75
	33.6	810	2.66
β-FeMoO₄	12.9	110	6.81
	26.2	220	3.40
	27.3	-202	3.26

Table 3.2 – XRPD Peak list for Figure 3.7 with associated d-spacing and lattice planes.

As Figure 3.7 shows, β-FeMoO$_4$ and Mo$_4$O$_{11}$ are both present after a reduction step in

catalyst preparation. However Fe$_2$(MoO$_4$)$_3$ and MoO$_3$ are still present. This was despite

reducing in 10% hydrogen in argon for 2 hours at 460°C. This can be attributed to hydrogen and octane exhibiting a different ability to reduce the catalyst.

The peak at 23.0° is indicative of $Fe_2(MoO_4)_3$ showing the (220) lattice plane with a spacing of 202 Å. This peak is 100% intensity. When compared with the peak at 26.2° which is indicative of β-$FeMoO_4$ (220) (340 Å) which is also 100% intensity we see that the ratio of β-$FeMoO_4$ to $Fe_2(MoO_4)_3$ is approximately 2:1.

Relative intensity ratios suggest a molybdenum excess to iron of approximately 3:1.
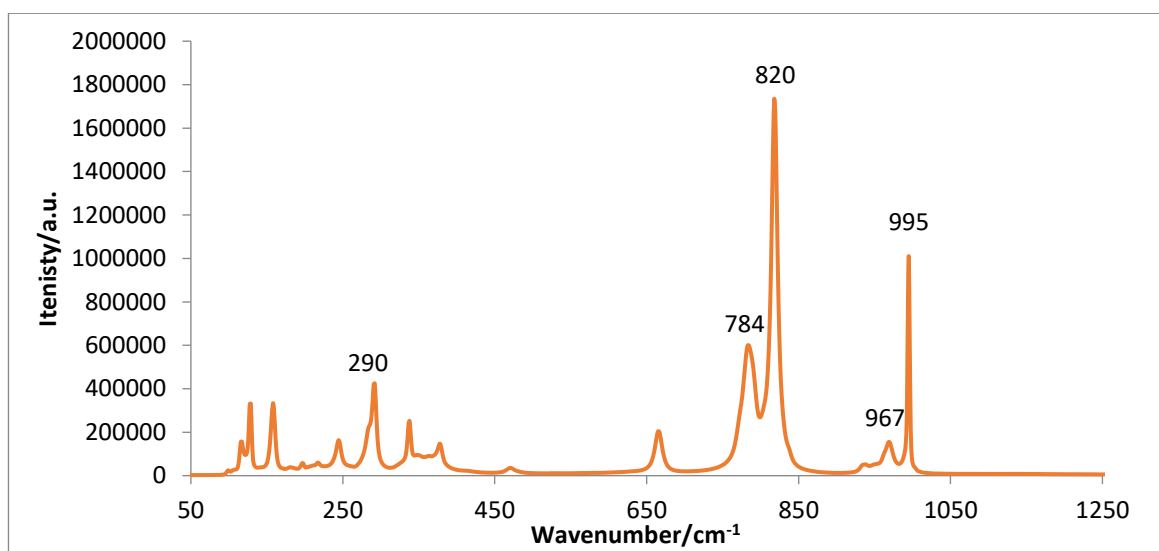
Figure 3.8- Raman spectra of iron molybdate catalyst before reduction step in catalyst preparation
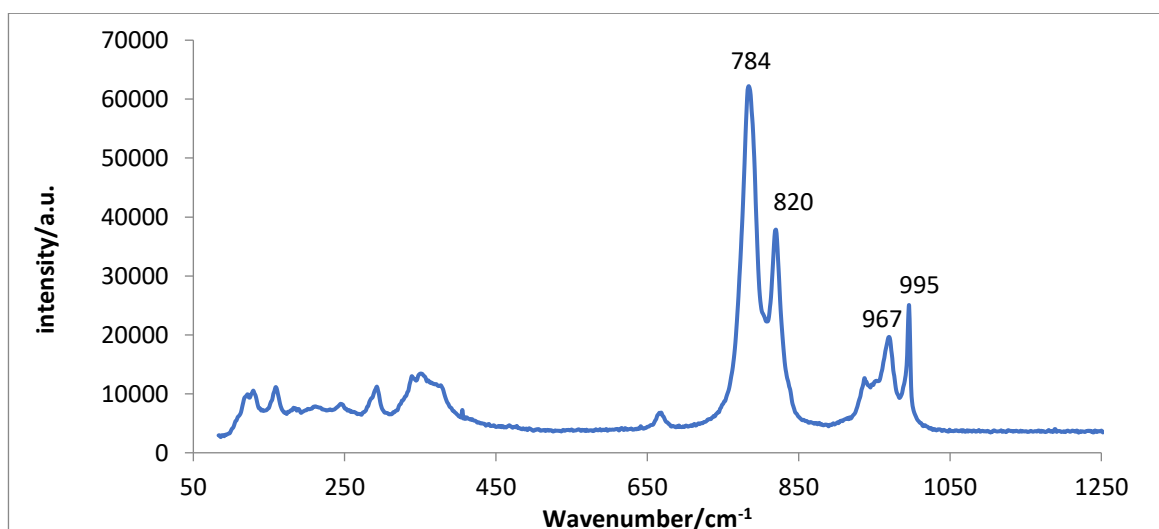
Figure 3.9- Raman spectra of iron molybdate after reduction in catalyst preparation

The Raman spectra in Figure 3.8 shows a reduction has occurred when compared to Figure 3.9 which shows an as prepared iron molybdate catalyst. Peaks at 995cm^{-1} are indicative of the terminal molybdenum oxygen bond in MoO_3. Peaks at 819cm^{-1} are indicative of antisymmetric Mo-O-Mo stretching vibrations in MoO_3. The peaks at 784cm^{-1} and 967cm^{-1} are molybdenum – oxygen vibrations in iron molybdate.[14] The difference in spectra and lower intensity of the peaks at 995 and 821cm^{-1} indicate the reductive phase transition from MoO_3 to Mo_4O_{11} in the bulk molybdenum of the catalyst.

3.5.4 CATALYTIC ACTIVITY OF A PRE-REDUCED IRON MOLYBDATE

A pre-reduced iron molybdate catalyst was tested (1% *n*-octane, 0.2mL catalyst, C:O 8:1). The reductive step is outlined in the experimental chapter. For clarity it is also presented here. Calcined in flowing air (5mL/min) at 260 °C for 4 hours using a heating ramp rate of 5 °C a minute. A final reduction step was then performed by placing the catalyst in a calcination furnace under a 10% hydrogen in argon atmosphere (5mL/min) at 460 °C using a heating ramp rate of 5 °C for 2 hours.

Figure 3.10 – Reaction of 1% *n*-octane (GHSV 1000h[-1], C:O 8:1) over a pre-reduced iron molybdate catalyst. Temperature range from 350-550ºC

Using a pre-reduced iron molybdate catalyst clearly affects selectivity and activity. Although the activity was considerably lower than the highest seen with a $Fe_2(MoO_4)_3$ catalyst (see Figure 3.3) with an octane conversion of *ca.*19% compared to *ca.*52%, there are considerably less carbon oxides present. Selectivity to octenes is also higher, which given that one of the aims of this chapter was to maximise octene selectivity, showed that a pre-reduced iron molybdate was a superior catalyst. This again is similar to previous findings in the group.[2] In Figure 3.7 oxygen consumption rises with temperature and conversion. This provides evidence of oxidative dehydrogenation (ODH) occurring.

Reductive pre-treatment of the catalyst results in reductive phase change of the iron molybdate present in the catalyst. As the catalyst has a molybdenum excess, molybdenum oxides are present, once the reductive pre-treatment occurs, the molybdenum forms Mo_4O_{11} in the place of MoO_3.

This difference in composition of the catalyst leads to very different results. With a pre-reduced catalyst higher selectivity to octenes (the desired products) are observed, and lower selectivity to carbon oxides is found. Overall activity appears to be lower in the pre-reduced catalyst, possibly as a result of the lower levels of burning seen, as a high proportion of activity in the unreduced catalyst can be attributed to the formation of carbon oxides. It would appear the pre-reduced catalyst, $(FeMoO_4 + Mo_4O_{11})$ is a better catalytic system for the oxidative dehydrogenation of *n*-octane to octenes than the unreduced catalyst $(Fe_2(MoO_4)_3 + MoO_3)$.

3.6 EFFECT OF ALTERING THE GHSV ON THE REACTION

Altering the gas hourly space velocity (GHSV) and contact time can alter catalytic activity and selectivity.[15] To see the if octene production could be optimised, the GHSV of the reaction was varied from $1000h^{-1}$ to $4000h^{-1}$. The pre-reduced iron molybdate catalyst was tested (1% *n*-octane, 0.2mL catalyst, C:O 8:1).

Figure 3.11 – Reaction of 1% *n*-octane (GHSV 4000h⁻¹, C:O 8:1) over a pre-reduced molybdate catalyst. Temperature range from 350-550°C

As can be seen, increasing the GHSV and lowering the contact time of the *n*-octane over the catalyst alters the catalytic selectivity. Octenes are the major product between 350-450°C*.* Most strikingly carbon oxides (COx) are not produced at lower temperatures. At temperatures of 450°C and above, catalytic selectivity to COx remains below 20%. At higher temperatures, as with 1000h⁻¹ GHSV, aromatics become the main product.

The result suggests that 4000h⁻¹ is a more suitable GHSV than 1000h⁻¹ for optimising octene production. 400°C appears to be the optimal temperature for giving a good balance between activity and selectivity to octenes

Aromatic selectivity also varies considerably when the contact time is varied. The aromatic selectivity data was examined to observe the effect of altering the GHSV.
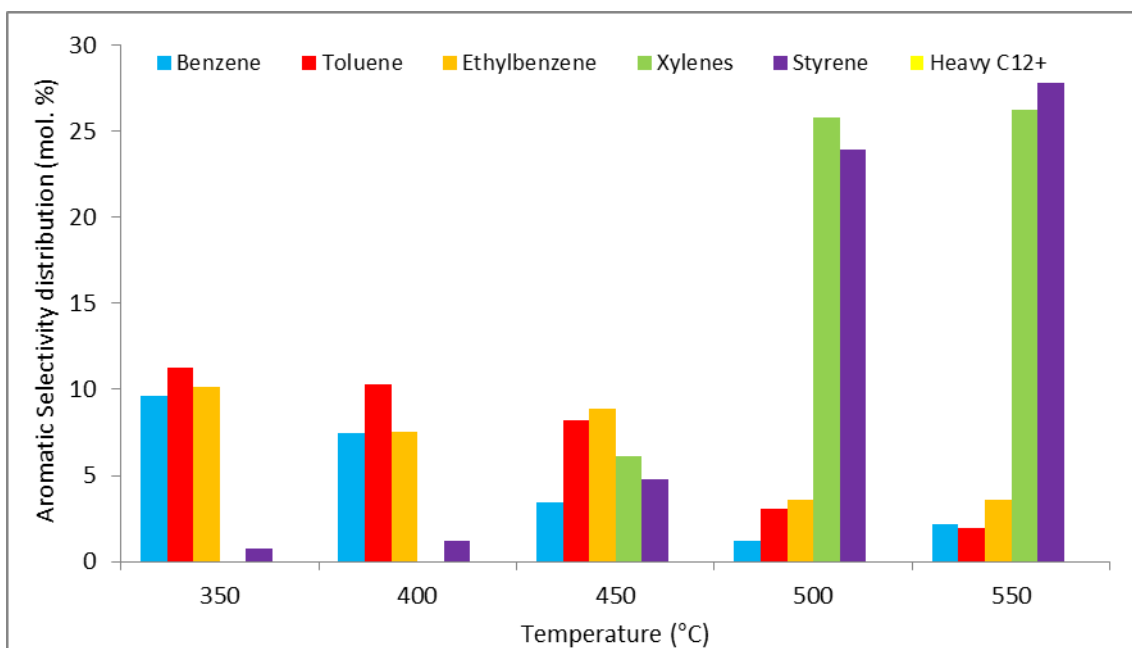
Figure 3.12 – Aromatic selectivity distribution during the reaction of 1% *n*-octane (GHSV 1000h^{-1}, C:O 8:1) over a pre-reduced iron molybdate catalyst. Temperature range from 350-550°C

At 1000 h^{-1} benzene, toluene, ethylbenzene with a trace amount of styrene are present at all temperatures tested. As the temperature increases xylene is produced with selectivity to styrene increasing. This is similar to the findings of Friedrich *et al*[8] where 4% *n*-octane was passed over a magnesium vanadate catalyst. That work showed styrene as the main product as temperature increased. At lower temperature six and seven carbon (C6-C7) aromatics were found to be the main products, whereas eight carbon (C8) aromatics were the main products as the temperature was raised to >450 °C. Ethylbenzene, a C8 aromatic that is present in significant concentrations at lower temperatures, decreases sharply as the temperature increases past 450°C.
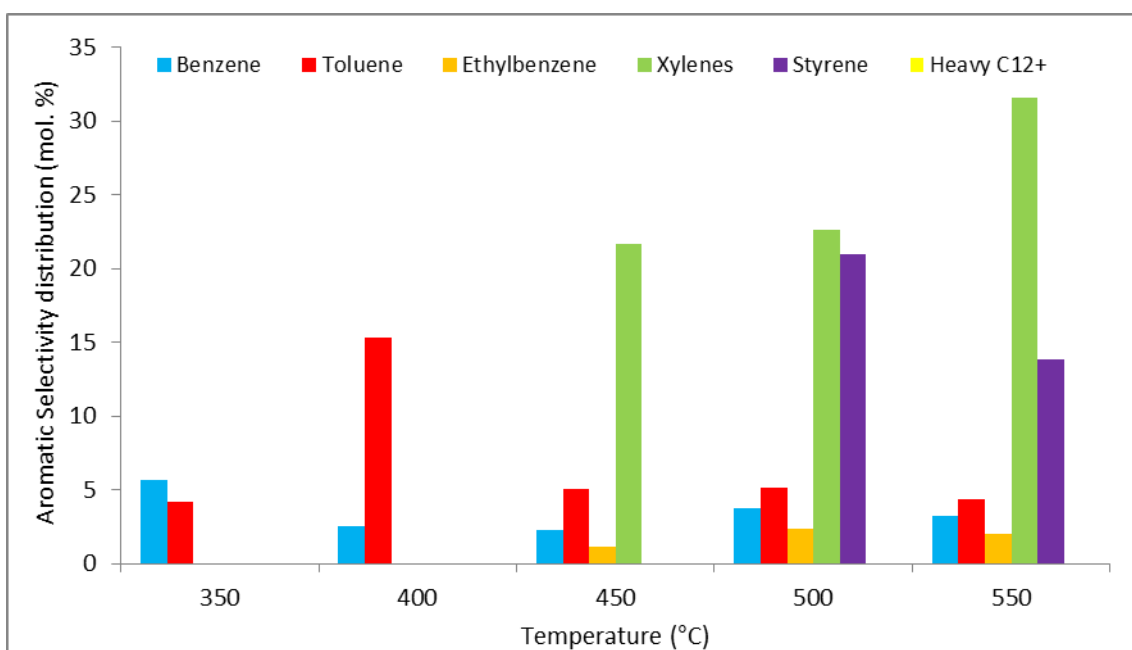
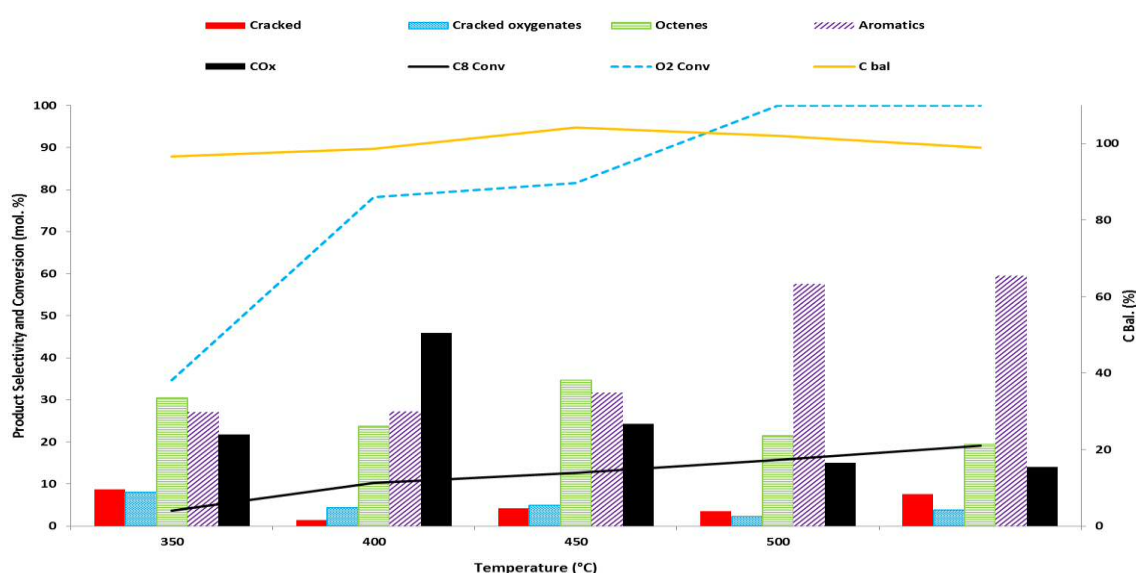**Figure 3.13 – Aromatic selectivity distribution during the reaction of 1% *n*-octane (GHSV 4000h⁻¹, C:O 8:1) over a pre-reduced iron molybdate catalyst. Temperature range from 350-550°C**

At 4000h^{-1} a similar broad trend to figure 1000h^{-1} is observed. At lower temperatures the aromatics present are benzene and toluene, and at higher temperatures greater selectivity towards C8 aromatic species. At lower temperatures (350-400°C) lower overall selectivity to aromatics is observed with higher GHSV. Ethylbenzene and styrene are also not present at 4000h^{-1} when the temperature <450°C. Xylene is the major C8 aromatic product seen with lower contact time.

Clearly altering the GHSV alters catalytic selectivity, higher GHSV (lower contact time) leads to more octenes being produced. Lower GHSV (higher contact time) sees greater selectivity to aromatics and COx species. The product distribution of the aromatics also changes with GHSV. Higher GHSV sees only toluene and benzene present at 400°C and below, while at the same temperature range with lower GHSV, ethylbenzene and styrene are both produced. Higher GHSV also results in xylene as the major aromatic product at higher temperatures, while lower GHSV results in the production of styrene as the main product. Different contact times therefore may favour different ring closing positions at high temperatures. Aromatic formation at lower temperatures sees

benzene and toluene formed which suggests the remaining carbon fraction is what leads to the cracked products seen, or forms carbon laydown at the surface.

3.6.1 INCREASING THE GHSV OF THE REACTION TO 6000H^{-1}

As 4000h^{-1} GHSV was shown to give a higher yield of octenes than 1000h^{-1} GHSV, 6000h^{-1} GHSV was tested (1% *n*-octane, 0.2mL catalyst, C:O 8:1).
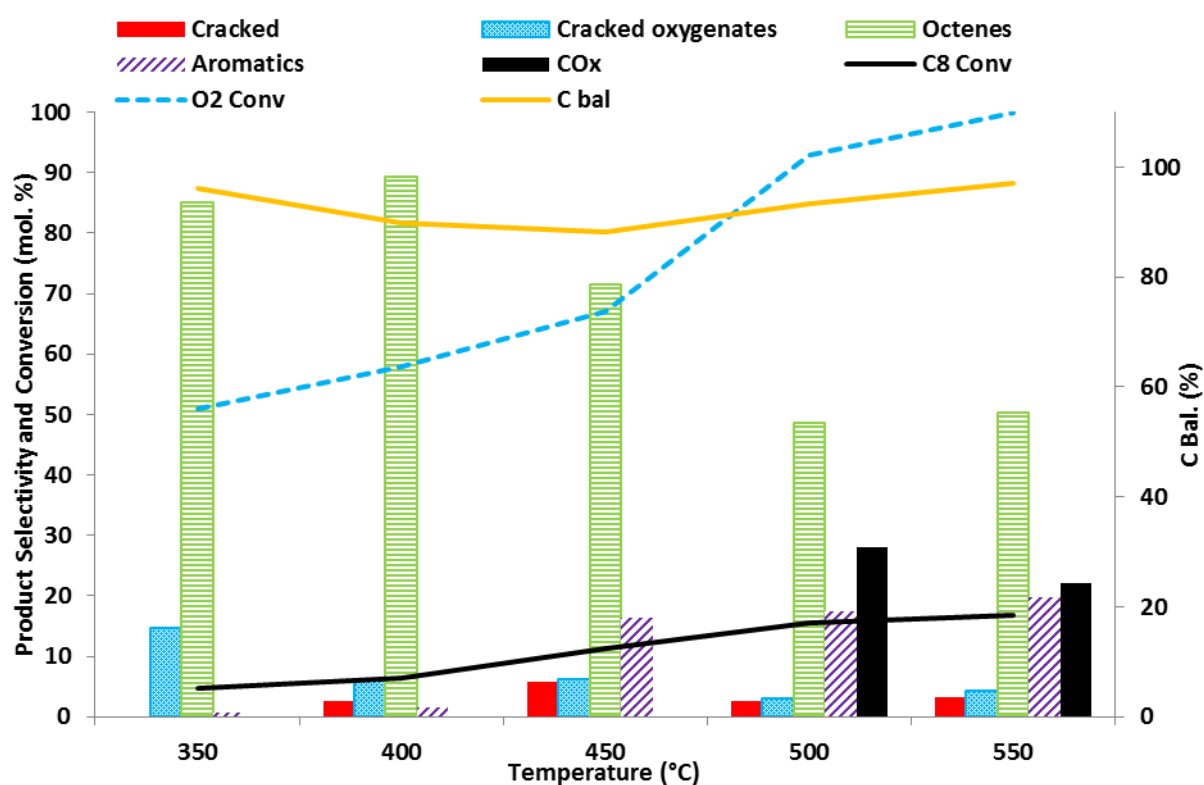
Figure 3.14 –Reaction of 1% *n*-octane (GHSV 6000h^{-1}, C:O 8:1) over a pre-reduced iron molybdate catalyst. Temperature range from 350-550°C

The selectivity to octenes is at *ca.*91% at 400°C when the GHSV is raised to 6000h^{-1}. Octenes remain the dominant product throughout, 400°C offers the highest selectivity with an octane conversion of *ca.*6.5%. This octane conversion is lower than at experiments done at 400°C with lower GHSVs. This is not unexpected as a lower contact time over the catalyst could result in less reactant being converted to products.[16] At 350°C cracked oxygenates, chiefly propanoic acid and pentanol. are present at higher concentrations than seen in any of the temperature ranges at lower

GHSVs. At higher temperatures selectivity to carbon oxides and aromatics rises. The aromatic species formed are examined below in Figure 3.15.

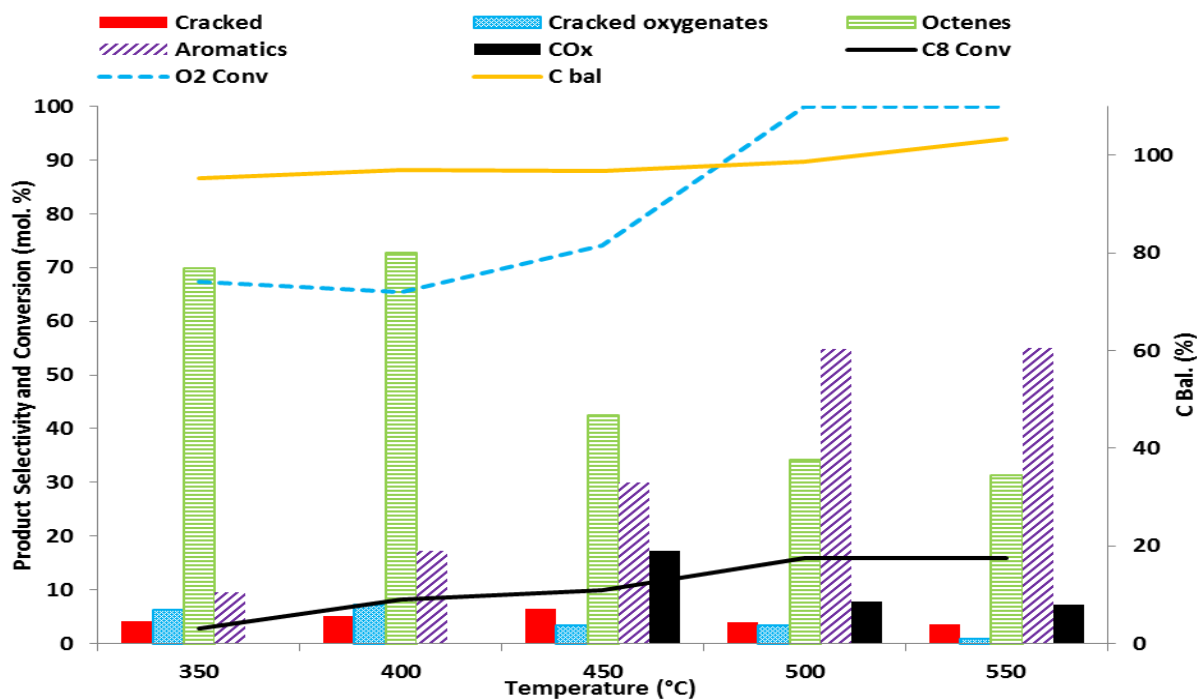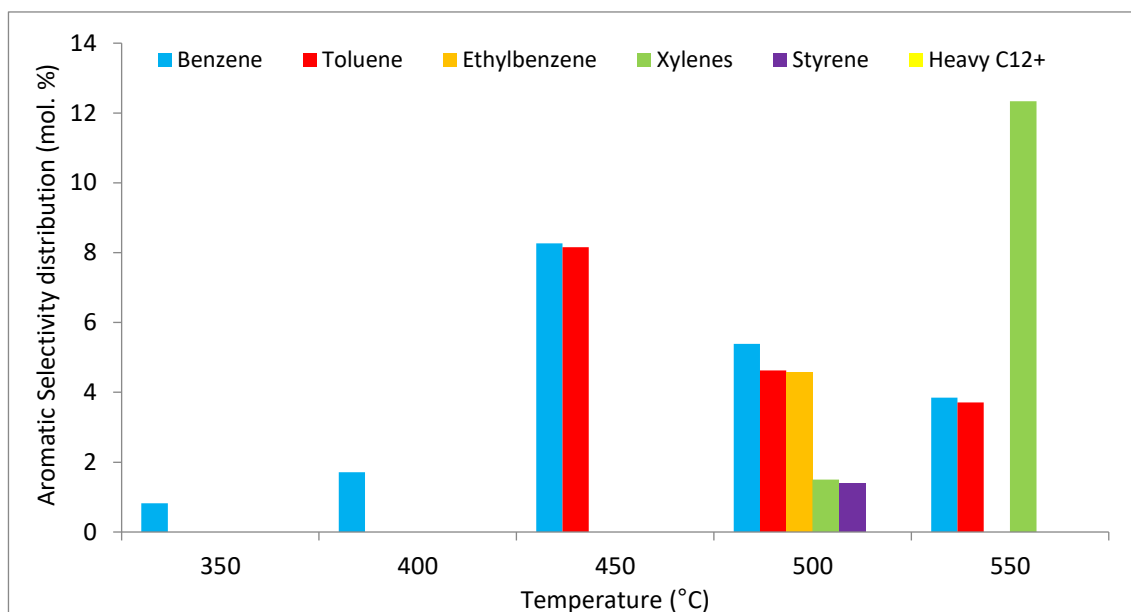**Figure 3.15 – Aromatic selectivity distribution during the reaction of 1% *n*-octane (GHSV 6000h^{-1}, C:O 8:1) over a pre-reduced iron molybdate catalyst. Temperature range from 350-550ºC**

As can be seen in Figure 3.15 between 350-450ºC no 8 carbon aromatics are seen, only benzene at lower temperatures before toluene is observed at 450ºC. This is in marked contrast to the aromatic species produced at the 350-450ºC temperature range with a GHSV of 1000h^{-1} (see Figure 3.12) where C8 aromatics such as ethylbenzene and styrene are present at 350ºC. The only C8 aromatic seen in any notable levels is xylene at 550ºC.

The aromatic data seen at 1% *n*-octane, 8:1 carbon to oxygen ratio, over the pre-reduced iron molybdate catalyst, gives the following trends: Firstly at lower temperatures, benzene and toluene are the main aromatic products, this is notable because a C8 feedstock in octane is being fed into the reactor, this suggest would suggest some level of cracking then aromatisation. Secondly, at 1000h^{-1} GHSV some C8 aromatics are observed from 350ºC and above, this is not seen at higher GHSVs. Thirdly, at higher temperatures we see C8 aromatics, at 1000h^{-1} GHSV the highest

selectivities at 500-550°C are to both xylene and styrene (see Figure 3.10), at higher GHSVs (figures 3.9 and 3.11) it is to xylene. Finally, if styrene is produced, COx is also being produced, if the corresponding main product selectivity chart is checked.

3.6.2 COMPARISON OF VARIOUS GHSVS AT 1% *N-OCTANE*

As shown previously, altering the GHSV affects the catalytic activity and selectivity. Below are two charts showing the catalytic data at two set temperatures; 400°C and 550°C, with the GHSV being only parameter altered.

Figure 3.16 – Catalytic activity and selectivity during the reaction of 1% *n*-octane (Temperature held at 400°C, C:O 8:1) over a pre-reduced iron molybdate catalyst. Gas hourly space velocity range from 1000-6000h^{-1}

As Figure 3.16 shows higher GHSV increases selectivity to octenes. Lower GHSV leads to higher aromatic formation, presumably at the expense of octenes. The notable difference between 1000h^{-1} GHSV at 400°C and 4000h^{-1} GHSV is the formation of carbon oxides. No carbon oxides are produced at 4000 and 6000h^{-1} GHSV when at 400°C. Lower GHSV also leads to greater oxygen consumption (see the blue dotted

line) and conversion (black solid line). Octane conversion falls from a high of *ca.*10.3% at 1000h^{-1} to *ca.*6.2% at 6000h^{-1}.
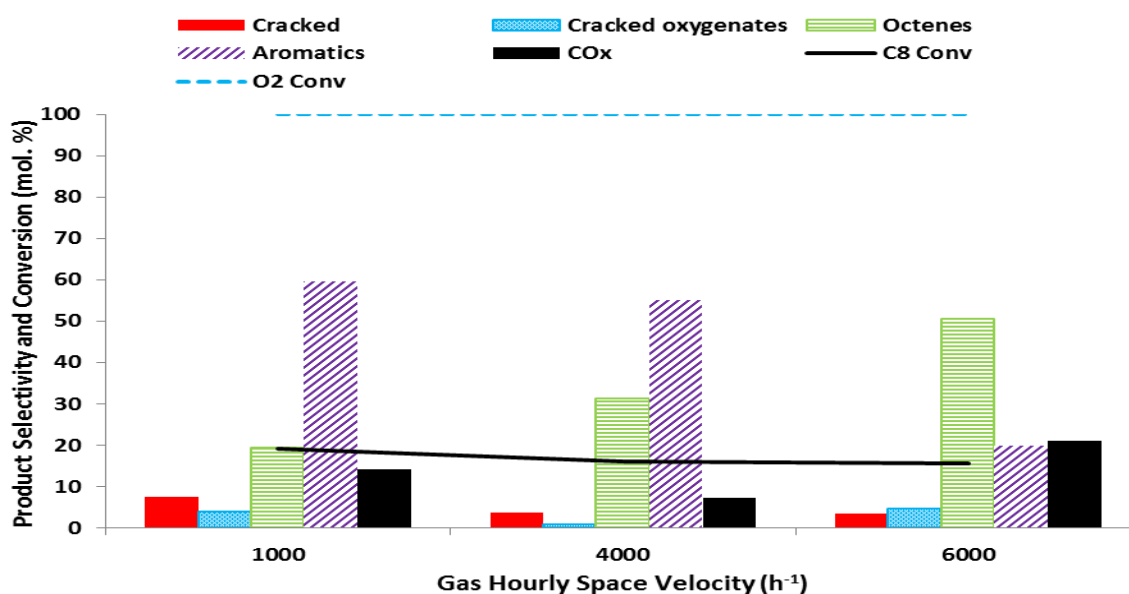
Figure 3.17 – Catalytic activity and selectivity during the reaction of 1% n-octane (Temperature held at 550°C, C:O 8:1) over a pre-reduced iron molybdate catalyst. Gas hourly space velocity range from 1000-6000h^{-1}

Altering the GHSV at 550°C shows similar trends. Lower GHSV leads to higher octane conversion, presumably from greater contact time at the catalyst surface. As can be seen on Figure 3.17, conversion goes from *ca.*19.5% at 1000h^{-1} GHSV down to *ca.*15.7% at 6000h^{-1} GHSV. Higher gas hourly space velocity also shows the same trend to greater octene selectivity, as in Figure 3.18. At this higher temperature, a lower GHSV also shows greater levels of cracked products. No oxygen was observed at 550°C which suggested that oxygen consumption was at 100%.

Higher GHSV (lower contact time) leads to lower octane conversion, as expected. However selectivity to octenes increases with higher GHSV, while levels of aromatics produced falls. Once 4000h^{-1} GHSV at 400°C is reached no carbon oxide is detected and a corresponding fall in oxygen consumption is observed.

3.6.3 ALTERING THE CARBON TO OXYGEN (C:O) RATIO AT 1% *N*-OCTANE

Another parameter that can be altered in addition to temperature and GHSV is the carbon to oxygen (C:O) ratio. In all of the results shown in this chapter so far, the C:O ration has been 8:1. That is, 8 carbon atoms to one oxygen in the gas feed of octane, oxygen and helium (as a carrier gas) being fed into the catalytic reactor bed. Other C:O ratios were tested and the results are shown in this section. Firstly a "lean" gas mixture was tested with a C:O ratio of 2:1. Then a gas "rich" mixture with a C:O ratio of 12:1 was tested. Temperatures of 400°C and 550°C were tested, as 400°C has been shown to be the optimal temperature for octene production, while 550°C produces aromatics as the major products. Anaerobic testing, that is, a C:O ratio of 8:0 is explored in depth in the next chapter so is not discussed here.
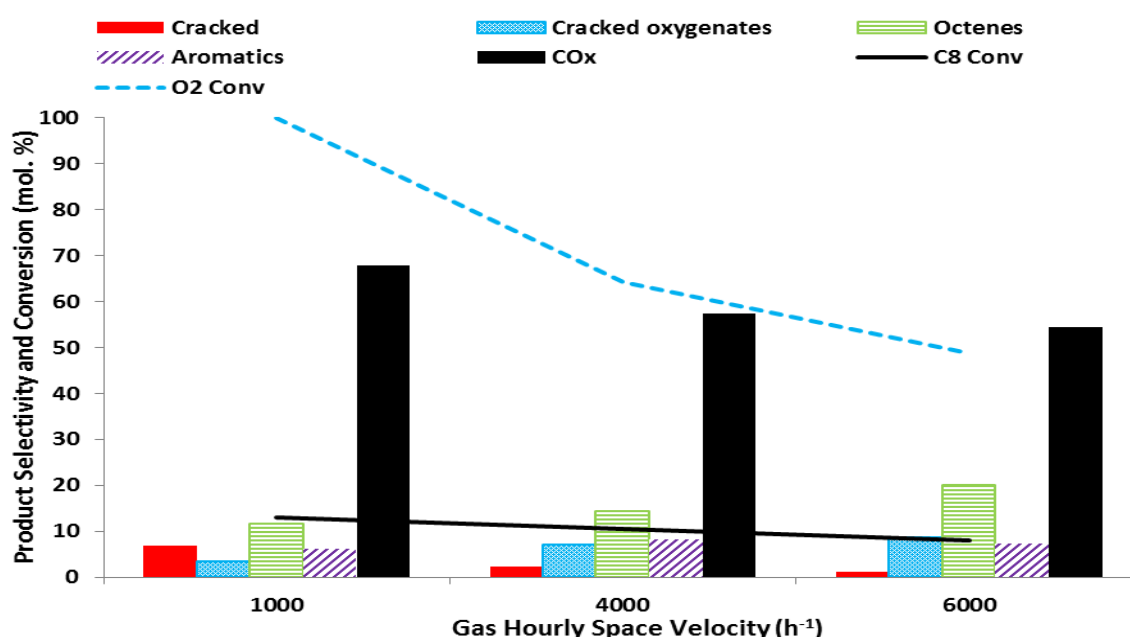
Figure 3.18 – Catalytic activity and selectivity during the reaction of 1% n-octane (Temperature held at 400°C, C:O 2:1) over a pre-reduced iron molybdate catalyst. Gas hourly space velocity range from 1000-6000h^{-1}

As expected, raising the level of oxygen in the gas feed increased the production of carbon oxides compared to a C:O ratio of 8:1. Octane conversion is also higher at *ca.*13.8% at 1000h^{-1} GHSV, than the 10.3% seen in Figure 3.14. This trend in higher conversion is also seen at higher GHSV. Octene production increased as GHSV increased from *ca.*11.7% at 1000h^{-1} to *ca.*20.1% at 6000h^{-1}. Clearly from the perspective of optimising octenes production a C:O ratio of 2:1 is inferior to 8:1.
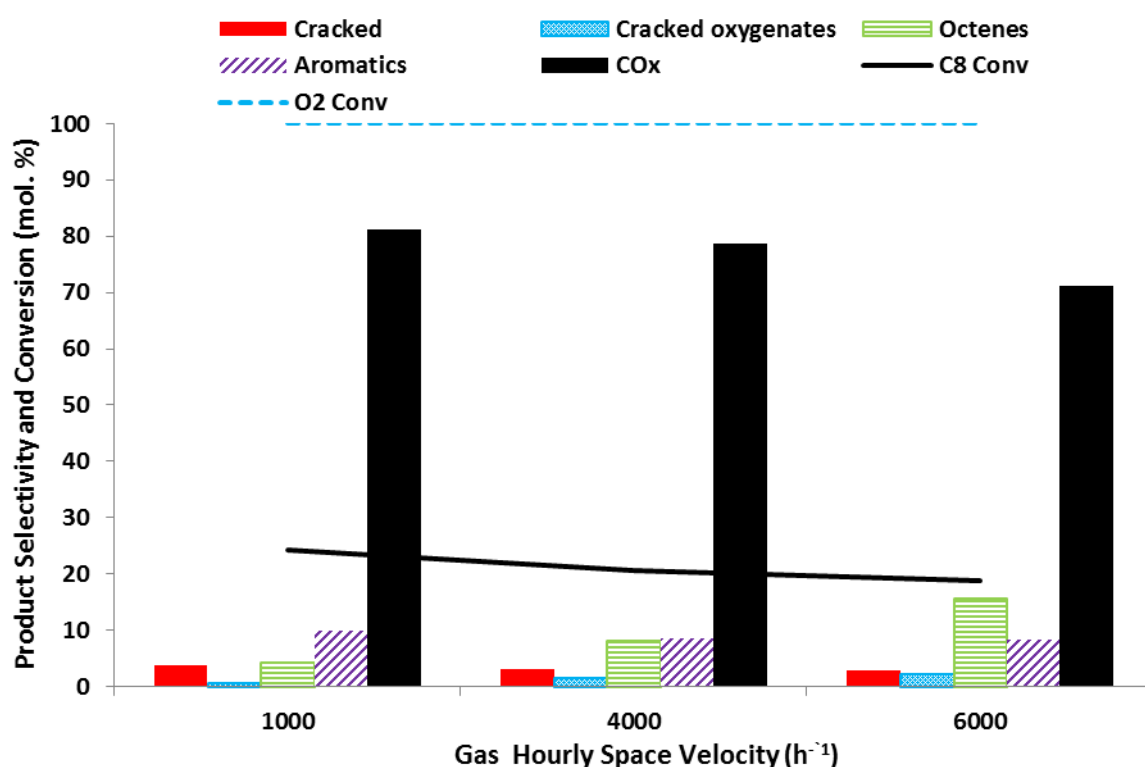
Figure 3.19 – Catalytic activity and selectivity during the reaction of 1% n-octane (Temperature held at 550°C, C:O 2:1) over a pre-reduced iron molybdate catalyst. Gas hourly space velocity range from 1000-6000h^{-1}

As Figure 3.19 shows there is a high octane conversion when the C:O ratio is 2:1 and the temperature is held at 550°C. The highest conversion once again, is found with the highest contact time at *ca.*23.9% . However the main selectivity is to carbon oxides.
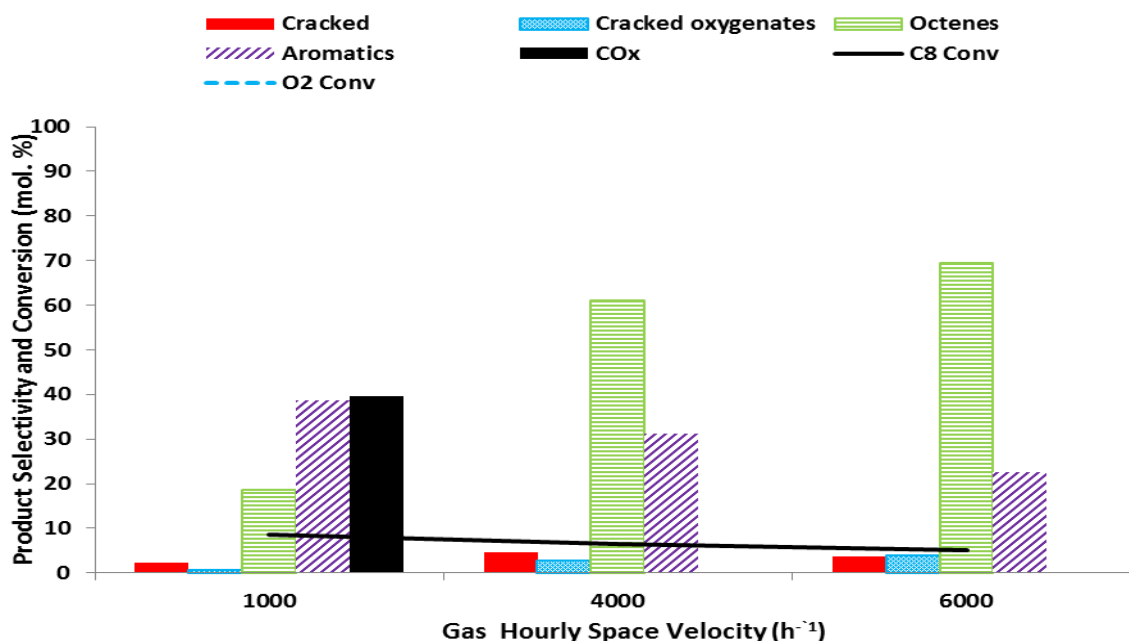
Figure 3.20 – Catalytic activity and selectivity during the reaction of 1% n-octane (Temperature held at 400°C, C:O 12:1) over a pre-reduced iron molybdate catalyst. Gas hourly space velocity range from 1000-6000h^{-1}

Compared to a carbon to oxygen ratio of 8:1 lower octane conversion is observed (see Table 3.3). Higher GHSV sees an increase in selectivity to octenes and no carbon oxides produced above 4000h^{-1}. Aromatic species are the secondary product formed. In comparison to the 8:1 C:O experiment at 400°C (see Figure 3.14) higher concentrations of aromatic species are seen at 12:1 C:O ratios. This means that an 8:1 C:O ratio is superior for octene production than 12:1, as both selectivity to octenes and octane conversion are higher.

Gas hourly space velocity (h^{-1})	Octane conversion (%) at 8:1 C:O ratio	Octane conversion (%) at 12:1 C:O ratio
1000	10.3	8.2
4000	8.7	6.4
6000	6.2	5.1

Table 3.3 – Comparison of octane conversion over varying GHSV between differing carbon to oxygen ratios at 400°C
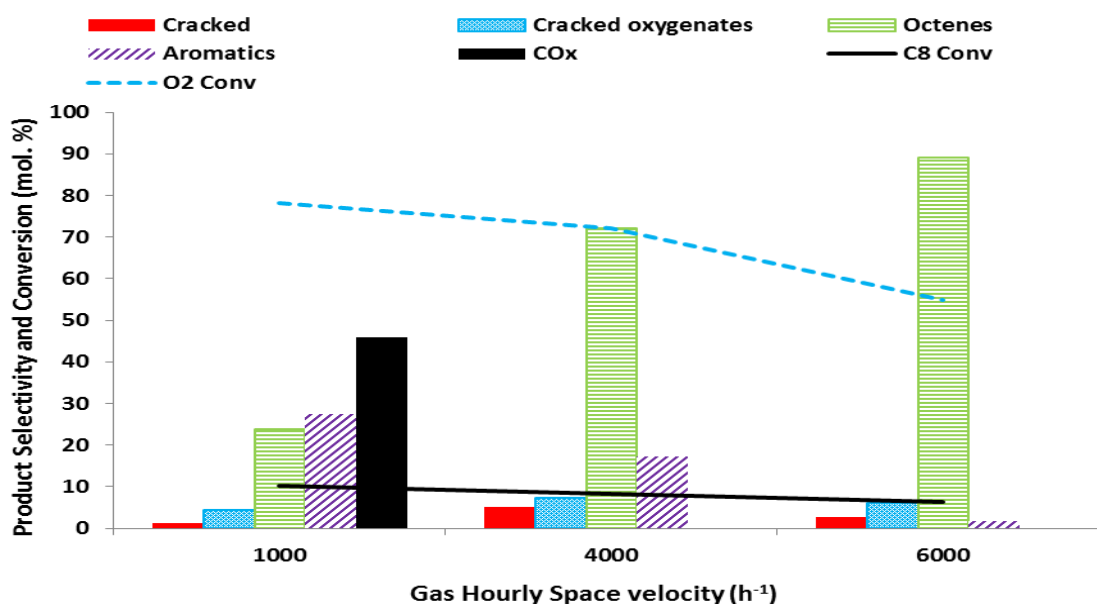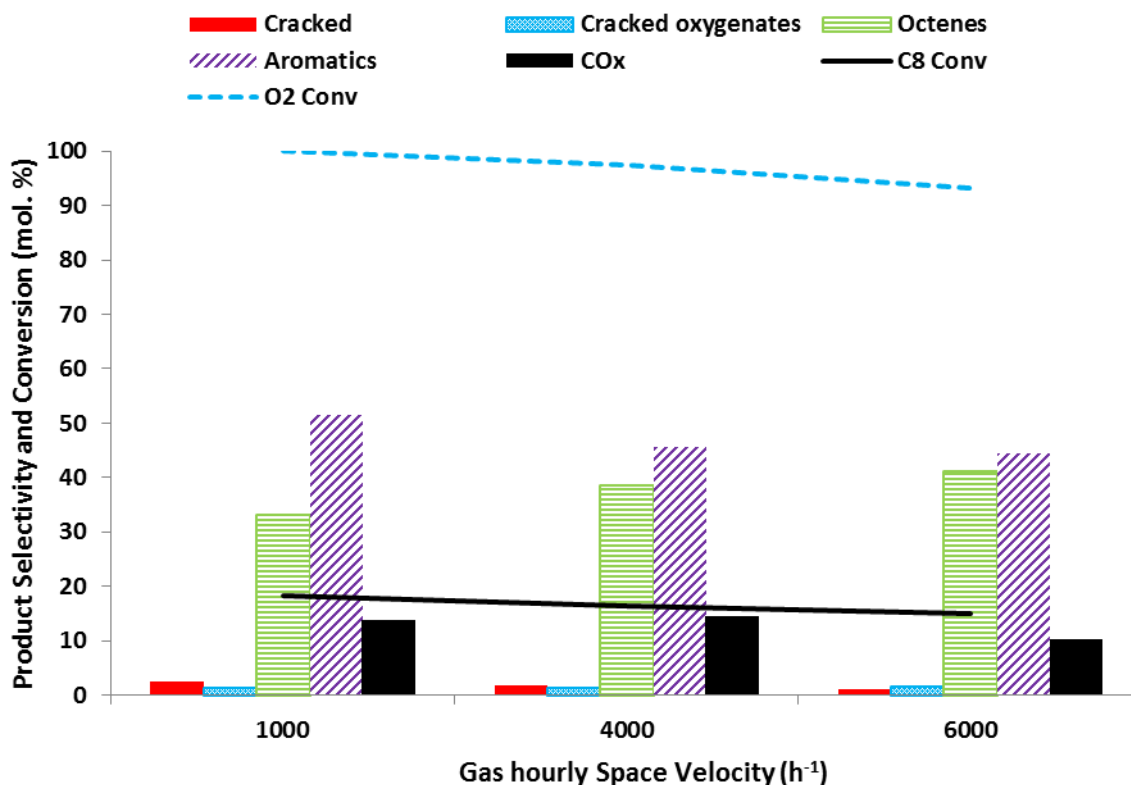
Figure 3.21 – Catalytic activity and selectivity during the reaction of 1% n-octane (Temperature held at 400°C, C:O 12:1) over a pre-reduced iron molybdate catalyst. Gas hourly space velocity range from 1000-6000h^{-1}

Again the higher carbon to oxygen ratio results in lower octane conversion. Selectivity is similar to 8:1 C:O. The main difference of having a higher proportion of octane relative to oxygen in the gas feed is that higher selectivity to aromatics.

Having a gas lean (C:O 2:1) feed into the reactor results in a very high selectivity to carbon oxides. Conversion, and thus catalytic activity, is higher than a carbon of oxygen ratio of 8:1 but the desired product of octenes is only produced at low levels.

Having a gas rich (C:O 12:1) feed into the reactor results in similar selectivity seen when the carbon to oxygen ratio is 8:1. However conversion (see Table 3.3) is lower and leads to an overall yield of octenes that is lower than when the C:O ratio is 8:1.

3.7 CATALYTIC TESTING OF THE PURE PHASE COMPONENTS OF THE CATALYST

Iron molybdate catalysts with an excess of molybdenum[7,14,17] will have several different species present. Both iron molybdate and molybdenum oxides[7] of varying types. As discussed at the beginning of this chapter, the catalyst tested underwent a reductive pre-treatment, which produced ferric molybdate ($FeMoO_4$) and MoO_3, Mo_4O_{11} and MoO_2 species. This was confirmed by XPRD (see figures 3.4 and 3.6). In this section the pure phase species; $FeMoO_4$, MoO_3 and MoO_2 were tested. Mo_4O_{11} is difficult to prepare, and is best understood as a partially reduced MoO_3 species[18], so was not tested.

For each species a catalytic activity and selectivity study at $4000h^{-1}$ is shown between 350-550°C. Then activity and selectivity profiles over varying GHSVs are considered at 400°C (shown above to optimal for octene production) and 550°C (which has the highest activity and a high selectivity to aromatics). Aromatic selectivity is also shown. Each "pure phase" species was obtained from Sigma-Aldrich and was checked by XPRD and Raman spectroscopy to confirm purity.

3.7.1 FeMoO$_4$– Ferrous Molybdate
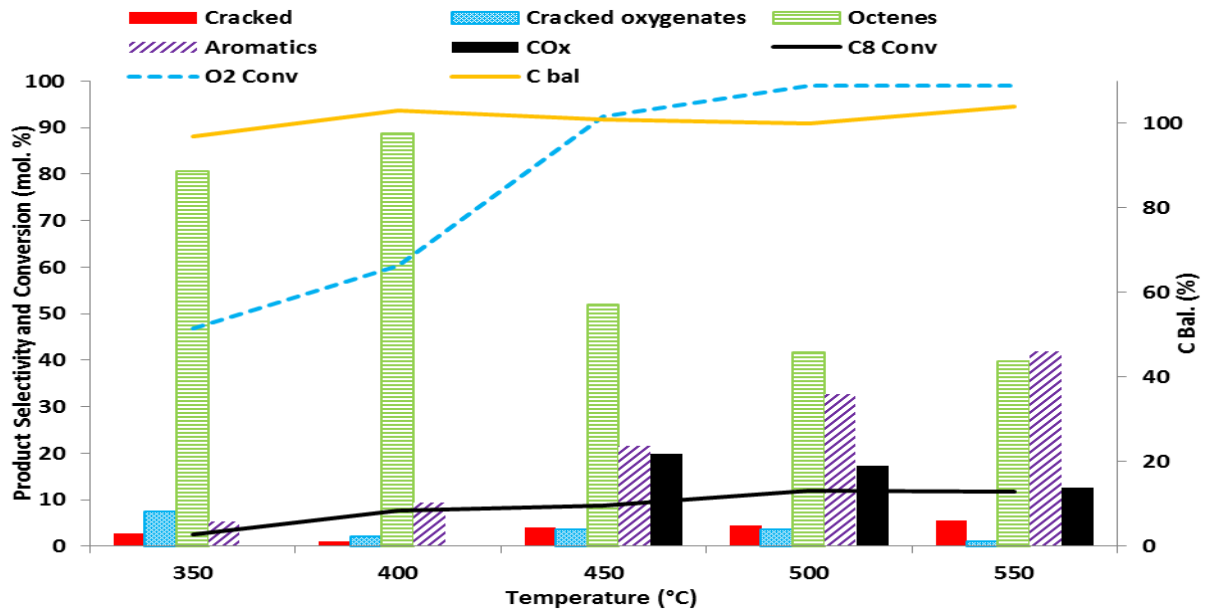
Figure 3.22 –Reaction of 1% *n*-octane (GHSV 4000h^{-1}, C:O 8:1) over pure phase FeMoO$_4$. Temperature range from 350-550°C

Figure 3.22 shows that FeMoO$_4$ is very similar in selectivity to the pre-reduced catalyst but with a higher selectivity to octenes, with a catalytic selectivity of *ca.*85% at 400°C. This compares to *ca.*73% at the same conditions for the pre-reduced catalyst. This would suggest FeMoO$_4$ is an active component of the catalyst. However octane conversion is lower (see Table 3.4), suggesting that the molybdenum oxide species also play a catalytic role in reaction.[7] Much lower levels of aromatics at lower temperatures are produced when pure phase FeMoO$_4$ is used as a catalyst instead of a catalyst with molybdenum oxides present.

Species	Pre-reduced catalyst, molybdenum excess	Pure phase FeMoO$_4$
Octane conversion at 400°C	8.7%	7.8%
Selectivity to octenes at 400°C	73.2%	85.4%
Octane conversion at 550°C	14.7%	11.6%
Selectivity to octenes at 550°C	28.5%	38.2%

Table 3.4 – Comparison of octane conversion and selectivity to octenes at 400°C & 550°C between pure phase FeMoO$_4$ and a pre-reduced iron molybdate catalyst with 2.7:1 molybdenum to iron excess. (8:1 C:O, 4000h^{-1}, 1% *n*-octane)

As we will see further in this section, pure molybdenum oxides do have a high selectivity to aromatic species. The absence of these would offer an explanation for the low levels of aromatic species formed between 350-400°C when a pure FeMoO$_4$ catalyst is used.
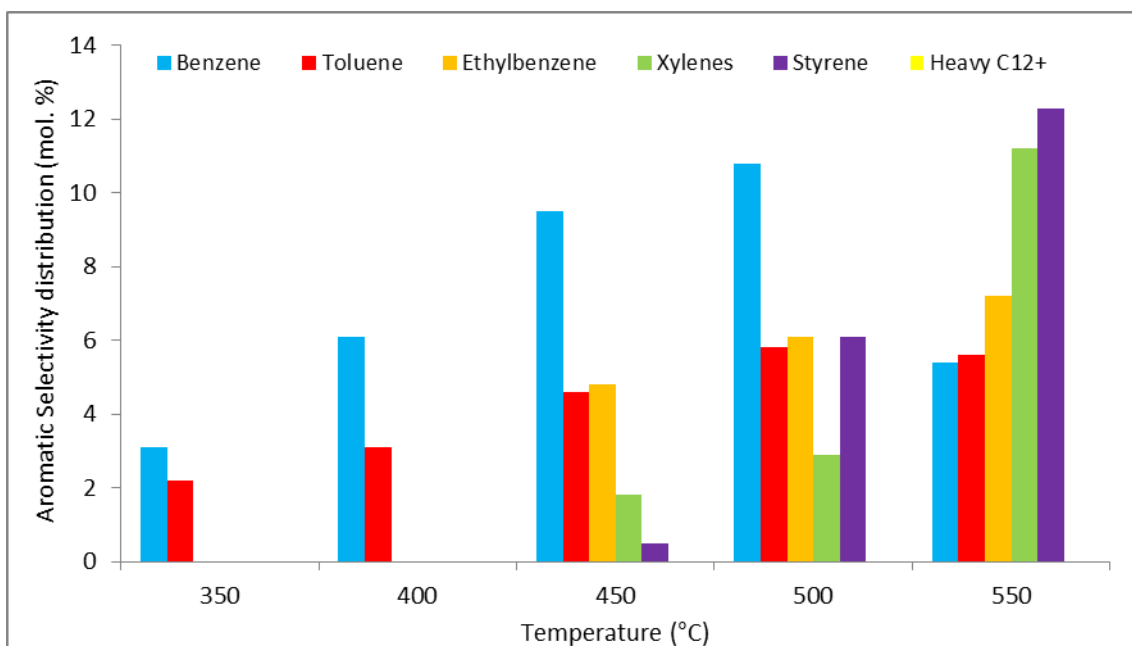
Figure 3.23 – Aromatic selectivity distribution during the reaction of 1% *n*-octane (GHSV 4000h^{-1}, C:O 8:1) over a FeMoO$_4$ catalyst. Temperature range from 350-550°C

Aromatic selectivity shows one notable difference to a pre-reduced catalyst at the same conditions (see Figure 3.13). As with a catalyst that has a molybdenum excess, FeMoO$_4$ produces benzene and toluene at lower temperatures, before 8-carbon

aromatics (styrene, ethylbenzene and xylene) appear at higher temperatures. Notably however, high levels of benzene are seen even at 500°C when FeMoO$_4$ was the catalyst. With the pre-reduced catalyst this was not seen. Benzene and toluene are minor products at 500°C. Having 6 and 7-carbon aromatics formed from an 8-carbon feedstock suggests cracking in addition to an aromatisation reaction.

This higher level of cracking could be attributed to more exposed iron species at the surface of the catalyst.[19,20] It has been widely postulated that the surface of iron molybdate catalysts have a monolayer of molybdenum oxide at the catalyst surface.[21] It would be expected that a catalyst with a 1:1 iron to molybdenum ratio would not have such a layer of molybdenum oxide, and iron sites would be present at the surface. X-ray photoelectron spectroscopy confirmed a greater proportion of iron sites at the surface in FeMoO$_4$ than a catalyst with a molybdenum excess. The data showing how pure phase iron molybdate has a higher percentage of iron at the surface is shown in Table 3.9 at the end of this chapter. Pure phase FeMoO$_4$ has >14% of the surface as iron while with the pre-reduced catalyst with a molybdenum excess, the value is <7%.

3.7.2 MoO3 – Molybdenum trioxide.

Molybdenum trioxide possesses the Mo(VI) oxidation state . It is reduced to MoO$_2$ which possesses the Mo(IV) oxidation state. Transient species such as Mo$_4$O$_{11}$ also exist, where some of the MoO$_3$ in the lattice lose its terminally bonded oxygen before complete reduction to MoO$_2$.[18,22]

As MoO$_3$ is still present in the pre-reduced iron molybdate catalyst tested throughout this chapter, it was of interest to see how it would act as a catalyst for the reaction of 1%-*n*-octane.
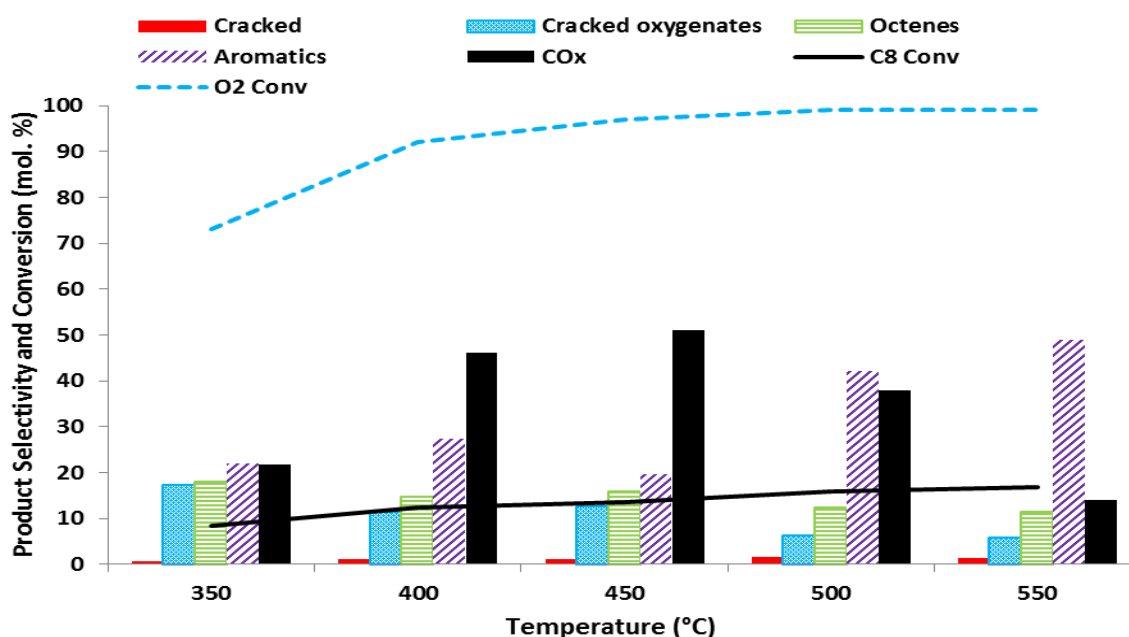
Figure 3.24 –Reaction of 1% *n*-octane (GHSV 4000h^{-1}, C:O 8:1) over a pure phase MoO$_3$ catalyst. Temperature range from 350-550ºC

Molybdenum trioxide decomposes from temperatures of 350ºC and above. This is different from FeMoO$_4$. It also shows low selectivity to octenes and high selectivity to aromatics. Cracked oxygenates are also observed in higher concentrations than when FeMoO$_4$ or the pre-reduced iron molybdate catalyst was tested at the same conditions. Activity was relatively high with the lowest octane conversion seen at 350ºC being *ca.*8.3%. This high activity is likely due to the ready selectivity to carbon oxides.
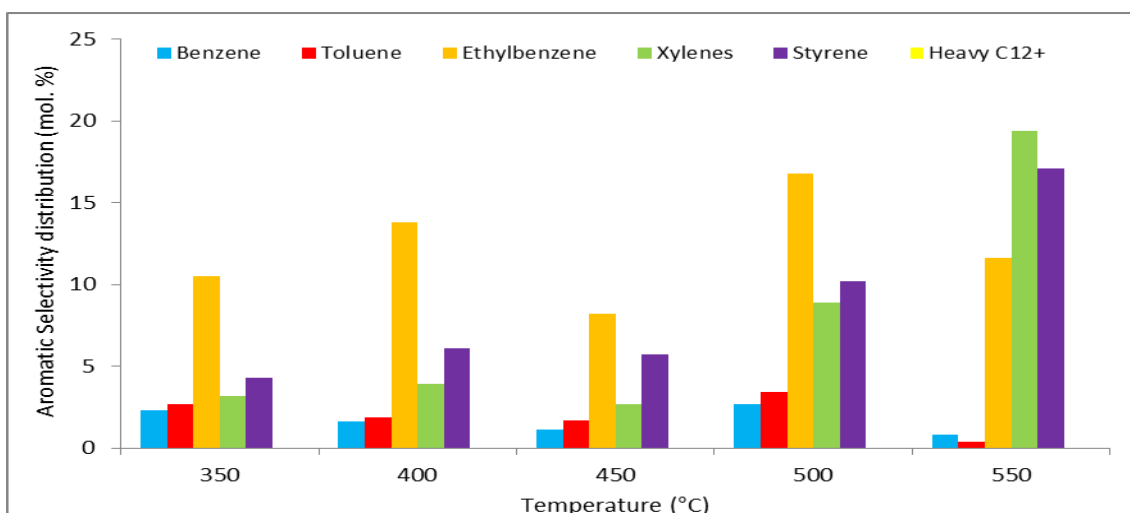
Figure 3.25 – Aromatic selectivity distribution during the reaction of 1% *n*-octane (GHSV 4000h^{-1}, C:O 8:1) over a MoO$_3$ catalyst. Temperature range from 350-550ºC

As can be seen in Figure 3.25, MoO_3 has very high selectivity to 8-carbon aromatic species. Very low levels of toluene and benzene are observed but none in high levels. This is in direct contrast to $FeMoO_4$ (see Figure 3.23) which produced high levels of benzene. This suggests that MoO_3 acts at lower temperatures as the main species causing aromatisation with $FeMoO_4$ causing cracking of the 8-carbon aromatic to benzene or toluene. At higher temperatures, both $FeMoO_4$ and MoO_3 produce high levels of aromatics. With MoO_3 xylenes and styrene replace ethyl benzene as the temperature increases.

Increasing the gas hourly space velocity to $6000h^{-1}$ sees aromatic selectivity rise at the expense of carbon oxides, but burning still at all the temperature profiles tested.

3.7.3 MoO_2 – Molybdenum dioxide

The last pure phase species examined to see its catalytic activity and selectivity on *n*-octane. MoO_2 is produced, as seen at the beginning on this chapter (see Figure 3.6) when iron molybdate catalysts reach temperatures of $460^{\circ}C$ and above. As MoO_2 can be thought of as a MoO_3 molecule minus the terminally bonded oxygen, it was of interest to see how a molybdenum surface with oxygen vacancies would act.
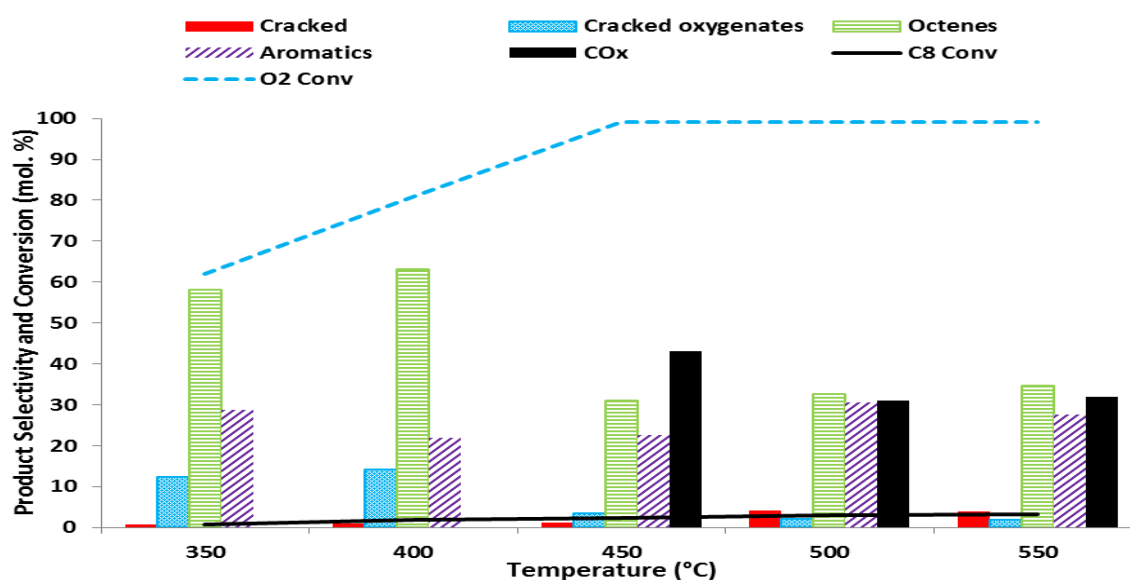
Figure 3.26 –Reaction of 1% *n*-octane (GHSV $4000h^{-1}$, C:O 8:1) over a pure phase MoO_2 catalyst. Temperature range from 350-550°C

It is immediately apparent that MoO_2 has a very low catalytic activity, with octane conversions no higher than *ca.*3.2%. This is in contrast with MoO_3 which had considerably higher conversion. Unlike MoO_3, MoO_2 shows high selectivity to octenes at 400^oC (*ca.*63.4%). This selectivity to octenes is still lower than that exhibited by $FeMoO_4$. No burning or selectivity to carbon oxides is shown at 400^oC or lower. Appreciable levels of cracked oxygenates are observed at lower temperatures before dropping sharply at 450^oC and above. A slight increase in cracked products is seen at 500^oC and 550^oC. This cracking can also be seen in the aromatic selectivities.

Figure 3.27 – Aromatic selectivity distribution during the reaction of 1% *n*-octane (GHSV 4000h^{-1}, C:O 8:1) over a MoO_2 catalyst. Temperature range from 350-550ºC

Interestingly the majority of aromatic species produced are "heavy" aromatics with carbon chains of 12 or longer. The most common species formed were naphthalene and ethyl-napthalene. Very low levels of benzene and toluene are seen until 500^0C and 550^oC when cracking occurs in higher levels (see Figure 3.26). At higher temperatures 8-carbon chain aromatics start to be formed. This is in contrast to MoO_3 which produced 8-carbon aromatics from 350^oC.

FeMoO$_4$ as a catalyst shows similar selectivity to the pre-reduced catalyst, however conversion is slightly lower. This suggests that the active species for catalytic ODH is FeMoO$_4$. Further work on pure FeMoO$_4$, namely time on line (TOL) studies and anaerobic studies, is shown in chapter 4. Benzene is formed readily which suggests iron sites are responsible for catalytic cracking.

MoO$_3$ is highly selective to aromatics and carbon oxides. It also forms higher levels of cracked oxygenates than the pre-reduced catalyst. It has a higher catalytic activity than FeMoO$_4$. 8-carbon aromatics are seen at lower temperatures when the GHSV is 4000h^{-1} unlike the pre-reduced catalyst and FeMoO$_4$. It would appear that the terminally-bonded oxygen on MoO$_3$ is highly active in a Mars-Van Krevelen ODH style mechanism.

This hypothesis is supported by the very low catalytic activity exhibited by MoO$_2$ as there is no terminally bonded oxygen present just a surface vacancy. MoO$_2$ does exhibit higher selectivity to octenes than MoO$_3$. It does not burn at 400°C when the gas hourly velocity is 4000h^{-1}, like FeMoO$_4$ and the pre-reduced catalyst. The major aromatic species produced are 12 carbon chain or larger. As the temperature increases higher levels of styrene and xylene are observed in line with other results. Clearly the oxygen vacancy on MoO$_2$ encourages the formation of naphthalene and ethyl-napthalene.

3.8 SCALING UP THE PROCESS – INCREASING *N*-OCTANE TO 10% OF THE GAS FEED

All of the work shown far was conducted with the concentration of *n-octane* in the gas feed being 1%. As in industry this would not be feasible, the Honeywell UOP method uses much higher concentrations of alkane[23], the concentration of *n*-octane was raised to 10% to see what effect it would have on the reaction.

The carbon to oxygen ratio was kept at 8:1, this having been found to be the optimal ratio, GHSV was kept at 4000h^{-1}, 0.2mL of catalyst was used. The catalyst used was the pre-reduced iron molybdate catalyst. In short all conditions except *n*-octane

concentration was kept the same. 10% *n*-octane in the gas feed was used as the lower explosive limit of *n*-octane is 1.1% and the upper explosive limit is 7%.
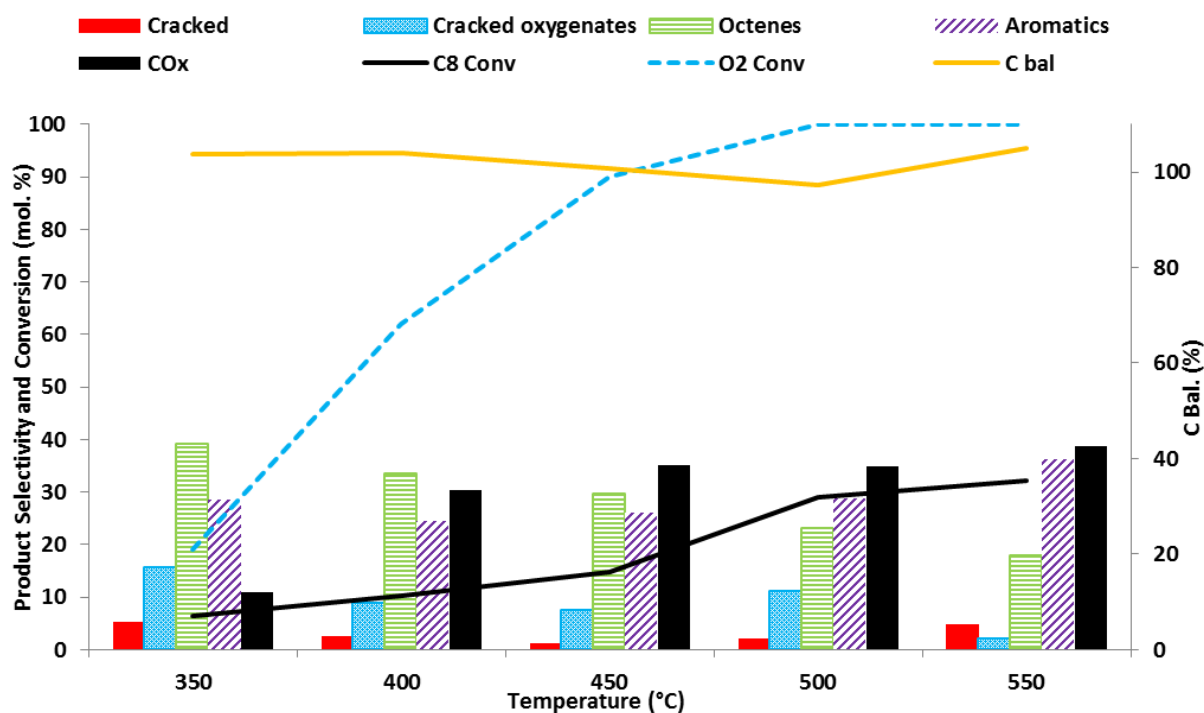
Figure 3.28 –Reaction of 10% *n*-octane (GHSV 4000h^{-1}, C:O 8:1) over a pre-reduced iron molybdate catalyst. Temperature range from 350-550°C

The first result of note was that using a higher concentration of *n*-octane in the gas feed was that production of carbon oxides was occurring at 350°C and 400°C using identical conditions where no CO$_x$ was produced when the percentage of *n*-octane was 1%. Higher temperatures once again saw high levels of aromatics formed. Conversion levels were similar to when 1% *n*-octane was used. With this finding and referencing earlier results shown in this chapter, the GHSV was raised to observe whether burning could be eliminated at lower temperatures and thus increase selectivity to octenes.
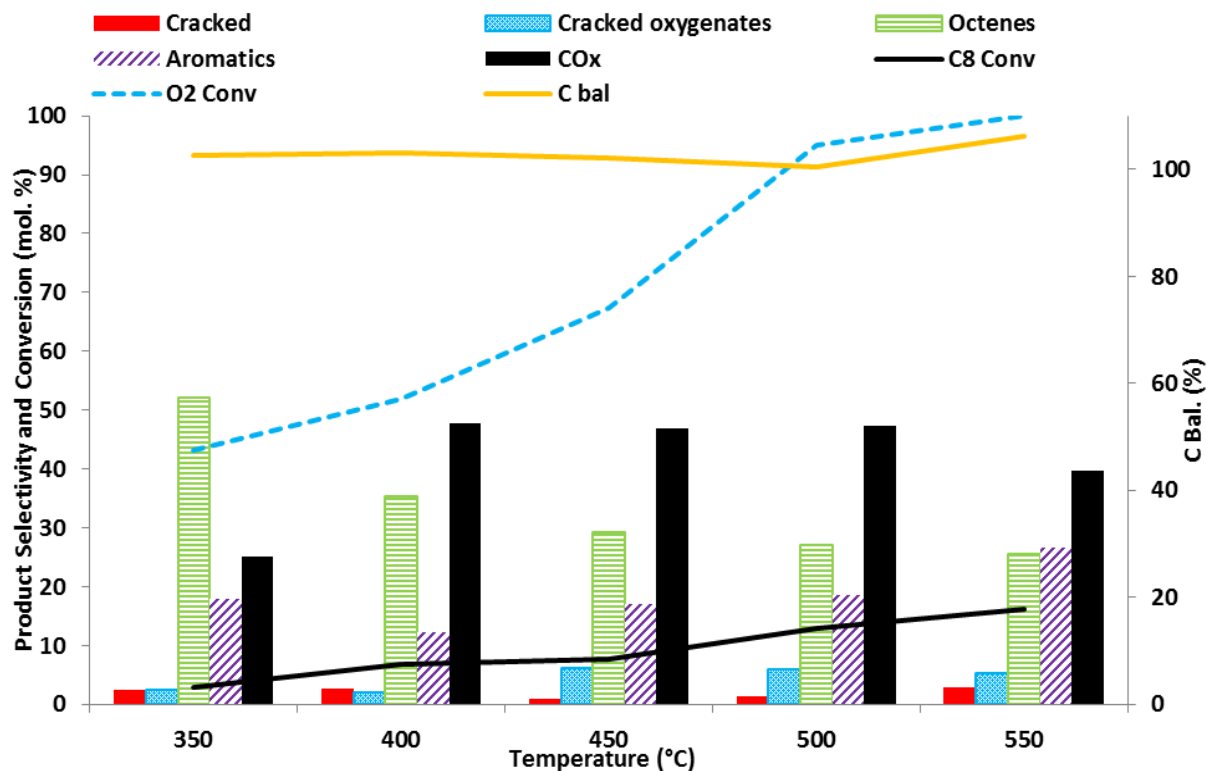
Figure 3.29 –Reaction of 10% *n*-octane (GHSV 6000h^{-1}, C:O 8:1) over a pre-reduced iron molybdate catalyst. Temperature range from 350-550°C

As can be seen production of CO$_x$ was still high. A higher GHSV led to lower oxygen consumption from 350-450°C. In contrast to Figure 3.28, CO$_x$ are the dominant product at 550°C whereas when the GHSV was 4000h^{-1} it was aromatic species. However increasing the GHSV did result on octenes becoming the main product at 350°C.

Clearly to eliminate burning the GHSV would need to be raised to a higher level, although this required some alteration of the reactor as using high gas flows over the catalyst led to back-pressure issues.
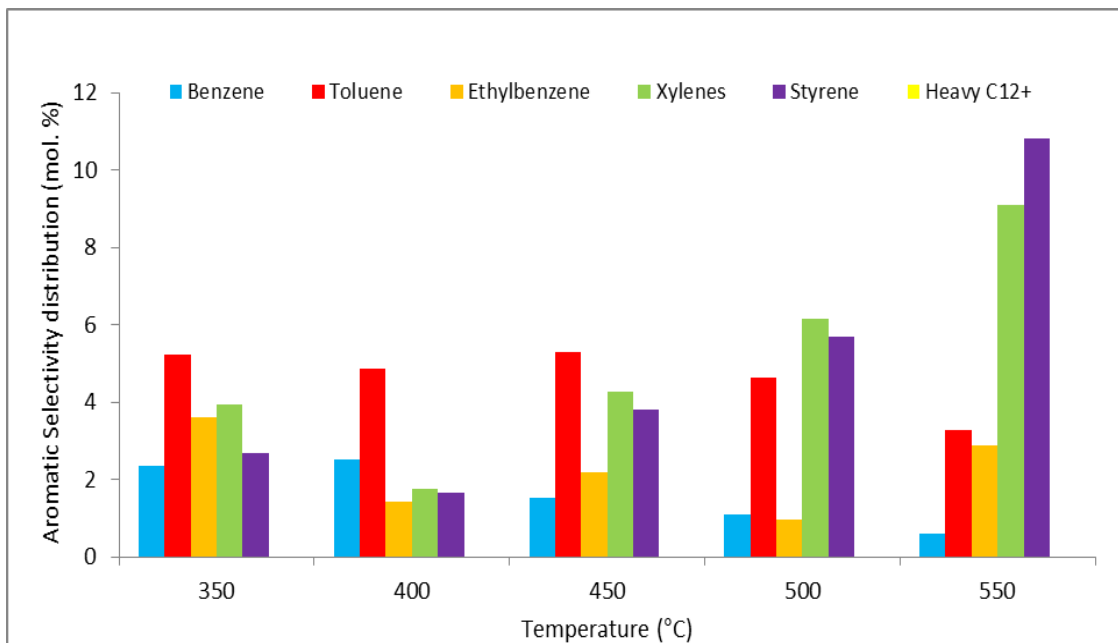
Figure 3.30 – Aromatic selectivity distribution during the reaction of 10% *n*-octane (GHSV 6000h^{-1}, C:O 8:1) over a pre-reduced iron molybdate catalyst. Temperature range from 350-550°C

Considering the aromatic selectivity when the GHSV was 6000h^{-1}, it is notable that 8 carbon chain aromatics are formed at low temperatures. This is consistent with earlier findings showing that C8 aromatics are formed whenever burning occurs. Once again, higher temperatures see xylene and styrene being formed at high levels.

When the GHSV was raised to 12,000h^{-1} carbon oxides were still being formed at 350°C and 400°C. Another experiment was run with the GHSV at 16,000h^{-1}.
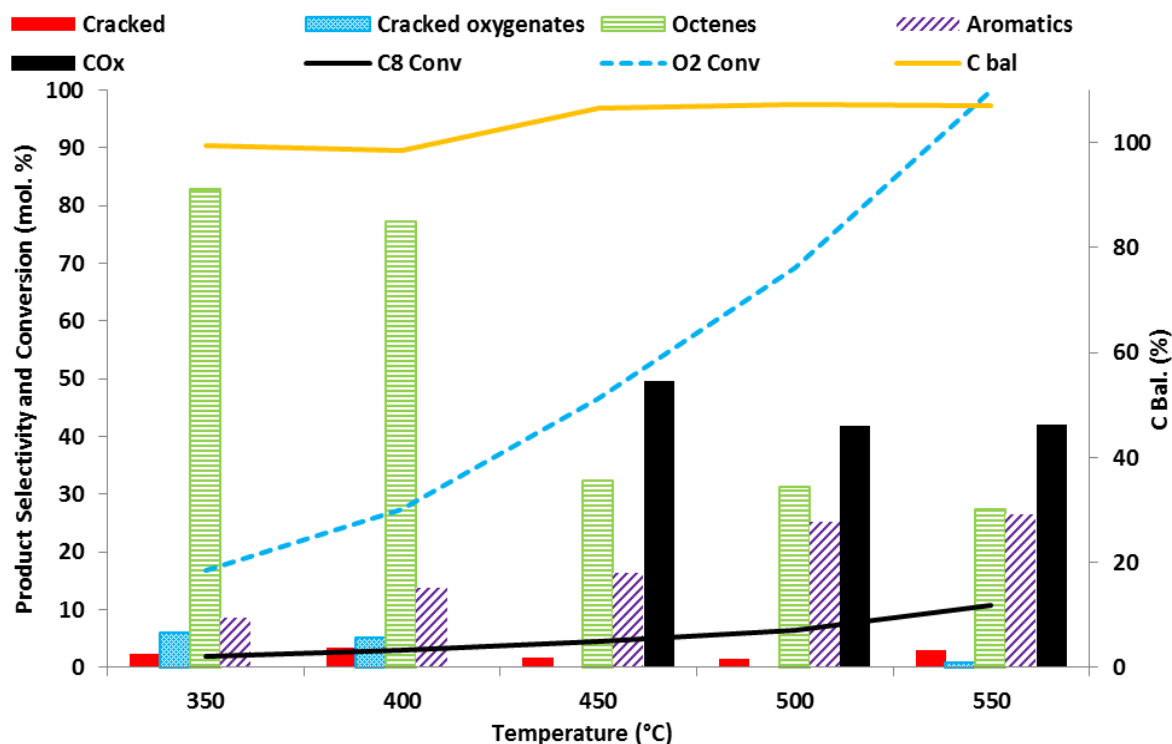
Figure 3.31 –Reaction of 10% *n*-octane (GHSV 16,000h^{-1}, C:O 8:1) over a pre-reduced iron molybdate catalyst. Temperature range from 350-550ºC

As can be seen, raising the GHSV to 16,000h^{-1} stops selectivity to CO$_x$ at lower temperatures, with octenes being the main product. At 400ºC there is *ca.*77.1% selectivity to octenes. However from the standpoint of maximising octene production, this comes at a price. An octane conversion of only *ca.*3.2% is observed. While this gives a higher overall yield of octenes than at 400ºC, 4000h^{-1}, 1% *n*-octane, it is not as high as hoped. Table 3.5 (below) shows a comparison of CO$_x$ free octene production at 400ºC for both 1% and 10% *n*-octane

n-octane percentage in gas feed	Selectivity to octenes (mol %) at 400ºC	Octane conversion (mol %)	Yield of octenes in gas feed (%)
1% *n*-octane	73.2	8.7	0.06
10% *n*-octane	77.1	3.2	0.25

Table 3.5 – Comparison of octane conversion and selectivity to octenes for 1% *n*-octane at 4000h^{-1} and 10% *n*-octane at 16,000h^{-1}

As table 3.5 shows although 10% *n*-octane produces a greater concentration of octenes without burning at 16,000h⁻¹ than 1% *n*-octane does at 4000h⁻¹ it is not ten times greater. In fact it is more likely to be 4 times greater. This lower yield can be attributed directly to the low conversion of *n*-octane. This is turn can be attributed to the higher GHSV required with greater *n*-octane concentrations in the gas feed. Clearly there is a trade-off.

Although there is no concretely defined target for conversion and selectivity to octenes, this work would like it to be as high as possible. As a point of reference the UOP-PACOL process that uses dehydrogenation to convert *n*-paraffins to olefins has a reported conversion rate of 12-13% with a selectivity to olefins >90%.[24] For this process to compete with that both activity and selectivity need to be higher. The selectivity to octenes is the most important as they are the desired product. Although oct-1-ene would be desirable, this process and the UOP-PACOL process both produce internal alkenes (olefins). These are still valuable however as they can be further functionalised.
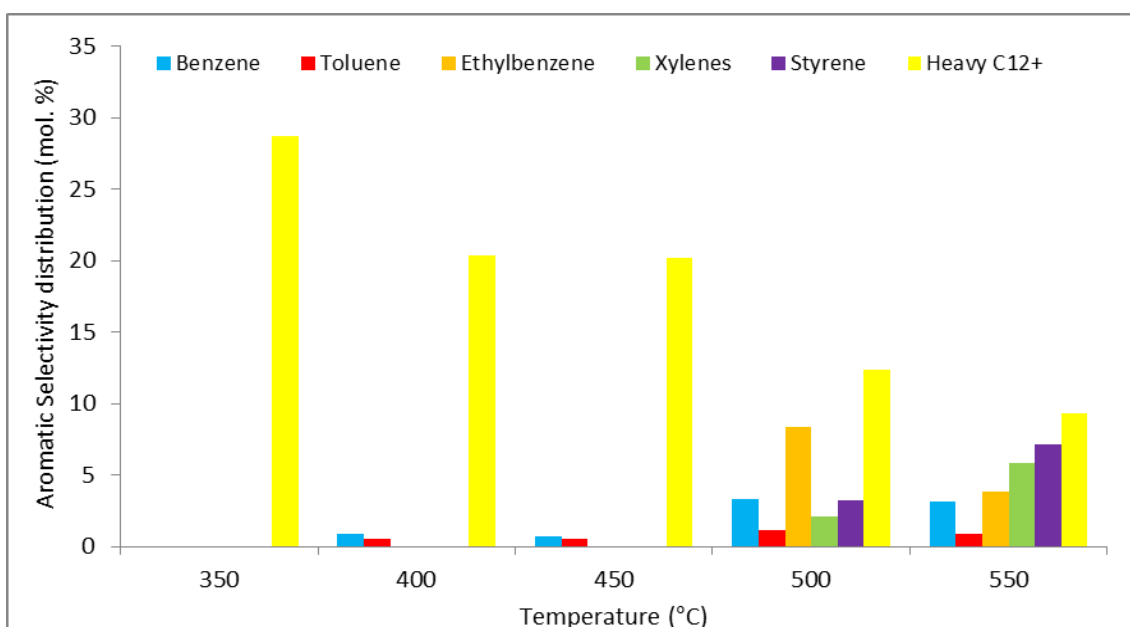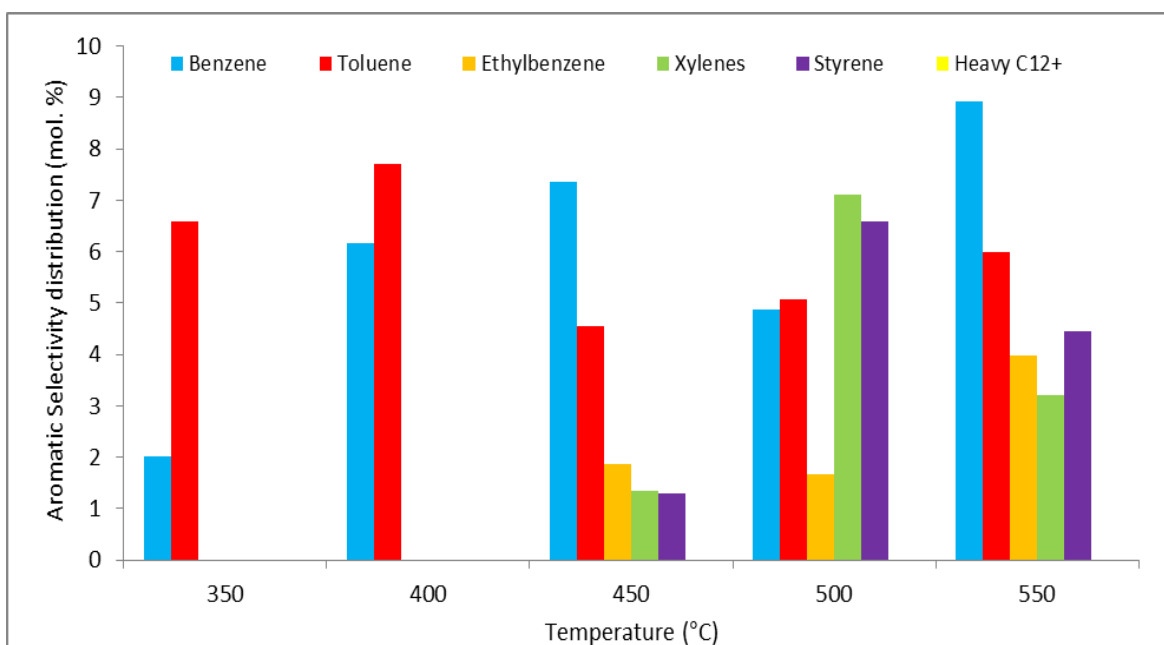

Figure 3.32 – Aromatic selectivity distribution during the reaction of 10% *n*-octane (GHSV 16000h⁻¹, C:O 8:1) over a pre-reduced iron molybdate catalyst. Temperature range from 350-550ºC

The aromatic species produced over the various temperatures at 16,000h^{-1} are comparable to those produced with 1% *n*-octane at 4000h^{-1} GHSV (see Figure 3.13). Toluene and benzene produced from 350-400°C with 8 carbon chain aromatics being produced once burning occurs at 450°C and above. Curiously higher levels of benzene are seen at 550°C than in Figure 3.13. This could be attributed to greater surface coverage of olefin on the catalyst surface and more iron sites coming into contact with the alkane, leading to cracking, similar to what was observed when pure phase FeMoO$_4$ was tested.

Catalyst testing was then done with the temperature kept at 400°C and various GHSVs tested to see at what contact time burning occurs. This was to see if the process could be "fine tuned" to obtain the highest octane conversion without combustion occurring.
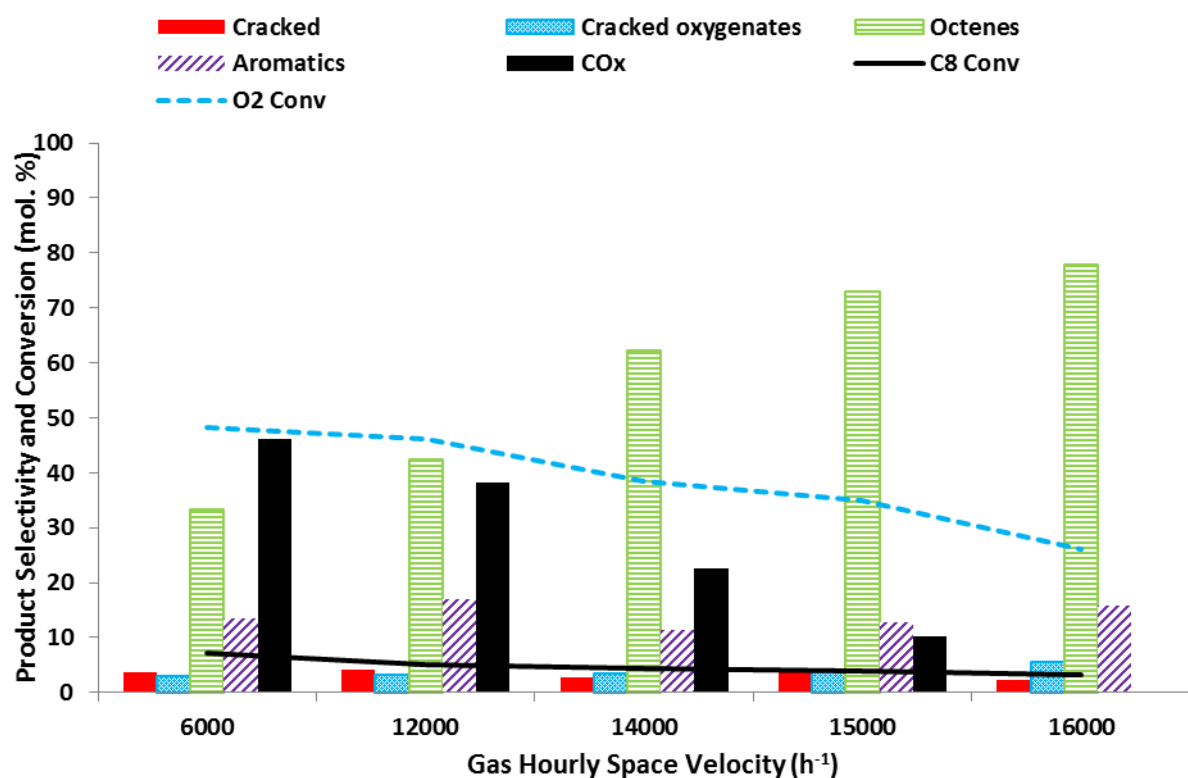
Figure 3.33 –Reaction of 10% *n*-octane (Temperature 400°C, C:O 8:1) over a pre-reduced iron molybdate catalyst. GHSV range from 6000-16,000h^{-1}

As Figure 3.33 shows burning occurs until 16,000h^{-1}. Less CO$_x$ is produced as the GHSV is raised but this comes as the cost of decreasing conversions. This is expected as a

shorter contact time on the catalyst surface will lead to lower conversions of the *n*-octane to products. Equally a higher contact time will lead to more thermodynamically stable products (such as CO_2) being produced.

Scaling up the process and increasing the percentage of octane in the gas feed is feasible. However much higher GHSVs were required for a combustion free conversion of *n*-octane to octenes. The same contact times at 1% *n*-octane resulted in burning when 10% *n*-octane was used. This may be due to a surface coverage issue as greater levels of alkane come into contact with iron sites on the catalyst surface. Although using a higher concentration of alkane in the gas feed results in a greater concentration of alkenes being produced, there is a trade-off, as the higher GHSVs required result in lower conversions. Selectivity remained largely the same as 1% *n*-octane when considering the species produced, no heavy aromatics for example, were observed. As contact times were shortened lower oxygen consumption was observed as *n*-octane conversion dropped, this is again expected as the reaction appears to proceed by an oxidative dehydrogenation mechanism.

3.9 CATALYST CHARACTERISATION

Earlier in the chapter X-ray Powder Diffraction (XRPD) patterns and Raman spectra were presented, showing the effect of the pre-reduction step in catalyst preparation. Other analytical techniques to observe the effect on the catalyst structure post reaction, and to elucidate details about the catalyst such as the exact ratio of molybdenum to iron present.

3.9.1 SURFACE AREA MEASUREMENTS

Brunauer-Emmet-Teller measurements were used to show the surface area of the catalyst before and after the reaction.

Surface area before reaction (m^2g^{-1})	Surface area after reaction (m^2g^{-1})
1.3	4.2

Table 3.6 – Different surface areas of the pre-reduced iron molybdate catalyst before and after reaction. 1% *n*-octane, 4000h^{-1}, 550°C, 8:1 C:O

After being placed in the reactor the catalyst has a higher surface area. This is most likely due to MoO_3 being reduced and forming Mo_4O_{11} and MoO_2 species as MoO_3 has a very low surface area.[25] MoO_3 is recorded in the literature[7]as having a low surface area (*ca.* 1.0m^2g^{-1}). The formation of MoO_2 and Mo_4O_{11} species from the loss of terminal oxygen species from surface MoO_3, could be acting to disrupt the surface layer of MoO_3 that is observed on iron molybdate catalysts.[21] This disruption would then lead to defect sites thus increasing surface area.[26]

3.9.2 THERMOGRAVIMETRIC ANALYSIS

Thermal gravimetric analysis (TGA) was performed before (fresh catalyst) and after (used catalyst) to observe what mass had been lost. The catalyst had been taken up to 550°C at a C:O ratio of 8:1 under a flow of 1% *n*-octane.

A ramp rate of 5 °C per minutes was used. The sample atmosphere was 10% oxygen in argon. Flow rate was 10ml/min. Sample mass was 0.12g.
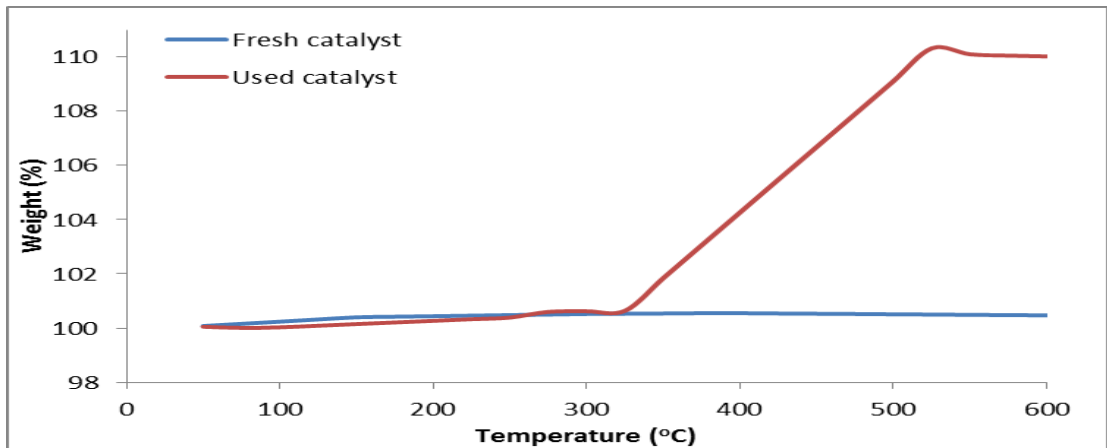
Figure 3.34 – TGA of catalyst before being undergoing reaction with *n*-octane (blue line) and after (red line). Conditions of 1% *n*-octane, 4000h^{-1}, 550°C and 8:1 C:O used

The weight gain in the used catalyst is likely due to the molybdenum being re-oxidised from Mo_4O_{11} and MoO_2 to MoO_3. This would come from the oxygen in the gas feed. This is also consistent with the surface area change. XPS which is examined in Chapter 4 confirms that there is some low level carbon deposition, potentially therefore the gain in mass may be down to sp2 and sp3 carbon species oxidising at the catalyst surface. Osswald *et al* suggest that this process would occur between 375-450°C which overlaps with the range in which there is mass gain in the TGA shown in Figure 3.34.[27] This is important to note as carbon deposition could be removed by varying the rate of gas flow to 40ml/min and high temperatures.

3.9.3 XRPD OF CATALYST POST-REACTION
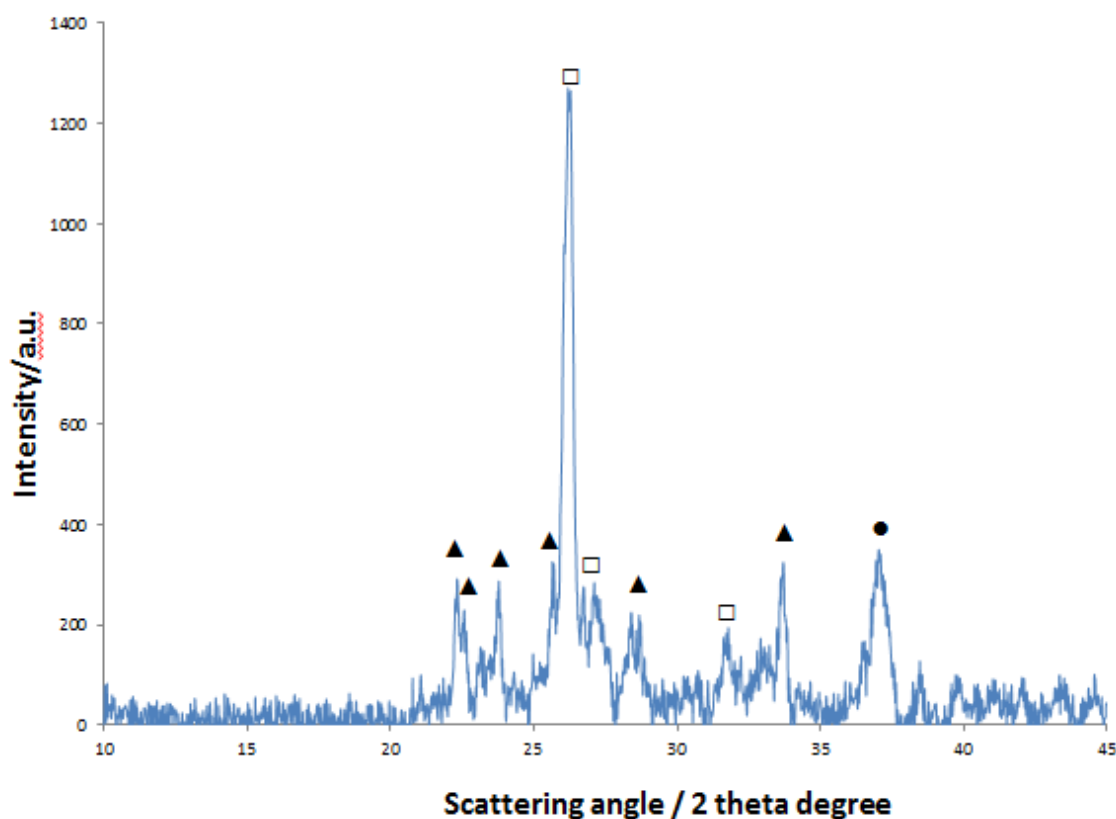
Figure 3.35- XRPD of a pre-reduced iron molybdate catalyst post reaction. Phases present: β-FeMoO$_4$ (□) and Mo$_4$O$_{11}$(▲) and MoO$_2$ (●). Conditions used in reaction 1% *n*-octane, 4000h^{-1}, 550°C and 8:1 C:O

Species	Peak (2 theta degrees)	Lattice Plane	d-spacing (Å)
Mo$_4$O$_{11}$	22.2	211	4.00
	22.5	501	3.95
	23.7	311	3.75
	25.5	601	3.48
	27.3	610	3.26
	34.6	602	2.56
MoO$_2$	37.1	-211	2.42
β-FeMoO$_4$	26.2	220	3.40
	27.3	-202	3.26
	31.6	112	2.83

Table 3.7 – XRPD Peak list for Figure 3.35 with associated d-spacing and lattice planes.

These results show that reduction does take place in the reactor. Oxygen depleted molybdenum species (Mo$_4$O$_{11}$ and MoO$_2$) are observed in the catalyst. This oxygen

depletion would explain why the spent catalyst gains mass in TGA (reoxidation of the sample would explain weight gain), and why the catalyst exhibits greater surface area post reaction. XPS studies (below) confirm that oxygen depleted molybdenum species exist at the surface. This is in line with the XRPD.

3.9.4 RATIO OF MOLYBDENUM TO IRON IN THE CATALYST

The catalyst was prepared with a ratio of 2.7:1 molydenum to iron excess, and XRPD patterns confirm that free molybdenum oxide species are present in the catalyst, so it is likely that there is a molybdenum excess. Energy dispersive X-Ray (EDX) spectroscopy and Microwave Plasma- Atomic Emission (MP-AES) Spectroscopy was carried out on the catalyst before it was tested in the reactor, to see what molybdenum to iron ratio is present at the catalyst .

Ratio of Mo/Fe found using EDX	Ration of Mo/Fe found using MP-AES
2.4	2.7

Table 3.8 – Ratios of molybdenum to iron present using EDX and MP-AES spectroscopy

Clearly both spectroscopic methods show that there is an excess of molybdenum present. EDX shows a lower level of molybdenum than MP-AES which gives a 2.7:1 ratio, which was what the catalyst preparation aimed for.

3.9.5 XPS STUDIES AT THE CATALYST SURFACE

X-ray photoelectron studies were carried out on the molybdenum rich, pre-reduced catalyst before and after the reaction and on the pure phase $FeMoO_4$ before reaction.

Deconvolution of the XPS spectra into special peaks was done via a Microsoft Excel macro "eXPFIT" in which Shirley-type background subtraction was selected. This works on the assumption that the shapes of the lines is Gaussian.

Peaks for Mo(VI) were seen in the molybdenum rich catalyst before reaction. After reaction this shifted to peaks for Mo(IV), Mo(V) and Mo(VI) all being present. This concurs with the XRPD that reduction of the catalyst occurred inside the reactor.
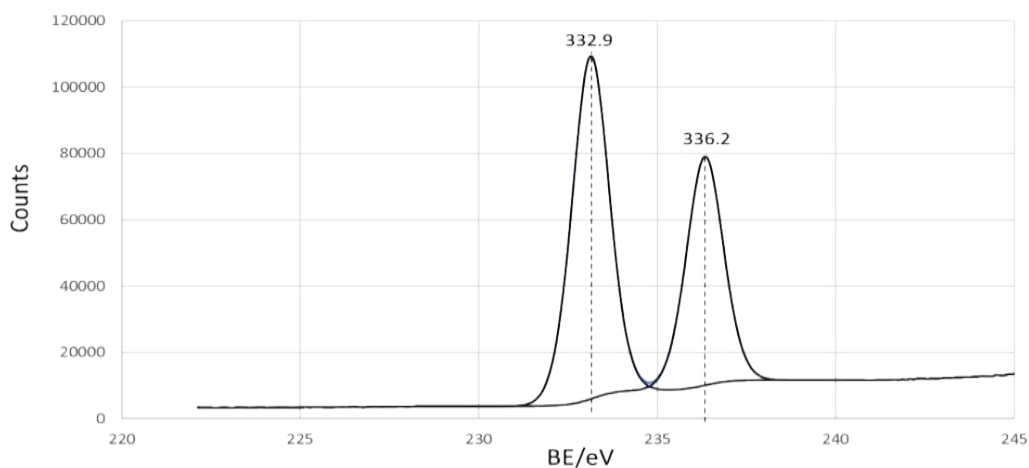
Figure 3.36 XPS spectra of pre-reduced iron molybdate before undergoing reaction with *n*-octane

The peak at 232.9 eV in Figure 3.36 is indicative of Mo 3d 5/2 at (VI) oxidation state, which is corresponds to MoO_3. The peak at 236.2 corresponds to Mo 3d 3/2 at the (VI) oxidation state.
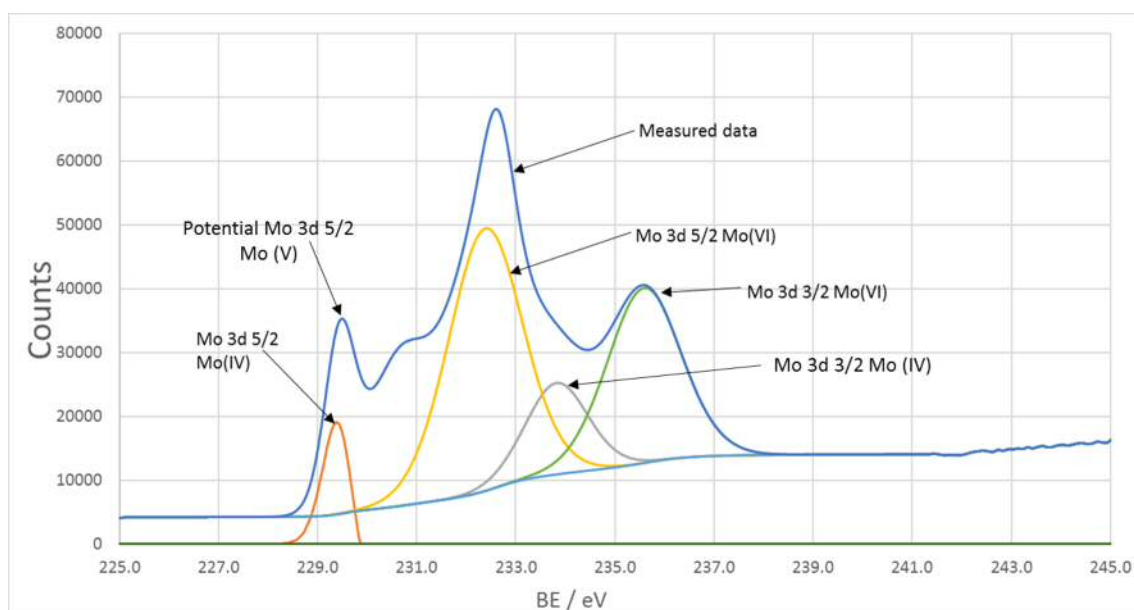
Figure 3.37 XPS spectra of pre-reduced iron molybdate after undergoing reaction with *n*-octane. Conditions of 1% *n*-octane, 4000h^{-1}, 550°C and 8:1 C:O used

Figure 3.37 shows the XPS spectra of the pre-reduced iron molybdate catalyst after undergoing reaction with *n*-octane. Peaks corresponding to molybdenum in the +4, +5 and +6 oxidation states were observed. The binding energies (BE) at 233.15 eV and 236.3 eV are indicative of Mo (VI) with spins indicated on Figure 3.37. This could indicate the presence either of MoO_3 or Mo_4O_{11} at the catalyst surface. The peaks at 229.8 eV and 233.0 eV are indicative of Mo (IV), this would suggest there is a presence of $MoO_2.$ The data for assigning these peaks come from the NIST X-ray photoelectron spectroscopy database. Finally, work by Spevak[28] suggests that an Mo (V) species can be observed at 230.7 eV, this oxidation state could either be from the Mo (VI) being reduced by the X-rays, or be indicative of Mo_4O_{11}. These findings correspond to the XRPD shown in Figure 3.35.
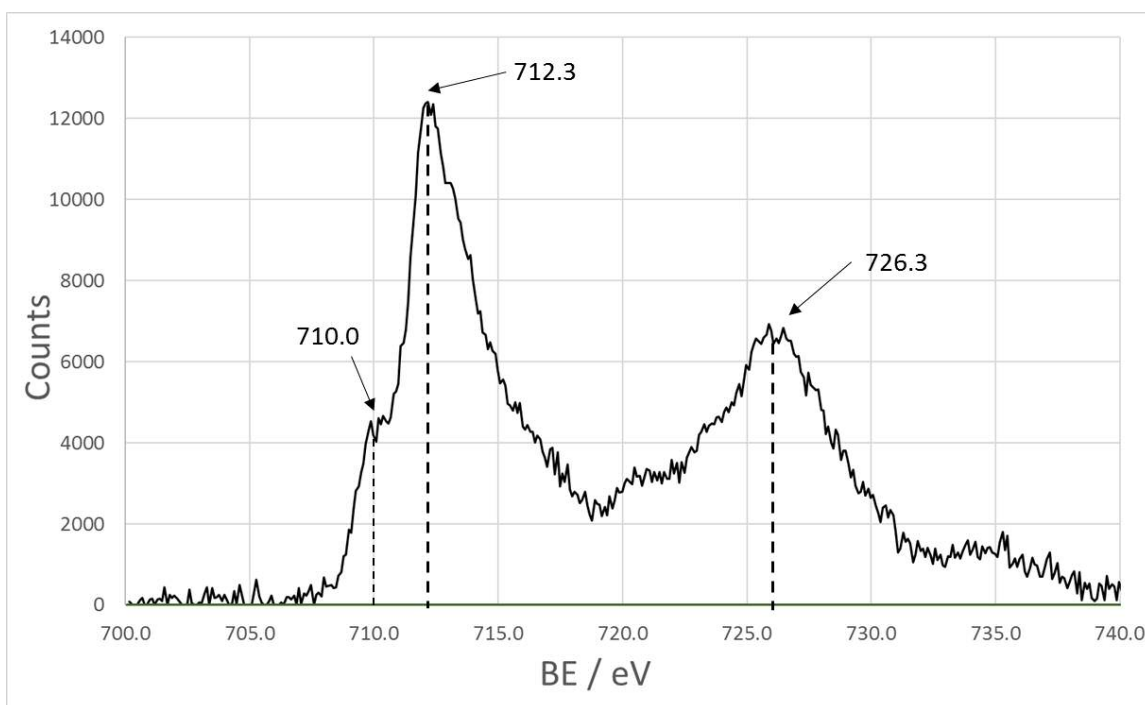
Figure 3.38 XPS spectra of pre-reduced iron molybdate before undergoing reaction with *n*-octane. Conditions of 1% *n*-octane, 4000h^{-1}, 550°C and 8:1 C:O used

Figure 3.38 shows the XPS spectra of the pre-reduced iron molybdate catalyst after undergoing reaction with *n*-octane. Peaks corresponding to iron in the +2 and +3 oxidation states were observed. The peak at 710.0 eV corresponds to Fe 2p 3/2 spin of iron in the +3 state. This correlates with the XRPD done at the beginning of this chapter

in Figure 3.7 which showed $Fe_2(MoO4)_3$ still present in the catalyst even after the pre-reduction step. The narrow peak at 712.3 eV is indicative of Fe 2p 3/2 species of iron in the +2 oxidation state, indicating the presence of $FeMoO_4$, although iron chloride which was used as a precursor for the catalyst preparation also exists in the +2 state. The broad peak at 726.3 eV corresponds to Fe 2p 1/2 species indicating the possible existence of Fe_2O_3 on the catalyst surface.[29,30]
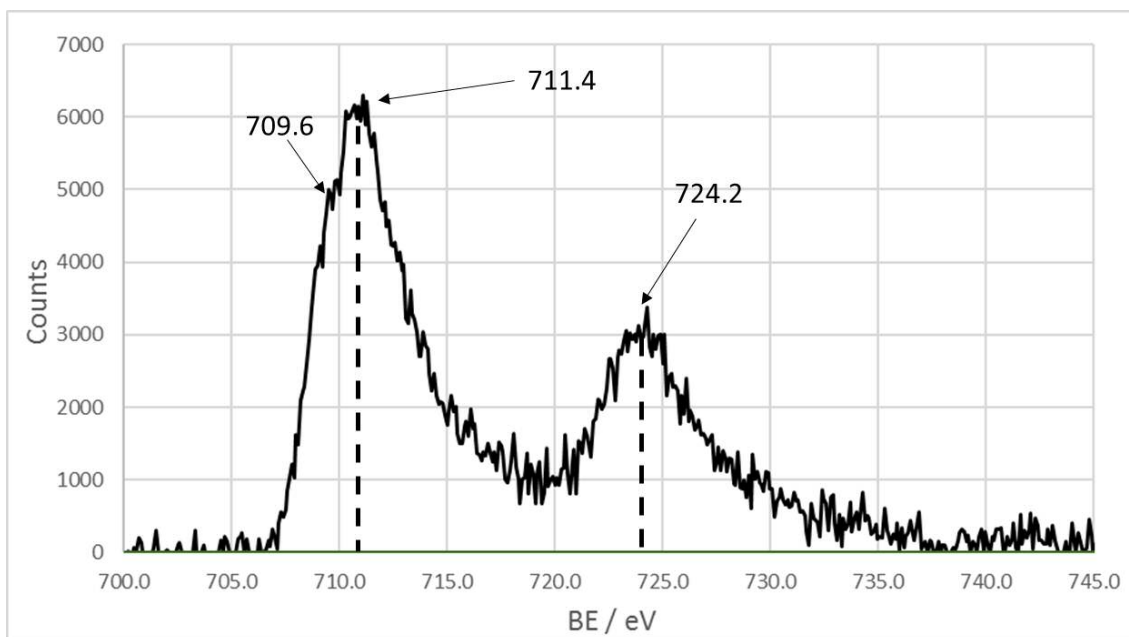
Figure 3.39 XPS spectra of pre-reduced iron molybdate after undergoing reaction with *n*-octane. Conditions of 1% *n*-octane, 4000h^{-1}, 550°C and 8:1 C:O used

As figure 3.39 shows, post-reaction there is a much subtler peak indicating the presence of iron in the +3 oxidation state (709.6 eV, Fe 2p 3/2 species). This implies a near-full reduction to $FeMoO_4$ which is in agreement with the XRPD shown in Figure 3.35. The peak at 711.4 eV BE is indicative of Fe 2p 3/2 and the peak at 724.2 eV BE is indicative of Fe 2p 1/2. Both of these show iron in the +2 oxidation state.[30]

Analysis of the catalyst surface showed the ratios of iron molybdenum and oxygen present before and after the reaction (see Table 3.9).

Catalyst	Fe present (%)	Mo present (%)	Oxygen present (%)
Before reaction with 1% *n-octane*	6.67	25.15	68.18
After reaction with 1% *n-octane*	3.74	30.39	65.87
Pure Phase FeMoO$_4$ before reaction	14.47	18.45	67.08

Table 3.9 – Showing the composition of the catalyst surface (%) before and after reaction with 1% *n*-octane, 4000h^{-1}, 550°C, 8:1 C:O. Also shown is pure phase FeMoO$_4$ before reaction

As Table 3.9 shows, after the reaction, higher levels of molybdenum are seen at the catalyst surface but with lower levels of oxygen present. This suggests that some level of reduction is occurring with molybdenum migration to the surface. This is supported by the XRPD above.

As also shown in Table 3.9, FeMoO$_4$ has more iron sites present at the surface. This offers an explanation as to why it had higher selectivity to cracked products and benzene/toluene aromatic species. Iron sites cause the cracking of the *n*-octane molecules.

SUMMARY OF CHAPTER 3

An iron molybdate catalyst, with a molybdenum excess to iron of 2.7:1, causes oxidative dehydrogenation (ODH) of *n*-octane to octenes, chiefly *trans* 2-octene and t*rans* 3-octene.

Ferric molybdate and molybdenum trioxide, the oxidised common form of iron molybdate, is highly selective to carbon oxides and only gives a low yield of octenes. However ferrous molybdate and reduced molybdenum oxide species (FeMoO$_4$ +

Mo$_4$O$_{11}$) show greater selectivity to octenes. This is in keeping with findings by Stern and Grasselli[31] which showed ODH of propane over molybdate catalysts with the formula AMoO$_4$ where A is a cation with a +2 oxidation state.

At 1% *n*-octane with a 8:1 carbon to oxygen ratio, and a gas hourly space velocity (GHSV) of 4000h^{-1}, carbon oxide free ODH is observed at 400°C*. With a selectivity of *ca.*73.2% to octenes and a *n*-octane conversion of *ca.*8.7%. Lower GHSV leads to the formation of carbon oxides and aromatics, as longer contact times of the substrate at the catalyst surface leads to the formation of more thermodynamically stable products. Experiments at higher GHSVs lead to similar results but with lower conversions observed, falling to 6.5% *n*-octane conversion at 6000h^{-1}.

Higher temperatures (450°C and above) lead to the formation of aromatics and carbon oxides. With aromatics being the main products formed from *n*-octane (>50% selectivity) at 550°C*. Having a higher temperature and greater energy in the system could lead to the alkane bonding to the catalyst in numerous places, forming an octa-tri-ene species which could then cyclise in an intramolecular Diels-Alder style mechanism.[32]

There is a pattern when considering the aromatic species formed. At lower temperatures, when no CO$_x$ is formed, the only two aromatics seen are benzene and toluene. This suggests that cracking is occurring before or after cyclisation as 6 and 7 carbon chain products are formed from an 8 carbon feedstock. It may be that iron sites at the surface cause this cracking. Indeed when pure phase FeMoO$_4$ was used as a catalyst, a much higher proportion of the aromatics formed was benzene. Although fewer aromatics were formed overall at low temperatures when FeMoO$_4$ was used as a catalyst. XPS confirmed that the ratio of iron at the surface of FeMoO$_4$ was much higher than the catalyst with a molybdenum excess.

At higher temperatures and lower GHSVs as CO$_x$ is formed, longer 8-chain aromatics are produced. These are ethylbenzene, xylene and styrene. At the highest temperature

tested (550°C) the major aromatic products were xylenes and styrene, while ethylbenzene was observed at its highest concentrations at 450° or below if there was a low GHSV. When pure MoO_3 was used, 8 carbon chain aromatics were the main species formed, so it is reasonable to suggest that is the molybdate rich parts of the catalyst surface that cause cyclisation. When pure phase MoO_2 was used the main aromatic species formed was ethyl-napthalene, clearly incorporating 2 *n*-octane molecules at the surface before desorption as a heavy aromatics.

Altering the carbon to oxygen (C:O) ratio also had an effect on selectivity. Increasing the level of oxygen in the gas feed increased selectivity to carbon oxides significantly (>55% across all temperature and GHSV profiles), as expected. While increasing the level of alkane in the feed led to similar results to an 8:1 C:O but with lower conversions (drop of 1-2%) observed. Previous work on propane ODH found that the reaction rate of the alkane in a Mars-Van Krevelen ODH mechanism is close to one and close to zero with oxygen.[33] This is consistent with the findings here, as conversions with a 12:1 C:O ratio only decreased slightly compared to conversions with an 8:1 ratio. The increase in conversion seen for an oxygen rich species can be attributed to the formation of high levels of CO_x, which may not be formed by an MvK-ODH pathway.

Using the pure phase components of the catalyst showed that $FeMoO_4$ is highly selective to octenes (*ca.*85%), but with a slightly lower catalytic activity than the molybdenum rich catalyst (7.3%). MoO_3 showed high activity (between 9-20% *n*-octane conversion across temperature profiles) but was mainly selective to aromatics and carbon oxides (20-50% depending on temperature profile), and at 350°C cracked oxygenate species. This is likely to due to the labile terminal oxygen bonded to the molybdenum. MoO_2 which lacks that terminal oxygen shows very low catalytic activity (*n*-octane conversions of less than 3.2%) and its main selectivity is to heavy aromatics.

Finally the level of *n*-octane can be increased from 1% to 10% in the gas feed. However the GHSV must be altered as formation of CO_x occurs more readily when the

percentage of *n*-octane in the gas feed is higher. This may be due to greater surface coverage of the catalyst.

Bibliography

1   S. Pradhan, J. K. Bartley, D. Bethell, A. F. Carley, M. Conte, S. Golunski, M. P. House, R. L. Jenkins, R. Lloyd and G. J. Hutchings, *Nat. Chem.*, 2012, **4**, 134–139.
2   B.R. Yeo, PhD, Cardiff University 2014.
3   T. Konya, T. Katou, T. Murayama, S. Ishikawa, M. Sadakane, D. Buttrey and W. Ueda, *Catal. Sci. Technol.*, 2013, **3**, 380–387.
4   Y. S. Yoon, W. Ueda and Y. Moro-oka, *Catal. Lett.*, 1995, **35**, 57–64.
5   C. Doornkamp and V. Ponec, *J. Mol. Catal. Chem.*, 2000, **162**, 19–32.
6   S. K. Bhattacharyya, K. Janakiram and N. D. Ganguly, *J. Catal.*, 1967, **8**, 128–136.
7   K. Routray, W. Zhou, C. J. Kiely, W. Grünert and I. E. Wachs, *J. Catal.*, 2010, **275**, 84–98.
8   H. B. Friedrich and A. S. Mahomed, *Appl. Catal. Gen.*, 2008, **347**, 11–22.
9   M. I. Fadlalla and H. B. Friedrich, *Catal. Sci. Technol.*, 2014, **4**, 4378–4385.
10 J. E. Macintyre, *Dictionary of Inorganic Compounds*, CRC Press, 1992.
11 Sleight et al, *Inorg Chem*, 1968, **7**, 1093.
12 J. A. Rodriguez, J. C. Hanson, S. Chaturvedi, A. Maiti and J. L. Brito, *J. Phys. Chem. B*, 2000, **104**, 8145–8152.
13 W. Ueda, K. Asakawa, C.-L. Chen, Y. Moro-oka and T. Ikawa, *J. Catal.*, 1986, **101**, 360–368.
14 A. P. V. Soares, M. F. Portela and A. Kiennemann, *Catal. Rev.*, 2005, **47**, 125–174.
15 G. Veser, in *Handbook of Heterogeneous Catalysis*, Wiley-VCH Verlag GmbH & Co. KGaA, 2008.
16 G. K. Boreskov, *Heterogeneous Catalysis*, Nova Publishers, 2003.
17 P. Adkins, H.; W. R., *J Am Chem Soc*, 1931, **53**, 1512.
18 O. G. D'Yachenko, V. V. Tabachenko and M. Sundberg, *J. Solid State Chem.*, 1995, **119**, 8–12.
19 A. Cimino, M. Boudart and H. Taylor, *J. Phys. Chem.*, 1954, **58**, 796–800.
20 E. Ogata, K. Horie and X.-Y. Wei, *Prepr. Pap. Am. Chem. Soc. Div. Fuel Chem.*
21 A. P. V. Soares, M. F. Portela and A. Kiennemann, *Catal. Rev.*, 2005, **47**, 125–174.
22 T. Bhaskar, K. R. Reddy, C. P. Kumar, M. R. V. S. Murthy and K. V. R. Chary, *Appl. Catal. Gen.*, 2001, **211**, 189–201.
23 US7737312 B2, Patent. Production of linear alkyle benzene. I, Greager. 2010/
24 N. B. of C. Engineers, *The Complete Technology Book on Detergents (2nd Revised Edition)*, Niir Project Consultancy Services, 2013.
25 G. Jin, W. Weng, Z. Lin, N. F. Dummer, S. H. Taylor, C. J. Kiely, J. K. Bartley and G. J. Hutchings, *J. Catal.*, 2012, **296**, 55–64.
26 H. Knözinger and P. Ratnasamy, *Catal. Rev.*, 1978, **17**, 31–70.
27 S. Osswald, G. Yushin, V. Mochalin, S. O. Kucheyev and Y. Gogotsi, *J. Am. Chem. Soc.*, 2006, **128**, 11635–11642.
28 P. Spevak, University of Western Ontario, 1993.

29 M. C. Biesinger, B. P. Payne, A. P. Grosvenor, L. W. M. Lau, A. R. Gerson and R. S. C. Smart, *Appl. Surf. Sci.*, 2011, **257**, 2717–2730.

30 I. Uhlig, R. Szargan, H. W. Nesbitt and K. Laajalehto, *Appl. Surf. Sci.*, 2001, **179**, 222–229.

31 D. L. Stern and R. K. Grasselli, *J. Catal.*, 1997, **167**, 550–559.

32 E. Ciganek, in *Organic Reactions*, John Wiley & Sons, Inc., 2004.

33 Kinetics of the Oxidative Dehydrogenation of Propane over a VMgO Catalyst, http://www.jenergychem.org/EN/abstract/abstract8419.shtml, (accessed 4 July 2016).

CHAPTER 4 – TIME ON LINE STUDIES, PROPOSED MECHANISM AND ANAEROBIC STUDIES.

4.1 INTRODUCTION

This chapter follows on directly from findings in chapter 3, which examined the use of an iron molybdate catalyst formed of $FeMoO_4 + Mo_4O_{11}$ for the oxidative dehydrogenation (ODH) of *n*-octane to octenes. In this chapter, the effects of prolonged use and oxygen depletion on the performance of the catalyst are investigated. This was done to give information on the possible mechanism of the catalyst. A great deal of work has been done on the use of metal molybdates for the oxidative dehydrogenation of shorter chain alkanes, such as propane.[1–3] It is assumed that molybdate species use a Mars-Van Krevelen type mechanism to cause the ODH of an alkane to alkene.[4–6] If this is the case with an iron molybdate catalyst, then removing the oxygen from the gas feed should stop the reaction. However a time lapse may be seen, as residual lattice oxygen still converts alkane to alkene, before the reaction stops.

In addition, studies on catalyst lifetime and reusability were done, and a molybdenum rich catalyst comprising of $FeMoO_4 + Mo_4O_{11}$ was compared with pure phase $FeMoO_4$ catalyst that had no molybdenum excess.

4.2 TIME ON LINE STUDY, EFFECT OF HIGH TEMPERATURE ON CATALYST PERFORMANCE

An iron molybdate catalyst ($FeMoO_4 + Mo_4O_{11}$) with a molybdenum to iron excess of 2.7:1, prepared as described in Chapter 2, pre-reduced under flowing hydrogen at 460°C was used. Reactor conditions used 1% *n*-octane, 0.2mL catalyst C:O 8:1. The catalyst was tested at 400°C to maximise octene production. It was then taken to

550°C and held for 15h before being cooled to 400°C to observe if there was any difference in catalytic activity.
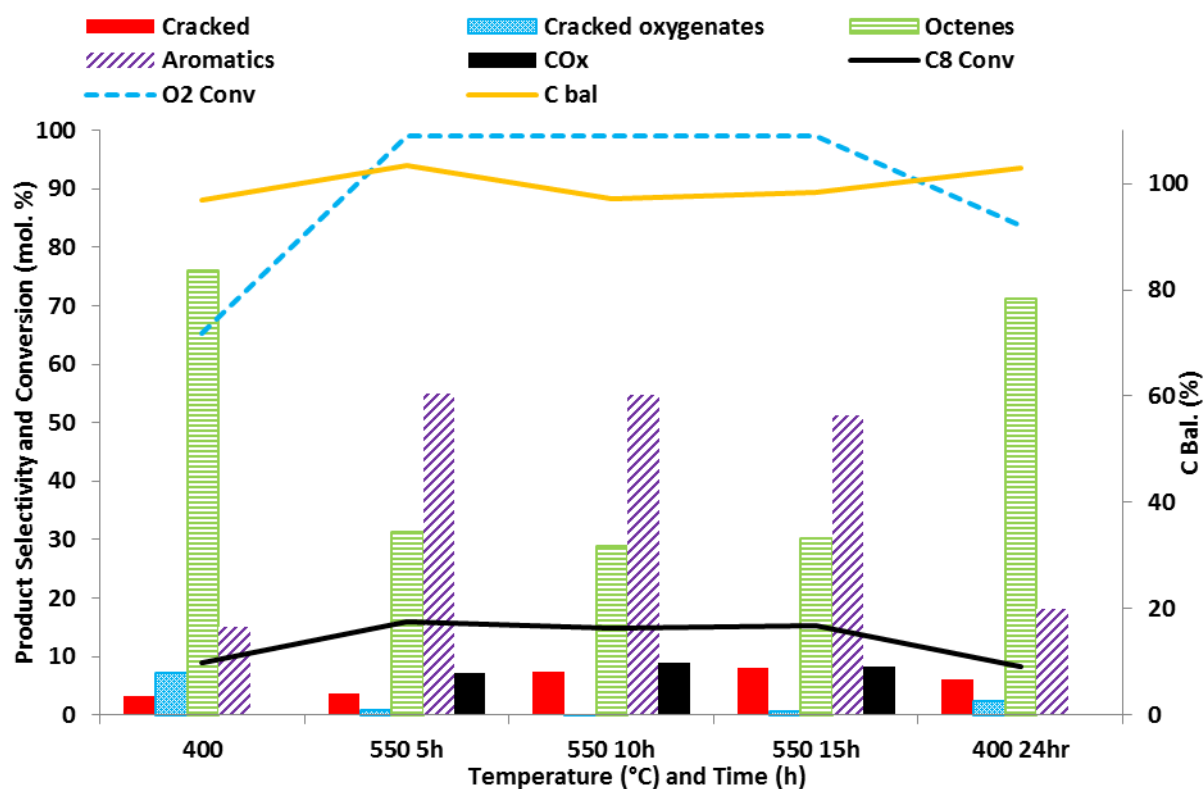
Figure 4.1 - **Reaction of 1% *n*-octane (GHSV 4000h^{-1}, C:O 8:1) over a pre-reduced iron molybdate catalyst. Temperature range from 400-550°C over a period of 24 hours. 15 hours spent at 550°C**

As can be seen in Figure 4.1, the temperature can be raised from 400°C where octene production is maximised, to 550°C which sees combustion and high levels of aromatic production, before returning to 400°C and seeing similar levels of octene production as before. Notable differences are the higher oxygen consumption between 400°C at 0h and 24h, lower levels of cracked oxygenates are observed and slightly higher levels of aromatics and cracked products are seen.

Molybdenum, in the form of MoO_3, can sublime at temperatures as low as 550°C if there is a flow of gas[7], so it was of interest to observe whether the catalyst would be stable if exposed to those temperatures for a prolonged period.
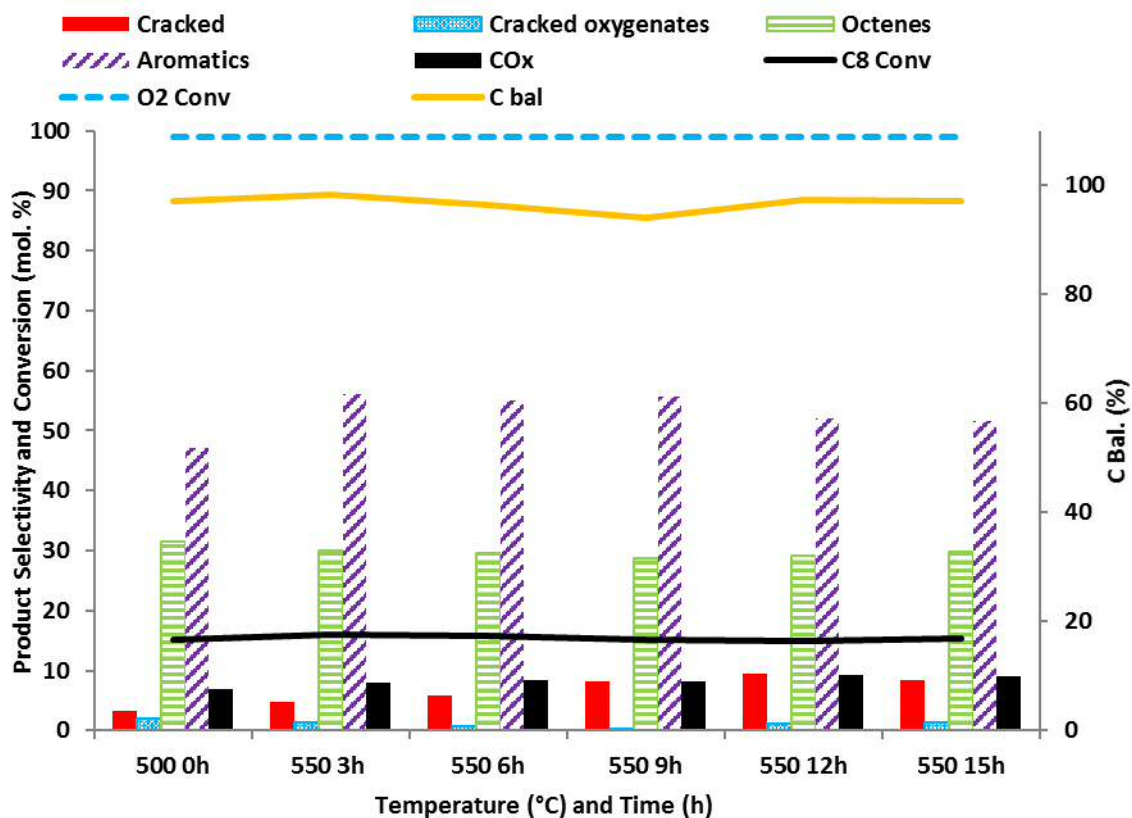
Figure 4.2 – Reaction of 1% *n*-octane (GHSV 4000h^{-1}, C:O 8:1) over a pre-reduced iron molybdate catalyst. Temperature held constant at 550°C over a period of 15 hours.

Figure 4.2 shows the time online data from Figure 4.1 in more detail when the catalyst was kept at 550 °C as can be seen the catalyst is kept at steady state conditions.

4.3 TIME ON LINE STUDY – CATALYST LIFETIME

An iron molybdate catalyst (FeMoO$_4$ + Mo$_4$O$_{11}$) was tested for 48hrs at 400°C to observe catalyst lifetime for octene production.
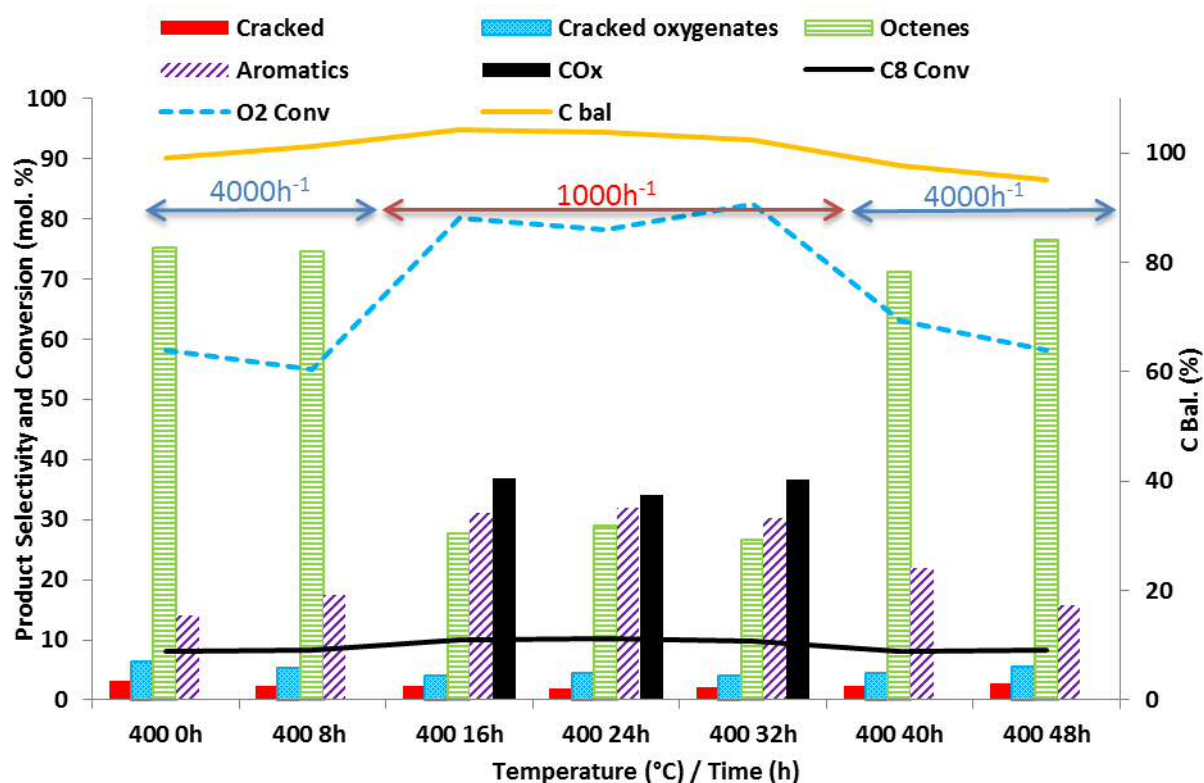
Figure 4.3 – TOL reaction of 1% *n*-octane (400°C, C:O 8:1) over a pre-reduced iron molybdate catalyst. GHSV range from 1000h^{-1}–4000h^{-1} over a period of 48 hours.

Figure 4.3 shows the iron molybdate catalyst held at 400°C for 48 hours. The GHSV was lowered from 4000h^{-1} to 1000h^{-1} after 15 hours and raised to 4000h^{-1} again after 33 hours. After 48 hours the catalyst was showing similar selectivity and conversions as at the beginning. This shows the catalyst longevity and tunability as the conditions can be altered and reset without lasting effect on the distribution and yield of products.

As found in chapter 3, lower GHSV leads to higher conversions and oxygen consumption, indicative of an oxidative dehydrogenation mechanism, but lower selectivity to octenes, and higher selectivity to carbon oxides and aromatics.

4.4 PROPOSED MECHANISMS FOR FORMATION OF OCTENES AND AROMATICS FROM *N*-OCTANE

Stern and Grasseli[8] proposed the following mechanism (Figure 4.4) for how the oxydehydrogenation of propane over nickel and cobalt molybdate catalysts can lead to total oxidation and the formation of carbon oxides.
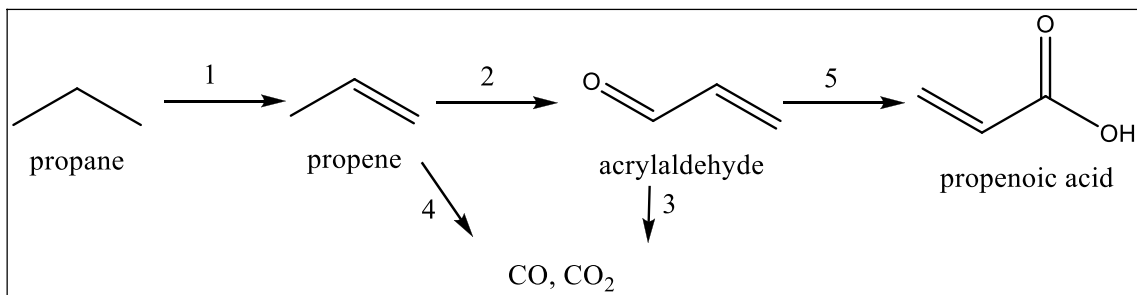
Figure 4.4 – Proposed mechanism for oxidation of propane over molybdate catalysts[8]

If an assumption is made that *n*-octane forms aromatic species more readily rather than oxygenate species (in contrast to propane), then it would appear a similar mechanism is occurring with an iron molybdate catalyst and *n*-octane at 400°C. This assumption however assumes that the formation of aromatics comes from a sequential pathway via alkenes which have been formed via alkanes.

At higher gas hourly space velocities octenes are formed more readily, while a lower GHSVs greater selectivity to carbon oxides and aromatics is observed. At $4000h^{-1}$ step 1, the conversion from alkane to alkene, occurs and the shorter contact time allows the bulk of the hydrocarbon to be removed before sequential steps can occur. While at $1000h^{-1}$ step 1 occurs, the alkene is formed, but due to greater contact time at the catalyst surface, aromatisation or total oxidation occurs, leading carbon oxide formation and high levels of aromatics at the expense of the desired alkene product.

To probe the nature of the mechanism several studies were done in this work. Varying the GHSV altered the selectivity of products. This would suggest that contact time of reactants and products at the catalyst surface affects the nature of the reaction. Intermediates or products such as octene could be used as a feedstock to observe if sequential reactions are responsible for secondary products. The carbon to oxygen ratio was varied in the previous chapter to observe how the selectivity and conversion changed. In this chapter anaerobic studies were done to observe if the nature of gaseous oxygen is different in character to lattice oxygen. This would also offer a strong indicator of whether the reaction mechanism is Mars-Van Krevelen or not.

A proposed mechanism scheme based on Stern and Grasseli's model is shown in Figure 4.5. It is based on the difference in selectivity shown through varying contact times and temperatures shown in chapter 3 and briefly here.
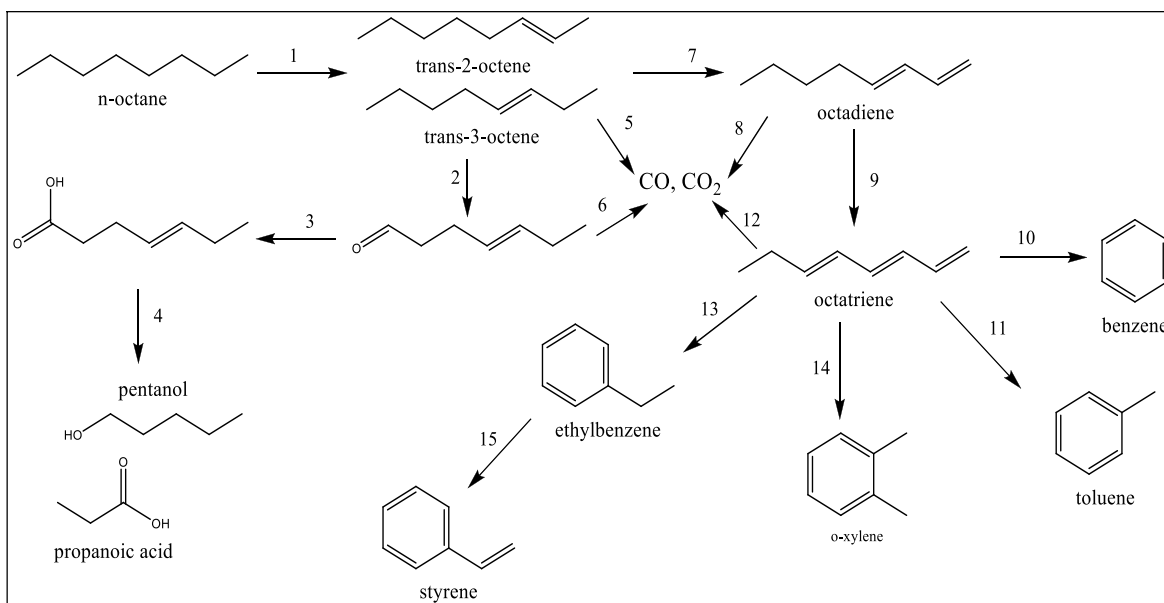
Figure 4.5 -Proposed mechanism for oxidation and oxidative dehydrogenation of *n-octane* over an iron molybdate catalyst

The mechanism shown in Figure 4.5 is an attempt to adapt the mechanism proposed by Stern and Graselli shown in Figure 4.4. It is based on observations made on how contact time effects selectivity. Firstly that high GHSV (low contact time), leads to high selectivity to octenes and cracked oxygenates. Secondly that lower GHSVs (a higher contact time for the *n-octane* to be in contact with the catalyst), leads to carbon oxides and aromatics being the dominant products, see Figure 4.6. Thirdly, within the formation of aromatics, higher GHSV sees only benzene and toluene formed, while lower GHSV results in styrene, xylene and ethylbenzene being produced.

One of the problems with this mechanism are that octa-dienes are not observed as products. This is in direct contrast to the Honeywell UOP PACOL process which sees octa-dienes being produced when conditions make the catalyst "over-active".[9] A second problem is that the formation of aromatic species and carbon oxides also occurs at higher temperatures regardless of GHSV. While the oxidative dehydrogenation of shorter chain (C_5 and lower) has been widely studied,[10] there is considerably less literature on longer chain alkane ODH.

Literature on shorter chain alkane ODH indicates consecutive reactions leading to carbon oxides, I have attempted to portray this in Figure 4.5.[11] Grabowski notes that the nature of the alkane used as a feedstock strongly influences reactivity.[11] This makes generating a potential set of reaction pathways based on literature of propane or butane ODH very difficult. A further complicating factor is that the nature of the active site of the catalyst used in this work has yet to be elucidated. In an ideal scenario a catalyst site which only undergoes the C-H abstraction required for ODH would be the one studied. This is not possible. Furthermore the catalyst system used is a mixed metal oxide, the interplay and synergy between the molybdenum oxide species and the iron molybdate phase further complicates matters. This phenomenon has been discussed in the literature concerning methanol oxidation over an iron molybdates system.[12,13]

It should be stressed that the mechanism shown in Figure 4.5 is hypothetical and an early attempt to clarify what is a complicated reaction mechanism.
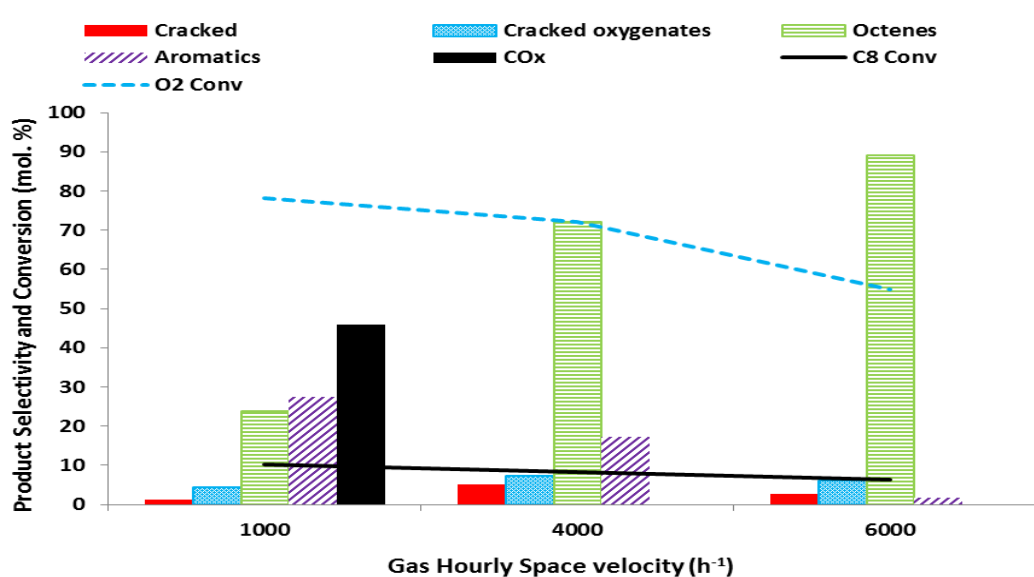
Figure 4.6 – Catalytic activity and selectivity during the reaction of 1% *n*-octane (Temperature held at 400°C, C:O 8:1) over a pre-reduced iron molybdate catalyst. Gas hourly space velocity range from 1000-6000h^{-1}

A flaw with the proposed mechanism is that octadienes and octatrienes are not seen. It could be assumed that these species are adsorbed strongly to the catalyst surface and only desorb once cyclisation and aromatisation has occurred. Work by Pradhan *et*

al[14] also proposed this. Work done by Davis *et* al[11] and Paal[17] suggests that an octatriene or octadiene could be an intermediate leading to cyclic aromatic products as part of a dehydrocyclisation reaction. The octatriene surface intermediate, being highly unsaturated and bound to the surface at multiple points in the carbon chain would not desorb readily.[17] However later work done by Davis[15] suggests that cyclisation of the alkane may occur prior to unsaturation and aromatisation (see Figure 4.7). This suggests two pathways, one forming 1,2 – dimethylcyclohexane, which leads to the formation of xylene, and another pathway forming ethylcyclohexane which can form ethylbenzene and styrene. It has also been shown in the literature[15,16] that benzene and toluene could be formed by cracking, producing methane and ethane or carbon laydown at the catalyst surface.
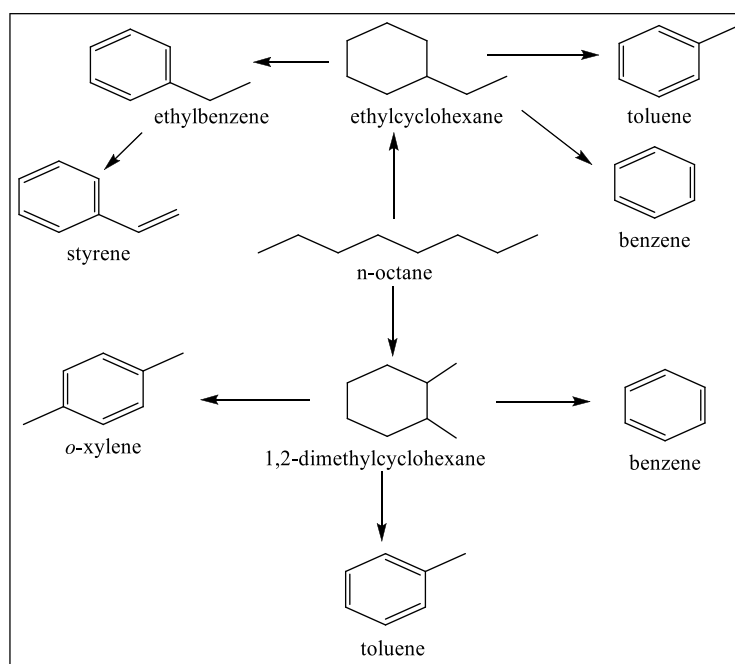
Figure 4.7 Aromatic formation from the reaction of n-octane by a cyclisation reaction followed by oxidative dehydrogenation rather than via an octatriene intermediate.

In an attempt to elucidate the mechanism by which aromatics are formed oct-1-ene was used as a substrate in place of *n*-octane. If the reaction proceeds by an octadiene/octatriene intermediate then the use of oct-1-ene as a feedstock would cause higher levels of aromatisation than produced with *n*-octane.[18]

4.5.1 REACTION OF OCT-1-ENE.

As oct-1-ene is more reactive than *n*-octane it would be expected that oct-1-ene would show higher conversion.[18] The first experiment was done at 13.3ml/min to mimic 4000h^{-1} GHSV in a blank stainless steel tube to see how the oct-1-ene reacted in the absence of a catalyst.
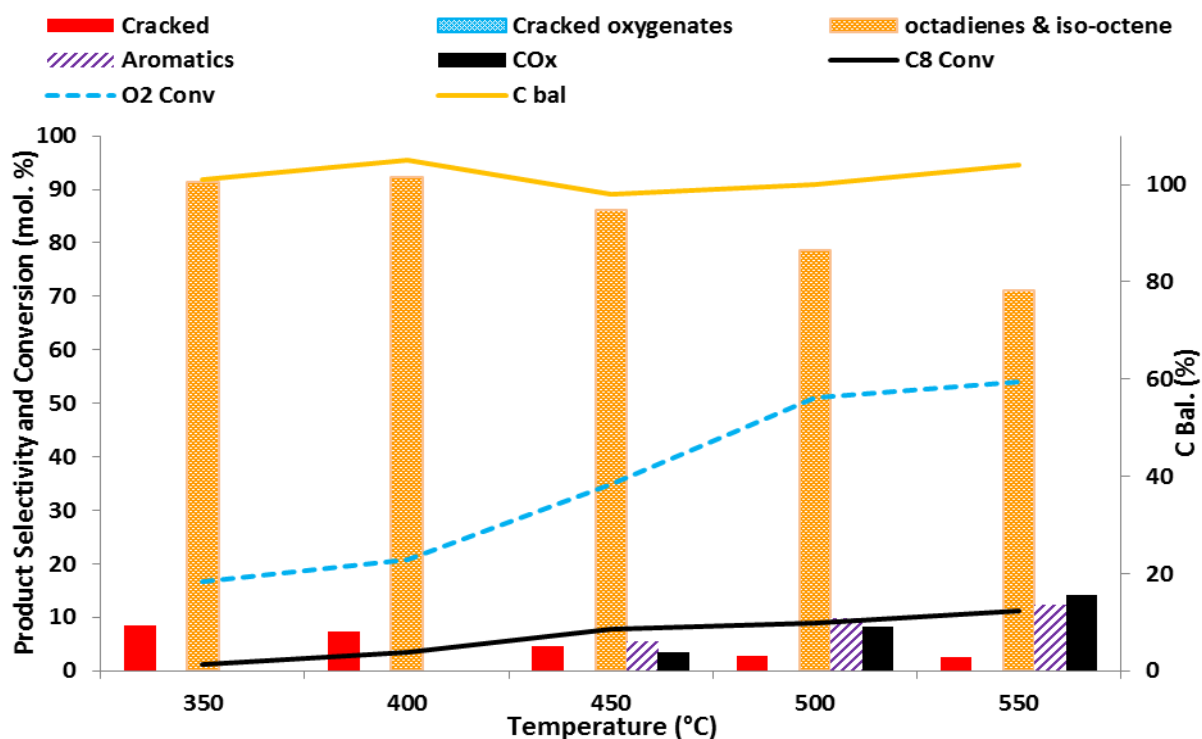
Figure 4.8 - **Reaction of 1% oct-1-ene (13.3ml/min, C:O 8:1) through a blank tube. Temperature range from 350-550°C**

As can be seen the oct-1-ene is converted to octadienes and iso-octene even in the absence of a catalyst, due to the temperature of the furnace. The conversion to iso-octene from oct-1-ene is unsurprising it is a more stable isomer. Low levels of aromatics are observed from ≥450°C. Catalytic cracking is seen in from 350-550°C. Low levels of CO_x are seen from ≥450.
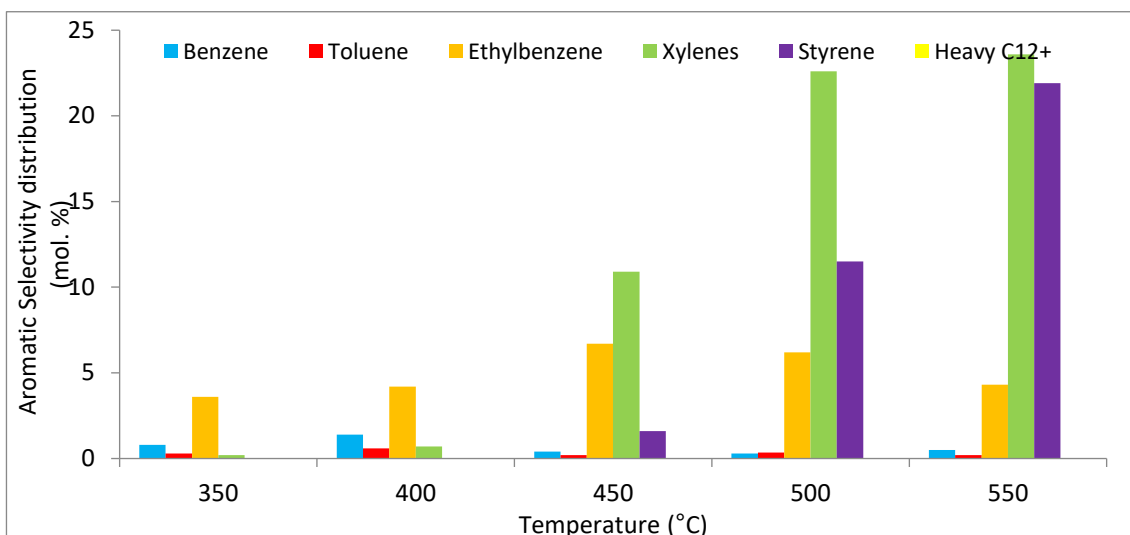
Figure 4.9 - **Aromatic selectivity Reaction of 1% oct-1-ene (13.3ml/min, C:O 8:1) through blank stainless steel tube. Temperature range from 350-550°C**

As can be seen from the aromatic selectivity, oct-1-ene shows high selectivity to xylene at 450°C and above, with styrene being produced at ≥500°C (although in concentrations of ≤3%). This would suggest that 2,7 ring closure is favoured when oct-1-ene is produced to yield xylene as the dominant product.

4.5.2 REACTIVITY OF 1% OCT-1-ENE OVER PRE-REDUCED IRON MOLYBDATE CATALYST
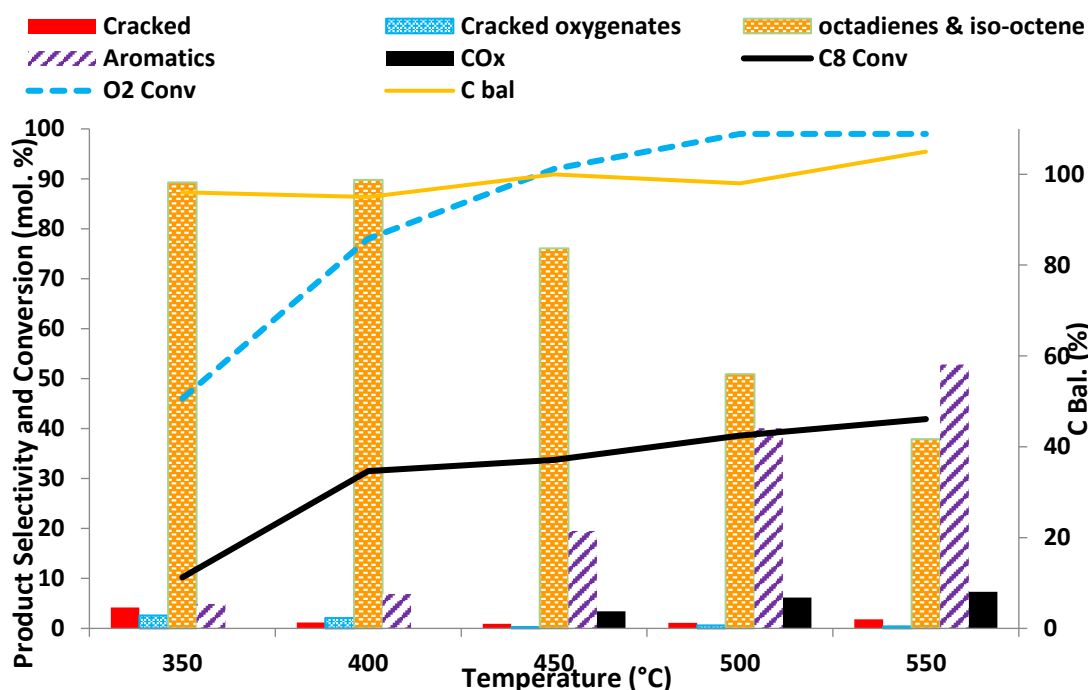
Figure 4.10 - **Reaction of 1% oct-1-ene (GHSV 4000h^{-1}, C:O 8:1) over a pre-reduced iron molybdate catalyst. Temperature range from 350-550°C**

Once a catalyst is added, much higher activity is observed, with conversions as high as *ca*.42% at 500°C being observed. Considering the greater reactivity of oct-1-ene compared to *n*-octane this is to be expected. At ≤400°C selectivity of *ca*.90% is observed for octadienes and iso-octene. As the temperature increases above 400°C more aromatics are seen, with very low levels of CO_x (≤7.5%) produced.

However aromatic selectivity is lower than when *n*-octane was used as a substrate (Table 4.1). This does not indicate that aromatic formation follows an octadiene/octatriene intermediate. Aromatic formation may be formed by ring closure and subsequent oxidative dehydrogenation. This process is favoured by higher contact times and temperatures. The lower selectivity to aromatics exhibited by oct-1-ene is due to its greater reactivity, thus conversion to octadienes/iso-octenes occurs preferentially to ring closure.

Temperature sampled / °C	Selectivity to aromatics (mol. %) when n-octane used as a substrate	Selectivity to aromatics (mol. %) when oct-1-ene used as a substrate
350	9.6	4.9
400	17.2	6.7
450	30.1	19.5
500	53.9	40.2
550	55.1	52.8

Table 4.1 – Comparison of aromatic selectivity when 1% *n*-octane and 1% oct-1-ene are reacted over a pre-reduced catalyst at 4000h^{-1}
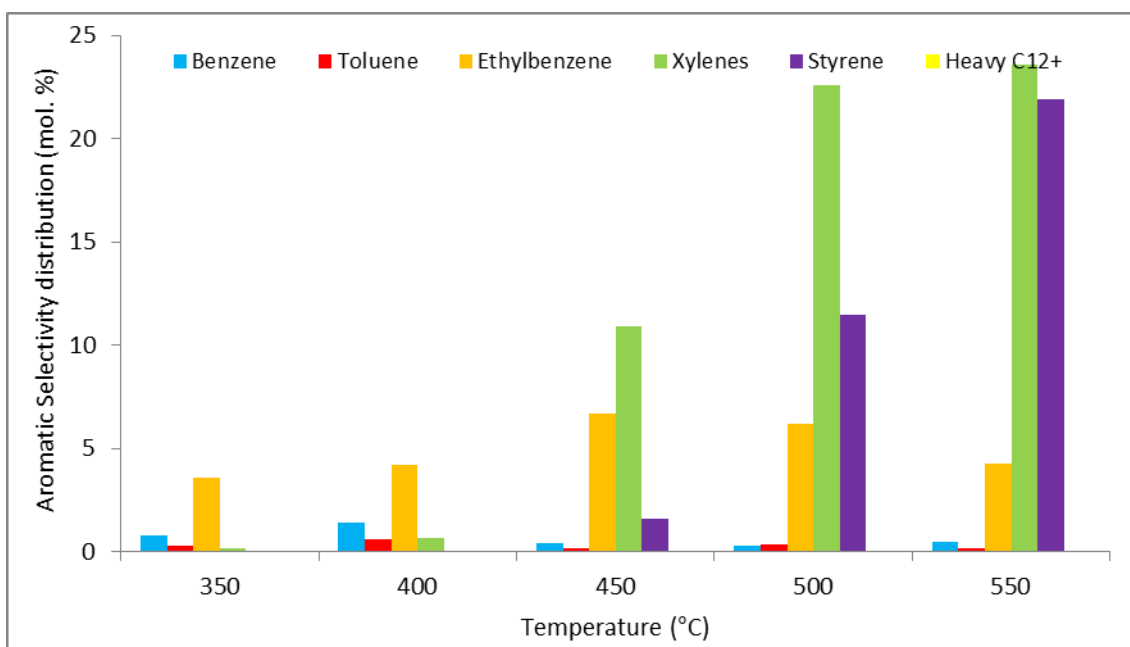
Figure 4.11 - Aromatic selectivity Reaction of 1% oct-1-ene (4000h^{-1}, C:O 8:1) over a pre-reduced iron molybdate catalyst. Temperature range from 350-550°C

Aromatic selectivity shows in contrast to *n*-octane, that oct-1-ene produces ethylbenzene at low temperatures, when reacted over a pre-reduced iron molybdate catalyst. Very low levels of benzene and toluene are detected, which could indicate lower carbon laydown at the catalyst surface. At ≥450°C *o*-xylene becomes the dominant product, although high levels of styrene are produced at 550°C. Ethylbenzene production did not increase with temperature, unlike xylene and styrene, this may indicate that it is an intermediate to forming styrene.

4.5.3 EFFECT OF ALTERING C:O AND GHSV RATIO WITH THE REACTION OF OCT-1-ENE

Work with *n*-octane shows that temperatures of ≥500°C and low GHSV results in the production of aromatics as the dominant product, while higher GHSV and temperatures of ≤400°C result in octenes as the main product. Introducing more oxygen to the gas feed led to greater levels of carbon oxides produced and greater activity across all temperatures tested, while a greater proportion of *n*-octane to oxygen led to lower conversions and activity.

Oct-1-ene was expected to follow a similar trend, with higher GHSVs maximising octadiene and iso-octene production, while lower GHSVs would maximise aromatic and carbon oxide production. Greater ratios of oxygen to carbon in the gas feed was expected to cause greater carbon oxide production. While more carbon to oxygen was expected to result in lower oct-1-ene conversions due to depressed catalytic activity from a lack of oxygen.
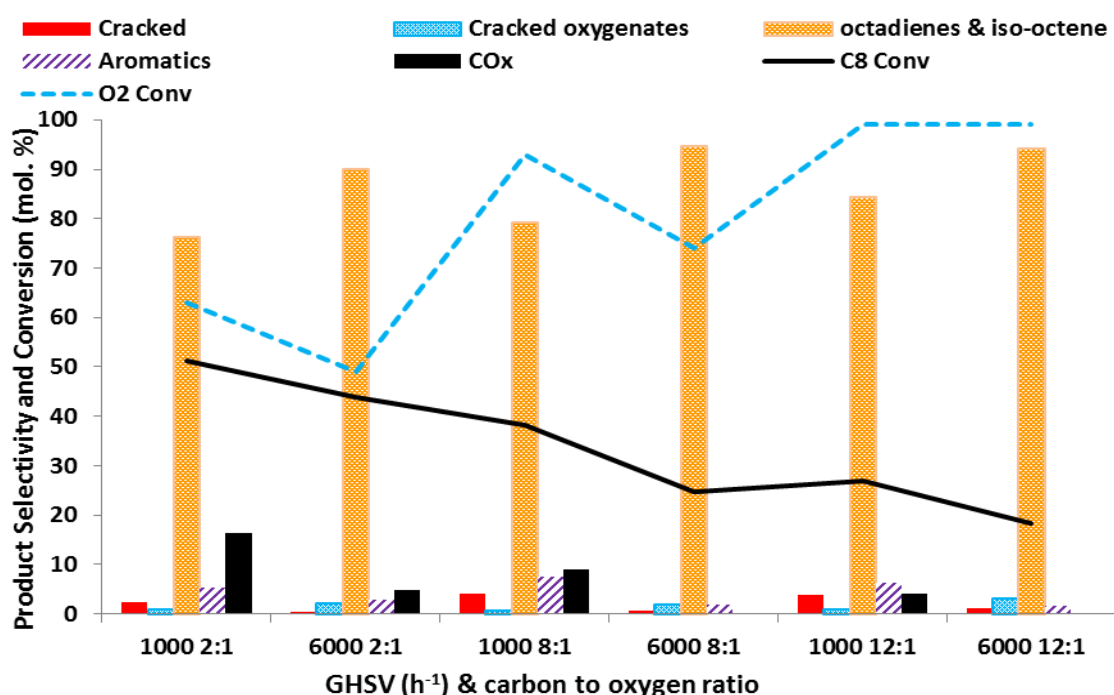
Figure 4.12 - **Reaction of 1% oct-1-ene (temperature held at 400°C) over a pre-reduced iron molybdate catalyst over a range of C:O ratios and GHSV**

Figure 4.12 shows that greater levels of oxygen in the gas feed lead to higher oct-1-ene conversions. Lower GHSV also gives higher conversions. Where conversion rises so does oxygen consumption, showing oxidative dehydrogenation (ODH) is occurring. Where less oxygen was present (12:1 C:O) in the gas feed, lower conversions were observed, while all oxygen was consumed, again suggesting ODH is occurring. Higher levels of oxygen present in the gas feed (2:1 C:O) resulted in the formation of carbon oxides. Low GHSV (1000h^{-1}) across all carbon to oxygen ratios resulted in the formation of carbon oxides and higher levels of cracked products.

These findings are similar to the results observed with *n*-octane, indicating the same mechanism. Lower GHSVs (higher contact times) favour the production of carbon oxides and also result in higher conversions. Higher GHSVs (lower contact times) result in lower conversions but greater selectivity to octadienes. If the carbon to oxygen ratio is 2:1 higher conversion is observed but carbon oxides are formed. If C:O ratio is 12:1 lower conversion but greater selectivity to octadienes is found.
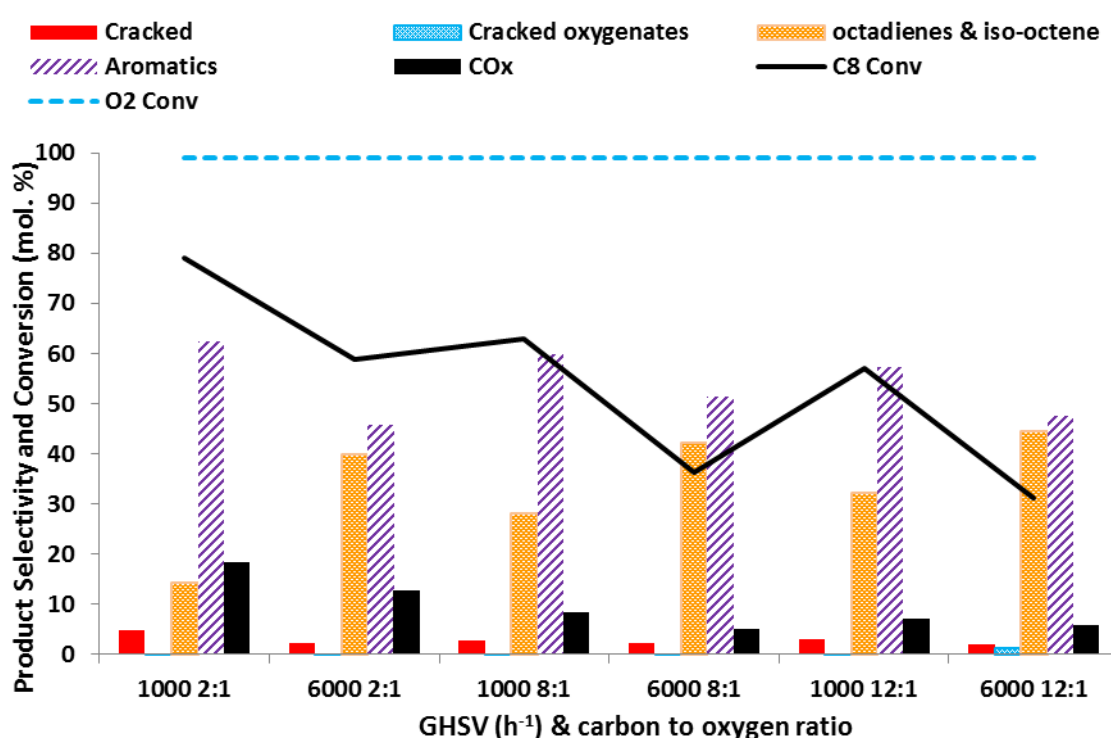
Figure 4.13 - **Reaction of 1% oct-1-ene (temperature held at 550°C) over a pre-reduced iron molybdate catalyst over a range of C:O ratios and GHSV**

Figure 4.13 also shows that lower GHSV leads to higher oct-1-ene conversions. Greater levels of oxygen present in the gas feed lead to greater oct-1-ene conversion, this is indicative of ODH occurring.

At 550°C aromatic species are the main products formed. Oxygen consumption across all carbon to oxygen profiles is 100%, again indicative of ODH occurring. Lower selectivity to carbon oxides is observed with oct-1-ene as the substrate when compared to *n*-octane. Higher substrate conversions are also seen. This is due to the alkene being more reactive than the alkane.

In summary, it appears that the aromatisation occurs via a dehydrocyclisation mechanism rather than an octadiene/triene intermediate. It was expected that if aromatisation occurred via the latter pathway then placing oct-1-ene in the reactor in place of *n*-octane would lead to a greater selectivity to aromatics. This was not the case (see table 4.1). Across all temperature profiles n-octane showed greater selectivity to aromatics than oct-1-ene. Oct-1-ene also showed greater reactivity than *n*-octane.

4.6 DEHYDROGENATION STUDIES

The data presented so far in both this chapter and chapter 3 has focused on studies where a mixture of 1% alkane/alkene, with a varying concentration of oxygen (ranging 12:1 carbon atoms to oxygen atoms down to 2:1 carbon atoms to oxygen atoms) and the remainder of the gas feed (*ca*.96-98.5%) being helium as a carrier gas, being passed over a pre-reduced iron molybdate catalyst. In Chapter 3 a 10% alkane concentration with an 8:1 carbon to oxygen ratio was also tested.

This section examines the effect of removal of the oxygen from the reaction feed. The previous results indicate catalytic oxidative dehydrogenation is occurring with oxygen consumption rising with increased conversion and overall conversions becoming higher with increased oxygen concentrations in the gas feed. Molybdates are also noted for being ODH catalysts.[1,2]

If oxygen is removed from the system then it would be expected that the ODH reaction would cease to occur.[19] However molybdates intercalated in a hydrotalcite have been shown to exhibit dehydrogenation of cyclohexane.[20]

It was therefore of interest to examine the effect of removing oxygen totally from the catalytic system. It was initially expected that there would be some initial catalytic activity as the oxygen rich molybdates continued ODH via a Mars-Van Krevelen style mechanism[21], before seeing a drop in activity as the lattice oxygen in the iron molybdate catalyst was not replenished.

The first experiment was done at a GHSV of 4000h[-1] with a range of temperatures to observe any catalytic activity. The system was run under anaerobic conditions for 15 hours before any sampling was undertaken, to ensure any residual oxygen was purged.
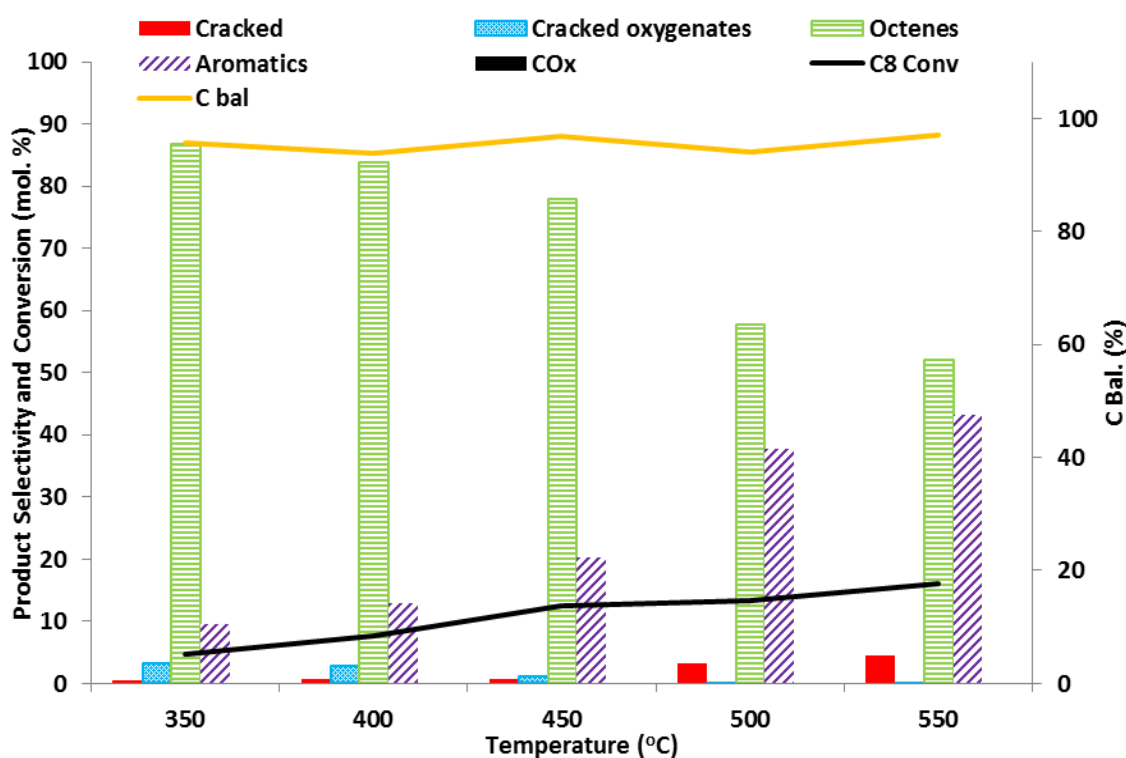
Figure 4.14 - **Reaction of 1% *n*-octane (anaerobic conditions, 4000h[-1]) over a pre-reduced iron molybdate catalyst temperature range 350-550°C**

Figure 4.14 showed a reaction occurring. With *n*-octane conversions of *ca.*16.5% at 550°C exhibited and octenes as the main product. Carbon oxides, produced at temperatures of ≥450°C at the conditions of Figure 4.14 when oxygen was present in the system, are not produced. This suggested that carbon oxides are produced from

oxygen species from the gas phase rather than via the bulk lattice oxygen present in iron molybdate. The presence of cracked oxygenates at lower temperatures showed that oxygen was still present in the system, from the catalyst lattice.

As the temperature increased selectivity to aromatics and cracked products increased. Octenes were the main product, even at 550°C. This was not the case when oxygen was present in the same conditions, as aromatics and carbon oxides were produced in greater levels than octenes.

An experiment to observe the effect of altering GHSV was then undertaken.
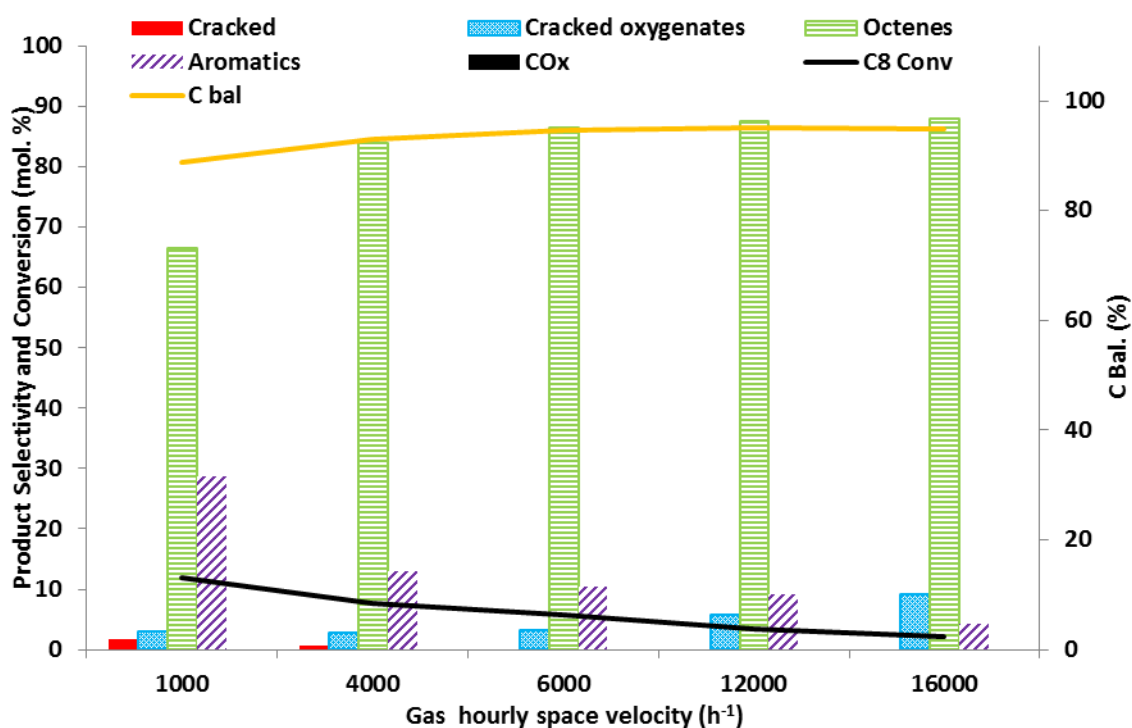
Figure 4.15 - **Reaction of 1% *n*-octane (anaerobic conditions, 400°C) over a pre-reduced iron molybdate catalyst GHSV range 1000-16,000h^{-1}**

Across all of the GHSVs tested in Figure 4.15 cracked oxygenates were observed. This indicated the presence of oxygen in the system. No carbon oxides were observed at lower GHSV. Lower GHSV resulted in greater *n*-octane conversion and greater selectivity to aromatics with high conversions. Higher GHSV resulted in greater selectivity to octenes.

Figures 4.13 and 4.14 showed a reaction was occurring without oxygen but whether it was catalytic ODH or dehydrogenation (DH) occurring was unclear. ODH with the remainder of lattice oxygen from the catalyst could have been occurring, resulting in the presence of cracked oxygenate products.

A time on line (TOL) study was done to observe if activity and selectivity altered over time in an anaerobic environment.
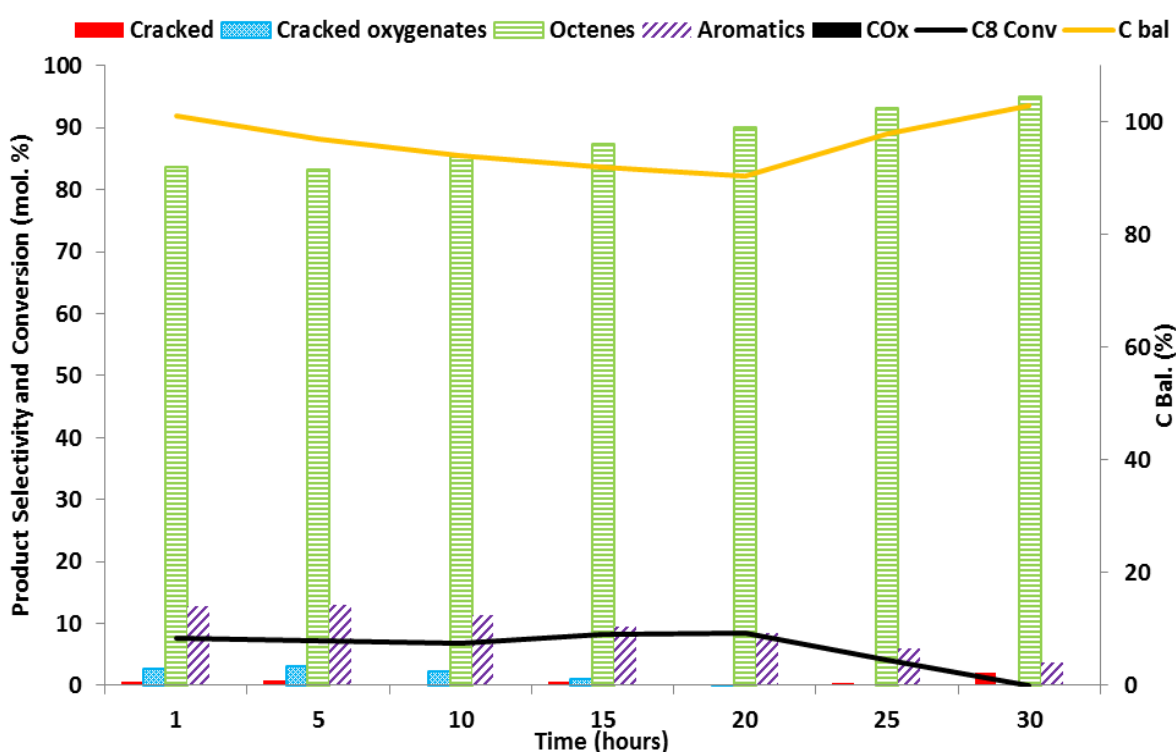
Figure 4.16 – TOL study of the reaction of 1% *n*-octane (anaerobic conditions, 400°C, 4000h^{-1}) over a pre-reduced iron molybdate catalyst. Lasting 30 hours

Figure 4.16 shows that selectivity to octenes increases as the reaction progresses. Selectivity to cracked oxygenates drops from *ca.*2.7% after 1 hour to *ca.*0.3% after 20 hours, before not being seen at 25 and 30 hours. This suggests that lattice oxygen is being removed as the reaction continues in an anaerobic environment. Selectivity to aromatics drops slightly from *ca.*12.9% to *ca.*6.5% through the reaction. Conversion decreases notably after 20 hours. By 30 hours the lattice oxygen is exhausted and oxidative dehydrogenations is no longer occurring. The carbon balance drops

considerably during the reaction until 20 hours. This may suggest carbon laydown is occurring. Analysis was done on the catalyst after the TOL anaerobic study.

This finding shows that the pre-reduced iron molybdate catalyst proceeds by an oxidative dehydrogenation mechanism, the continuing catalytic activity for more than 25 hours without the presence of oxygen suggests that the a Mars-Van Krevelen is occurring, with lattice oxygen still abstracting hydrogen atoms from the alkane. However with no oxygen present, this lattice oxygen is not replaced.

The absence of carbon oxides, when the reaction is run without oxygen, indicates that it is an oxygen species from the gas phase that forms carbon oxides. Lattice oxygen species do not act so. This may mean that carbon oxides are formed via a Langmuir-Hinshelwood or Eley-Rideal style mechanism.

4.6.1 ANALYSIS OF THE CATALYST AFTER ANAEROBIC TOL REACTION

The structure of the catalyst after being deprived of oxygen and being reacted with 1% *n*-octane (see Figure 4.16). X-ray powder diffraction (XRPD) was carried out.
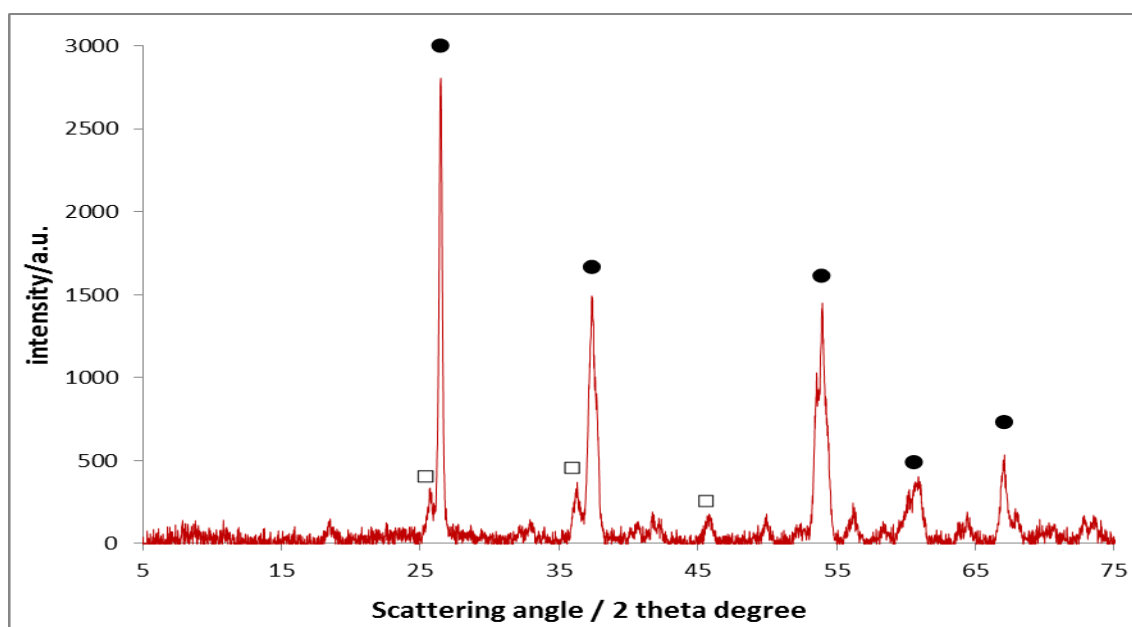
Figure 4.17- XRPD of a pre-reduced iron molybdate catalyst post TOL study. Phases present: β-FeMoO₄ (□) and MoO₂ (●). (1% *n*-octane, 4000h⁻¹, 400°C and anaerobic conditions, 30 hours on line).

Species	Peak (2 theta degrees)	Lattice Plane	d-spacing (Å)
MoO$_2$	26.0	-111	3.42
	37.1	-211	2.42
	53.9	-213	1.69
	57.4	-303	1.60
	66.6	-402	1.40
B-FeMoO$_4$	26.2	220	3.40
	36.3	400	2.47

Table 4.2 – XRPD Peak list for Figure 4.17 with associated d-spacing and lattice planes.

Figure 4.17 shows that after a 20 hour reaction without the presence of oxygen, there are no Mo$_4$O$_{11}$ species present. MoO$_2$ is present. This suggests the free molybdenum in the bulk of the pre-reduced iron molybdate catalyst has been reduced from a +6 to a +4 oxidation state. This correlates with the results in Figure 4.16 where the cracked oxygenate species stop being produced as the reaction progresses, along with the eventual drop in catalytic conversion, suggesting the stripping of lattice oxygen. This is consistent with a Mars-Van Krevelen ODH mechanism.[21] Figure 4.17 also shows the presence of β-FeMoO$_4$ which has not been reduced further.

Ultra-violet Raman spectroscopy was carried out on the catalyst sample.
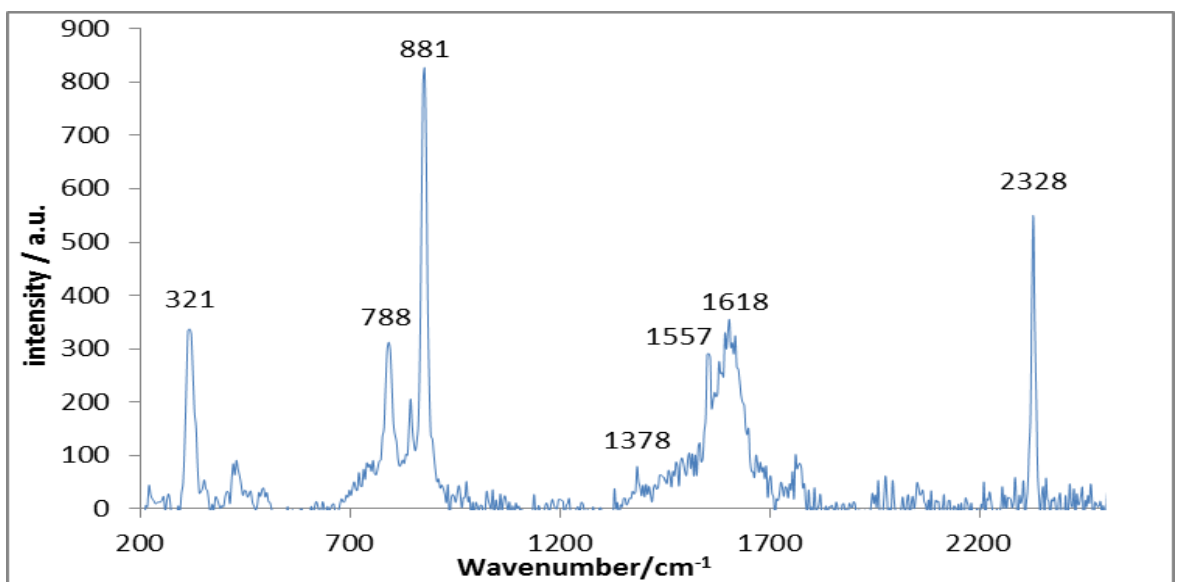
Figure 4.18- UV Raman spectra of pre-reduced iron molybdate catalyst post TOL study (1% *n*-octane, 4000h^{-1}, 400°C, anaerobic conditions, 30 hours on line)

The peaks at 881cm^{-1} in Figure 4.18 indicate of antisymmetric Mo-O-Mo stretching vibrations in molybdenum oxides. The absence of peaks at *ca.*995cm^{-1} shows no terminal molybdenum oxygen bonds are detected. This would suggest that it is MoO_2 that is present in the bulk lattice not Mo_4O_{11} or MoO_3. The peak at 788cm^{-1} is indicative of the molybdenum oxygen bond stretching in iron molybdate. The spectra indicates that the catalyst sample has been reduced to a MoO_2 + $FeMoO_4$ system. This is also shown in the XRPD in Figure 4.17.

The peaks at 1378cm^{-1}, 1557cm^{-1}, 1618cm^{-1} and 2328cm^{-1} suggest the presence of graphitic carbon at the catalyst surface.[22–24] The peak at 1378cm^{-1} is indicative of the D-mode of carbon. The peaks at 1557cm^{-1} and 1618cm^{-1} are indicative of G-band splitting, with the peak 1557cm^{-1} being the G-peak and 1618cm^{-1} the D'-peak.[22] The peak at 2328cm^{-1} is the 2D(G*) band, which is indicative of graphitic sp2 materials.[23,25] Carbon nanotubes could be a structure formed which would exhibit sp2 hybridisation. Figure 4.18 with the difference in D and G bands and the presence of a sharp G* band indicates the presence of single walled carbon tubes (SWNT) or graphene.[26]

Carbon nanotubes have been shown to be produced on molydates.[27,28] Lamoroux *et al* [29] have shown the production of single walled carbon nanotubes via an $FeMoO_4$ phase.

X-ray photo electron spectroscopy (XPS) was then done on the catalyst sample to observe if carbon is present on the surface. Two experiments were carried out, firstly XPS was run on a sample that had been exposed to oxidative dehydrogenation. Conditions of 8:1 C:O ratio, 4000 h^{-1}, 400°C, 30 hrs on-line. Then XPS was carried out on another sample which had been deprived of oxygen. Anaerobic conditions of 4000 h^{-1}, 400°C, 30 hrs on-line.

Figure 4.19 – XPS spectra of surface of pre-reduced iron molybdate after undergoing catalytic testing with oxygen. Conditions of 8:1 C:O ratio, 4000 h^{-1}, 400°C, 30 hrs online.

As can been seen in Figure 4.19 a low level peak corresponding to a C (1s) species is observed at *ca.*284.9 eV, this corresponds with C-C bonds, the peaks being centred at 284.9eV suggests sp3 carbon. There is a second peak of low intensity at the binding energy of 289.2 eV, the literature indicates this is C (1s) of trace levels of C=O bonds seen at 289 eV.[30] However after the anaerobic testing a much stronger, more intense carbon peak was observed. This gives further evidence to suggest carbon laydown is occurring when oxygen is removed from the system.[30,31]
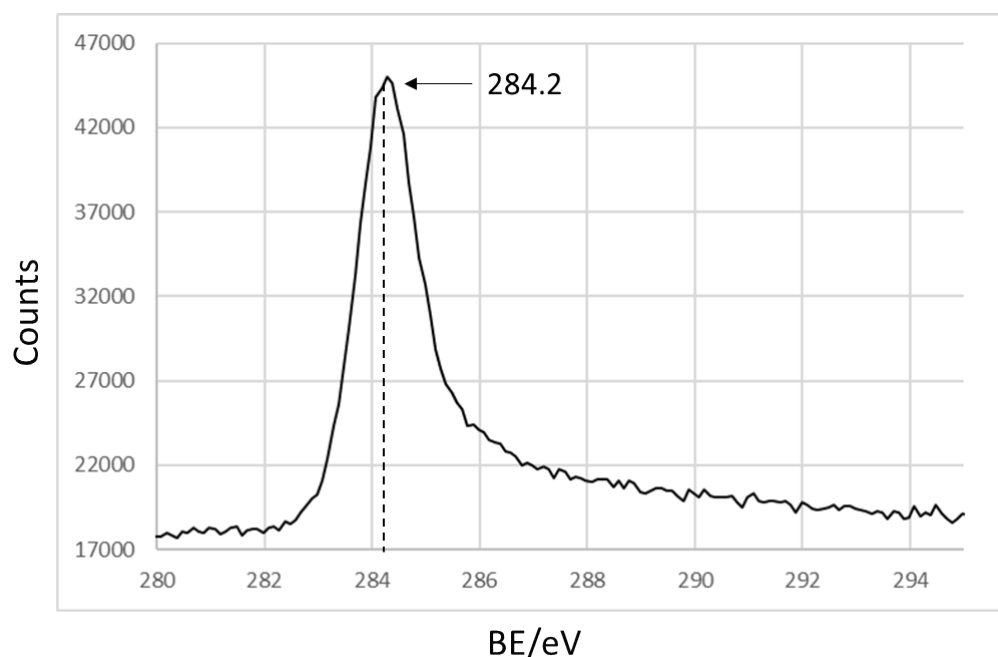
Figure 4.20 – XPS spectra of surface of pre-reduced iron molybdate after undergoing catalytic testing without oxygen. Anaerobic conditions of 4000 h^{-1}, 400°C, 30 hrs on-line.

Although Figure 4.20 looks simple, one peak with a binding energy (BE) of 284.2 eV, it can be inferred from the long asymmetric tail toward higher binding energy that the presence of sp2 carbon at the catalyst surface is likely post reaction.[32] The peak shift of 0.7 eV from Figure 4.19 also indicates the presence of sp2 type carbon in Figure 4.20 as proposed by Estrade-Szwarckopf.[33] This shift in XPS data from Figure 4.19 to 4.20 and the much higher intensity of counts suggests carbon laydown, potentially of sp2 hybridised graphitic type materials as suggested by Li *et al*[34].

4.6.2 Catalytic activity of pure phase $FeMoO_4$ in an anaerobic environment

Having hypothesised that bulk lattice oxygen from the Mo_4O_{11} phase of the pre-reduced iron molybdate causes ODH to still occur in an anaerobic environment, pure phase $FeMoO_4$ was tested to observe activity.
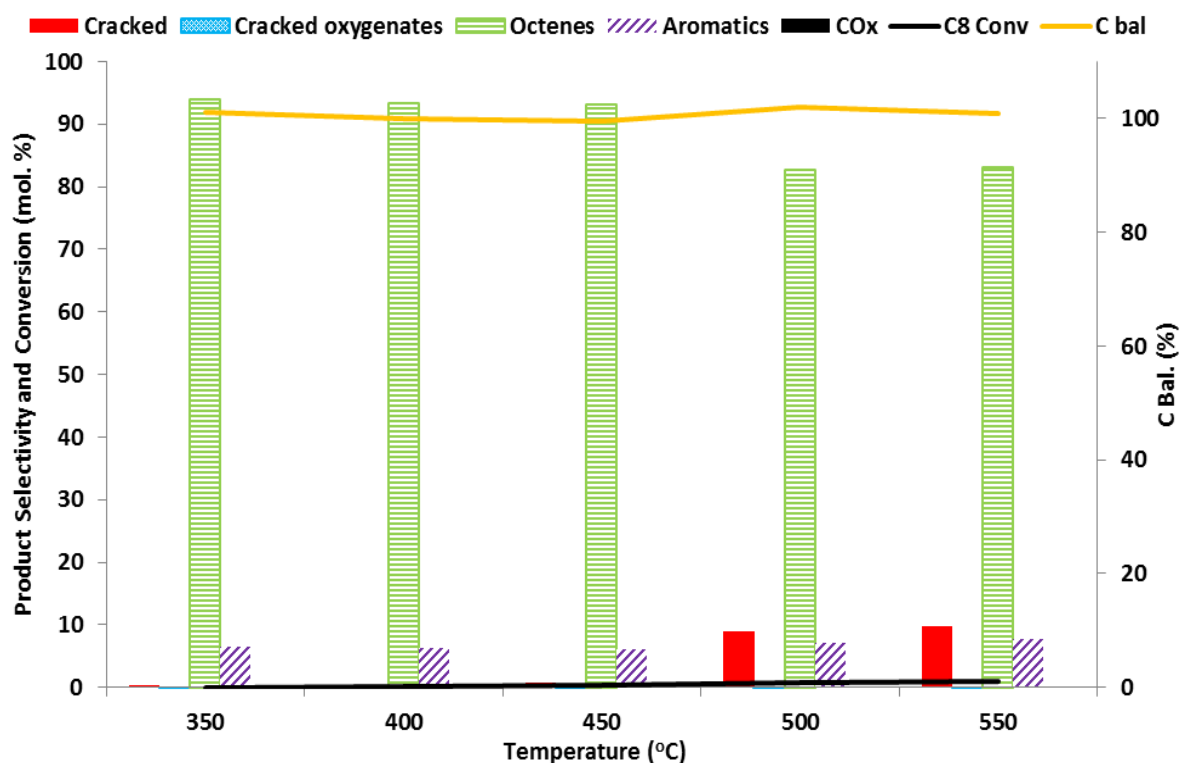
Figure 4.21 - **Reaction of 1% *n*-octane (anaerobic conditions, 4000h^{-1}) over a pure phase FeMoO$_4$ catalyst, temperature range 350-550°C**

Figure 4.21 illustrates how pure phase FeMoO$_4$ exhibits no catalytic activity when no oxygen was present in the system. This was expected as there was no molybdenum oxides present from which lattice oxygen could be used.

These findings confirm that the pre-reduced iron molybdate catalyst proceeds by an oxidative dehydrogenation system. When oxygen is removed from the system, the catalyst still exhibits activity due to the lattice oxygen present, this can be attributed to the oxygen rich Mo$_4$O$_{11}$ species in the catalyst. This was proven by testing pure phase FeMoO$_4$ as a catalyst when oxygen is not present, no activity was observed. After a period of 30 hours the lattice oxygen is exhausted and the catalyst ceases to be active. The catalyst once inactive possesses a structure of bulk MoO$_2$ + FeMoO$_4$. UV Raman and XPS show that a layer of carbon is deposited on the surface that is not observed when oxygen is present in the system. Molybdenum at the surface shows a combination of molybdenum oxygen states, with Mo(VI) being attributed to the

FeMoO$_4$ phase, and Mo(V) and Mo(IV) states being attributed to the reduced molybdenum.

It was also shown that carbon oxides are not produced when the system is deprived of oxygen. Cracked oxygenates are initially formed before the catalyst undergoes reduction. This indicates that carbon oxides are formed through a surface reaction involving gaseous oxygen, and is not formed via the Mars-Van Krevelen mechanism that produces cracked oxygenates, octenes and aromatic species.

4.7 RE-INTRODUCTION OF OXYGEN TO THE SYSTEM AFTER REDUCTION

As demonstrated in the previous section, the catalyst when deprived of oxygen will cease to be active after lattice oxygen has been removed. In this section the effect of reintroducing oxygen to the system will be examined. It was of interest to observe the effect that reduction would have on activity and selectivity, as Figure 4.17 shows, the catalyst system after oxygen removal is comprised of MoO$_2$ + FeMoO$_4$.

As seen in chapter 3, FeMoO$_4$ is an active ODH catalyst with a high selectivity to octenes. MoO$_2$ exhibits much lower activity but with high selectivity to heavy aromatics such as naphthalene.

The pre-reduced iron molybdate catalyst that has been exposed to anaerobic conditions, at 400°C, 4000h^{-1}, for 30 hours will be referred to as **the oxygen depleted catalyst** to avoid confusion.
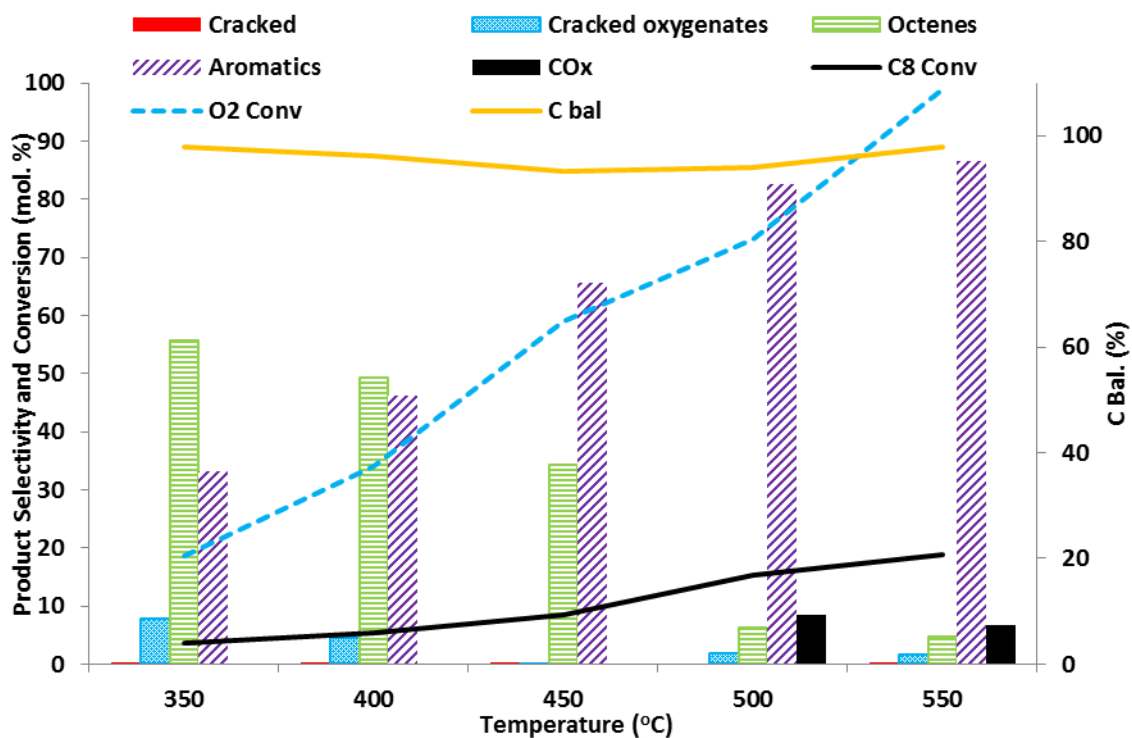
Figure 4.22 - **Reaction of 1% *n*-octane (C:O 8:1, 4000h^{-1}) over an oxygen depleted iron molybdate catalyst, temperature range 350-550°C**

Figure 4.22 shows that after re-introduction of oxygen to the gas feed the oxygen depleted catalyst exhibits very different activity and selectivity to its prior state. Selectivity to aromatics is much higher and greater levels of cracked oxygenates are seen. Carbon oxides are observed only at ≥500°C and selectivity to them is lower than a pre-reduced Mo_4O_{11} + $FeMoO_4$ system exhibits. Cracked products even at high temperatures are negligible.

The *n*-octane conversion rises in line with oxygen consumption, showing that oxidative dehydrogenation is occurring once more.
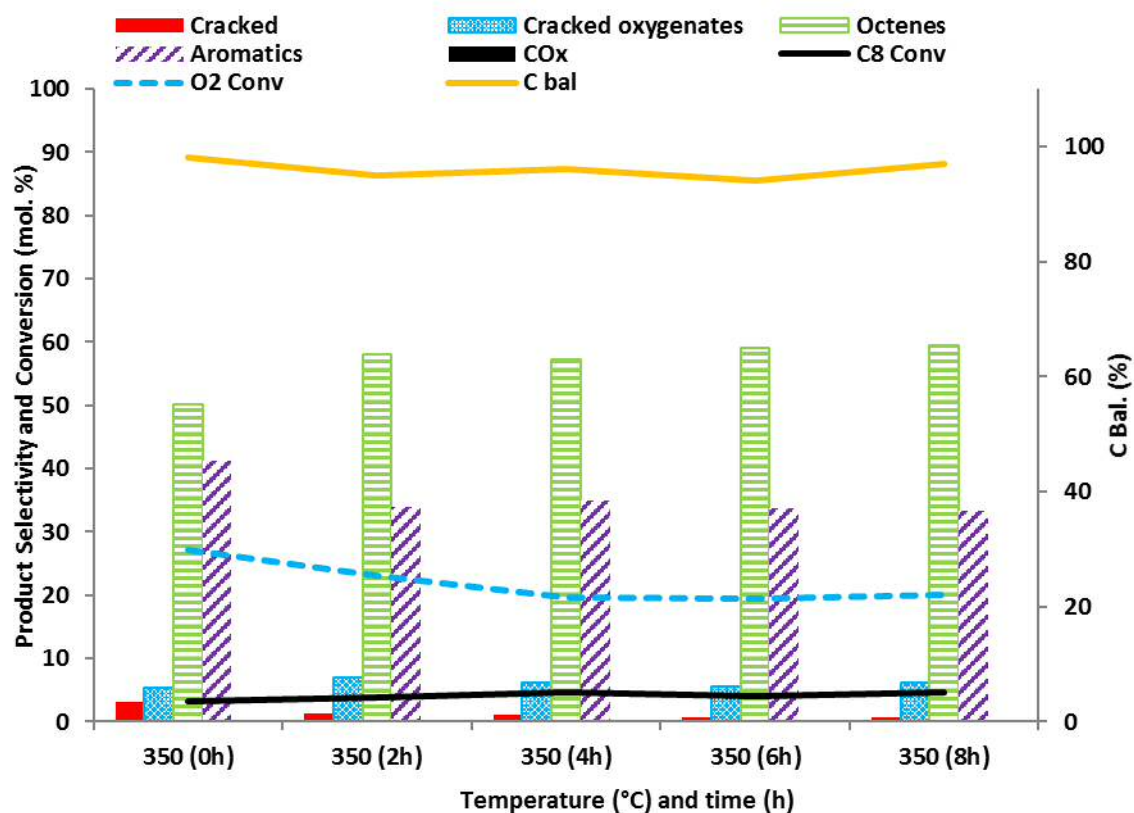
Figure 4.23 - **Reaction of 1% *n*-octane (C:O 8:1, 4000h⁻¹) over an oxygen depleted iron molybdate catalyst, temperature kept constant at 350°C for a period of 8 hours.**

To ensure the reaction in Figure 4.22 was steady state and that oxygen re-adsoprtion to the lattice was not influencing results, the reactor was kept at 350°C for 8 hours with a gas flow of 1% *n*-octane and oxygen. Figure 4.23 shows the reaction is steady state.

Considering the high selectivity to aromatics it is worth comparing the results in Figure 4.22 to the results obtained for the reaction of *n*-octane over a MoO_2 catalyst shown in Figure 4.24.
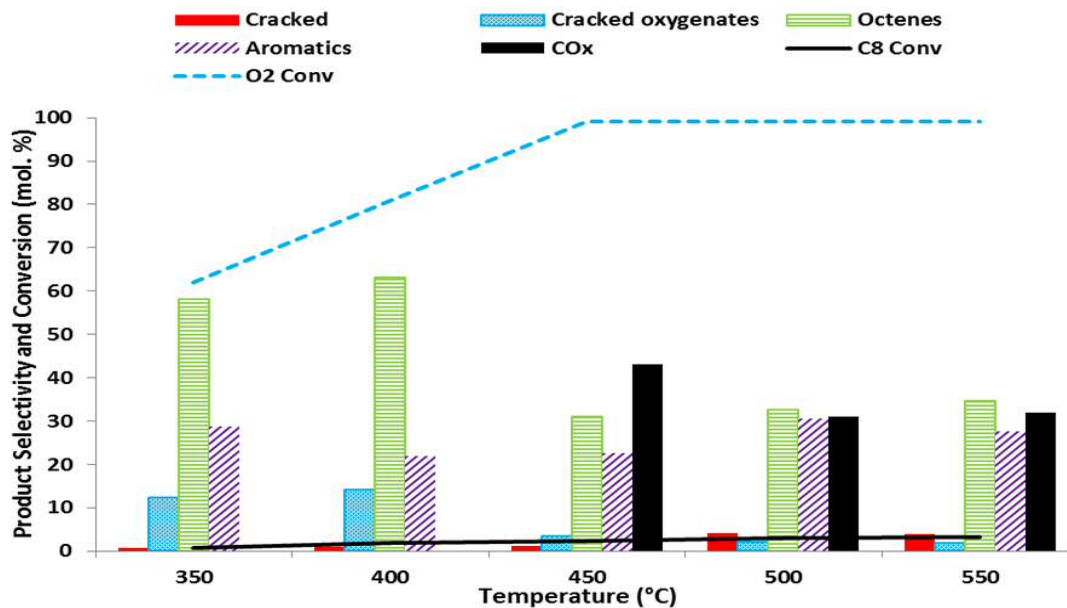
Figure 4.24 - **Reaction of 1% *n*-octane (C:O 8:1, 4000h^{-1}) over MoO$_2$ catalyst, temperature range 350-550°C**

Although there are some similarities (relatively high levels of cracked oxygenates at lower temperatures) between the results in Figures 4.22 and 4.24 there are obvious differences. This indicates that it is not only MoO$_2$ that is having an effect on the products.

Equally of interest are the aromatic species formed.
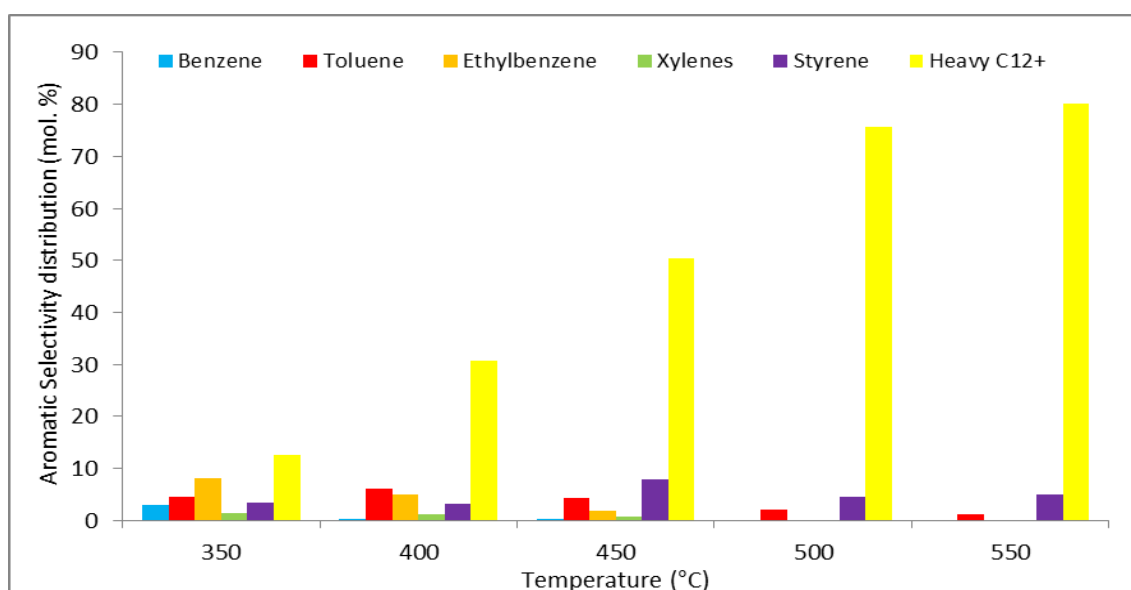
Figure 4.25 - **Aromatic selectivity Reaction of 1% *n*-octane (4000h^{-1}, C:O 8:1) over an oxygen depleted iron molybdate catalyst. Temperature range from 350-550°C**

Figure 4.25 shows how after being oxygen deprived the catalyst produces "heavy" (12 carbons or greater) aromatics, mainly naphthalene and naptha-2-ene. As temperature increases so does selectivity to these large aromatic species. Again it is worth comparing these results to when MoO_2 was used as a catalyst in the same conditions.
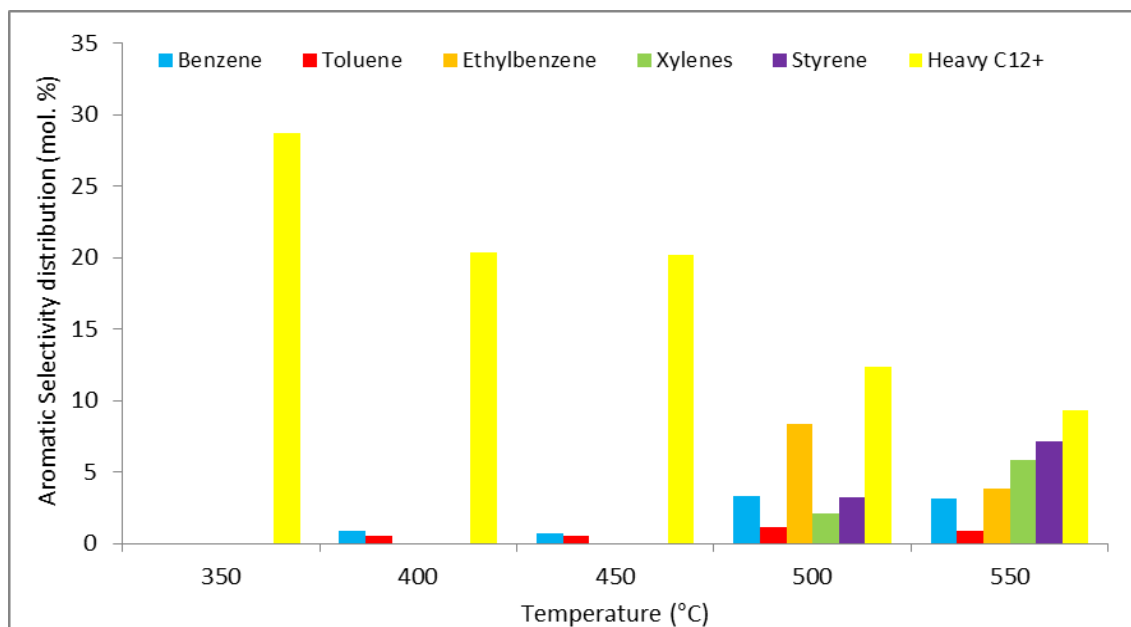
Figure 4.26 - **Aromatic selectivity Reaction of 1% *n*-octane (4000h^{-1}, C:O 8:1) over a MoO_2 iron molybdate catalyst. Temperature range from 350-550°C**

The data in Figure 4.26 appears to show the opposite trend to that of Figure 4.25. As the temperature increases with a MoO_2 catalyst the selectivity to heavy aromatics drops, and greater levels of 8 carbon chain aromatics are produced.

The production of high levels of 12 (and higher) carbon aromatics with an oxygen depleted catalyst may therefore be due to a combination of MoO_2 and the carbon laydown at the surface of the catalyst. Potential carbon chain growth on the molybdenum[31,35–37] could lead to polyaromatic formation which at higher temperatures desorbs from the surface, giving the high selectivity for heavy aromatics. As noted earlier in the chapter, carbon deposits on the catalyst surface occur in when *n*-octane is passed over the catalyst in an anaerobic environment.

The effect of gas hourly space velocity on the activity and selectivity was then tested. The temperature of 400°C was chosen as the constant as it was interest to observe if carbon oxides would be produced at lower temperatures.
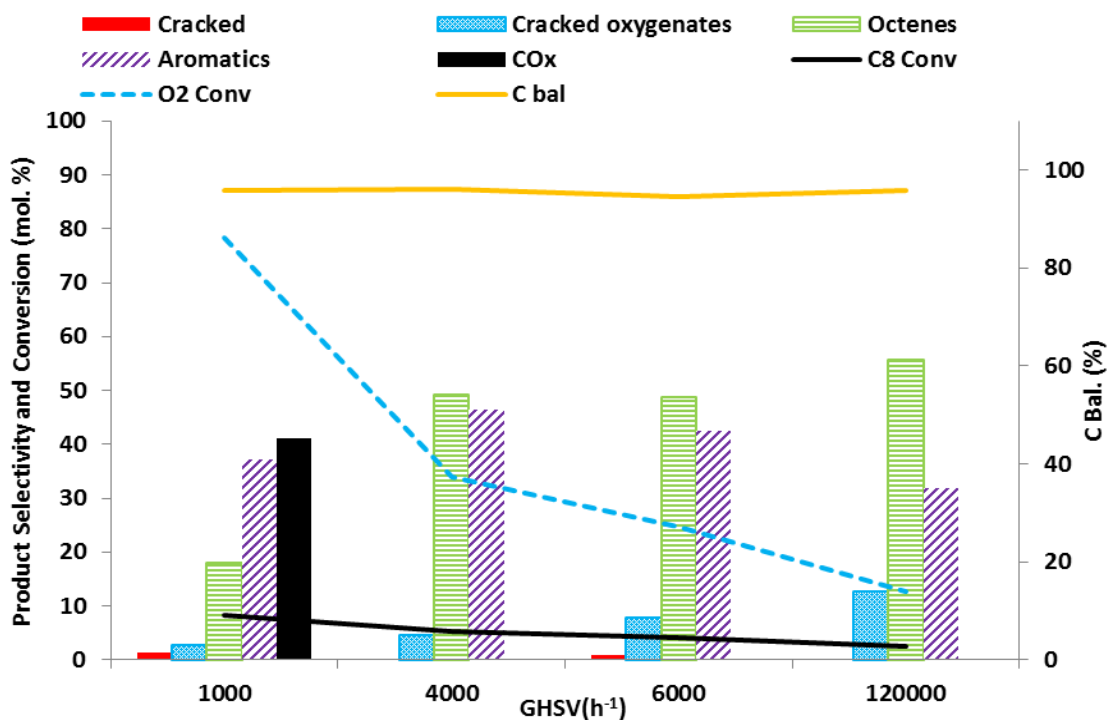
Figure 4.27 - **Reaction of 1% *n*-octane (400°C, C:O 8:1) over an oxygen depleted iron molybdate catalyst. GHSV range from 1000-12,000h^{-1}**

Figure 4.27 shows that at higher GHSVs conversion drops in line with oxygen consumption as would be expected with an ODH reaction. As GHSV rises so does selectivity to octenes and cracked oxygenates. When GHSV was at 1000h^{-1} carbon oxides were observed, suggesting that higher contact time allowed the surface reaction producing COx to occur.

When aromatic selectivity was examined (see Figure 4.28) higher GHSVs resulted in lower levels of polyaromatic hydrocarbons produced. This suggests that that lower contact times of *n*-octane to the catalyst surface mean it is less likely for polyaromatic hydrocarbons to form.
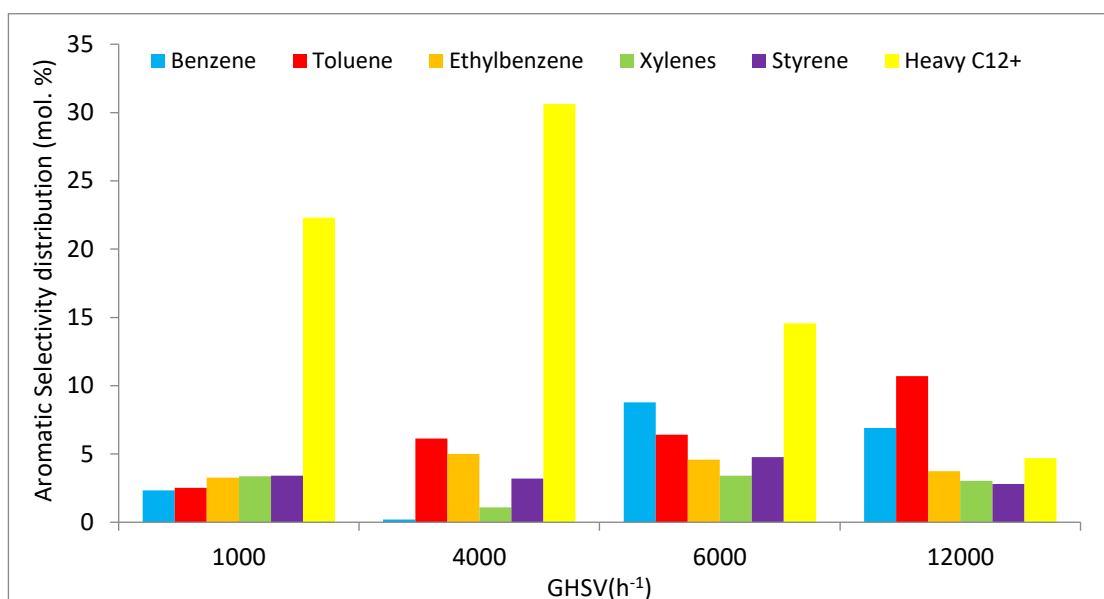
Figure 4.28 - **Aromatic selectivity Reaction of 1% *n*-octane (400°C, C:O 8:1) over an oxygen depleted iron molybdate catalyst. GHSV range from 1000-12,000h^{-1}**

SUMMARY OF CHAPTER 4

The pre-reduced iron molybdate acts as a catalyst for an oxidative dehydrogenation reaction. Catalytic activity rises in line with oxygen consumption. When oxygen is removed from the system and *n*-octane is passed over the catalytic activity is observed for up to 30 hours, although conversions decline after 20 hours in an anaerobic environment.

High selectivity to octenes was observed when there was no oxygen in the gas feed and no carbon oxides were produced. This indicates that carbon oxide production is produced from oxygen in the gas phase and not lattice oxygen in the molybdate. Cracked oxygenates were still produced when there was no oxygen in the gas feed suggesting they are produced via lattice oxygen in Mo_4O_{11}.

When pure phase $FeMoO_4$ was tested as catalyst for *n*-octane with no oxygen in the gas feed, no catalytic activity was observed. This shows that it is the Mo_4O_{11} species in the pre-reduced iron molybdate catalyst that provide the lattice oxygen required for activity. This confirms that the oxidative dehydrogenation proceeds by a Mars-Van Krevelen style mechanism.

Time on line studies showed that the carbon balance dropped when n-octane was passed over the catalyst with no oxygen present in the gas feed. Analysis by both XPS and UV Raman confirmed that carbon laydown was occurring. The data from UV Raman indicated that the carbon was of graphitic sp2 structure.

XRPD and UV Raman analysis showed that the molybdenum species were reduced from Mo_4O_{11} to MoO_2. $FeMoO_4$ phases remained unchanged.

When oxygen was reintroduced to the system after the catalyst had been reduced to $FeMoO_4$ + MoO_2, selectivity of products was very different. Low levels of carbon oxides were observed only ≥500°C. Selectivity to aromatics increased notably. At lower temperatures relatively high levels of cracked oxygenates were observed. The majority of aromatic products were polyaromatic hydrocarbons. The production of these is a point of interest, it has been found that MoO_2 showed a high selectivity to polyaromatics but the role of deposited carbon may also play a role. Raising the GHSV increases the selectivity to octenes and limits the production of polyaromatic hydrocarbons.

Altering the substrate to oct-1-ene showed that it is more reactive than n-octane. Oct-1-ene does not show higher selectivity to aromatic species than n-octane. This was of interest as the nature of aromatic formation was of interest. Two possible routes of formation were suggested. Either an octane molecule undergoes ODH to form an octa-diene/octatriene which then cyclises via an internal diels-alder style mechanism, or a dehydrocyclisation mechanism which then undergoes further removal of hydrogen to form an aromatic system. In the case of the former it was hypothesised that if octene was used as a substrate then selectivity to aromatics would rise compared to octane. This did not happen, selectivity to aromatics was actually slightly lower overall temperature profiles tested. This finding indicates that aromatics are formed via a cyclisation reaction before undergoing aromatisation.

It was also found that altering the GHSV and temperature for a period of 24 hours or more did not affect catalyst performance, as long as there was a flow of oxygen present, this suggests a degree of tunability.

Bibliography

1   Y. S. Yoon, W. Ueda and Y. Moro-oka, *Catal. Lett.*, 1995, **35**, 57–64.

2   Y. S. Yoon, W. Ueda and Y. Moro-oka, *Top. Catal.*, 1996, **3**, 265–275.

3   W. Ueda, Y.-S. Yoon, K.-H. Lee and Y. Moro-oka, *Korean J. Chem. Eng.*, 1997, **14**, 474–478.

4   M. M. Barsan and F. C. Thyrion, *Catal. Today*, 2003, **81**, 159–170.

5   D. L. Stern and R. K. Grasselli, *J. Catal.*, 1997, **167**, 550–559.

6   S. Pietrzyk, M. L. Ould Mohamed Mahmoud, T. Rembeczky, R. Bechara, M. Czernicki and N. Fatah, in *Studies in Surface Science and Catalysis*, ed. G. F. F. and K. C. Waugh, Elsevier, 1997, vol. 109, pp. 263–271.

7   Smolik, Petti, Schuetz, .

8   D. L. Stern and R. K. Grasselli, *J. Catal.*, 1997, **167**, 560–569.

9   N. B. of C. Engineers, *The Complete Technology Book on Detergents (2nd Revised Edition)*, Niir Project Consultancy Services, 2013.

10 S. ALBONETTI, F. CAVANI and F. TRIFIRÒ, *Catal. Rev.*, 1996, **38**, 413–438.

11 R. Grabowski, *Catal. Rev.*, 2006, **48**, 199–268.

12 C. Brookes, P. P. Wells, N. Dimitratos, W. Jones, E. K. Gibson, D. J. Morgan, G. Cibin, C. Nicklin, D. Mora-Fonz, D. O. Scanlon, C. R. A. Catlow and M. Bowker, *J. Phys. Chem. C*, 2014, **118**, 26155–26161.

13 K. Routray, W. Zhou, C. J. Kiely, W. Grünert and I. E. Wachs, *J. Catal.*, 2010, **275**, 84–98.

14 S. Pradhan, J. K. Bartley, D. Bethell, A. F. Carley, M. Conte, S. Golunski, M. P. House, R. L. Jenkins, R. Lloyd and G. J. Hutchings, *Nat. Chem.*, 2012, **4**, 134–139.

15 B. H. Davis, *Catal. Today*, 1999, **53**, 443–516.

16 B. Shi and B. H. Davis, *J. Catal.*, 1996, **162**, 134–137.

17 T. Paal, *Acta Chim AcadSciHung*, 273.

18 M. I. Rozengart, I. N. Fundyler, K. Y. Burshtein and T. Y. Krimond, *Bull. Acad. Sci. USSR Div. Chem. Sci.*, 1974, **23**, 1186–1188.

19 H. H. Kung, in *Advances in Catalysis*, ed. H. P. and W. O. H. D.D. Eley, Academic Press, 1994, vol. 40, pp. 1–38.

20 T. Baskaran, J. Christopher and A. Sakthivel, *RSC Adv.*, 2015, **5**, 98853–98875.

21 C. Doornkamp and V. Ponec, *J. Mol. Catal. Chem.*, 2000, **162**, 19–32.

22 A. C. Ferrari and J. Robertson, *Philos. Trans. R. Soc. Lond. Math. Phys. Eng. Sci.*, 2004, **362**, 2477–2512.

23 A. C. Ferrari and J. Robertson, *Phys. Rev. B*, 2000, **61**, 14095–14107.

24 A. C. Ferrari and J. Robertson, *Phys. Rev. B*, 2001, **64**, 075414.

25 J. Schwan, S. Ulrich, V. Batori, H. Ehrhardt and S. R. P. Silva, *J. Appl. Phys.*, 1996, **80**, 440–447.

26 M. S. Dresselhaus, A. Jorio, M. Hofmann, G. Dresselhaus and R. Saito, *Nano Lett.*, 2010, **10**, 751–758.

27 E. Flahaut, A. Peigney, W. S. Bacsa, R. R. Bacsa and C. Laurent, *J. Mater. Chem.*, 2004, **14**, 646–653.

28 W. E. Alvarez, B. Kitiyanan, A. Borgna and D. E. Resasco, *Carbon*, 2001, **39**, 547–558.

29 E. Lamouroux, P. Serp, Y. Kihn and P. Kalck, *Appl. Catal. Gen.*, 2007, **323**, 162–173.

30 S. Stankovich, D. A. Dikin, R. D. Piner, K. A. Kohlhaas, A. Kleinhammes, Y. Jia, Y. Wu, S. T. Nguyen and R. S. Ruoff, *Carbon*, 2007, **45**, 1558–1565.

31 Y. Li, X. Zhang, X. Tao, J. Xu, F. Chen, W. Huang and F. Liu, *Chem. Phys. Lett.*, 2004, **386**, 105–110.

32 S. T. Jackson and R. G. Nuzzo, *Appl. Surf. Sci.*, 1995, **90**, 195–203.

33 H. Estrade-Szwarckopf, *Carbon*, 2004, **42**, 1713–1721.

34 X. Li, J. Zhang, L. Shen, Y. Ma, W. Lei, Q. Cui and G. Zou, *Appl. Phys. A*, 2009, **94**, 387–392.

35 Y. Li, X. B. Zhang, X. Y. Tao, J. M. Xu, W. Z. Huang, J. H. Luo, Z. Q. Luo, T. Li, F. Liu, Y. Bao and H. J. Geise, *Carbon*, 2005, **43**, 295–301.

36 Y. Li, X. B. Zhang, X. Y. Tao, J. M. Xu, F. Chen, L. H. Shen, X. F. Yang, F. Liu, G. V. Tendeloo and H. J. Geise, *Carbon*, 2005, **43**, 1325–1328.

37 M. Hu, Y. Murakami, M. Ogura, S. Maruyama and T. Okubo, *J. Catal.*, 2004, **225**, 230–239.

5

CHAPTER 5 –USING NICKEL AND COBALT MOLYBDATES AS CATALYSTS FOR THE OXIDATIVE DEHYDROGENATION OF *N*-OCTANE.

5.1 INTRODUCTION

This chapter examines the performance of nickel and cobalt molybdates as catalysts for the oxidative dehydrogenation (ODH) of *n*-octane. As both nickel molybdate[1–3] and cobalt molybdate[4,5] have been shown to catalyse the ODH of propane to propene, propane was also tested as a substrate to observe activity.

Cobalt molybdate has already been shown as a catalyst for the ODH of *n*-octane.[6] Fadlalla and Friedrich found that the aromatic species of ethyl benzene, xylene and styrene were the main products formed. Higher temperatures led to higher selectivity to aromatic species formed. They found that altering the carbon to oxygen ratio from 8:1 to 2:1 led to an increase in conversion but greater selectivity to carbon oxides. These results were similar to findings with iron molybdate in the $FeMoO_4$ phase, presented in previous chapters.

As both nickel and cobalt molybdates have received much more attention in the literature as ODH catalysts compared to iron molybdates (more known as a catalyst for the oxidation of methanol to formaldehyde[7–9]) it was of interest to observe how they compared to an iron molybdate catalyst for the ODH of *n*-octane.

As both nickel and cobalt form molybdates have the formula of $NiMoO_4$ and $CoMoO_4$ with both nickel and cobalt in a +2 oxidation state, no pre-reduction step needed in the preparation of the catalysts (see Chapter 2 for full details). The pre-reduction step was used for the iron molybdate catalyst to convert it from the ferric form $Fe_2(MoO_4)_3$ where iron is in a +3 oxidation state, to the ferrous form, $FeMoO_4$, where iron is in a +2 oxidation state.

Catalysts with a molybdenum molar excess of 1.5:1 were synthesised for both nickel and cobalt molybdates. Nickel and cobalt molybdates with no molybdenum excess were also synthesised, to create pure phase $NiMoO_4$ and $CoMoO_4$. It has been reported[10] that nickel molybdate with an excess of molybdenum is particularly active, for the conversion of *n-* butane to maleic anhydride.[11]

5.2 CHARACTERISATION OF CATALYSTS

X-ray powder diffraction (XRPD) and Raman spectroscopy was used to confirm the structures of the catalysts prepared.
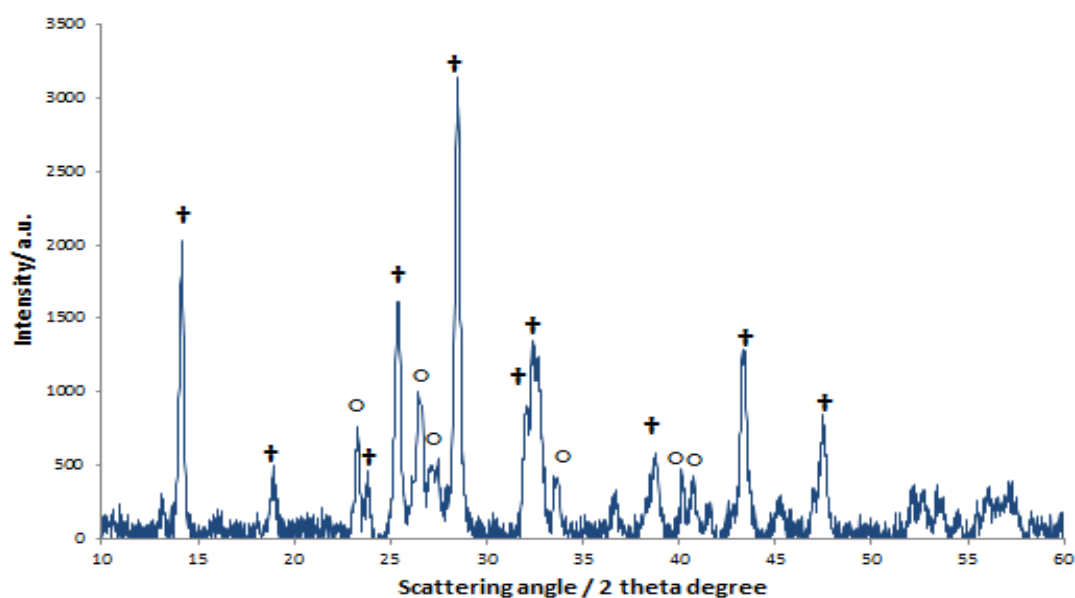
Figure 5.1- XRPD of a cobalt molybdate catalyst prepared with a Co:Mo ratio of 1:1

Phases present: $CoMoO_4$ (†) and MoO_3 (o)

Species	Peak (2 theta degrees)	Lattice Plane	d-spacing (Å)
MoO$_3$	23.3	011	3.86
	25.2	200	3.42
	26.2	111	3.42
	33.8	-211	2.62
	41.5	310	2.14
	42.1	220	2.04
CoMoO$_4$	12.5	001	7.09
	18.9	-201	4.70
	23.7	021	3.76
	25.1	-112	3.55
	28.5	220	3.13
	32.2	312	2.77
	38.3	022	2.78
	38.3	202	2.34
	43.3	023	2.09
	46.8	-204	1.94

Table 5.1 – XRPD Peak list for Figure 5.1 with associated d-spacing and lattice planes.[12]

The presence of MoO$_3$ phases may indicate that some cobalt oxides could be present as the 1:1 molar ratio of molybdenum to cobalt suggests that no MoO$_3$ should be formed. However no such cobalt phases were observed in the XRPD. The preparation of the catalyst was via a pH controlled co-precipitation technique, thus some cobalt may have not precipitated out form the reaction mixture, leaving free molybdenum to form MoO$_3$ *post*-calcination.
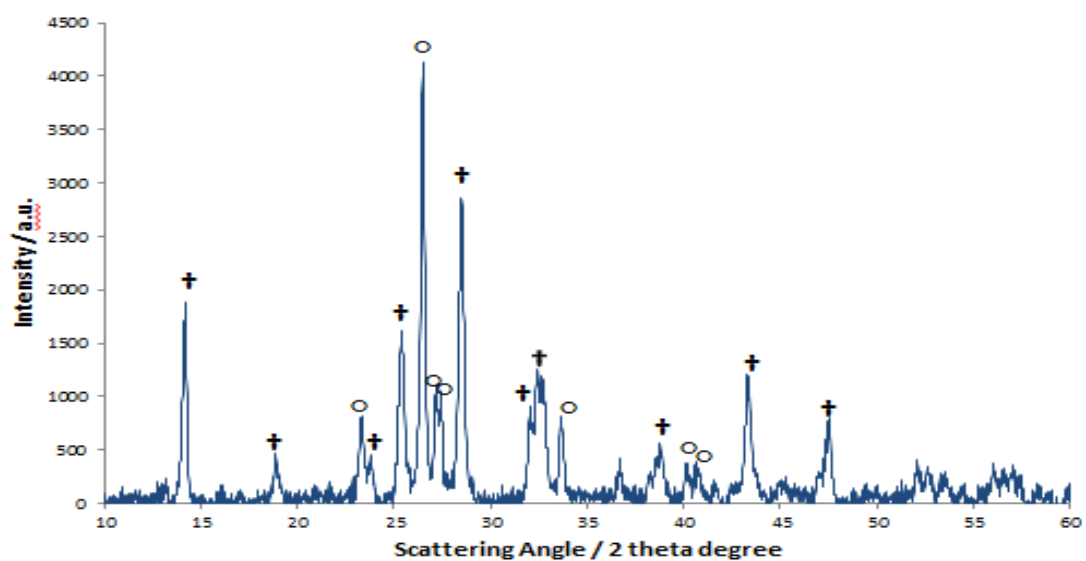
Figure 5.2- XRPD of a cobalt molybdate catalyst prepared with a Co:Mo ratio of 1:1.5

Phases present: CoMoO₄ (†) and MoO₃ (○)

Species	Peak (2 theta degrees)	Lattice Plane	d-spacing (Å)
MoO₃	23.3	011	3.86
	25.2	200	3.42
	26.2	111	3.42
	33.8	-211	2.62
	41.5	310	2.14
	42.1	220	2.04
CoMoO₄	12.5	001	7.09
	18.9	-201	4.7
	23.7	021	3.76
	25.1	-112	3.55
	28.5	220	3.13
	32.2	312	2.77
	38.3	022	2.78
	38.3	202	2.34
	43.3	023	2.09
	46.8	-204	1.94

Table 5.2 – XRPD Peak list for Figure 5.2 with associated d-spacing and lattice planes.

As Figures 5.1 and 5.2 show, the molybdenum trioxide content present in the catalyst increased when increasing the ratio of Mo/Co in preparation. Relative intensity ratios indicated a presence of 25% MoO₃ for the 1:1 Mo/Co catalyst, and a presence of 55% for the 1.5 ratio.

It should be noted that using relative intensity ratios is only a semi-quantitative technique that estimates the ratios of the phases present in the samples. XRPD is a bulk technique, it may not give an accurate depiction of the catalyst surface.

Species	Wavenumber / cm^{-1}									
CoMoO$_4$	946(s)	940(s)	895(vw)	880(w)	704(m)	700(m)	695 (m)			
NiMoO$_4$	963(vs)	916(s)	709(s)	494(m)	420(m)	389(m)	373(m)	179(m)		
MoO$_3$	996(vs)	820(vs)	667(m)	380(w)	337(m)	292(m)	284(s)	247(w)	218(w)	199(w)

TABLE 5.3 - RAMAN ABSORPTION PEAKS FOR COBALT MOLYBDATE, NICKEL MOLYBDATE AND MOLYBDENUM TRIOXIDE[11,13]
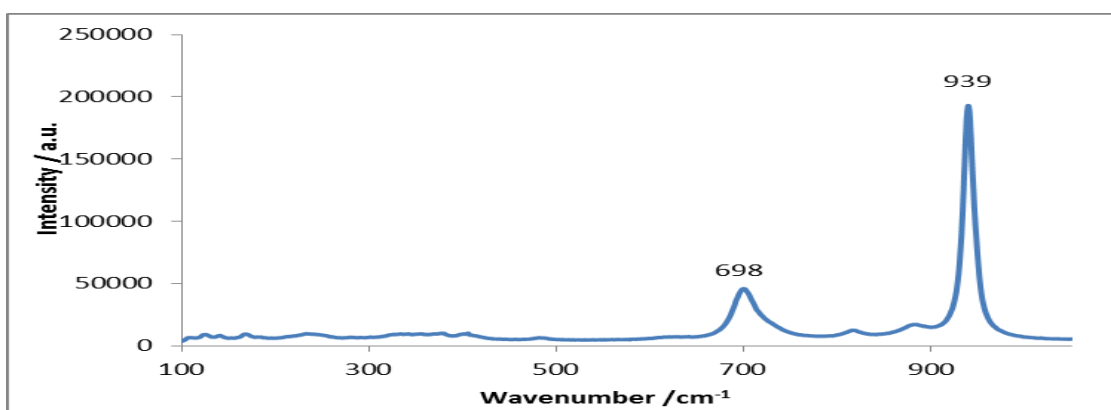
Figure 5.3 – Raman spectra of a cobalt molybdate catalyst with a Co:Mo ratio of 1:1

Figure 5.3 shows only peaks corresponding to CoMoO$_4$ suggesting no molybdenum excess was present when the catalyst was prepared with a 1:1 cobalt to molybdenum ratio. Figure 5.4 confirmed that molybdate excess was present when the catalyst was prepared with a molybdenum excess of 1.5:1.
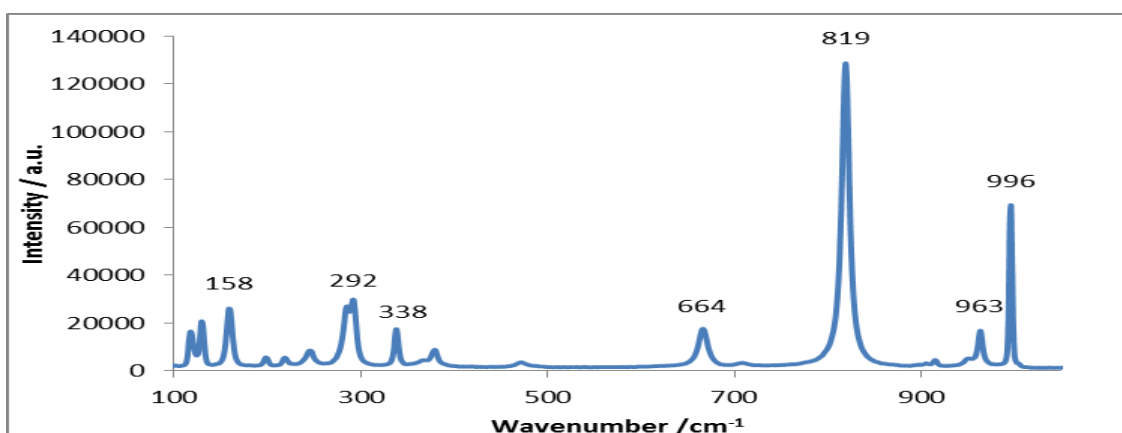
Figure 5.4 – Raman spectra of a cobalt molybdate catalyst with a Co:Mo ratio of 1:1.5
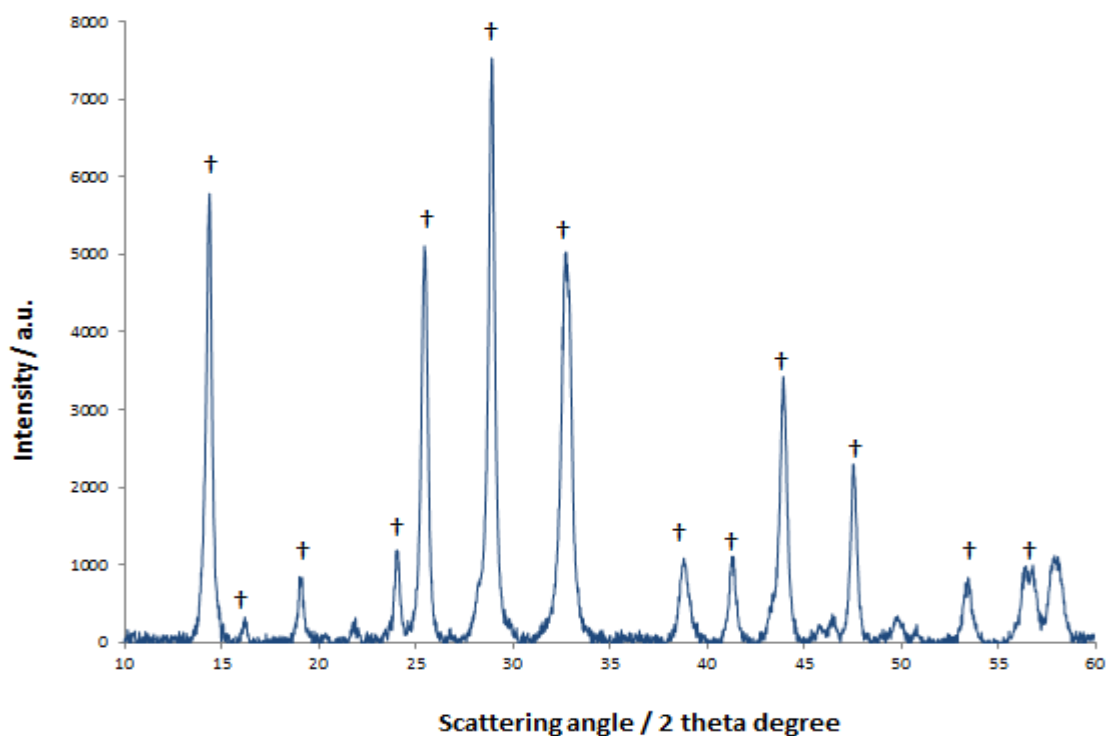
Figure 5.5- XRPD of a nickel molybdate catalyst prepared with a Ni:Mo ratio of 1:1 Phases present: NiMoO$_4$ (†)

Species	Peak (2 theta degrees)	Lattice Plane	d-spacing (Å)
NiMoO$_4$	14.3	110	6.19
	16.2	011	5.50
	19.0	101	4.67
	23.9	-121	3.71
	25.3	-112	3.51
	28.9	220	3.09
	32.6	022	2.75
	38.8	-132	2.32
	41.4	040	2.18
	43.8	330	2.06
	47.5	-204	1.92
	53.3	510	1.72
	55.2	-202	1.66

Table 5.4 – XRPD Peak list for Figure 5.5 with associated d-spacing and lattice planes.

No molybdenum trioxide phases were observed, suggesting that the nickel molybdate prepared with a 1:1 nickel molybdenum molar ratio is pure phase NiMoO$_4$.
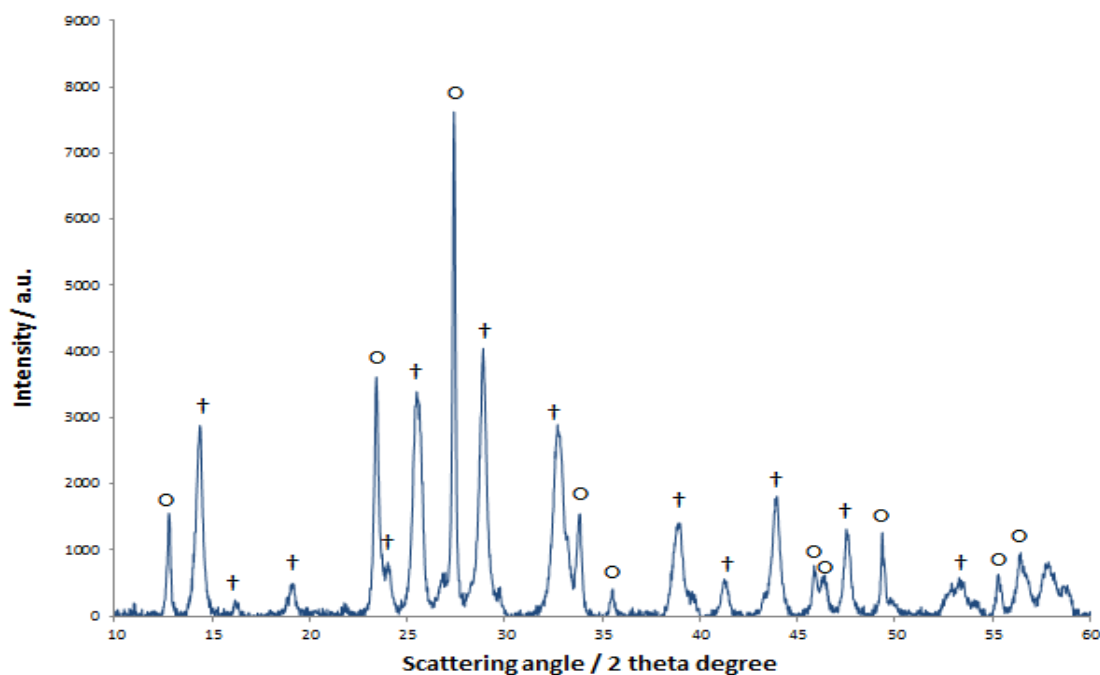
Figure 5.6- XRPD of a nickel molybdate catalyst prepared with a Ni:Mo ratio of 1:1.5 Phases present: NiMoO₄ (†) and MoO₃ (○)

Species	Peak (2 theta degrees)	Lattice Plane	d-spacing (Å)
MoO₃	23.3	011	3.86
	25.2	200	3.42
	26.2	111	3.42
	33.8	-211	2.62
	35.2	102	2.56
	44.5	-311	2.04
	46.7	022	1.93
	49.1	122	1.86
	55.1	-131	1.67
	57.5	411	1.60
NiMoO₄	14.3	110	6.19
	16.2	011	5.50
	19.0	101	4.67
	23.9	-121	3.71
	25.3	-112	3.51
	28.9	220	3.09
	32.6	022	2.75
	38.8	-132	2.32
	41.4	040	2.18
	43.8	330	2.06
	47.5	-204	1.92
	53.3	510	1.72
	55.2	-202	1.66

Table 5.5 – XRPD Peak list for Figure 5.6 with associated d-spacing and lattice planes.

Preparing the catalyst with a molybdenum excess led to the formation of both nickel molybdate ($NiMoO_4$) and molybdenum trioxide (MoO_3).
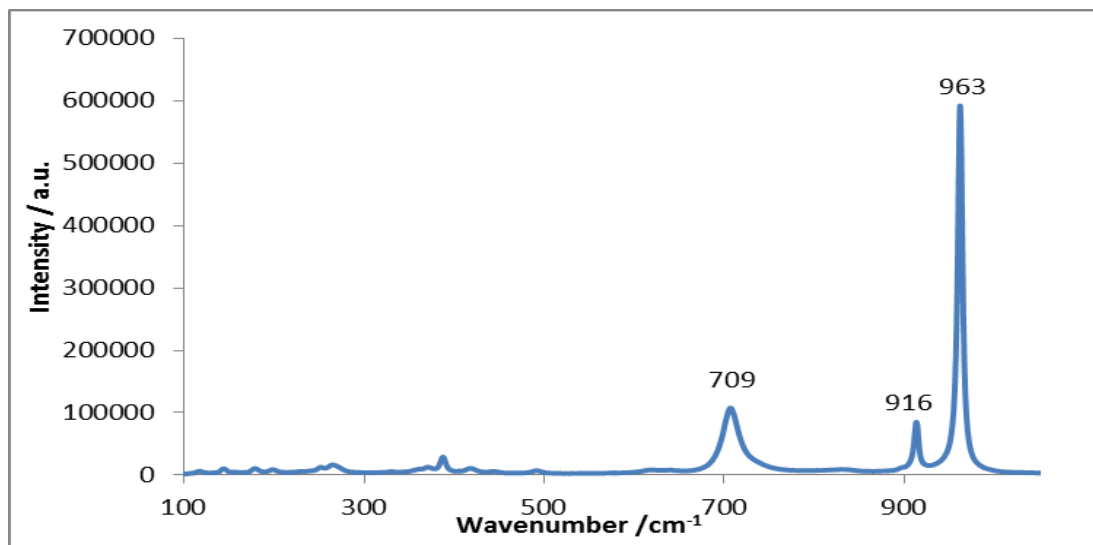
Figure 5.7 – Raman spectra of a nickel molybdate catalyst with a Ni:Mo ratio of 1:1

A similar trend to cobalt molybdate was seen with nickel molybdate. No molybdenum trioxide was detected when the catalyst was prepared with a 1:1 molar ratio of nickel and molybdenum. MoO_3 was observed when the catalyst was prepared with a molybdenum excess.
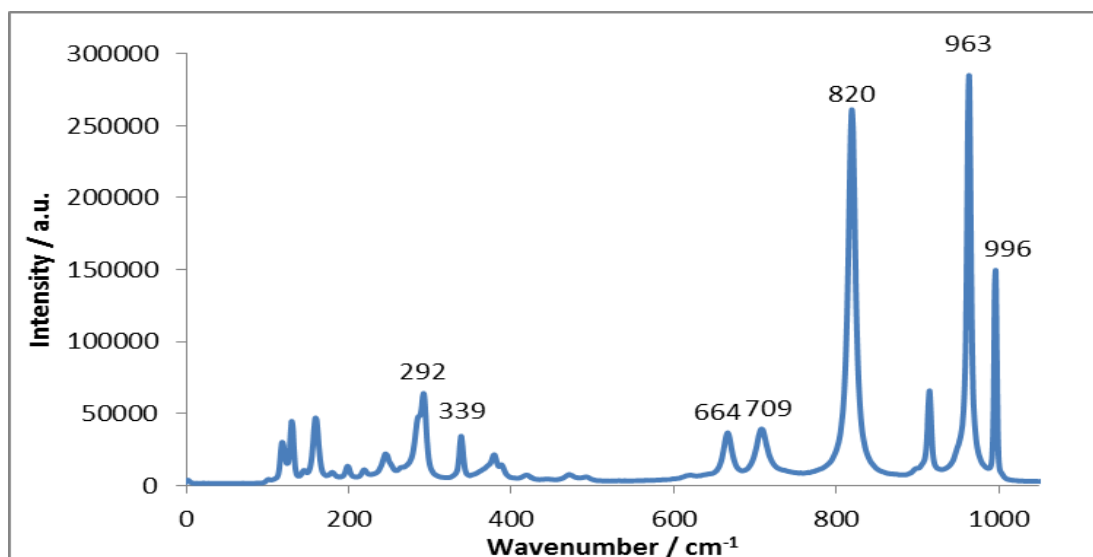
Figure 5.8 – Raman spectra of a nickel molybdate catalyst with a Ni:Mo ratio of 1:1.5

After the findings, microwave plasma – atomic emission spectroscopy (MP-AES) analysis was used upon the catalysts to obtain a more quantitative measure of the molybdenum excess present in the catalysts.

Molybdenum ratio used in catalyst preparation	Molybdenum excess found by AES - cobalt molybdate	Molybdenum excess found by AES – nickel molybdate
1.0 (no excess)	1.0 (no excess)	1.0 (no excess)
1.5	1.2	1.4

Table 5.6 – Molybdenum excess relative to cobalt or nickel in catalysts calculated via MP-AES analysis

Analysis by MP-AES showed that preparing the catalysts with a molybdenum excess did lead to the material having excess molybdenum. Nickel molybdate showed a greater molybdenum excess than cobalt molybdate. This finding was consistent with what was found via XRPD and Raman spectroscopy on the cobalt molybdate. No MoO_3 was observed for the XRPD of pure phase $NiMoO_4$.

5.3 – CATALYTIC TESTING OF CATALYSTS FOR PROPANE OXIDATIVE DEHYDROGENATION

The catalysts were tested for the oxidative dehydrogenation of propane. Due to experimental constraints the catalytic testing was run on a separate reactor to the octane oxidative dehydrogenation reactor. Full details of this are found in Chapter 2.

It should be noted for Figures 5.9-5.12 that although there is a steep increase in conversion above 500 °C, it is likely homogeneous gas phase catalytic processes may be taking place. This is an observation that is well documented in the literature.[14,15] Blank experiments done (no catalyst present) showed a propane conversion to produce carbon oxides once the temperature rose above 500°C. This propane conversion with a blank test was lower (*ca.*10-15% in total*)* than the catalytic tests outlined in Figure 5.9-5.12 but still substantial.
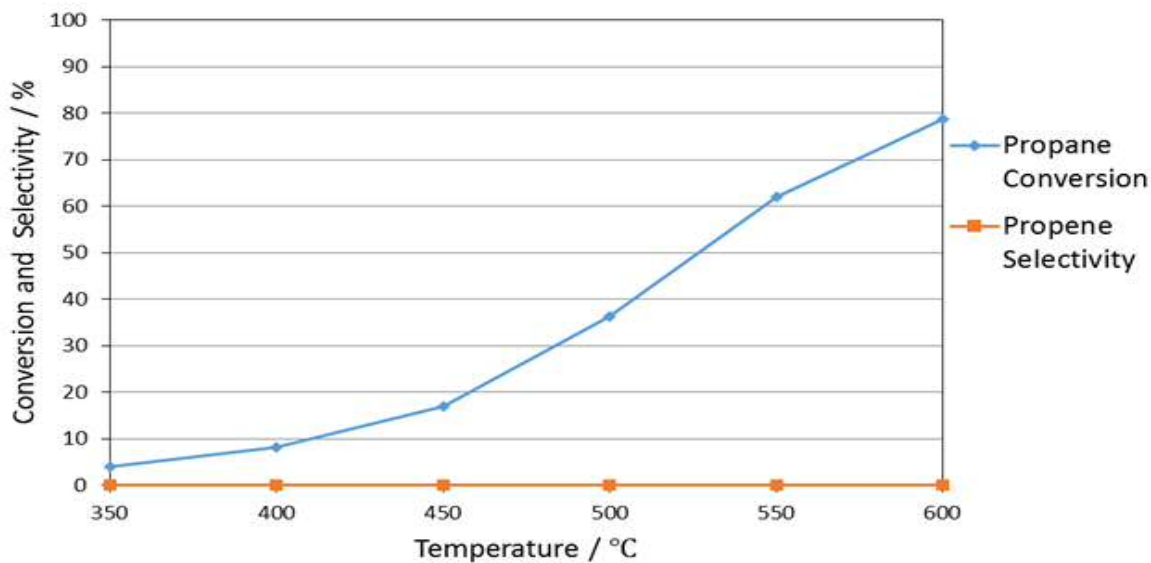
Figure 5.9 - **Reaction of 4.75% propane (GHSV 4000h^{-1}, C:O 3:2) over a cobalt molybdate catalyst (1:1 Co:Mo). Temperature range from 350-600 °C**

As seen in Figure 5.9 a pure phase $CoMoO_4$ catalyst with no molybdenum excess shows very little selectivity to propene. Propane conversion increases with temperature but this was due to the formation of carbon oxides and homogeneous gas-phase reactions.

Figure 5.10 - **Reaction of 4.75% propane (GHSV 4000h^{-1}, C:O 3:2) over a cobalt molybdate catalyst (1:1.5 Co:Mo). Temperature range from 350-600 °C**

As seen in Figure 5.10 a cobalt molybdate catalyst with an excess of molybdenum shows a much higher selectivity to propene. Activity was similar to Figure 5.9.

Selectivity to propene falls as temperature increases. The increase in activity was due to the formation of carbon oxides and likely homogeneous reactions.

The high selectivity to carbon oxides may be caused by the relatively high oxygen to carbon levels. Unfortunately with the set-up of the reactor and time constraints it was not possible to alter the carbon to oxygen ratios sufficiently to perform a full study on this. However the purpose of this section was simply to observe if the catalysts exhibited activity in converting propane to propene and if so, which catalyst was most active and selective. This could then be compared to catalytic activity for ODH of *n*-octane.
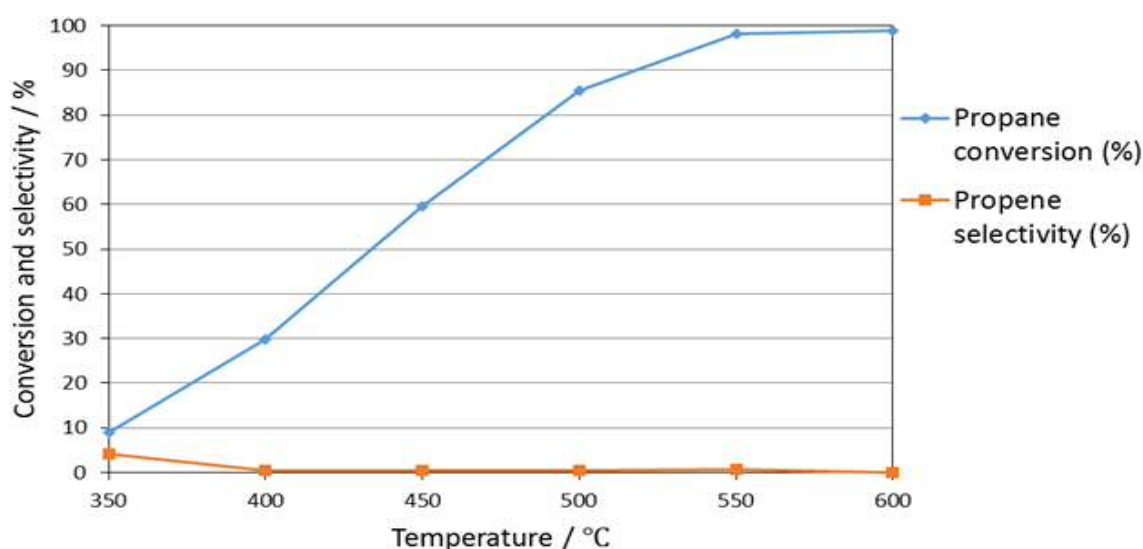
Figure 5.11 - Reaction of 4.75% propane (GHSV 4000h^{-1}, C:O 3:2) over a nickel molybdate catalyst (1:1 Ni:Mo). Temperature range from 350-600 °C

As seen in Figures 5.12 and 5.13, nickel molybdate shows higher conversions of propane than cobalt molybdate, suggesting it was a more active catalyst. Pure phase NiMoO$_4$ with no molybdenum excess shows no selectivity to propene beyond 350 °C. At 550 °C the near complete conversion of propane was occurring, attributable to carbon oxides.

Nickel molybdate with a molybdenum excess shows greater selectivity to propene with slightly lower conversions until 600 °C. This follows the same trend as cobalt molybdate. Results show cobalt molybdate with a molybdenum excess was the best catalyst, exhibiting lower propane conversions but much higher selectivity to propene

across all temperature profiles. Nickel molybdate with an excess of molybdenum formed other products such as acrolein and acrylic acid at lower temperatures.

The results indicate that molybdenum excess was needed for the oxidative dehydrogenation of propane to propene.
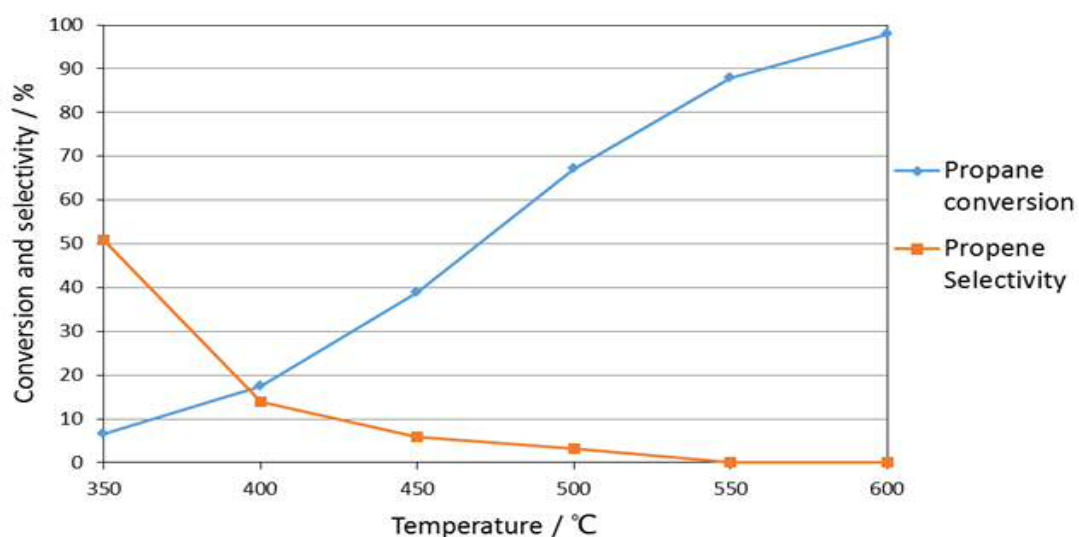
Figure 5.12 - **Reaction of 4.75% propane (GHSV 4000h^{-1}, C:O 3:2) over a cobalt molybdate catalyst (1:1.5 Ni:Mo). Temperature range from 350-600 °C**

5.4 CATALYTIC TESTING FOR THE OXIDATIVE DEHYDROGENATION OF *N*-OCTANE.

The catalysts were then tested for ODH of *n*-octane. Two tests were run at different carbon to oxygen ratios. Firstly each catalyst was tested at a 3:2 carbon to oxygen ratio to compare results as closely as possible to the ODH of propane. Then each catalyst was tested at an 8:1 carbon to oxygen ratio. This was to compare the activity and selectivity of nickel and cobalt molybdates with that of iron molybdate. Cobalt molybdate results could also be compared to work done by Fadlalla and Friedrich.

5.4.1 CATALYTIC TESTING FOR THE OXIDATIVE DEHYDROGENATION OF *N*-OCTANE WITH A 3:2 CARBON TO OXYGEN RATIO.

Figure 5.13 - Reaction of 1% *n*-octane (GHSV 4000h^{-1}, C:O 3:2) over a cobalt molybdate catalyst (1:1 Co:Mo). Temperature range from 350-550 °C

Figure 5.13 shows that a CoMoO$_4$ catalyst with no molybdenum excess shows high selectivity to carbon oxides. This can be attributed to the ratio of carbon to oxygen. Previous results in Chapter 3 and Chapter 4, showed with an FeMoO$_4$ catalyst that increasing the level of oxygen in the gas feed relative to carbon, led to much greater selectivity to carbon oxides.

As temperature increased so did selectivity to aromatics. Selectivity to octenes was low. This could be attributed to the *n*-octane that does not from carbon oxides rapidly cyclising before undergoing ODH. This was found in Chapter 4. This is an area where cobalt molybdate differs from iron molybdate. Oxygen conversion rises in line with *n*-octane conversion, as would be expected for an ODH process.

Figure 5.14 - Reaction of 1% *n*-octane (GHSV 4000h^{-1}, C:O 3:2) over a cobalt molybdate catalyst (1:1.5 Co:Mo). Temperature range from 350-550 °C

Cobalt molybdate with a molybdenum excess (Figure 5.13) shows lower *n*-octane conversions, suggesting lower catalytic activity than pure phase CoMoO$_4$ (Figure 5.14). The opposite trend was seen for propane conversions. Selectivity to carbon oxides was very high. Selectivity to octenes was higher at temperatures of ≤450 °C in Figure 5.14 than Figure 5.13. Selectivity to aromatics increases as temperature increases. Oxygen conversion rises in line with hydrocarbon conversion.
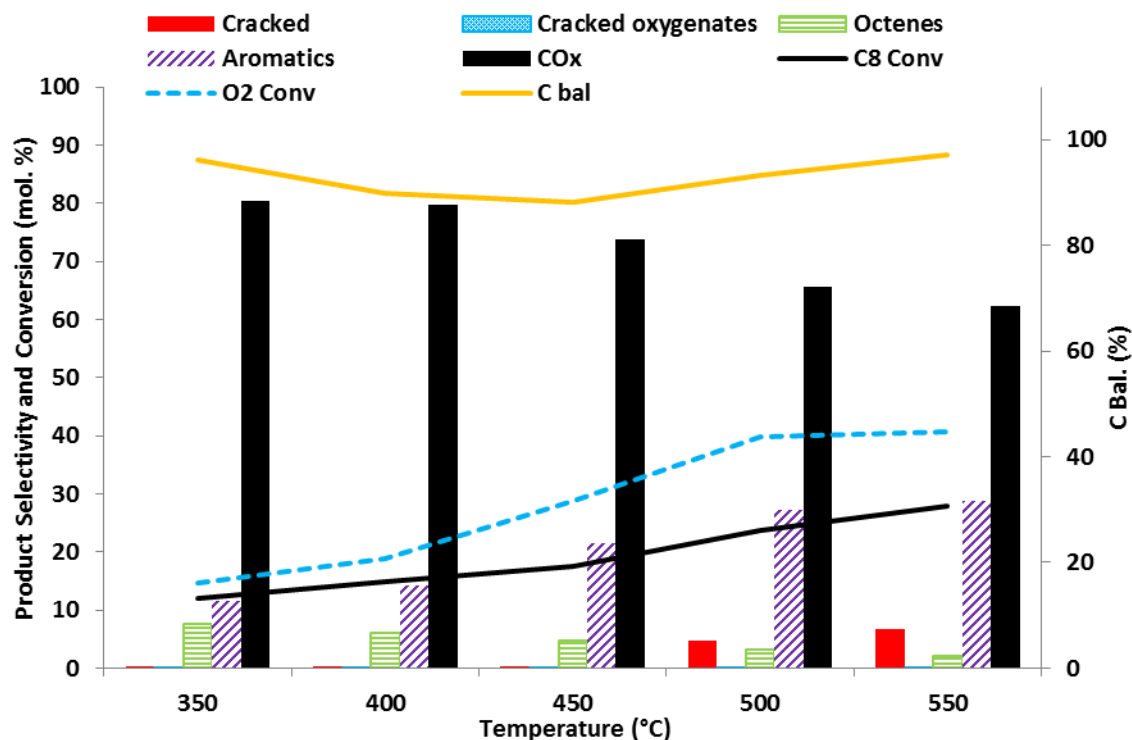
Figure 5.15 - **Reaction of 1% *n*-octane (GHSV 4000h^{-1}, C:O 3:2) over a nickel molybdate catalyst (1:1 Ni:Mo). Temperature range from 350-550 °C**

Pure phase NiMoO$_4$ with no molybdenum excess shows high selectivity to carbon oxides with the relatively high level of oxygen to carbon as expected. NiMoO$_4$ as a catalyst exhibited similar *n*-octane conversions to the cobalt molybdate catalysts. Unlike the cobalt molybdate catalysts, NiMoO$_4$ exhibits higher selectivity to aromatics across all temperatures profiles.

At temperatures of ≥500 °C significant levels of cracked products, chiefly methane, were observed. This could be attributable to the presence of nickel oxide which is a methanation catalyst.[16,17] The lack of hydrogen in the oxidised reaction atmosphere is a likely reason that the selectivity to methane does not rise above *ca.*9%. However some hydrogen will be present from the dehydrogenation of *n*-octane to aromatics at the catalyst surface, which could result in methane formation.

Previous work has been done suggesting that catalytic processes which result in the dehydrogenation of ethylbenzene to styrene would produce the hydrogen required to also catalytically convert carbon oxides to methane.[18] If a similar trend was occurring it would offer an explanation as to why selectivity to carbon oxides fell in Figure 5.15 as

selectivity to cracked products (chiefly methane) rose. Work by Park *et al*[19] showed how CO_2 can be used for the oxidative dehydrogenation of ethylbenzene to styrene using a ceria-zirconia catalyst. McFarland and Park[20] demonstrated how a palladium and magnesium catalyst over silica is active for the methanation of CO_2. Work done by Ravindram[21] and Yamasaki[22] has shown that nickel catalysts exhibiting this catalytic behaviour.
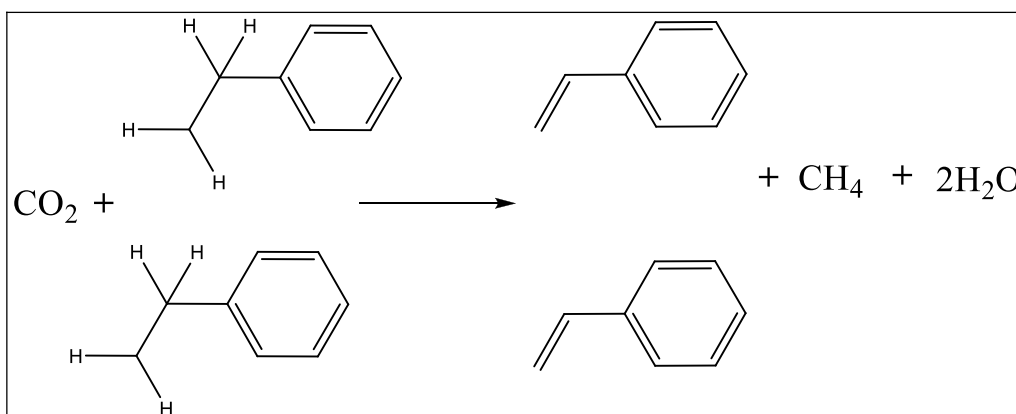
Figure 5.16 Proposed reaction for the conversion of ethylbenzene to styrene and production of methane using carbon dioxide over a nickel catalyst.

Figure 5.16 illustrates the proposed reaction for the production of methane when *n*-octane is passed over a nickel molybdate catalyst. Figure 5.23 (toward the end of this chapter) shows that pure phase nickel molybdate produces high levels of ethylbenzene between 350-450 °C but at 500 °C and above styrene is the major aromatic product produced. There is also a notable increase in selectivity to toluene which may also be producing methane as a by-product.
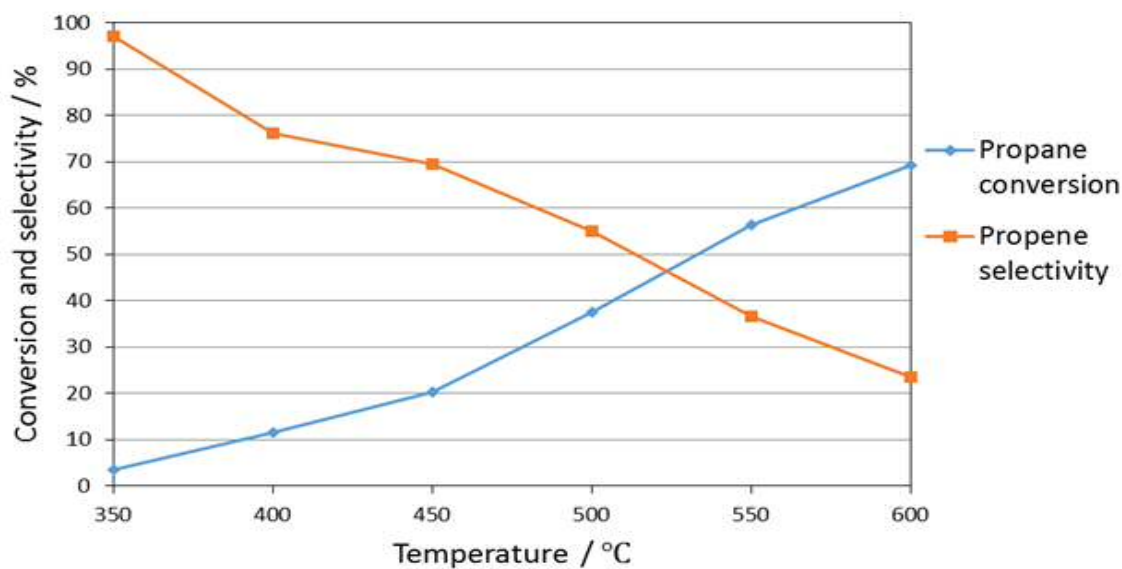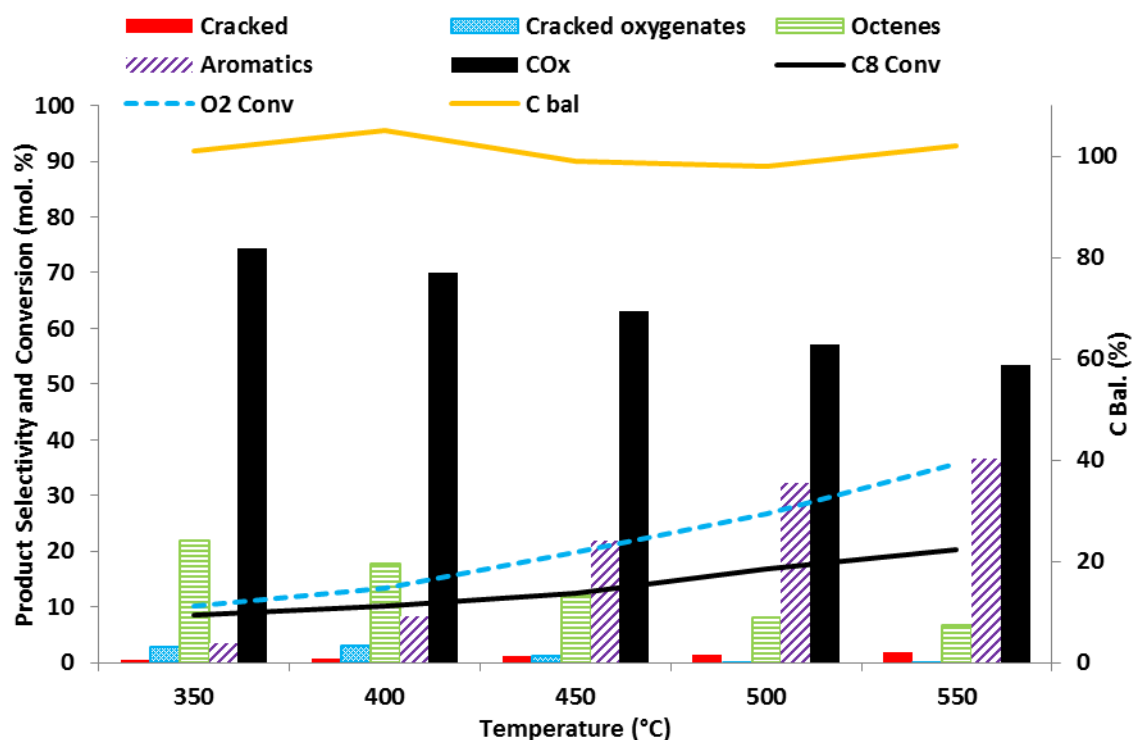
Figure 5.17 - **Reaction of 1% *n*-octane (GHSV 4000h⁻¹, C:O 3:2) over a nickel molybdate catalyst (1:1.5 Ni:Mo). Temperature range from 350-550 °C**

A nickel molybdate catalyst with a molybdenum excess showed lower conversions than a pure phase $NiMoO_4$ catalyst.

At temperatures of ≤400 °C octenes were more favoured selectively than aromatic species and higher levels of cracked oxygenates were observed. Cracked products were not prominent at higher temperatures unlike when pure phase $NiMoO_4$ was used as a catalyst. This could be due to the molybdenum rich surface preventing the formation of nickel oxide which would cause the production of methane (a cracked product).

In summary, cobalt and nickel catalysts with a molybdenum excess (of 1.5:1 Mo:Co/Ni) were superior catalysts for the production of octene from *n*-octane via ODH. Pure phase $CoMoO_4$ and $NiMoO_4$ catalysts (possessing no molybdenum excess) exhibited higher conversions but lower selectivity to the alkene. This trend is the same as found with the ODH of propane under the same conditions.

However while cobalt molybdate catalyst with a molybdenum excess gave the highest selectivity to propene, a nickel molybdate catalyst yielded the best performance for selectivity to octenes.

5.4.2 CATALYTIC TESTING FOR THE OXIDATIVE DEHYDROGENATION OF *N*-OCTANE WITH AN 8:1 CARBON TO OXYGEN RATIO.

The catalysts were tested in a more gas rich system to directly compare them to the iron molybdate catalyst tested in previous Chapters, where the majority of catalytic testing had occurred with an 8:1 carbon to oxygen ratio.
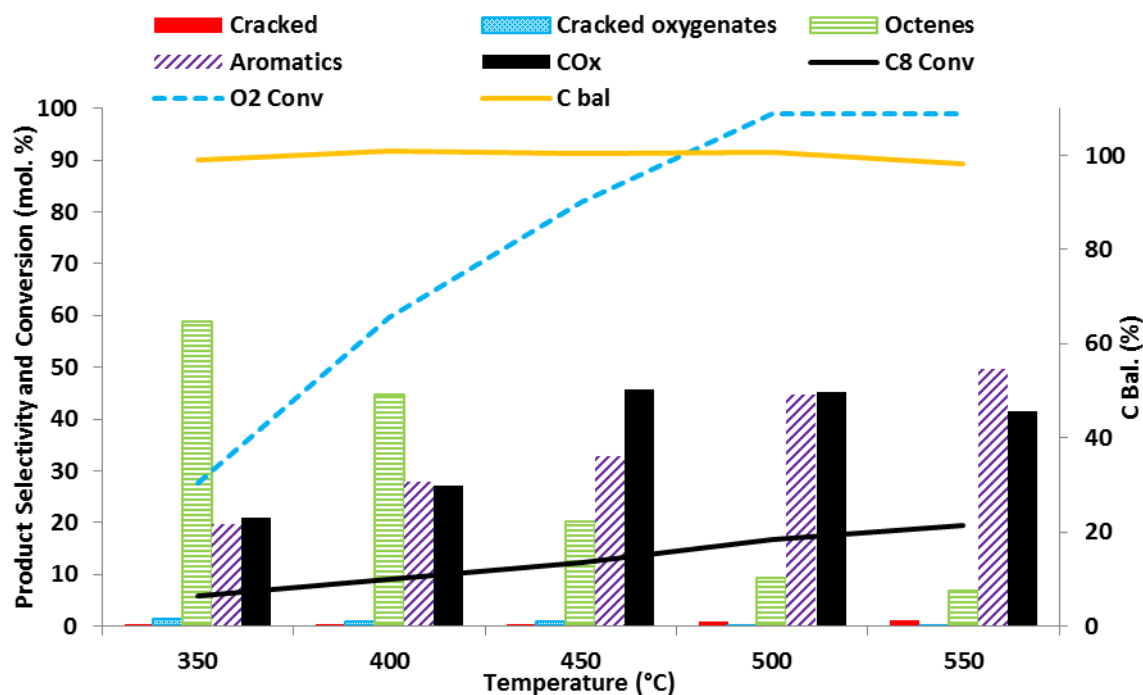
Figure 5.18 - **Reaction of 1% *n*-octane (GHSV 4000h^{-1}, C:O 8:1) over a cobalt molybdate catalyst (1:1 Co:Mo). Temperature range from 350-550 °C**

As seen in Figure 5.18, the use of lower levels of oxygen to carbon sees a notable difference in selectivity. Carbon oxide selectivity was much lower, and at temperatures of ≤400 °C octenes were the major product. As temperature increases selectivity to aromatics increases while octene selectivity decreases. Oxygen conversions reach 100% from 500 °C.

Conversion was lower than when a 3:2 carbon to oxygen ratio was tested with the same catalyst (Figure 5.13) but this would be expected, as limiting the level of oxygen would limit catalyst activity in a catalytic ODH system.
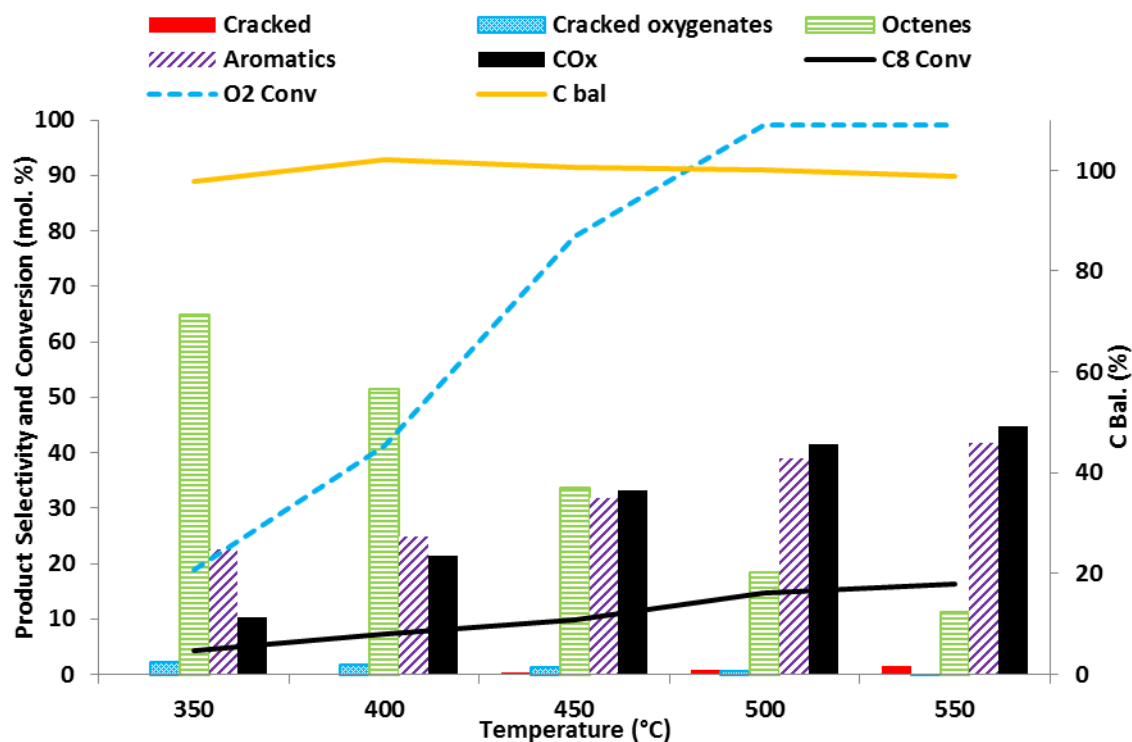
Figure 5.19 - Reaction of 1% *n*-octane (GHSV 4000h^{-1}, C:O 8:1) over a cobalt molybdate catalyst (1:1.5 Co:Mo). Temperature range from 350-550 °C

A cobalt catalyst with a molybdenum excess (Figure 5.19) showed even higher selectivity to octenes than pure phase $CoMoO_4$. Higher levels of cracked oxygenates were observed with a cobalt molybdate catalyst with molybdenum excess. This suggests that cracked oxygenates were produced via oxygen species from the molybdenum trioxide lattice (something discussed in Chapter 4 with iron molybdates). At higher temperatures aromatic species and carbon oxides were the main products.

As *n*-octane conversion with a cobalt molybdate catalyst is very similar to a pure phase $CoMoO_4$ catalyst, and exhibiting higher selectivity to octenes, it appears that cobalt molybdate with a molybdenum excess is a superior catalyst to pure phase $CoMoO_4$ for the ODH of *n*-octane. This finding was also seen with propane ODH.

Aromatic product distribution was very similar between both catalysts and so will be examined against nickel molybdate later in this chapter.
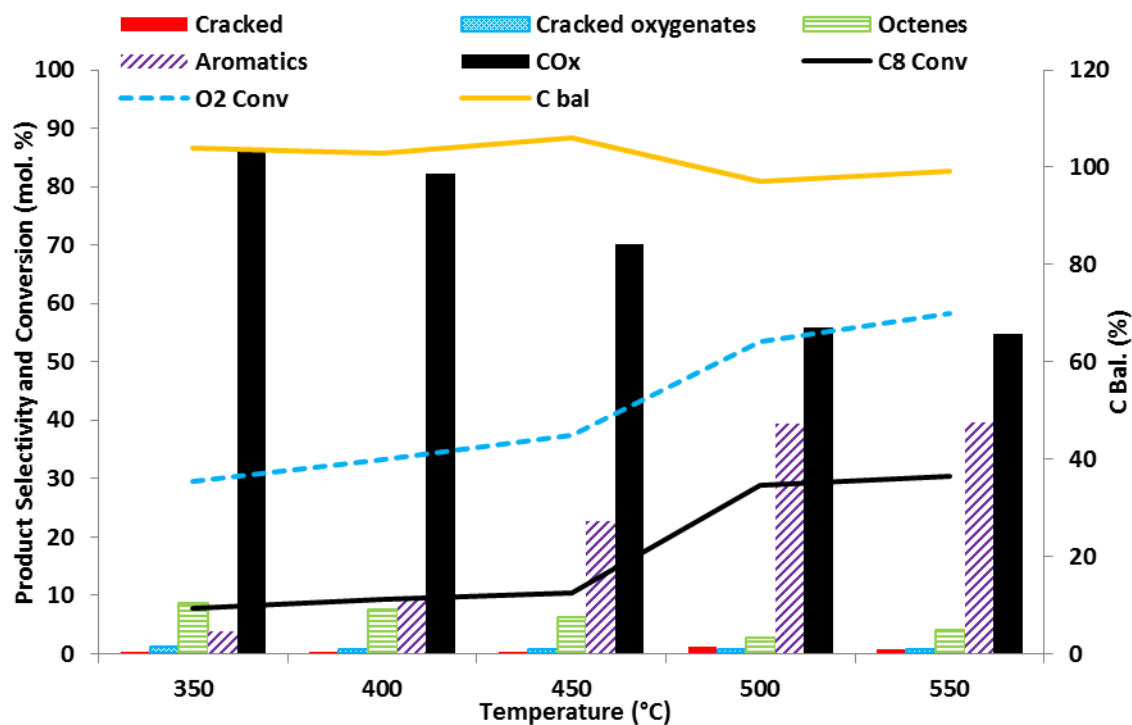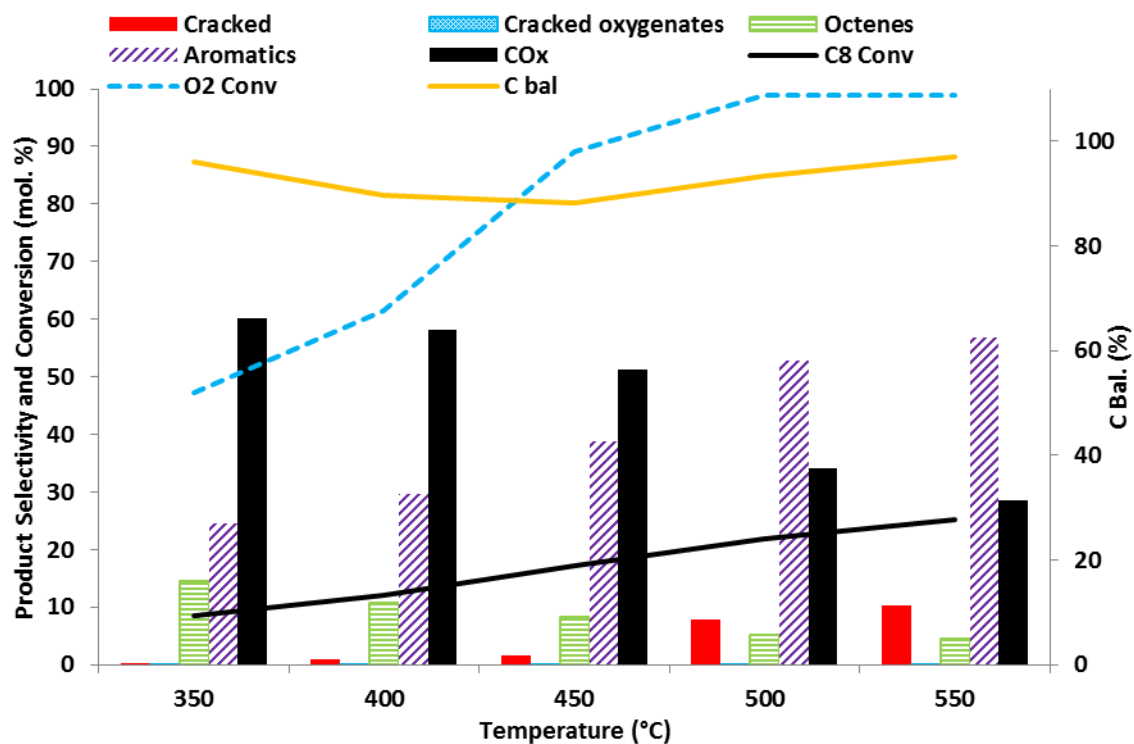
Figure 5.20 - Reaction of 1% *n*-octane (GHSV 4000h^{-1}, C:O 8:1) over a nickel molybdate catalyst (1:1 Ni:Mo). Temperature range from 350-550 °C

Nickel molybdate (catalytic data shown in Figure 5.20) was not as promising a catalyst for the ODH of *n*-octane. High selectivity to carbon oxides was observed, even with a greater proportion of carbon to oxygen in the gas feed. Aromatic species were the secondary product formed at lower temperatures, as the temperature increased aromatic selectivity increased.

At ≥500 °C a significant proportion of products are cracked species, particularly methane. This is likely due to nickel oxide at the catalyst surface, due to the ability of nickel oxide to be a methanation catalyst and is discussed earlier in relation to Figure 5.15.[16,17]

While pure phase NiMoO$_4$ showed low selectivity to octenes compared to cobalt molybdates, it shows high selectivity to aromatics, especially at ≥500 °C. NiMoO$_4$ has been shown by Ozkan and Schrader[11] to be catalytically active in the formation of maleic anhydride from C4 hydrocarbons. This suggests that it is an active dehydrocyclisation catalyst which may explain the formation of aromatics. Work by Pillay *et al*[23] showed that nickel molybdate catalysts form benzene from *n*-hexane.
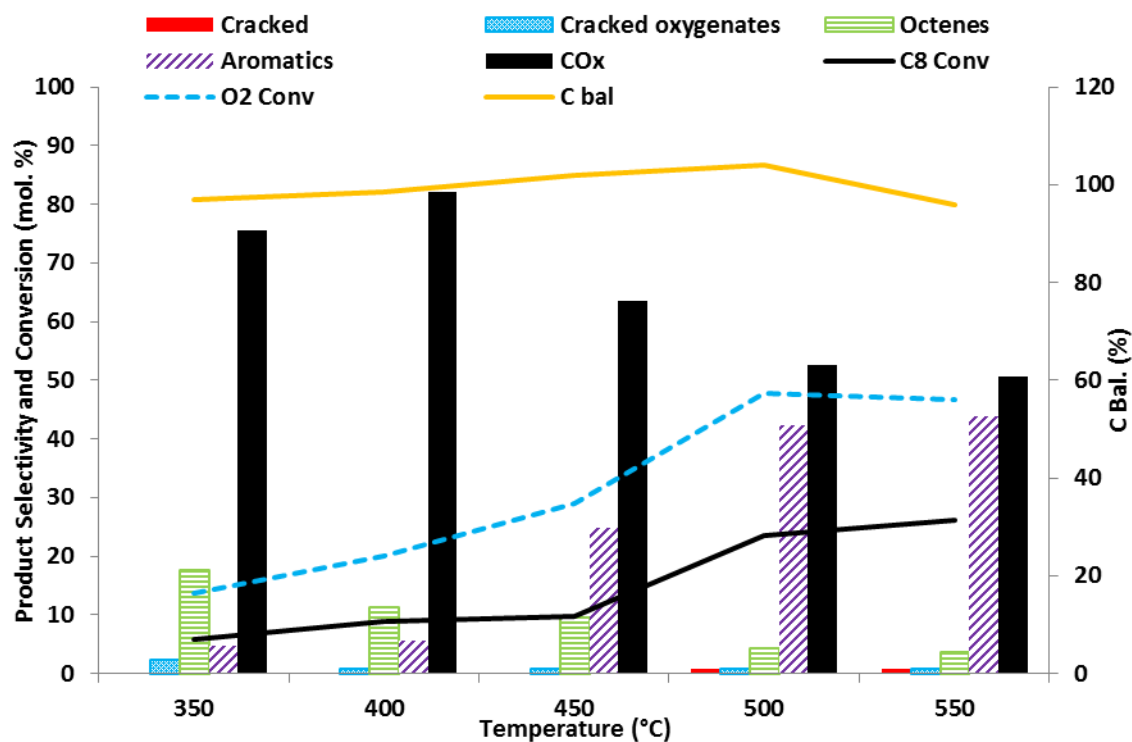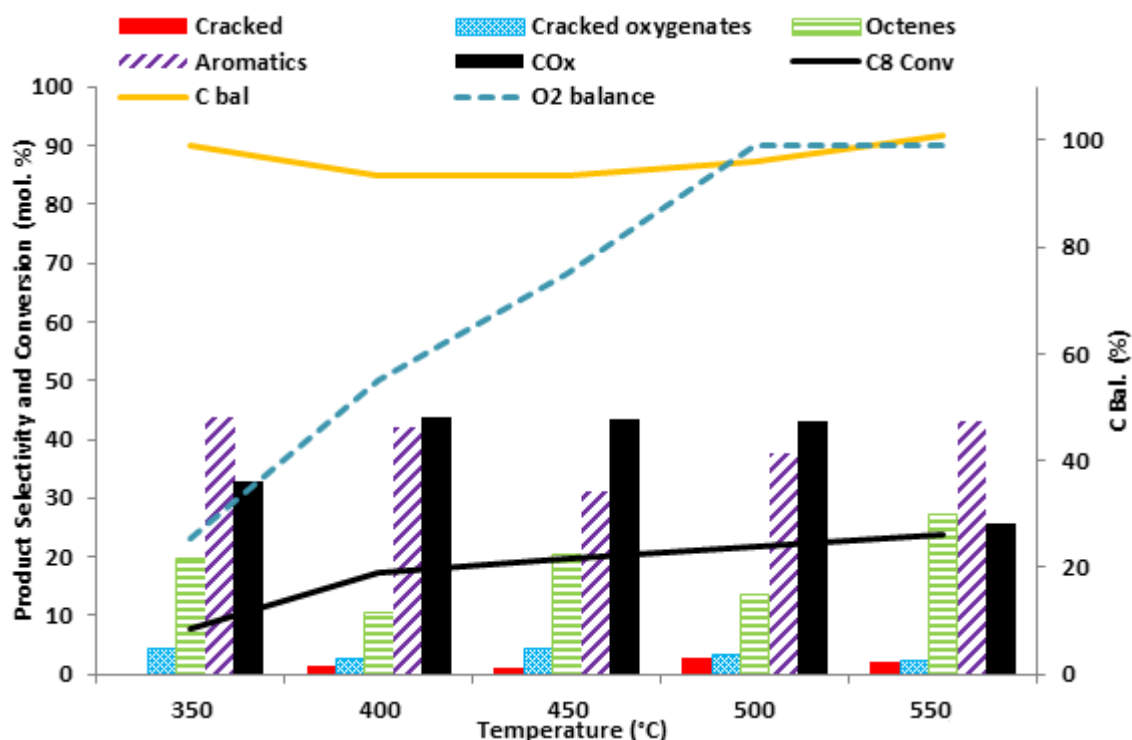
Figure 5.21 - **Reaction of 1% *n*-octane (GHSV 4000h⁻¹, C:O 8:1) over a nickel molybdate catalyst (1:1.5 Ni:Mo). Temperature range from 350-550 °C**

Nickel molybdate with a molybdenum excess showed lower selectivity to carbon oxides at ≤450 °C when compared to pure phase $NiMoO_4$. Higher selectivity to octenes was observed, and higher levels of cracked oxygenates were observed. Cracked products were observed but not in the same concentration as when pure phase $NiMoO_4$ was used. This may be due to the molybdenum excess preventing the formation of nickel oxide particles at the catalyst surface.

Aromatic selectivity between pure phase $NiMoO_4$ and nickel molybdate with a molybdenum excess was very similar. The differences between the aromatic product distribution produced from cobalt and nickel molybdate catalysts are shown in Figures 5.23 and 5.24 and discussed.
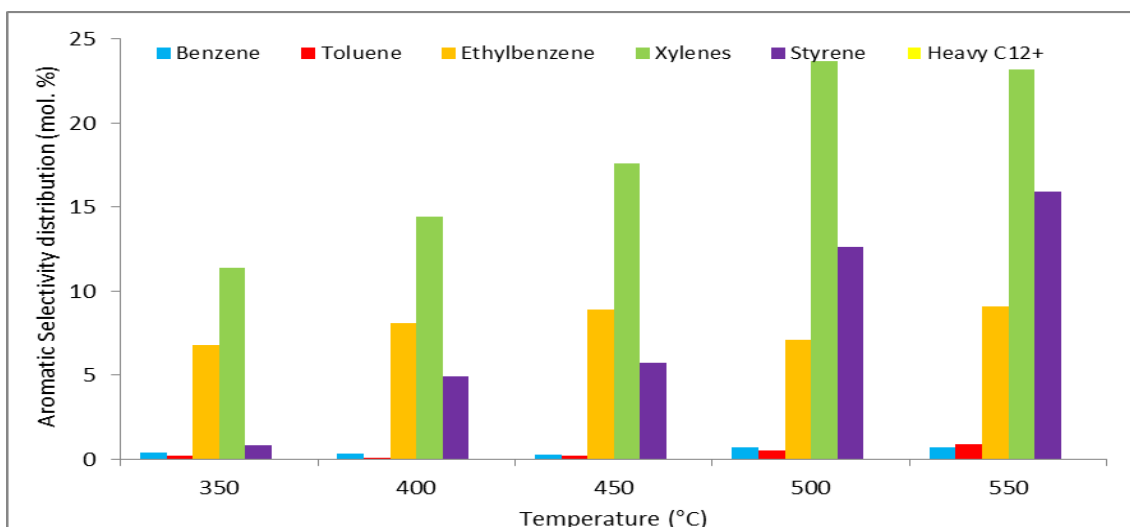
Figure 5.22 - **Aromatic selectivity of 1%** *n*-**octane (4000h^{-1}, C:O 8:1) over a cobalt molybdate catalyst (1:1 Co:Mo). Temperature range from 350-550 °C**

Cobalt molybdates show high selectivity to benzene across all temperature profiles. As temperature increases so does selectivity to styrene. The selectivity to ethyl benzene decreases and temperature increases.

Nickel molybdate shows high selectivity to ethyl benzene at lower temperatures and styrene at higher temperatures. There is an increase in benzene and toluene at higher temperatures as the level of cracked products increases, suggesting aromatic formation followed by cracking. The increase in styrene selectivity occurring as methane selectivity increases, fits with the proposed mechanism in Figure 5.16 with CO_2 acting to oxidatively dehydrogenate ethyl benzene.
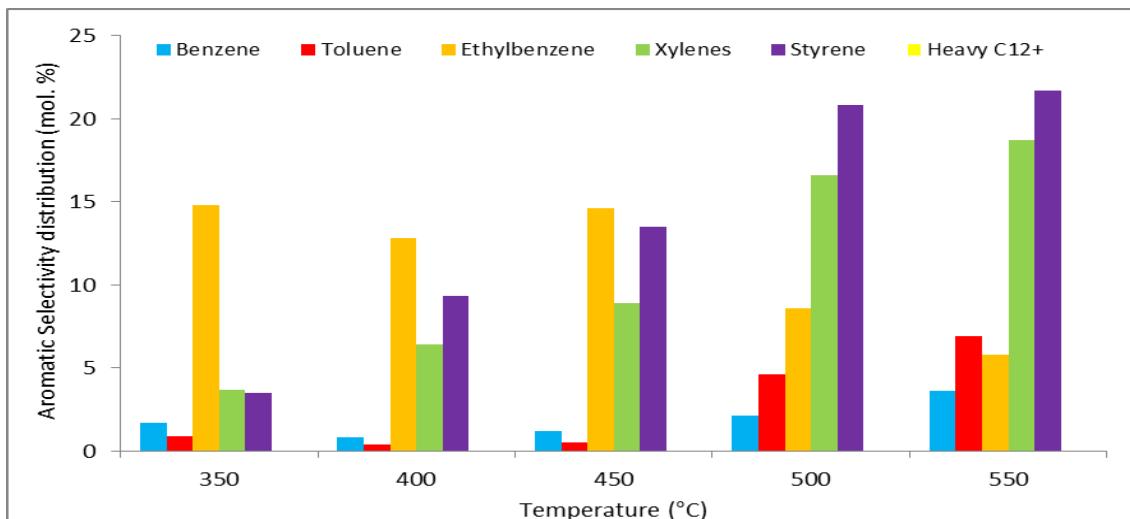
Figure 5.23 - **Aromatic selectivity of 1% *n*-octane (4000h^{-1}, C:O 8:1) over nickel molybdate catalyst (1:1Ni:Mo). Temperature range from 350-550 °C**

5.5 CONCLUSIONS AND SUMMARY OF CHAPTER 5

Nickel and cobalt molybdates show activity as catalysts for the oxidative dehydrogenation of *n*-octane to octenes. A greater level of carbon to oxygen gives greater selectivity to octenes. A lower carbon to oxygen ratio results in very high selectivity to carbon oxides.

Cobalt and nickel catalysts with a molybdenum excess exhibit higher selectivity to octenes than pure phase nickel and cobalt molybdate (NiMoO$_4$ and CoMoO$_4$). This may be due to a synergistic effect between the different phases.[23] When a catalyst with a molybdenum excess is tested, there are levels of cracked oxygenate products compared to pure phase catalysts. Pure phase nickel molybdate, when tested at higher temperatures produces notable selectivity (ca.10%) to cracked products, chiefly methane. This is likely due to the formation of nickel oxide. When a nickel molybdenum catalyst with a molybdenum excess was tested, this was not seen. This suggests excess molybdenum is required to prevent segregation of nickel particles at the catalyst surface.

Cobalt molybdate showed much higher selectivity to octenes than nickel molybdate. Nickel molybdate showed greater selectivity to aromatic products. Lower *n*-octane

conversions were found than those reported by Fadlalla and Friedrich[6] for pure phase cobalt molybdate at 8:1 C:O. However as they did not report on product distribution at these conditions, selectivity cannot be compared. It should be noted that this work was with 1% *n*-octane while work done by Fadlalla and Friedrich was at 10%.

Comparing cobalt and nickel molybdates to iron molybdate, iron molybdate shows the lowest conversions at the conditions tested (8:1 C:O, 4000h^{-1}, 350-550 °C). However iron molybdate at those conditions does not produce carbon oxides until 450 °C. Cobalt and nickel molybdates produces carbon oxides at all temperature profiles examined. Iron molybdate shows the highest selectivity to octenes of the three molybdates tested.

Comparing pure phase $CoMoO_4$, $NiMoO_4$ and $FeMoO_4$ at 400 °C, iron molybdate appears the most impressive catalyst for the ODH of *n*-octane.

Catalyst	*n*-octane conversion at 400 °C (mol %)	Selectivity to octenes at 400 °C (mol %)
$FeMoO_4$	7.8	85.4
$CoMoO_4$	7.3	51.4
$NiMoO_4$	12.1	10.8

Table 5.7 – Comparison of catalyst conversion of *n*-octane and selectivity to octenes at 400 °C, 4000h^{-1}, 8:1 C:O

Work done by Igleslia *et al*[24] which tested the effect of Lewis acidity of molybdate catalysts on propane ODH, found that increasing Lewis acidity increased the difference in activation energy between combustion of propene (lower in energy) and propane ODH (higher energy). Therefore greater Lewis acidity of molybdates results in greater levels of combustion and thus carbon oxide production with lower selectivity to propene.

If the ODH of *n*-octane is assumed to be similar in nature to propane ODH, which has been demonstrated in this chapter then any difference in Lewis acidity between cobalt molybdate and nickel molybdate would result in differences in activity and selectivity. Ouqour *et al*[25] demonstrated that nickel molybdate is more Lewis acidic than cobalt

molybdate. This finding would corroborate with findings in this work which shows nickel molybdate exhibiting high selectivity to carbon oxides through combustion, which is due to its greater Lewis acidity. Cobalt molydate with its lower Lewis acidity exhibited consistently lower selectivity to carbon oxides than nickel molybdate. This may be one reason between the differences in catalytic performance.

Bibliography

1   D. Levin and J. Y. Ying, in *Studies in Surface Science and Catalysis*, ed. S. T. O. R.K. Grasselli A. M.Gaffney and J. E.Lyons, Elsevier, 1997, vol. 110, pp. 367–373.
2   W. Ueda, Y.-S. Yoon, K.-H. Lee and Y. Moro-oka, *Korean J. Chem. Eng.*, 1997, **14**, 474–478.
3   C. Mazzocchia, C. Aboumrad, C. Diagne, E. Tempesti, J. M. Herrmann and G. Thomas, *Catal. Lett.*, **10**, 181–191.
4   D. L. Stern and R. K. Grasselli, *J. Catal.*, 1997, **167**, 560–569.
5   Y. S. Yoon, W. Ueda and Y. Moro-oka, *Top. Catal.*, 1996, **3**, 265–275.
6   M. I. Fadlalla and H. B. Friedrich, *Catal. Sci. Technol.*, 2014, **4**, 4378–4385.
7   Abaulina, L.I., Kustova, G.N., Klevtsova, R.F., Popov, B.I., Bibin, V.N., Melekhina, V.A., Kolomiichuk, V.N., Boreskov, G.K., *Kinet Catal Engl Transl*, 1976, **17**, 1126.
8   P. Adkins, H.; W. R., *J Am Chem Soc*, 1931, **53**, 1512.
9   M. Carbucicchio and F. Trifirò, *J. Catal.*, 1976, **45**, 77–85.
10 N. Fujikawa, K. Wakui, K. Tomita, N. Ooue and W. Ueda, *Catal. Today*, 2001, **71**, 83–88.
11 U. Ozkan and G. L. Schrader, *J. Catal.*, 1985, **95**, 120–136.
12 I. J. A. Smith G.W., *Acta Crystallogr*.
13 H. Jeziorowski, H. Knoezinger, P. Grange and P. Gajardo, *J. Phys. Chem.*, 1980, **84**, 1825–1829.
14 V. P. Vislovskiy, T. E. Suleimanov, M. Y. Sinev, Y. P. Tulenin, L. Y. Margolis and V. Cortés Corberán, *Catal. Today*, 2000, **61**, 287–293.
15 L. Y. Margolis and V. N. Korchak, *Russ. Chem. Rev.*, 1998, **67**, 1073–1082.
16 T. Van Herwijnen, H. Van Doesburg and W. A. De Jong, *J. Catal.*, 1973, **28**, 391–402.
17 J. Happel, I. Suzuki, P. Kokayeff and V. Fthenakis, *J. Catal.*, 1980, **65**, 59–77.
18 US3424808 A, 1969.
19 D. R. Burri, K.-M. Choi, J.-H. Lee, D.-S. Han and S.-E. Park, *Catal. Commun.*, 2007, **8**, 43–48.
20 J.-N. Park and E. W. McFarland, *J. Catal.*, 2009, **266**, 92–97.
21 G. M. Shashidhara and M. Ravindram, *React. Kinet. Catal. Lett.*, **37**, 451–456.
22 M. Yamasaki, H. Habazaki, K. Asami, K. Izumiya and K. Hashimoto, *Catal. Commun.*, 2006, **7**, 24–28.
23 B. Pillay, M. R. Mathebula and H. B. Friedrich, *Appl. Catal. Gen.*, 2009, **361**, 57–64.
24 K. Chen, A. T. Bell and E. Iglesia, *J. Phys. Chem. B*, 2000, **104**, 1292–1299.
25 A. Ouqour, G. Coudurier and J. C. Vedrine, *J. Chem. Soc. Faraday Trans.*, 1993, **89**, 3151–3155.

6

CHAPTER 6 – CONCLUSIONS AND FUTURE WORK

6.1 CONCLUSIONS

An iron molybdate catalyst was shown to be active for the oxidative dehydrogenation (ODH) of *n*-octane. Performing a pre-reduction step on the catalyst prior to catalytic testing led to an improvement in selectivity to octenes as the product. The pre-reduced iron molybdate catalyst, composed of the two species $FeMoO_4$ + Mo_4O_{11}, performed the ODH of *n*-octane at 400°C without the formation of carbon oxides, providing an 8:1 carbon to oxygen ratio and a gas hourly space velocity (GHSV) of $4000h^{-1}$ or above was applied.

Temperatures of between 350-550°C were tested. Conversion of *n*-octane increased in line with temperature. At temperatures of or above 450°C carbon oxides were produced. Higher temperatures led to aromatic species or carbon oxides becoming the major products. Increasing GHSV led to lower conversions but increased selectivity to octenes. This was expected as increasing GHSV would lead to decreased contact time on the surface which would result in lower conversion.[1] This finding also indicated that the formation of carbon oxides and aromatics were formed over a longer timescale than octenes.

Increasing the carbon to oxygen ratio to a 12:1 C:O ratio led to greater octene selectivity but lower *n*-octane conversion. This offered evidence that the process was catalytic ODH as removing oxygen from the system would limit activity. Decreasing the carbon to oxygen ratio to 2:1 C:O increased conversions but led to a large increase in product selectivity to carbon oxides across all temperature profiles.

Most testing done was with a gas flow of 1% *n*-octane with an 8:1 C:O ratio and helium as a carrier gas. In Chapter 3, experiments where the *n*-octane concentration in the gas

flow was increased to *ca.*10% were discussed. The most notable finding when the concentration of *n*-octane was increased, was the shift in conditions which had resulted in ODH with no carbon oxide formation. When 1% *n*-octane was passed over the catalyst, an 8:1 carbon to oxygen ratio, at 400°C and 4000h^{-1} GHSV were the conditions which gave maximum conversion to octenes, while not producing carbon oxides. When the *n*-octane concentration increased to *ca.*10% however, gas hourly space velocity had to be increased from 4000h^{-1} to 16,000h^{-1} to attain a carbon oxide free reaction. This finding suggests considerable challenges ahead for scaling up the catalytic process, as increasing the GHSV leads to lower conversions.

Pure phases of the iron molybdate system were tested as catalysts to observe the activity and selectivity. Pure phase FeMoO$_4$ showed very similar activity and selectivity to a pre-reduced catalyst which possessed a molybdenum excess. This indicated that the active phase in the catalyst was FeMoO$_4$. Higher levels of cracked products were observed with pure phase FeMoO$_4$ this was suggested to be caused by iron particles at the catalyst surface. The molybdenum oxides of MoO$_3$ and MoO$_2$ were also tested. They showed lower activity than the pre-reduced iron molybdate catalyst and also higher selectivity to aromatic species. MoO$_2$ led to the formation of so called "heavy" aromatics such as ethyl naphthalene. MoO$_3$ exhibited a high selectivity to 8 carbon aromatic species and cracked oxygenates were produced in higher levels than when an iron molybdate catalyst was tested. Given the role of MoO$_3$ in the partial oxidation of methanol to formaldehyde[2,3] this finding is perhaps not surprising.

The pre-reduced iron molybdate catalyst underwent time on line studies to observe how holding the catalyst at 550°C for a prolonged period affected catalyst performance. The catalyst proved both durable and stable provided oxygen was available.

When oxygen was removed from the gas feed and *n*-octane was passed over the pre-reduced iron molybdate catalyst in an anaerobic atmosphere, activity was still observed for up to 30 hours. This was attributed to a time-lapse in the reaction, as the oxygen rich molybdenum lattice still retained the oxygen atoms to allow a Mars-Van

Krevelen[4] style mechanism to drive an ODH reaction. Iron molybdates have been associated with Mars-Van Krevelen mechanisms[5] so this finding is explicable.

It was found that carbon oxides were produced from oxygen present in the gas flow, while cracked oxygenates were formed from oxygen originating in the molybdate lattice. Product selectivity to octenes was higher when no oxygen was present in the gas feed. Carbon laydown was also observed with a sp2 type carbon material growing at the catalyst surface.

These findings are correlate with literature regarding nucleophilic and electrophilic oxygen. This work shows that lattice oxygen from an iron molybdate system possesses nucleophilic character while gas phase oxygen is electrophilic in nature.[6,7] Carbon laydown was unexpected but suggests that gas feed oxygen is required to replenish the catalyst surface.

Once the catalyst had ceased to exhibit activity in an anaerobic environment an irreversible change occurred. The catalyst was shown to have the bulk structure of $FeMoO_4$ + MoO_2. When oxygen was reintroduced into the gas feed with this system the *n*-octane was largely converted to "heavy" aromatic species such as naphthalene and ethyl naphthalene. It is unclear whether this was due to the presence of MoO_2 in the oxygen depleted catalyst or the effect of the carbon laydown at the catalyst surface. Lower selectivity to carbon oxides was also observed with the oxygen depleted catalyst.

Carbon oxides were attributed to oxygen species from the gas feed undergoing a surface reaction with the hydrocarbons. Cracked oxygenates were attributed to lattice oxygen from the molybdate excess. Cracked products appeared to be formed at high temperatures over iron particles at the catalyst surface. Octenes were formed via ODH using lattice oxygen. The formation of aromatic species, chiefly benzene, toluene, ethyl benzene, xylenes and styrene was also investigated. It had been suggested by Pillay *et al*[8] that the formation of aromatic species was from cyclisation via octene intermediate undergoing further ODH to an octadiene or octatriene, before undergoing a cyclisation. To test this oct-1-ene was used as a feedstock in place of *n*-octane, if Pillay *et al* suggested mechanism was correct it would be expected that

higher selectivity to aromatic species would be observed. This was not the case. Although oct-1-ene was much more reactive than *n*-octane, selectivity to aroamtics as a percentage of total products was actually lower with oct-1-ene as a substrate. The major product produced was octadienes. Thus it was suggested that the formation of aromatics is due to a cyclisation of the alkane followed by ODH to result in an aromatised system. It should be noted that no cyclic products such as cyclohexane were observed, as such this proposed mechanism comes with a significant caveat.

Nickel and cobalt molybdates have been shown within in existing literature[9,10] to be active ODH catalysts for small chain alkanes. More recently[8,11] they have been reported for ODH of hexane and octane. As such it was of interest to prepare and test the species before comparing them to iron molybdates.

Iron molybdate was shown to be a more promising catalyst for the ODH of *n*-octane to octene than cobalt and nickel molybdates. Pure phase $CoMoO_4$ and $NiMoO_4$ showed very high selectivity to carbon oxides at conditions where $FeMoO_4$ was highly selective to octenes.

Nickel and cobalt molybdates with a molybdenum molar excess exhibited more promising results for the ODH of *n*-octane than pure phase $CoMoO_4$ and $NiMoO_4$. Although *n*-octane conversion was lower, higher selectivity to octenes was observed. Cobalt molybdate with a molybdenum excess was the best of the cobalt and nickel molybdates tested.

6.2 FUTURE WORK

There are numerous directions this research could take for future work. Testing C_9-C_{20} hydrocarbons produced from the Fischer-Tropsch process as it would be of interest to observe if longer chain hydrocarbons act in the same manner as *n*-octane. Increasing the concentration of the alkane in the gas feed from 10% or above would be crucial in indicating if the catalyst could be an alternative to current processes such as the Honeywell UOP PACOL process.

Altering the catalyst volume or catalyst bed may also substantially alter results. Subtle changes of temperature around 400°C would also be of interest, to observe at what

temperature carbon oxide formation begins, and to maximise activity and selectivity to octenes.

Testing other molybdates for catalytic activity such as $MgMoO_4$ would be of interest as numerous molybdates have been tested for catalytic activity in the ODH of butane and propane.[12] Producing materials where the molybdenum is in a +5 oxidation state would also be an area to explore, as the redox state of molybdates may play a key role in the catalytic mechanism.

Tungstates could also be tested and compared to nickel, cobalt and iron molybdates. The effect of promoters such as alakali metals[13] on molybdates and tungstates could also be tested.

For the elucidation of how products are formed isotopic labelling experiments could be carried out. Using O^{18} in the gas feed would confirm beyond doubt whether an ODH-Mars-Van Krevelen mechanism is occurring. However aerobic and anaerobic studies done in Chapter 4 provide strong proof that the nature of the catalytic mechanism is Mars-Van Krevelen in nature. It has also been shown that the lattice oxygen of the iron molybdate catalyst is nucleophilic in nature, in direct contrast with the electrophilic nature of the oxygen from the gas phase which is required for the formation of carbon oxides.

From this it is possible to suggest some general trends regarding a possible mechanism.

Lower catalyst contact time increases the selectivity to octenes as the product. Higher contact times lead to higher selectivity toward aromatic species. Work in chapter 4 suggests that the reaction pathways are competing rather than sequential, and that a dehydrocyclization mechanism is responsible for the formation of aromatic species. However this work is inconclusive. Use of deuterium on the alkane feedstock could determine where hydrogen abstraction is occurring on the alkane chain using isotopic labelling. This would help elucidate if dehydrocyclization of the alkane is occurring. Higher contact time at lower temperatures also results in greater selectivity to carbon oxides, suggesting electrophilic oxygen from the gas feed inserts into an adsorbed

carbon chain at the catalyst surface in a competing manner to nucleophilic lattice oxygen which undergoes hydrogen abstraction. Low levels of cracked products such as methane and cracked oxygenates such as propan-1-ol were produced but in low concentrations.

Carbon oxides

Electrophilic oxygen insertion

n-octane —— *Oxidative dehydrogenation* —→ *Octene*

Dehydrocylisation

8 carbon aromatic species —— *Cracking* —→ **6 or 7 carbon aromatic species**
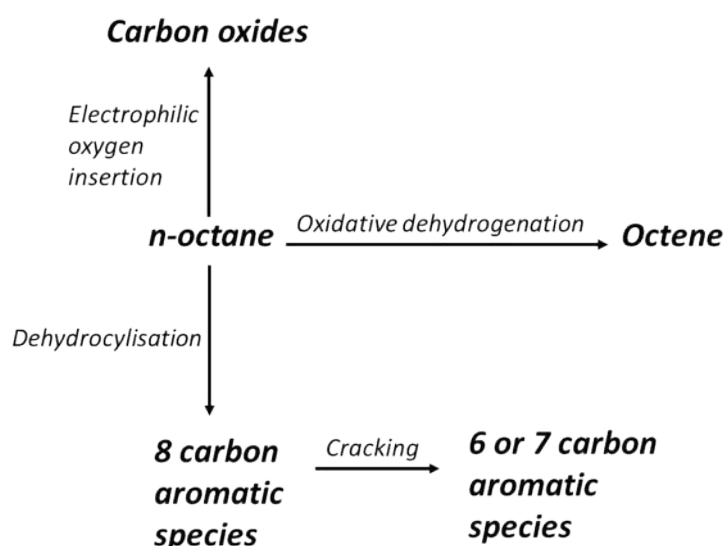
Figure 6.1 Proposed reaction pathways that *n*-octane undergoes

Figure 6.1 shows a proposed set of reaction pathways from the findings in this work. It is unlikely that octenes undergo no further reaction as work in Chapter 4 shows oct-1-ene undergoing aromatisation. However the majority of octenes formed in the reactions of *n*-octane were *trans* oct-3-ene. This would exhibit lower reactivity than oct-1-ene. I consider it still likely however that octenes once formed from *n*-octane would undergo further reactions forming carbon oxides or aromatic species. Future work could look at placing a gas feed of *trans* oct-3-ene into the reactor to observe what happens in the presence of an iron molybdate catalyst. This could be repeated with other isomers of octene.

There are many different directions future work could take. In the short term I would not alter the catalyst, keep using $FeMoO_4$ + MoO_3, and alter the other reaction variables. GHSV, concentration of hydrocarbon in the feed and the differences between alkanes and alkenes all offer intriguing alleyways of future work.

Bibliography

1   Fluid Catalytic Cracking VII:: Materials, Methods and Process Innovations, Elsevier, 2011.

2   J. S. Chung, R. Miranda and C. O. Bennett, J. Catal., 1988, **114**, 398–410.

3   J. Nováková, P. Jírů and V. Zavadil, J. Catal., 1970, **17**, 93–97.

4   C. Doornkamp and V. Ponec, J. Mol. Catal. Chem., 2000, **162**, 19–32.

5   M. P. House, phd, Cardiff University, 2007.

6   G. Centi, F. Cavani and F. Trifirò, Selective Oxidation by Heterogeneous Catalysis, Springer Science & Business Media, 2012.

7   R. H. Holm, Chem. Rev., 1987, **87**, 1401–1449.

8   B. Pillay, M. R. Mathebula and H. B. Friedrich, Appl. Catal. Gen., 2009, **361**, 57–64.

9   D. Levin and J. Y. Ying, in Studies in Surface Science and Catalysis, ed. S. T. O. R.K. Grasselli A. M.Gaffney and J. E.Lyons, Elsevier, 1997, vol. 110, pp. 367–373.

10 Y. S. Yoon, W. Ueda and Y. Moro-oka, Top. Catal., 1996, **3**, 265–275.

11 M. I. Fadlalla and H. B. Friedrich, Catal. Sci. Technol., 2014, **4**, 4378–4385.

12 L. M. Madeira, R. M. Martín-Aranda, F. J. Maldonado-Hódar, J. L. G. Fierro and M. F. Portela, J. Catal., 1997, **169**, 469–479.

13 R. M. Martin-Aranda, M. F. Portela, L. M. Madeira, F. Freire and M. Oliveira, Appl. Catal. Gen., 1995, **127**, 201–217.

Name and formula

Reference code:	00-022-0628

Common name:	β-Fe Mo O4
PDF index name:	Iron Molybdenum Oxide

Empirical formula:	$FeMoO_4$
Chemical formula:	$FeMoO_4$

Crystallographic parameters

Crystal system:	Monoclinic

a (Å):	10.2900
b (Å):	9.3940
c (Å):	7.0720
Alpha (°):	90.0000
Beta (°):	106.3100
Gamma (°):	90.0000

Calculated density (g/cm^3):	4.37
Volume of cell (10^6 pm^3):	656.10
Z:	8.00

RIR:	-

Subfiles and Quality

Subfiles:	Inorganic
	Corrosion
Quality:	Star (S)

Comments

General comments:	High-temperature, low pressure form.
Structure:	Isostructural with "Mn Mo O4" and "Mg Mo O4".
Unit cell data source:	Powder Diffraction.

References

Primary reference:	Sleight et al., *Inorg. Chem.*, **7**, 1093, (1968)

Peak list

No.	h	k	l	d [A]	2Theta[deg]	I [%]
1	1	1	0	6.81000	12.990	65.0
2	-2	0	1	4.66000	19.029	5.0
3	0	2	1	3.86000	23.022	15.0
4	2	0	1	3.55000	25.064	10.0
5	2	2	0	3.40000	26.189	100.0
6	-1	1	2	3.30000	26.998	20.0

```
 7   -2    0    2      3.26000      27.335       10.0
 8    1    1    2      2.82700      31.624       20.0
 9    0    2    2      2.75100      32.521       10.0
10   -2    2    2      2.67500      33.472       15.0
11   -3    1    2      2.67200      33.511       15.0
12    4    0    0      2.46900      36.358       10.0
13    0    4    0      2.34900      38.286       10.0
14   -1    3    2      2.34200      38.405        5.0
15   -4    0    2      2.33200      38.576        5.0
16    3    3    0      2.26900      39.691       35.0
```

Stick Pattern

Ref. Pattern : à-Fe Mo O4, 00-022-0628
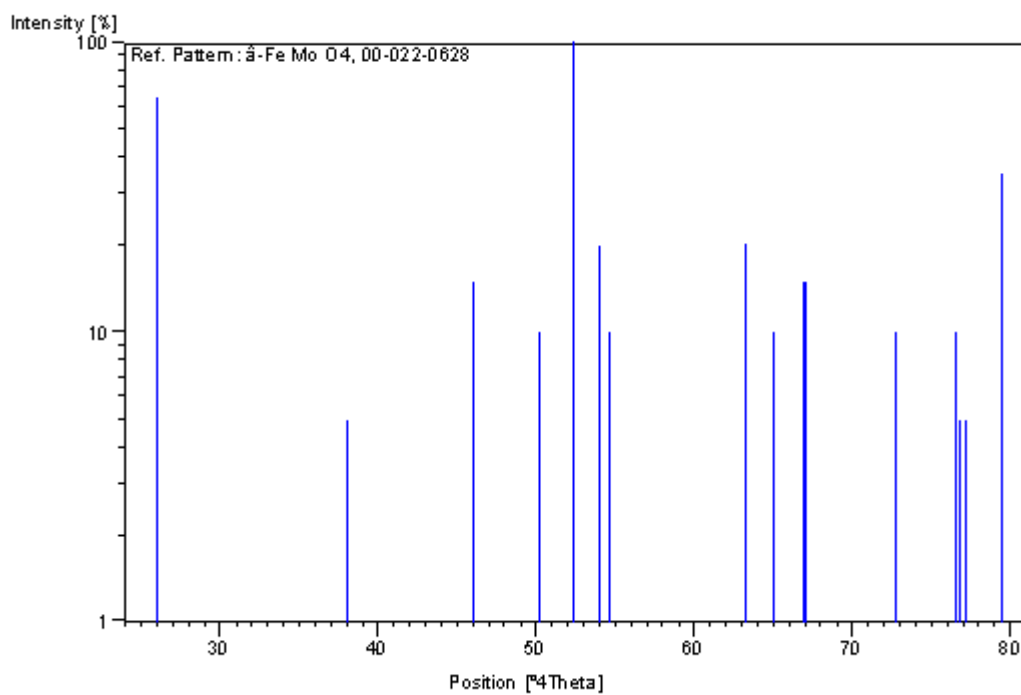
Name and formula

Reference code: 00-037-1445

Common name: β-Mo O3
PDF index name: Molybdenum Oxide

Empirical formula: MoO_3
Chemical formula: MoO_3

Crystallographic parameters

Crystal system: Monoclinic
Space group: P21/c
Space group number: 14

a (Å):   7.1220
b (Å):   5.3740
c (Å):   5.5650
Alpha (°):   90.0000
Beta (°):   91.8800
Gamma (°):   90.0000

Calculated density (g/cm^3):   4.49
Volume of cell (10^6 pm^3):   212.88
Z: 4.00

RIR: -

Status, subfiles and quality

Status:
Subfiles: Inorganic
                            Alloy, metal or intermetalic
                            Corrosion
Quality: Indexed (I)

Comments

Color: Yellow.
General comments: â-"Mo O3" is metastable, converting to the orthorhombic form
                            of "Mo O3" (á-"Mo O3") at elevated temperatures (above
                            ~350 C).
Sample preparation: Prepared by thermal treatment of a spray-dried molybdic acid
                            solution.
Melting point: Metastable.

References

Peak list

No.	h	k	l	d [A]	2Theta[deg]	I [%]
1	0	1	1	3.86200	23.010	100.0
2	2	0	0	3.55700	25.014	89.0
3	-1	1	1	3.42700	25.979	27.0
4	1	1	1	3.37300	26.403	23.0
5	0	0	2	2.78100	32.161	9.0
6	0	2	0	2.68500	33.344	19.0
7	-2	1	1	2.64900	33.810	24.0
8	-1	0	2	2.61900	34.210	25.0
9	2	1	1	2.58800	34.632	20.0
10	1	0	2	2.56200	34.995	16.0
11	3	1	0	2.17200	41.544	10.0
12	2	2	0	2.14400	42.112	15.0
13	-3	1	1	2.04100	44.347	10.0
14	0	2	2	1.93400	46.943	15.0
15	-1	2	2	1.87400	48.541	17.0
16	1	2	2	1.85500	49.071	14.0
17	4	0	0	1.78000	51.285	22.0
18	-2	2	2	1.71400	53.413	20.0
19	4	1	0	1.68600	54.372	15.0
20	-1	3	1	1.66500	55.116	23.0
21	4	1	1	1.60100	57.519	10.0
22	4	2	0	1.48200	62.634	15.0
23	-3	1	3	1.43200	65.084	10.0
24	3	1	3	1.38700	67.473	9.0
25	5	1	0	1.37600	68.085	8.0

Stick Pattern

Ref. Pattern: à-Mo O3, 00-037-1445
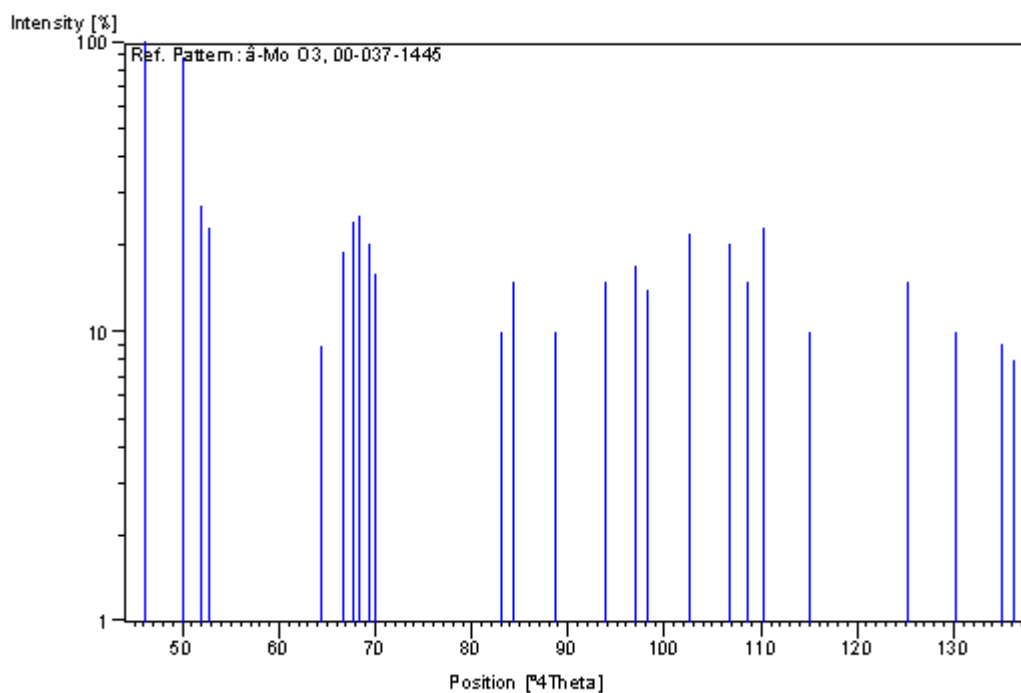
APPENDIX 3

Name and formula

Reference code:	00-005-0338
Common name:	χ-Mo4 O11
PDF index name:	Molybdenum Oxide
Empirical formula:	Mo_4O_{11}
Chemical formula:	Mo_4O_{11}

Crystallographic parameters

Crystal system:	Orthorhombic
Space group:	Pn21a
Space group number:	33
a (Å):	24.4000
b (Å):	5.4500
c (Å):	6.7230
Alpha (°):	90.0000
Beta (°):	90.0000
Gamma (°):	90.0000
Calculated density (g/cm^3):	4.16

Volume of cell (10^6 pm^3):   894.02
Z: 4.00

RIR: -

Status, subfiles and quality

Status: Marked as deleted by ICDD
Subfiles: Inorganic
                       Alloy, metal or intermetalic
Quality: Indexed (I)

Comments

Deleted by: Continuation of 00-005-0337.
Color: Reddish violet.

References

Primary reference: Magneli, a. et al., Univ. of Uppsala, Sweden., *Private Communication*
Structure: Asbrink, Kihlborg., *Acta Chem. Scand.*, **18**, 1571, (1964)

Peak list

No.	h	k	l	d [A]	2Theta[deg]	I [%]
1	2	0	0	12.30000	7.181	30.0
2	3	0	1	5.19000	17.071	10.0
3	4	0	1	4.53000	19.581	25.0
4	0	1	1	4.24000	20.935	45.0
5	2	1	1	4.00000	22.206	100.0
6	5	0	1	3.95000	22.491	65.0
7	3	1	1	3.75000	23.707	95.0
8	6	0	1	3.48000	25.577	85.0
9	1	0	2	3.33000	26.750	10.0
10	6	1	0	3.26000	27.335	20.0
11	3	0	2	3.11000	28.681	15.0
12	2	1	2	2.78700	32.090	50.0
13	5	0	2	2.77100	32.280	15.0
14	0	2	0	2.72200	32.878	60.0
15	3	1	2	2.70000	33.153	45.0
16	8	1	0	2.66300	33.627	70.0
17	6	0	2	2.59300	34.563	30.0
18	2	2	1	2.47300	36.297	10.0
19	7	0	2	2.42300	37.073	12.0
20	10	1	0	2.22500	40.510	30.0
21	2	0	3	2.20700	40.855	15.0
22	6	2	1	2.14600	42.071	35.0
23	7	2	1	2.04600	44.233	10.0
24	10	0	2	1.97500	45.912	30.0
25	5	2	2	1.94100	46.764	45.0
26	6	2	2	1.87700	48.459	40.0
27	11	0	2	1.85200	49.156	35.0
28	7	2	2	1.81000	50.375	30.0
29	7	1	3	1.78400	51.161	35.0
30	1	3	1	1.75000	52.230	10.0
31	2	3	1	1.73300	52.781	10.0
32	1	2	3	1.72600	53.012	50.0

33	13	1	1	1.71600	53.345	40.0
34	11	2	1	1.66600	55.080	15.0
35	9	1	3	1.64800	55.733	70.0
36	14	1	1	1.61200	57.091	30.0
37	12	2	1	1.58300	58.236	45.0
38	7	3	1	1.56700	58.888	15.0
39	8	3	0	1.56000	59.179	20.0
40	6	0	4	1.55500	59.388	25.0
41	11	2	2	1.53000	60.459	20.0
42	8	3	2	1.41500	65.965	15.0
43	4	2	4	1.39500	67.034	15.0
44	5	2	4	1.37300	68.255	20.0
45	4	4	0	1.33000	70.785	25.0
46	9	3	3	1.25100	76.012	40.0
47	10	3	3	1.22100	78.230	15.0
48	4	3	4	1.20900	79.157	20.0
49	15	3	2	1.14000	85.017	15.0
50	8	2	5	1.12100	86.811	20.0
51	17	2	3	1.10500	88.390	20.0

Stick Pattern
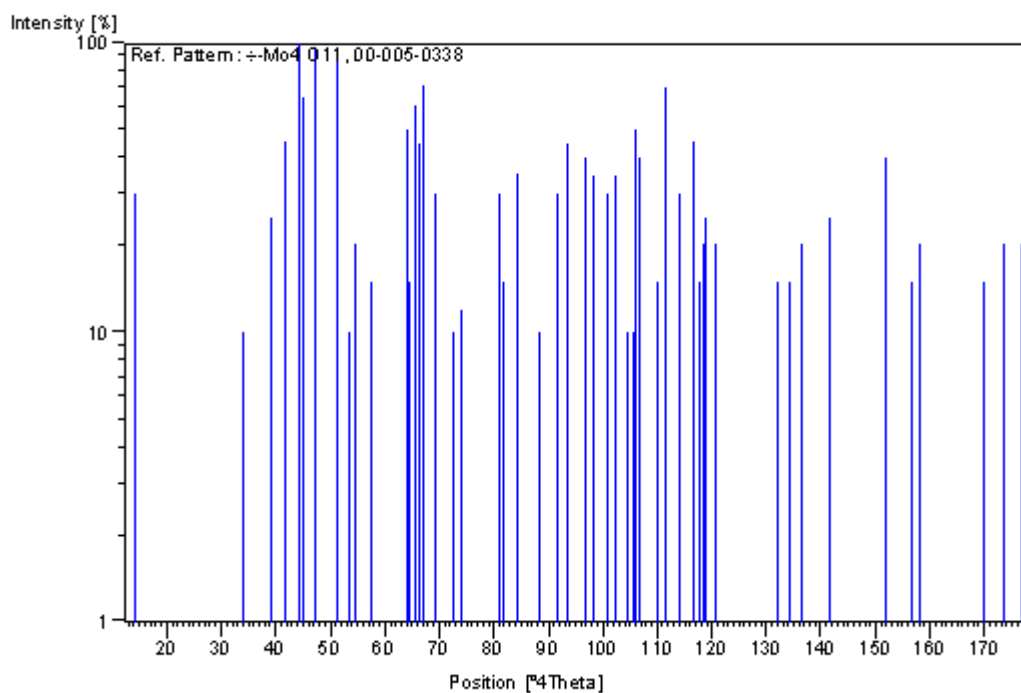
APPENDIX 4

Name and formula

Reference code: 00-032-0671

Mineral name: Tugarinovite, syn
PDF index name: Molybdenum Oxide

Empirical formula: MoO_2
Chemical formula: MoO_2

Crystallographic parameters

Crystal system: Monoclinic
Space group: P21/n
Space group number: 14

a (Å):   5.6068
b (Å):   4.8595
c (Å):   5.5373
Alpha (°):   90.0000
Beta (°):   119.3700
Gamma (°):   90.0000

Calculated density (g/cm^3):   6.46
Volume of cell (10^6 pm^3):   131.48
Z: 4.00

RIR: -

Subfiles and Quality

Subfiles: Inorganic
                           Mineral
                           Alloy, metal or intermetalic
                           Corrosion
                           Common Phase
                           Educational pattern
                           Forensic
                           NBS pattern
Quality: Star (S)

Comments

Color: Black.
Sample preparation: The sample was made at NBS, Gaithersburg, Maryland, USA,
                           Parker, H.S., by heating "Mo O3" in a Mo boat for 20 hours at
                           372 C in an atmosphere of 95% "N2" and 5% "H2" gases.
Additional pattern: To replace 00-005-0452 and 00-033-0929. See PDF 01-086-
                           0135.
CAS Number: 18868-43-4.
Additional diffraction line(s):   Plus 7 additional reflections to 1.0780.
Unit cell data source: Powder Diffraction.
Temperature: Pattern taken at 298 K.

References

Primary reference: *Natl. Bur. Stand. (U.S.) Monogr. 25*, **18**, 44, (1981)

Peak list

No.	h	k	l	d [A]	2Theta[deg]	I [%]
1	-1	0	1	4.80500	18.450	2.0
2	-1	1	1	3.42000	26.033	100.0
3	1	0	1	2.81300	31.785	4.0
4	2	0	0	2.44200	36.775	30.0
5	1	1	1	2.43700	36.853	30.0
6	-2	1	1	2.42600	37.026	70.0
7	-2	0	2	2.40300	37.393	35.0
8	2	1	0	2.18100	41.365	6.0
9	0	2	1	2.17100	41.564	2.0
10	-2	1	2	2.15600	41.867	5.0
11	-3	0	1	1.84100	49.469	11.0
12	2	1	1	1.72500	53.045	30.0
13	2	2	0	1.72300	53.112	35.0
14	-3	1	2	1.71100	53.514	40.0
15	-2	2	2	1.70900	53.581	35.0
16	-2	1	3	1.69760	53.970	20.0
17	-3	0	3	1.60330	57.429	1.0
18	3	1	0	1.54430	59.842	7.0
19	0	3	1	1.53600	60.198	13.0
20	0	1	3	1.52720	60.581	9.0
21	-3	2	1	1.46760	63.319	4.0
22	2	0	2	1.40570	66.458	4.0
23	-4	0	2	1.40190	66.661	20.0
24	-2	0	4	1.38450	67.611	5.0
25	3	0	1	1.35480	69.301	2.0
26	0	3	2	1.34480	69.891	1.0
27	-3	2	3	1.33810	70.293	1.0
28	-4	1	1	1.30330	72.461	5.0
29	-4	1	3	1.29120	73.250	5.0
30	-3	1	4	1.28290	73.802	1.0
31	4	0	0	1.22190	78.161	7.0
32	2	3	1	1.21750	78.498	10.0
33	1	3	2	1.21460	78.721	6.0
34	-2	3	3	1.20760	79.267	7.0
35	-2	2	4	1.20280	79.647	4.0
36	3	2	1	1.18370	81.197	2.0
37	1	2	3	1.17640	81.808	1.0
38	3	3	0	1.14850	84.242	2.0
39	0	3	3	1.14140	84.889	4.0

Stick Pattern

Ref. Pattern | Tugarinovite, syn, 00-032-0671
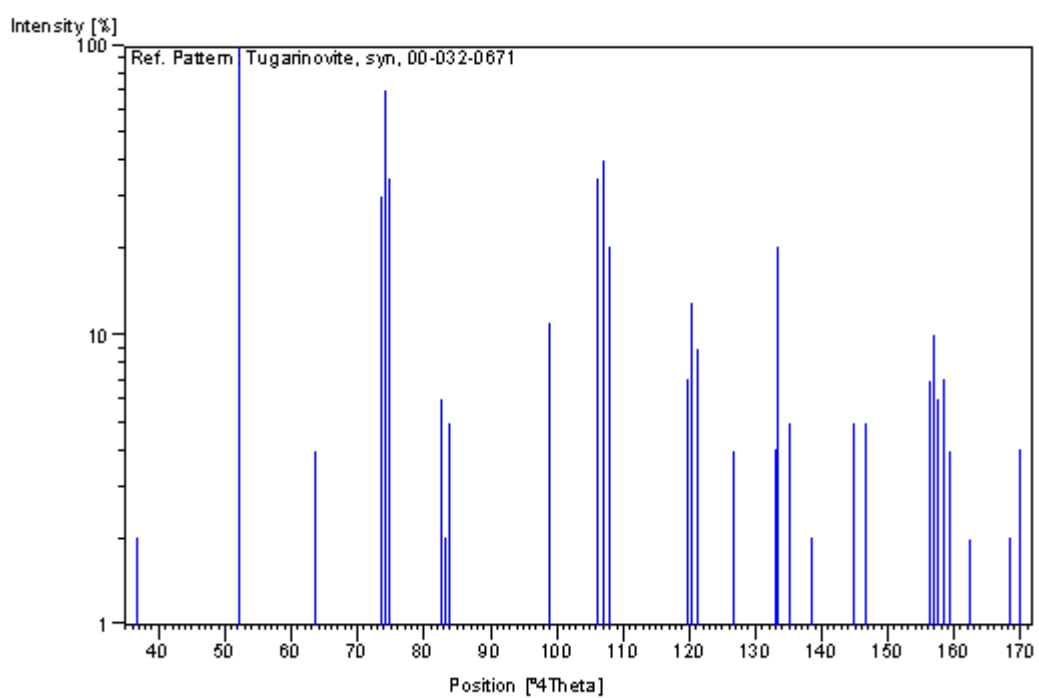
Name and formula

Reference code: 01-073-1331

Common name: cobalt molybdate
PDF index name: Cobalt Molybdenum Oxide

Empirical formula: $CoMoO_4$
Chemical formula: $CoMoO_4$

Crystallographic parameters

Crystal system: Monoclinic
Space group: C2/m
Space group number: 12

a (Å):   9.6660
b (Å):   8.8540
c (Å):   7.7550
Alpha (°):   90.0000
Beta (°):   113.8200
Gamma (°):   90.0000

Calculated density (g/cm^3):   4.79
Measured density (g/cm^3):   4.69
Volume of cell (10^6 pm^3):   607.16
Z: 8.00

RIR: 3.24

Subfiles and Quality

Subfiles: Inorganic
                         Corrosion
                         ICSD Pattern
Quality: Star (S)

Comments

ANX: ABX4.
Wyckoff Sequence: j3 i4 h g (C12/M1).
Additional pattern: See PDF 00-025-1434.
ICSD collection code: 23808.
Test from ICSD: Calc. density unusual but tolerable.

References

Primary reference: *Calculated from ICSD using POWD-12++*, (1997)
Structure: Smith, G.W., Ibers, J.A., *Acta Crystallogr.*, **19**, 269, (1965)

Peak list

No.	h	k	l	d [A]	2Theta[deg]	I [%]
1	0	0	1	7.09442	12.467	0.9
2	1	1	0	6.25670	14.144	100.0
3	-1	1	1	5.54375	15.974	7.4
4	-2	0	1	4.69979	18.867	15.4
5	0	2	0	4.42132	20.067	1.2
6	1	1	1	4.14196	21.436	3.4
7	0	2	1	3.75576	23.671	16.3
8	-1	1	2	3.55182	25.051	61.8
9	2	0	1	3.21453	27.729	5.1
10	2	2	0	3.12835	28.509	98.3
11	-3	1	1	3.02754	29.480	1.2
12	3	1	0	2.79952	31.942	4.7
13	-3	1	2	2.77187	32.270	58.9
14	0	2	2	2.76532	32.348	66.6
15	-1	3	1	2.72582	32.830	0.9
16	2	2	1	2.60113	34.452	0.1
17	-2	0	3	2.55890	35.039	0.1
18	1	3	1	2.49736	35.931	1.3
19	-1	1	3	2.45636	36.552	0.6
20	-4	0	1	2.40430	37.372	0.1
21	0	0	3	2.36481	38.020	1.5
22	-4	0	2	2.34844	38.295	15.6
23	2	0	2	2.34318	38.385	13.8
24	3	1	1	2.31650	38.845	1.6
25	-3	1	3	2.28938	39.323	0.7
26	0	4	0	2.21350	40.730	12.8
27	-3	3	1	2.17624	41.459	0.8
28	-4	2	1	2.11282	42.764	4.1
29	0	2	3	2.08557	43.351	43.1
30	1	1	3	2.02865	44.632	0.8
31	-2	4	1	2.00252	45.246	2.7
32	2	4	0	1.97931	45.806	3.3
33	-2	0	4	1.93874	46.821	25.4
34	-1	3	3	1.93244	46.983	14.1
35	4	0	1	1.90349	47.742	0.1
36	-4	2	3	1.88996	48.105	0.1
37	-2	4	2	1.87788	48.434	1.4
38	3	1	2	1.87454	48.526	1.4
39	-5	1	1	1.86209	48.872	0.6
40	-3	1	4	1.85297	49.128	3.3
41	-1	1	4	1.85077	49.190	3.2
42	-3	3	3	1.84792	49.271	2.4
43	2	4	1	1.82309	49.988	1.6
44	2	0	3	1.80414	50.550	0.1
45	0	0	4	1.77286	51.506	0.6
46	4	2	1	1.74869	52.272	1.1
47	1	5	0	1.73633	52.672	8.8
48	5	1	0	1.73427	52.740	9.2
49	-1	5	1	1.71831	53.268	0.7
50	1	3	3	1.70242	53.805	0.5
51	-2	4	3	1.67408	54.791	0.5
52	2	2	3	1.67073	54.911	1.8
53	-4	2	4	1.64949	55.679	11.7
54	0	2	4	1.64639	55.793	15.2
55	-4	4	1	1.62846	56.461	0.2
56	0	4	3	1.61603	56.935	1.9
57	-4	4	2	1.61124	57.120	13.7
58	3	3	2	1.60824	57.236	14.1
59	-5	1	4	1.59543	57.739	0.9

60	-1	3	4	1.59315	57.829	0.9
61	1	1	4	1.59123	57.906	0.8
62	-6	0	1	1.57521	58.552	0.9
63	4	4	0	1.56418	59.005	1.6
64	5	1	1	1.54908	59.638	0.7
65	-2	0	5	1.54466	59.826	0.4
66	-5	3	3	1.54264	59.913	0.3
67	3	1	3	1.53836	60.096	0.4
68	-4	4	3	1.51964	60.915	1.6
69	-6	2	2	1.51286	61.217	19.3
70	4	2	2	1.51077	61.311	16.2
71	-4	0	5	1.50104	61.751	1.0
72	-6	2	1	1.48406	62.537	0.2
73	0	6	0	1.47567	62.933	4.0
74	6	0	0	1.47377	63.023	4.3
75	-2	2	5	1.45842	63.764	5.1
76	-1	5	3	1.45547	63.909	4.6
77	0	6	1	1.44474	64.441	0.8
78	3	5	1	1.42494	65.447	1.5
79	-4	2	5	1.42146	65.627	9.5
80	-3	5	3	1.41848	65.782	11.9
81	2	6	0	1.39976	66.776	1.6
82	6	2	0	1.39832	66.854	1.6
83	5	3	1	1.38838	67.397	0.9
84	-6	2	4	1.38634	67.509	1.1
85	2	2	4	1.38266	67.713	1.0
86	3	3	3	1.38065	67.825	0.4
87	4	0	3	1.36342	68.801	0.6
88	5	1	2	1.35993	69.003	0.4
89	0	2	5	1.35105	69.521	0.5
90	2	6	1	1.34111	70.112	0.1
91	6	0	1	1.33927	70.222	0.1
92	-1	3	5	1.33639	70.396	0.3
93	-7	1	1	1.32551	71.061	0.1
94	1	1	5	1.30562	72.312	0.3
95	-5	5	2	1.30261	72.506	0.7
96	3	5	2	1.30108	72.605	0.6
97	-5	5	1	1.29737	72.846	0.7
98	-3	5	4	1.29381	73.079	4.3
99	3	1	4	1.29071	73.283	4.2
100	-6	4	1	1.28340	73.769	1.2
101	-2	6	3	1.27894	74.069	2.1
102	-6	2	5	1.26809	74.811	0.7
103	-5	5	3	1.26561	74.982	0.8
104	-4	6	1	1.25767	75.538	0.7
105	5	5	0	1.25134	75.988	4.1
106	2	6	2	1.24731	76.278	2.2
107	-4	4	5	1.24233	76.639	0.6
108	-7	3	3	1.24045	76.776	0.6
109	-5	1	6	1.22914	77.614	2.6
110	-1	1	6	1.22761	77.729	2.4
111	-7	3	1	1.22116	78.217	0.8
112	-6	4	4	1.21862	78.412	0.9
113	2	0	5	1.21612	78.604	1.0
114	-1	7	2	1.20250	79.670	5.8
115	6	0	2	1.20005	79.866	4.1
116	0	4	5	1.19454	80.309	0.5
117	5	1	3	1.19146	80.559	0.3
118	-3	3	6	1.18394	81.177	1.4
119	0	0	6	1.18240	81.305	1.0

```
120    -3    7    1      1.17737    81.726      0.7
121    -8    0    4      1.17422    81.993      3.0
122     4    0    4      1.17159    82.216      2.8
123    -8    0    1      1.16625    82.675      0.4
124    -8    2    3      1.16236    83.013      2.1
125     7    3    0      1.16133    83.103      2.6
126     6    2    2      1.15825    83.373      1.3
127     7    1    1      1.15515    83.647      0.4
128     6    4    1      1.14585    84.482      0.1
129     0    2    6      1.14224    84.812      0.6
130    -8    2    4      1.13539    85.445      1.0
131    -1    7    3      1.13437    85.540      0.8
132     4    2    4      1.13260    85.706      1.2
133    -8    2    1      1.12767    86.171      0.8
134    -8    0    5      1.11790    87.111      0.3
135    -3    7    3      1.11588    87.309      0.6
136     5    3    3      1.11353    87.540      0.3
137    -5    5    5      1.10875    88.014      0.1
138    -2    4    6      1.10675    88.214      0.3
139     1    1    6      1.10533    88.357      0.4
140    -3    1    7      1.09696    89.210      0.1
141     0    8    1      1.09352    89.566      0.1
```

Stick Pattern

190
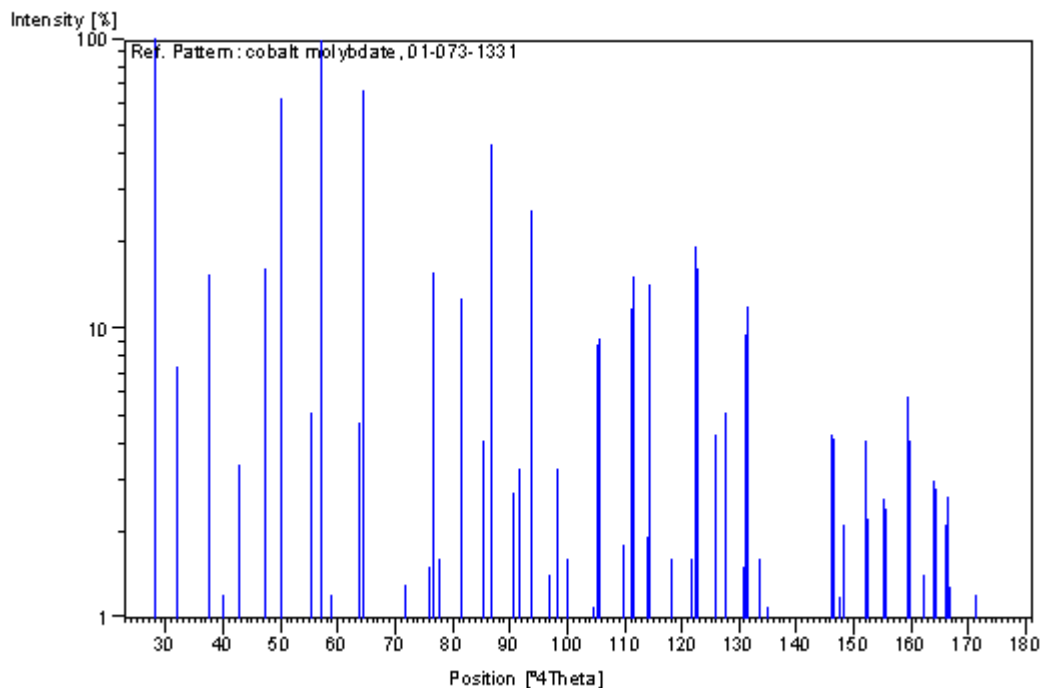
Name and formula

Reference code: 00-016-0291

PDF index name: Nickel Molybdenum Oxide

Empirical formula: $MoNiO_4$
Chemical formula: $NiMoO_4$

Crystallographic parameters

Crystal system: Monoclinic
Space group: P2/c
Space group number: 13

a (Å):   4.5800
b (Å):   5.6700
c (Å):   4.8700
Alpha (°):   90.0000
Beta (°):   89.3200
Gamma (°):   90.0000

Volume of cell (10^6 pm^3):   126.46
Z: 2.00

RIR: -

Subfiles and Quality

Subfiles: Inorganic
                         Corrosion
Quality: Indexed (I)

Comments

Sample preparation: High pressure modification formed at 60 kbar and 900 C.
Unit cell data source: Powder Diffraction.

References

Primary reference: Young, Schwartz., *Science*, **141**, 348, (1963)

Peak list

No.	h	k	l	d [A]	2Theta[deg]	I [%]
1	1	0	0	4.57000	19.408	20.0
2	0	1	1	3.69000	24.099	30.0
3	1	1	0	3.56000	24.993	50.0
4	1	1	1	2.88600	30.961	100.0
5	-1	1	1	2.86100	31.238	100.0
6	0	2	0	2.83400	31.544	10.0
7	0	2	1	2.44500	36.728	20.0

8	2	0	0	2.29000	39.312	10.0
9	1	2	1	2.16600	41.664	15.0
10	-1	1	2	2.00300	45.234	10.0
11	0	2	2	1.84900	49.241	30.0
12	2	2	0	1.78300	51.192	20.0
13	1	3	0	1.74700	52.326	40.0
14	2	0	2	1.67900	54.617	40.0
15	-2	0	2	1.66100	55.260	20.0

Stick Pattern

Ref. Pattern: Nickel Molybdenum Oxide, 00-016-0291